PREDICTIVE MODEL FOR THE PREVENTION OF WELD METAL HYDROGEN CRACKING IN HIGH-STRENGTH MULTIPASS WELDS

PEKKA NEVASMAA

Department of Mechanical Engineering,
University of Oulu

OULU 2003

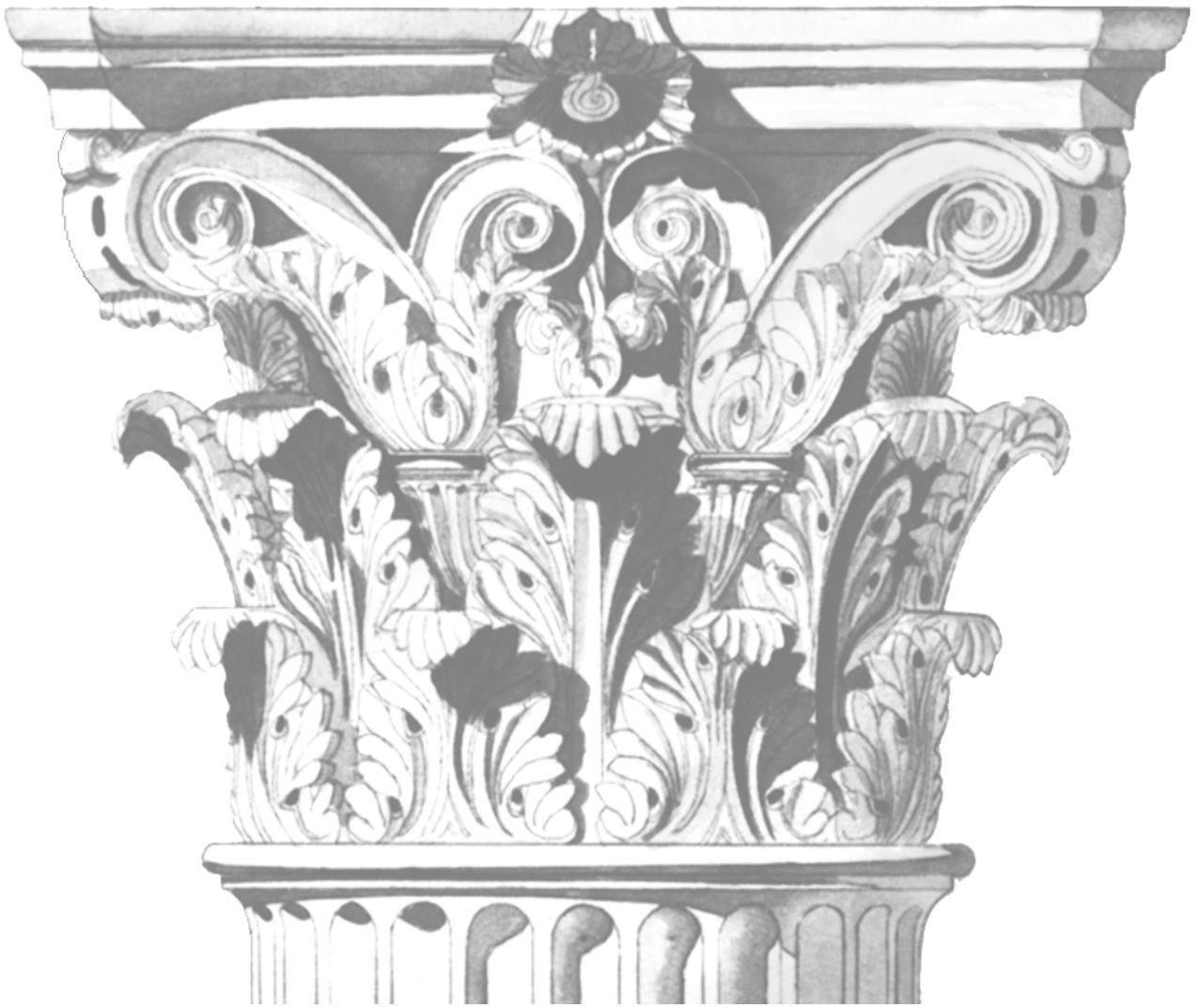

PEKKA NEVASMAA

PREDICTIVE MODEL FOR THE PREVENTION OF WELD METAL HYDROGEN CRACKING IN HIGH-STRENGTH MULTIPASS WELDS

Academic Dissertation to be presented with the assent of the Faculty of Technology, University of Oulu, for public discussion in Raahensali (Auditorium L10), Linnanmaa, on November 15th, 2003, at 12 noon.

OULUN YLIOPISTO, OULU 2003

Supervised by
Professor Pentti Karjalainen

Reviewed by
Professor Horst H. Cerjak
Doctor David A. Porter

ISBN 951-42-7181-5 (URL: http://herkules.oulu.fi/isbn9514271815/)

ALSO AVAILABLE IN PRINTED FORMAT
Acta Univ. Oul. C 191, 2003
ISBN 951-42-7180-7
ISSN 0355-3213 (URL: http://herkules.oulu.fi/issn03553213/)

OULU UNIVERSITY PRESS
OULU 2003

Nevasmaa, Pekka, Predictive model for the prevention of weld metal hydrogen cracking in high-strength multipass welds
Department of Mechanical Engineering, University of Oulu, P.O.Box 4200, FIN-90014
University of Oulu, Finland
Oulu, Finland
2003

Abstract

This thesis studies controlling factors that govern transverse hydrogen cracking in high-strength multipass weld metal (WM). The experiments were concerned with heavy-restraint Y- and U-Groove multipass cracking tests of shielded-metal arc (SMAW) and submerged-arc (SAW) weld metals. Results of tensile tests, hardness surveys, weld residual stress measurements and microstructural investigations are discussed. The analytical phase comprised numerical calculations for analysing the interactions between crack-controlling factors. The objectives were: (i) the assessment of WM hydrogen cracking risk by defining the Crack-No Crack boundary conditions in terms of 'safe line' description giving the desired lower-bound estimates, and (ii) to derive predictive equations capable of giving reliable estimates of the required preheat/interpass temperature T_0/T_i for the avoidance of cracking.

Hydrogen cracking occurred predominantly in high strength weld metals of $R_{p0.2} \approx 580$-900 MPa. At intermediate strengths of $R_{p0.2} \approx 500$-550 MPa, cracking took place in the cases where the holding time from welding to NDT inspection was prolonged to 7 days. Low strength WMs of $R_{p0.2} \leq 480$ MPa did not exhibit cracking under any conditions examined. Cracking occurrence was, above all, governed by WM tensile strength, weld diffusible hydrogen and weld residual stresses amounting to the yield strength. The appearance of cracking vanished when transferring from 40 to 6 mm thick welds. The implications of the holding time were more significant than anticipated previously. A period of 16 hrs in accordance with SFS-EN 1011 appeared much too short for thick multipass welds. Interpass time and heat input showed no measurable effect on cracking sensitivity, hence being of secondary importance. Equations were derived to assess the weld critical hydrogen content H_{cr} corresponding to the Crack-No Crack conditions as a function of either weld metal P_{cm}, yield strength $R_{p0.2}$ or weld metal maximum hardness $HV_{5(max)}$. For the calculation of safe T_0/T_i estimates, a formula incorporating: (i) WM strength as a linear function of either weld carbon equivalent CET or weld $HV_{5(max)}$, (ii) weld build-up thickness a_w in the form of *tanh* expression and (iii) weld diffusible hydrogen H_D in terms of a combined [*ln / power law*] expression was found descriptive.

Keywords: cold cracking, high-strength steels, hydrogen cracking, multipass welding, weld metal cracking

Preface

This work was principally carried out in two laboratories: VTT Industrial Systems (formerly: VTT Manufacturing Technology) and the University of Oulu during 1999–2002. Specifically and additionally, experimental cracking tests were performed at VTT, Oy ESAB and Mäntyluoto Works Oy, Finland, ESAB U.K Ltd, United Kingdom and Nippon Steel Corporation, Japan. Weld residual stress measurements were made in Helsinki University of Technology, Finland, whilst the University of Oulu was responsible for the permeation tests of hydrogen diffusivity, weld metal tensile tests and metallographic studies of welds. The non-destructive examination of the cracking test welds was performed jointly by Rautaruukki Oyj and VTT, Finland.

I would like to express my sincere gratitude to Professor Pentti Karjalainen, Dr. David Widgery and Dr. David Porter for their encouraging attitude, experimental work and valuable scientific comments concerning the analytical work. I am deeply indebted to Professor Nobutaka Yurioka for the opportunity to work in Nippon Steel Research Centre, Japan, as well as for the fruitful theoretical lectures and many discussions. I am very grateful to Lic.Tech. Mari-Selina Kantanen and PhD Longxiu Pan for their contribution as co-workers to the experimental part concerning metallographic studies of weld metal microstructures and measurements of hydrogen diffusion. The persistency and collaboration of Professor Risto Karppi regarding the arrangements of my working period in Japan, and the project management, is gratefully acknowledged. I have the pleasure in thanking MScTech Juha Lukkari for providing me with many rewarding research papers from recent works in this field.

I wish to thank all the colleagues and staff for their contribution to the various parts of the work during its lifetime, without whom this all would not have been possible. These thanks are, above all, due to Esko Kallinen, Esa Penttilä, Aarne Kanerva, Pentti Pajunen, S. Highland, A. Elmes and M. Andrews for the welding experiments, as well as to David Widgery, Juha Lukkari, Mika Siren, Janne Mononen, Janne Tamminen and Ari Joutsenvirta for supervising the welding work. Anssi Brederholm, Hans Gripenberg and Iikka Virkkunen who were conducting the residual stress measurements are gratefully acknowledged. It is my pleasure to thank MScTech Anssi Laukkanen for the many valuable and far-reaching discussions on numerical modelling of hydrogen diffusion and the associated effects on fracture resistance. I would also like to thank Mrs Hilkka

Hänninen, Mr Tuomo Hokkanen and Mr Erkki Makkonen for their patience in illustrating the figures and photos, as well as Arja Grahn, Erja Mörsky and Merja Asikainen for their secretarial work.

This work belonged to the Finnish R & D project "*Control of high-strength steel weld metal hydrogen cracking*" co-ordinated by VTT Industrial Systems. Financial support by the Graduate School of Metallurgy within the University of Oulu, ESAB Group Ltd, Rautaruukki Oyj, National Technology Agency (Tekes) and VTT Industrial Systems is gratefully acknowledged. Support in the form of labour as countless number of man-hours by Mäntyluoto Works Oyj and PPTH Steel Ltd is highly appreciated.

Finally, my dearest thanks are due to my wife Anu, my son Ilmari and my daughters Anniina and Leena for bearing their invidious share of the burden along the way, as well as for all the borrowed time I cannot pay back.

"After all this struggle, agony and pain – while now reaching finally my very destination,

Can't help feeling like a freight train – lost'n' lonely, as if I was abandoned in the station".

Espoo, November 2003 Pekka Nevasmaa

List of symbols and abbreviations

α	: ferrite
a	: activity of the diffusing mass
a_w	: weld build-up thickness (mm)
a_b	: height of an individual weld bead, bead size (mm)
AF	: acicular ferrite
BM	: base material, parent material
B/A	: weld (bead) overlap ratio according to bead-on-plate test
B_S	: bainite transformation (start) temperature
c	: concentration of the diffusing mass, e.g., hydrogen
CE_{IIW}	: IIW carbon equivalent (%)
CET	: German carbon equivalent based on chemical composition (%)
d	: weld bead penetration/overlap (mm)
d/h_w	: weld (bead) overlap ratio
D	: diffusion coefficient – general expression
D(T)	: diffusion coefficient as a function of temperature (cm^2/ sec)
D_i	: diffusion coefficient at a given interpass-temperature (cm^2/ sec)
D_H	: diffusion coefficient for hydrogen (cm^2/ sec)
E	: arc energy (in welding) (kJ/mm)
F	: weld groove shape factor
FCAW	: flux-cored (tubular wire) arc welding
FDM	: finite difference method
FEM	: finite element method
Fe_3C	: cementite
F_I	: specimen/groove severity parameter in terms of stress concentration
FS	: side-plate ferrite, lath-like ferrite side-plates resembling upper-bainite
FS(A)	: ferrite side-plates with aligned second-phase
FS(NA)	: ferrite side-plates with non-aligned second phase
γ	: activity coefficient of the mass
γ	: austenite
GBF	: pro-eutectoid grain boundary ferrite
GMAW	: gas-metal arc welding (i.e., MIG/MAG welding)

HAZ : heat-affected zone
H_D : weld diffusible hydrogen content per deposited weld metal (DM) conforming to ISO/IIW 3690-1977 (ml/100 g DM IIW)
H_F : weld diffusible hydrogen content per fused metal (ml/100 g FM IIW)
H_0 : initial diffusible hydrogen content in the weld (at high temperatures, immediately after solidification before cooling down to ambient temperature) according to e.g. ISO 3690 (in which case $H_0 = H_{D)}$ (ml/100 g DM IIW)
H_{max} : maximum hydrogen content/concentration in weld metal – general expression (ml/100 g)
H_{Rmax} : final local maximum hydrogen concentration in multipass weld metal (ml/100 g DM IIW)
H_{R100} : remaining weld diffusible hydrogen content at 100°C (ml/100 g DM IIW)
$H_{R100max}$: maximum remaining weld diffusible hydrogen content at 100°C (ml/100 g DM IIW)
$H_{Rmax(d=0)}$: maximum remaining weld diffusible hydrogen content under conditions of no dilution or weld overlap (ml/100 g DM IIW)
$H_{R100max(d=0)}$: maximum remaining weld diffusible hydrogen content at 100°C under conditions of no dilution or weld overlap (ml/100 g DM IIW)
$H_{Rmax(d > 0)}$: local final (maximum) hydrogen concentration in weld metal affected by dilution and weld overlap (ml/100 g DM IIW)
H_{cr} : weld critical hydrogen content with respect to cracking (ml/100 g DM IIW)
HV : Vickers pyramid hardness (HV)
HV_{ave} : average value of Vickers hardness (HV)
HV_{max} : maximum value of Vickers hardness (HV)
h : plate thickness (mm)
h_w : thickness of an individual weld bead layer (mm or cm)
J : flux of the diffusing mass
k : thermal efficiency of welding (acc. to EN 1011-1:1998)
l : number of weld bead layers
μ : chemical potential of a substance in the phase
M : martensite
M-A : martensite-austenite constituent
MAC : martensite-austenite-carbide (aligned) layers between ferrite laths
M_S : martensite transformation (start) temperature (°C)
N : number of individual weld beads
P_{cm} : Japanese welding index based on chemical composition (%)
$P_{D–D}$: integrated hydrogen diffusion-distance parameter
PF : polygonal ferrite
PWHT : post-weld heat treatment
Q : heat input (in welding) (kJ/mm)
R : the gas constant (cal/mol)
R_F : intensity of restraint against transverse shrinkage (MPa/mm∗mm)
R_e : yield strength – general expression (MPa)
$R_{e(WM)}$: yield strength of weld metal (MPa)
$R_{p0.2}$: yield strength at 0.2 mm elongation (MPa)

R_M	: ultimate tensile strength (MPa)
σ_{res}	: welding residual stress (MPa)
σ_{resL}	: weld longitudinal residual stress (MPa)
σ_{net}	: transverse net stress across the weld throat (MPa)
$\Sigma D\Delta t$	: thermal factor of hydrogen diffusion (cm^2)
$\Sigma D\Delta t_{(100)}$	: estimate for the thermal parameter of hydrogen diffusion $\Sigma D\Delta t$ from 500 to 100°C
SAW	: submerged-arc welding
SMAW	: shielded metal-arc welding (manual metal-arc welding)
τ	: thermal parameter of hydrogen diffusion (cm^2)
t	: time, in general (sec)
$t_{8/5}$	: weld cooling time between 800 to 500°C (sec)
$t_{500-100}$	: weld cooling time between 500 to 100°C (sec)
$t_{15/2}$	: weld cooling time from peak temperature to 200°C (sec)
t_{200}	: weld cooling time from peak temperature to 200°C (sec)
$t_{15/1.5}$	: weld cooling time from peak temperature to 150°C (sec)
t_{150}	: weld cooling time from peak temperature to 150°C (sec)
t_{100}	: weld cooling time from peak temperature to 100°C (sec)
t_i	: welding interpass time (min, sec)
Σt_i	: total interpass time during welding (min, sec)
Δt	: time integrated over the temperature range from T_m to T_i (sec)
T	: temperature, in the connection with diffusion equations (K)
θ	: temperature, in the connection with diffusion equations (°C)
T_0	: preheat temperature, in general (°C)
T_{cr}	: critical required preheat/interpass temperature for the avoidance of cracking (°C)
T_i	: weld interpass temperature (°C)
T_m	: melting temperature corresponding to approx. 1500°C (°C)
WM	: weld metal

Contents

1 Introduction: Current status of weld metal hydrogen cold cracking

Arc welding typically leads to the occlusion of hydrogen gas in the arc atmosphere into the solidifying weld metal, from which sc. diffusible hydrogen can diffuse into the various regions of the weldment as it cools down. Depending on metal's microstructure, concentration of weld diffusible hydrogen and the level of weld residual stress, the risk of *hydrogen-induced cold- cracking* in ferritic steel can arise when the weld cools down to below the 150–100°C temperature region. Generally, hydrogen cracking is of a delayed nature, i.e., cracks can appear several days after welding was completed. Usually, hydrogen cracks are sited either in the parent steel heat-affected zone or in the weld metal itself. One of the most effective precautions against weld hydrogen cracking is to use *preheating*, i.e., to heat up a sufficiently great volume of the weld area of a structural member prior to welding or, in the case of multipass welding, to apply *elevated interpass temperature* throughout the welding operation.

Recent developments in advanced steel processing routes have considerably improved base material quality by lowering carbon and impurities, thereby enhancing the resistance of the weld heat-affected zone (HAZ) to hydrogen cold cracking. From the end user's viewpoint, these developments have expanded the application boundaries for welding filler materials, challenging the consumable manufacturers to keep pace with the development of steel products. Presently, the industrial benefits brought by advanced steel are too often offset by the shift of hydrogen cold cracking problems to the weld metal (WM). Consequently, with increasing strength of parent plate and weld metal, required preheat may be dictated by the cracking sensitivity of the weld metal instead of the parent steel HAZ.

1.1 Hydrogen-induced cracking in weldments – general

Weld hydrogen cracking is attributable to three main factors: microstructure, hydrogen and stress. The causal factors governing the occurrence of hydrogen-induced cold

cracking in welded joints of ferritic structural steels are: (i) crack-sensitive, *hardened microstructure* containing martensitic and/or bainitic transformation products, (ii) sufficiently high, local weld hydrogen concentration in terms of *weld diffusible hydrogen content* and (iii) *elevated stress* caused by high structural restraint that is determined by structural rigidity, i.e., plate thickness and weld bead height (or weld build-up thickness). Hydrogen cracking sensitivity of weldments is a combination of these three primary factors[40].

The greatest risk of weld hydrogen cracking occurs when the weld cools down and temperatures of around 150–100°C are reached; above this temperature range, cracking is unlikely to initiate in ferritic structural steels[40]. A characteristic feature of hydrogen cold-cracking is its *delayed* nature, that is, crack initiation and especially propagation may take place several hours, or sometimes even days or weeks, after welding has been completed. The risk of cracking becomes apparent and raises as strength of parent steel and/or weld metal increases, and when welding thick plate sections that often employ multipass welding techniques[40].

Overall, there is very little information on the risk of weld metal hydrogen cracking in multipass welds, from which guidance on safe welding conditions can be derived[8]. Thus, welding guidelines in the current standards are quite limited in addressing the issue of avoiding hydrogen cracking in weld metal[8, 76]. AWS D1.1:1988[104] advises to conduct testing where it is feared there may be a risk. BS 5135:1984[105], in turn, proposes two approaches: (i) the use of consumables giving less than 2.5 ml/100 g DM hydrogen, or (ii) the application of 200°C post heat for 2–3 h. Whilst the former approach is outside the capabilities of most SAW and FCAW consumables, the latter approach has undesirable implications for, e.g., welding costs. Even the very recent European standards EN 1011-1:1998[1a] and EN 1011-2:2001[1b] do not give reliable guidance on how to assess the need of preheat for weld metal quantitatively. These standards do consider the possibility of weld metal cracking under certain conditions, however, they do not provide the user with any unified, scientifically validated methodology for the calculation of the actual level of ‘safe’ preheat temperature.

Simple, small-scale oblique *y*-groove Tekken, CTS and Implant tests are currently used for the assessment of HAZ hydrogen cracking of structural steels. The principal experiments employed for single-pass weld metals are the (symmetrical) Y-Groove Tekken test, the tensile restraint cracking (TRC) test, the gapped bead on plate (G-BOP) test and the Welding Institute of Canada (WIC) test. Applying only small-scale single-pass tests for weld metal, one cannot be convinced whether the results are really descriptive of the multiple pass welded structure. Testing full-scale products, on the other hand, indicates only the cracking susceptibility of the particular structure under certain welding conditions, but the results do not necessarily have any general relevance to other cases. Consequently, there are substantial gaps to be filled between the outcome of various cracking tests and a derivation of a unified prediction model for assessment of hydrogen cracking susceptibility in weld metal.

Of the calculation formulae predicting necessary preheat for weld metals, only few[2, 3, 12] are systematically based on experiments that actually involve multipass welding, the others being either modifications of previously existing formulae derived originally for the HAZ cracking cases[1b], or are solely based on the results of single pass cracking tests[7]. Single pass weld tests are of little assistance in the provision of

procedural guidance for multipass welds, principally because of the hydrogen retention characteristics of a much larger volume of weld metal in multipass welds, and because such factors as interpass time and -temperature are not encountered with single pass welds[8]. Therefore, suitability of data gained from single pass welding tests to reliable assessment of the hydrogen cracking risk in multipass weld metals can be questioned.

Every now and then, fabricators are still experiencing cases of hydrogen cold cracking in the welding of high strength steels and, increasingly, in the weld metal[76]. It is obvious that the status of knowledge on WM hydrogen cracking is not nearly as well advanced as that for the HAZ cracking. Even the few calculation formulae[2, 3, 11] that do exist for the assessment of hydrogen cracking risk in multipass weld metal can give greatly varying predictions, the differences in preheat temperature estimates becoming confusingly great. Presently, there is no consensus about the relevant primary parameters that should be included into such estimation procedures. For instance, different views exist on whether plate thickness should be considered, or not[2, 3, 76], and do increasing heat inputs actually result in beneficial or adverse effects with respect to WM cracking risk[8, 9, 11, 76].

Whether cracking takes place in the WM or HAZ depends on the actual chemical composition of the weld metal in relation to parent steel, as well as on the strength level in question. Generally, higher strength and greater contents of alloying elements in the weld metal tend to favour WM cracking, at the expense of HAZ cracking[40].

1.1.1 Hydrogen cracking in the HAZ

For CMn and microalloy/low-alloy high-strength steels, the heat affected zone (HAZ) cracking is generally the major form induced by hydrogen[13, 24, 25]. In practice, this covers steels with their yield strengths ranging from 350 to about 600 MPa. The most frequent types of HAZ cracks associated with common welding processes are *root crack*, *toe crack* and *underbead crack.*

Of these, underbead cracks are generally associated with shorter delay times and higher hydrogen levels than toe and root cracks, provided other factors are kept constant[41, 43]. Thus, lowering the hydrogen content effectively prevents underbead cracks in both fillet and butt welds. In multipass welding, however, underbead cracking may become a problem due to the effect of angular distortion (in the case it has not been prevented), this has been attributed to certain welding sequences[44]. As far as the HAZ cracking is concerned, the main problem in both single- and multipass welding of butt joints is usually root and/or underbead cracking. The restraint stress is highest after the first pass being laid, provided the weld is allowed to cool down to ambient temperatures[48]. The fact that the stress concentration is generally higher at the root than at the toe, further accentuates the appearance of root cracking at the expense of toe cracking[45].

The formation of HAZ underbead/root cracks is essentially governed by the transverse net stress σ_{net} across the weld and against transverse shrinkage, which, in turn, is determined by structural restraint and, to some extent, the weld metal strength. Since structural rigidity in thin plates is far too low to cause structural restraint and transverse

stresses high enough to promote cracking in the HAZ[1, 3], root and underbead cracking represent a potential risk merely in high-strength steel plates with thickness exceeding, say, 30 mm. This applies roughly to steel with yield strengths in the range of 355–460 MPa[34, 52], whereas for extra-high strength steel and with yield strengths exceeding 600 MPa, the critical thickness for the occurrence of the HAZ underbead/root cracking is lowered to 20–25 mm[52, 53]. Another application field where underbead/root cracks in the HAZ are often faced, are pipeline girth welds.

As the role of transverse stress σ_{net} is so decisive in the case of the HAZ underbead/root cracking, and the stress concentration at the root is relatively simple to model numerically and/or calculate analytically from the groove geometry, many of the current numerical methods[1b, 13] can predict safe preheat temperatures for the avoidance of cracking quite reliably.

1.1.2 Hydrogen cracking in weld metal

For extra-high strength steels of yield strength greater than 600 MPa and with weld metals of matching or overmatching strength, weld metal (WM) hydrogen cracking starts gradually to become the predominant form of hydrogen cracking[2, 3, 25]. Cracking in weld metal occurs either transverse or longitudinal to the weld direction, the orientation of cracks depending on the presence of gaps and notches and the direction of the controlling stress[3, 54]. In general, the susceptibility of weld metal to hydrogen cracking appears to increase with the strength and diffusible hydrogen of the weld metal. Consideration needs to be given to the risk of weld metal cracking, in particular, whenever making relatively thick restrained multipass butt welds[8].

In *single-pass welds*, the root gap or root bevel/face preparation provides a stress concentration with respect to stresses transverse to the weld. This leads to longitudinal hydrogen cracks in the weld metal[54], which is often the predominant form of cracking in high-strength pipelines where cracks can be encountered, not only in single-pass welds but, also, in the root run of multipass welds[26]. Many of the hydrogen-cracking tests, like the (oblique) *y*-groove Tekken test and Implant test, are designed to assess this kind of hydrogen cracking susceptibility and, often, predominantly in the HAZ instead of the weld metal.

In the case of high-strength *multipass welds* and relatively thick restrained plates, hydrogen cracking will generally occur transverse to the weld direction, growing either normal to the weld surface or at an orientation of ≈ 45° angle in the weld thickness direction. This latter morphology is called *Chevron cracking*[17b, 54]. In this form of cracking, the high longitudinal tensile stress causes slip bands to form at 45° angle in the weld thickness direction and the concentration of plastic strain in the intergranular proeutectoid grain-boundary ferrite GBF, coupled with transport of hydrogen into these regions, leads to crack initiation, c.f. *Fig. 3*. These cracks then link up by a ductile shear mechanism assisted by hydrogen[54]. Chevron cracking is often recognised in multipass submerged-arc (SAW) weld metals and, sometimes, in electroslag welds[54].

Most of the small-scale cracking tests for weld metals, e.g., the G-BOP, Y-Tekken and WIC test, are designed for single-pass welds[54]. Suitable cracking tests for multipass weld metals are sparse and not standardised within Europe. In Japan, Japanese Welding Association (JWA) has published a standard WES 1105-1985[19] entitled *"Cracking Test for Single-Bevel Groove Multi-layer Welds"*. This standard specifies a heavily restrained small-scale specimen of a size 300 x 600 mm, as well as defines quantitative crack size criterion. Despite this, different researchers and institutes, even in Japan, are still keenly devoted to different cracking test specimens and/or groove geometries. For example, Okuda et al[2] use a 500 x 400 mm U-grooved specimen, whereas Yurioka et al[3, 12] apply a symmetrically Y-grooved specimen of 300 x 300 mm size. At the TWI, U.K., an 800 x 400 mm size V-grooved specimen configuration is applied[8, 9]. Some of these experiments and applied test specimens are introduced in Chapter 1.6.

Because of the crucial role of longitudinal stress and accumulation of hydrogen – and in the absence of any groove geometry-dependent, geometrically defined stress concentration, the risk of WM transverse cracking in the filling runs is rather complicated to assess reliably either using small-scale test specimens or applying analytical calculation methods.

1.1.3 Characteristic appearance of hydrogen cracks

Fractographic examinations have revealed that hydrogen cracking is not associated with any unified micromechanism, but that cracking can occur by various modes, i.e., cleavage, quasi-cleavage, microvoid coalescence or in an intergranular manner along prior-austenite grain boundaries[42, 46, 54]. According to the microplasticity theory[50, 51], hydrogen in the lattice ahead of the crack tip assists and promotes whatever microscopic deformation and crack growth process the particular microstructure will inherently allow. The fracture mode in question will thereby depend on (i) weldment microstructure, (ii) the crack tip stress intensity level and (iii) the concentration of hydrogen[50, 51].

A characteristic feature of hydrogen cracking is that the crack propagation phase usually includes both transgranular and intergranular fracture morphologies[3, 54]. The highest susceptibility to hydrogen cracking is traditionally associated with intergranular cracking, and the lowest with microvoid coalescence, i.e., dimple formation. With increasing stress intensity, a transition from intergranular to cleavage/quasi-cleavage to microvoid coalescence occurs in the early stages of fracture[42], i.e., a transition from failure mechanisms involving negligible plasticity to those associated with high levels of plastic deformation. Investigations on fracture surfaces of cracked weld specimens have revealed[117] that the amount of crystalline area (resembling cleavage/quasi-cleavage fracture) increases with the carbon equivalent of weld metal and, hence, its strength.

Hydrogen cracks may vary in length, usually from a few microns to several mm:s[40]. Small cracks easily escape detection by normal NDT methods, such as radiography, magnetic particle inspection and ultrasonic inspection. In the case of extra-high strength steels and weld metals, microcracks of the size of a few tenths of a mm to a few mm:s may already become critical from the standpoint of structural integrity of a component[47].

Hydrogen cracks in weldments can act also as potential nuclei for later failures in manufacturing or service, e.g., by lamellar tearing, brittle fracture or fatigue.

1.2 Principal controlling factors of hydrogen induced cracking in weld metals

According to the present knowledge[2–7, 16–18, 21–23, 26, 37], the principal causal factors of weld metal hydrogen cold cracking have been identified as:

(i) sufficiently *high weld hydrogen concentration*, generally expressed in terms of weld initial diffusible hydrogen content, H_D or H_0
(ii) *susceptible microstructure*, described usually in terms of microstructural phases, GBF, M, and/or weld metal hardness HV or ultimate tensile strength R_M
(iii) *level (and tri-axiality) of weld residual tensile stress*, often assumed equivalent to the actual weld metal yield strength $R_{e(WM)}$.

It has been shown[3, 21] that hydrogen (micro)cracks appear in multipass weld metals when the weld hydrogen content exceeds a certain critical level that depends on the weld metal strength, plate/weld thickness and/or weld residual stress. These microcracks tend to locate mostly beneath the final weld bead layer, i.e., in the 2nd or 3rd last layer where weld hydrogen is likely to accumulate and remain the most[3]. These microcracks may gradually extend in length and grow further into characteristic transverse WM macrocracks[3b, 12].

The role of each factor is discussed separately in the following, with the emphasis on multipass welds, in particular.

1.2.1 Hydrogen

As the weld cools down, much of the hydrogen absorbed by the weld pool escapes from the solidified bead by diffusion. In general, the redistribution of hydrogen during cooling of the weld depends on the thermal history and hence the diffusion coefficient D(T) for hydrogen, as well as on the stress, especially, the triaxial states of stress close to notches and cracks[21, 22, 25]. In the case of transverse hydrogen cracking in multipass weld metal, the role of the latter factor becomes somewhat complicated, since there are no artificial gaps or bevelled faces inside the weld metal that could act as stress raisers.

In a certain temperature range (200–300°C) during cooling, part of the hydrogen in steel weldments looses its ability to move by diffusion. This part is called "residual hydrogen" in contrast to "diffusible hydrogen"[57]. The formation of residual hydrogen can be attributed to permanent trapping of hydrogen in sc. irreversible traps, for example voids with oxide layer on their surfaces and different chemical bonding mechanisms have been identified as sources for irreversible traps[58]. It is the diffusible hydrogen that is generally considered the predominant fraction of hydrogen in hydrogen cold-cracking of

welds[59, 60]. This has been explained by the fact that stress induced diffusion of hydrogen plays an important role in hydrogen crack initiation[61, 62], as well as by the observation that post heating even at relatively low temperatures (i.e., 100–150°C) already is effective in reducing the cracking risk[40].

It has been widely accepted[3b, 13, 24, 25, 40, 59, 63] that due to the removal of diffusible hydrogen from a weld during continuous cooling, it is not the *initial diffusible hydrogen content* H_0 according to ISO/IIW 3690[57], but the *remaining diffusible hydrogen content* at cold cracking temperatures, H_{R100}, that determines the cracking risk from the viewpoint of hydrogen factor. The choice of 100°C as a reference temperature is in agreement with hydrogen cracking temperatures[3, 24, 25]. It is known[3] that hydrogen diffusion and evolution from the weld is still quite active at around 150°C. However, the amount of decrease of diffusible hydrogen content in the bead on plate weld is found[3b] only 10–15% at temperatures below 100°C for 1 to 2 hours after welding. It is therefore reasonable to assume that the value of hydrogen content that is directly related to hydrogen cracking is satisfactorily represented by the value at 100°C[3b].

Consequently, the remaining weld diffusible hydrogen content H_{R100} that is responsible for the hydrogen cold-cracking in welds becomes always lower than the initial diffusible hydrogen H_0 absorbed by the weld pool. As far as hydrogen cracking in single-pass welds is concerned, e.g., HAZ underbead/root cracking, the description of hydrogen removal from a single bead during continuous post weld cooling applying the H_{R100} concept has been proved by the number of earlier works[3b, 13, 24, 25, 40, 59, 63]. The relationship between H_{R100} and H_0 depends essentially on the weld thermal cycle and diffusion coefficient $D(T)$ of hydrogen. A general description for the H_{R100}/H_0 ratio can be given using two alternative expressions[13, 63]:

$$(H_{R100} / H_0) = e^{(-A * \Sigma D \Delta t)} \quad (1a)$$

$$(H_{R100} / H_0) = e^{(-\beta_0 * \tau)} \quad (1b)$$

where H_{R100} is the remaining weld diffusible hydrogen content at 100°C, H_0 is the initial weld hydrogen content, $\Sigma D \Delta t$ (or τ) is a thermal factor, sc. *integrated thermal factor of hydrogen diffusion* in ferritic steel, and A and β_0 are material and geometry dependent constants, respectively[13, 22, 23, 63]. It can be seen that the H_{R100}/H_0 ratio decreases exponentially as the weld thermal content becomes greater, i.e., the weld cooling time is prolonged.

Measurements of H_{R100}, coupled with plots of the H_{R100}/H_0 ratio against the thermal diffusion factor $\Sigma D \Delta t$, have shown[69] that the slope varies with the weld metal strength, see *Fig. 1*. This was ascribed to differences in hydrogen diffusion rate as the WM composition changes. Consequently, values for constant A were derived[69] as 41, 46, 69, and 83 for R_M = 1800, 1300, 800 and 600 MPa welds, respectively. For basic electrodes, a general value of $A = 70$ has been proposed[13, 63].

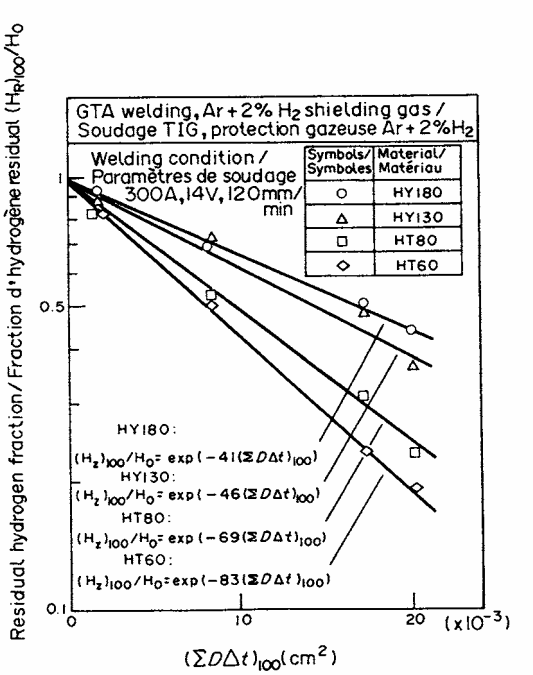

Fig. 1. Relationship between ΣDΔt and the ratio of the remaining (residual) weld diffusible hydrogen content at 100°C to the initial hydrogen content, H_{R100}/H_0, in HT60, HT80, HY130 and HY180 steels[69].

For Eq. (1), the complete weld thermal cycle is expressed in terms of *integrated thermal factor of hydrogen diffusion* ΣDΔt, or τ. The ΣDΔt incorporates the diffusion coefficient of hydrogen, D, at a certain temperature and the time interval Δt to which the D value applies. Theoretically, ΣDΔt should be determined by integrating over the complete weld thermal history, i.e., from T_m to T_i. In theoretical form, ΣDΔt can be written as[21–23]:

$$\Sigma D\Delta t = \tau = \int D(t)dt \tag{2a}$$

$$\Sigma D\Delta t = \Sigma D(\theta_j)\Delta t = \int D(\theta)\,(dt/d\theta)\,d(\theta) \tag{2b}$$

In order to avoid complex and tedious integration of time increments, and provided it is sufficient to consider the cracking conditions at a constant temperature, i.e., 100°C, the description of hydrogen diffusion over the weld thermal history from T_m to T_i can be simplified. This way, ΣDΔt can be expressed using an *approximative thermal factor of hydrogen diffusion*, $\Sigma D\Delta t_{(100)}$ that has been shown[13, 23–25] to approximate Eq. (2) comparatively well. The advantage of this simple 'engineering' factor is that for its numerical determination, only one parameter, namely, weld cooling time t is needed. Why cooling in the low temperature regime becomes important for H_{R100} stems from the fact that despite the decrease in the D values, the time available for hydrogen removal

increases considerably. This, in turn, is a direct consequence of the decaying exponential form of the post-weld cooling curve.

The use of $\Sigma D\Delta t_{(100)}$ in place of theoretical $\Sigma D\Delta t$ integrated over the complete weld thermal history is the possibility to calculate the $\Sigma D\Delta t_{(100)}$ factor within engineering accuracy directly from the recorded weld thermal history using e.g. t_{100} data. For this, three alternative empirical formulae have been proposed[13, 23, 25, 63, 77] (and validated) for calculating the estimates of $\Sigma D\Delta t_{(100)}$ on the basis of the weld cooling data:

$$\Sigma D\Delta t_{(100)} = (4.2\ t_{200} + 2.73\ t_{150} - 13) * 10^{-5} \quad (3a)$$

$$\Sigma D\Delta t_{(100)} = 6.87 * 10^{-4} * e^{[0.412\ (\log t_{100})^2 - 0.101\ (\log t_{100})]} \quad (3b)$$

$$\Sigma D\Delta t_{(100)} = \tau\ (T_R = 100°C) = (0.76\ t_{100} + 6.3\ t_{200}) * 10^{-5} \quad (3c)$$

where t_{200}, t_{150} and t_{100} are the corresponding weld cooling times from peak temperature to 200, 150 and 100°C, respectively.

The methodology based on H_{R100} being valid for single pass welds, the situation becomes more complex when multipass welds are concerned. Due to a number of repetitive thermal cycles of successive passes, part of the already solidified weld metal becomes re-melted, as welding proceeds. This re-melting of weld metal, in conjunction with the thermal effect elevating the temperature of those parts of the weld metal remaining in the solid state, cause part of the hydrogen present in the previous passes to become active again[3, 20–23]. There is good reason to believe that part of the thermodynamically stabilised residual hydrogen of the previous passes also becomes activated and may hence transform into diffusible state. Therefore, analysis of the dynamic behaviour of diffusible hydrogen in welds is even more important.

Previous work have shown[3, 20–23, 100] that in multipass welds the critical local (final) hydrogen concentration, H_{Rmax}, is governed by hydrogen diffusion and accumulation *throughout* the welding until finishing of the final layer. Therefore, H_{Rmax} in the filling runs where cracks usually locate, can differ not only from the initial weld diffusible hydrogen content H_0 according to ISO/IIW 3690[57], but also from the remaining weld diffusible hydrogen content $H_{R100max}$ according to Eq. (1) and characteristic of single pass welds.

The major practical difficulty is how to measure hydrogen distribution and a local maximum concentration in multiple-pass welds. Many attempts have been made[22,23,84,96,97] using several techniques, albeit only few have worked. Most methods are considered to fail because they are capable of measuring only hydrogen that is spontaneously evolved from welds. Since the final hydrogen distribution comprises also trapped hydrogen that is thermodynamically stabilised, forced extraction techniques are needed in order to determine a complete distribution of accumulated hydrogen[22]. Microsectioning of different weld regions at low temperature followed by hydrogen extraction[20, 22, 96, 97] and spot fusion of a weld cross section by laser beam followed by mass-spectrometric analysis of evaporated hydrogen[22, 84], are given as the most promising techniques. However, since both of these methods are technically very demanding and time consuming, they are not well suited to continual hydrogen control in production welding fabrication.

The earlier works[3, 20–22, 97, 100] have demonstrated that in multipass welding the hydrogen distribution across the weld thickness is non-uniform. Numerical FE and FD

modelling, as well as experimental techniques, in Japan reveal accordingly that the local hydrogen concentration H_{Rmax} in multipass welds increases in weldment thickness direction towards the filling runs as a result of diffusion and accumulation of hydrogen[19–23,100]. The results[20,100] demonstrate that in multiple-pass welds, H_{Rmax} reaches its maximum value at the height of 0.75–0.90 of the plate thickness (from the plate bottom), independently of the actual plate thickness, as shown in *Fig. 2a*.

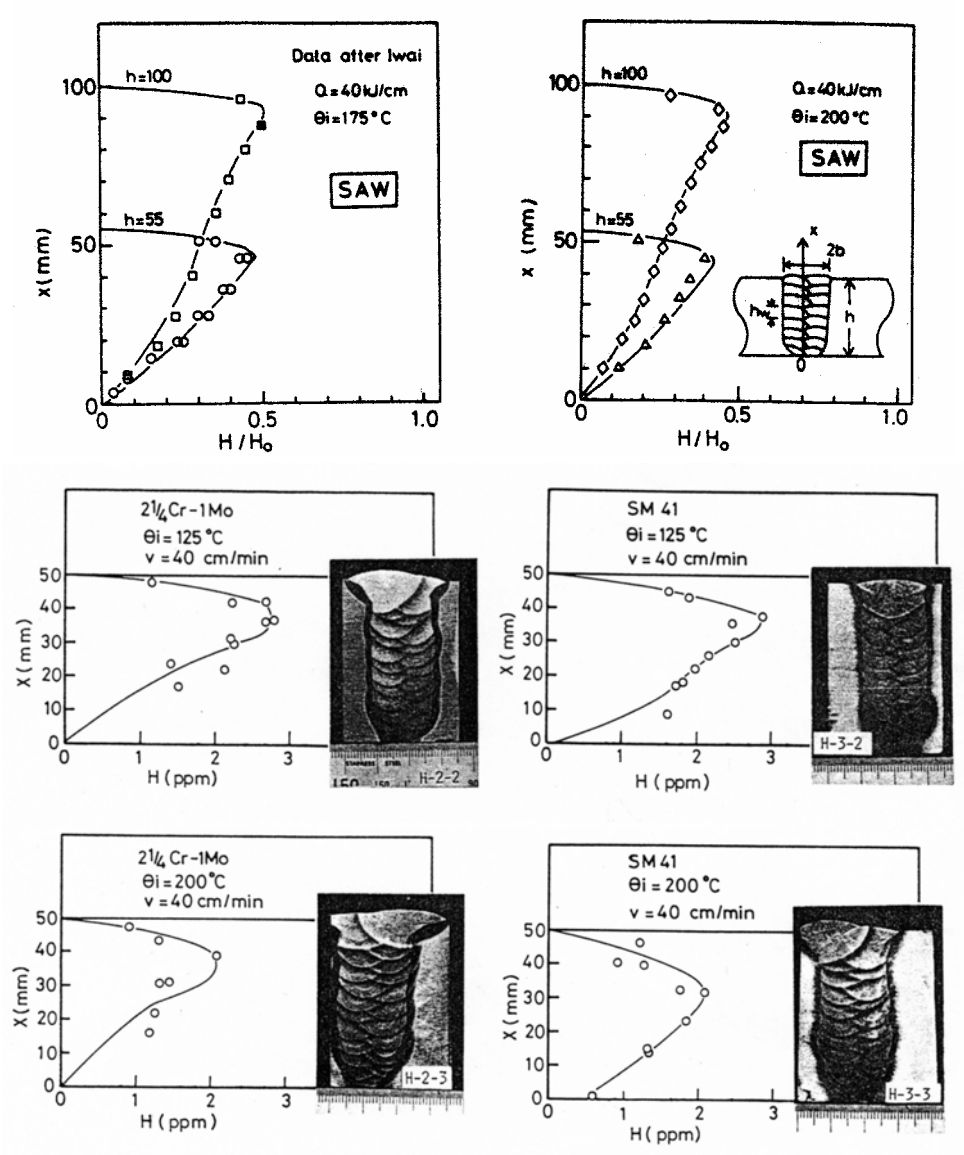

Fig. 2a. Examples of the measured/calculated hydrogen distributions in through-thickness direction of multipass weld[20].

This agrees with the findings that the crack density increases with the hydrogen concentration and towards the filling layers[76, 100, 106], as shown in *Fig. 2b*, as well as with the observation that most transverse hydrogen cracks tend to locate predominantly beneath the weld surface under the 2nd or 3rd last bead layer[3, 9, 12, 19–23, 76]. As this location also coincides with the peak value of weld longitudinal residual stress in weld thickness direction[19], it has been concluded that transverse cracking in multiple-pass weld metals actually results from the critical combination of high *local hydrogen concentration* and peak in weld *longitudinal tensile residual stress*[2,3,19,23]. Continuous hydrogen accumulation caused by repetitive weld thermal cycling and weld bead overlapping determines the *local (final) hydrogen concentration* H_{Rmax}[3, 20–22], which is the predominant hydrogen factor in hydrogen cold-cracking of multipass weld metals.

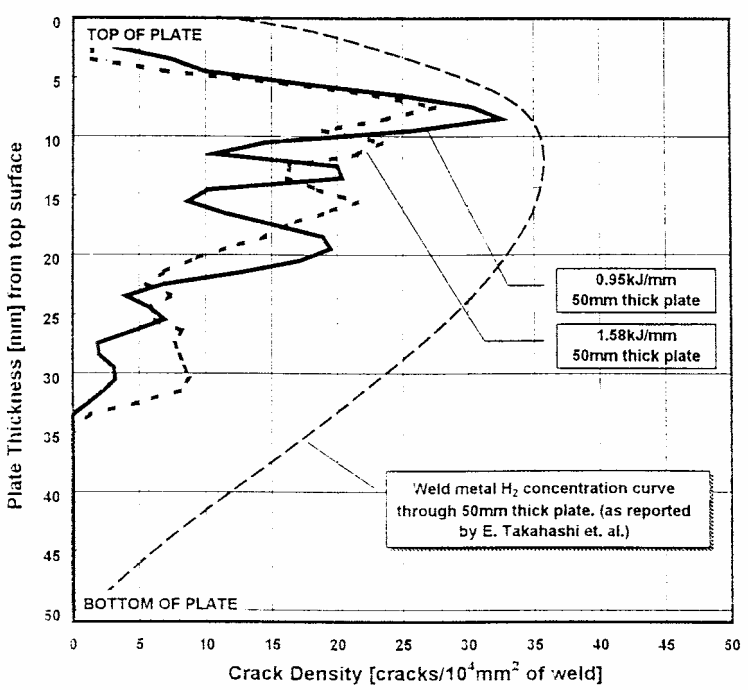

Fig. 2b. Crack distribution expressed in terms of crack density (CD) through the 50 mm thick FCAW multipass weld[76, 100].

It has been demonstrated[8, 9, 19–23] that in addition to the initial hydrogen content H_0, the local final hydrogen concentration H_{Rmax} in multipass welds depends on *complete weld thermal history*, *bead size* and *weld overlap* due to penetration of successive passes. As a consequence, the relationship between $H_{R100max}$ and H_0 that characterises the removal of hydrogen in single-pass welds and obeys Eq. (1), no longer prevails for multipass welding conditions. Factors affecting H_{Rmax} in multiple-pass welding, as well as methods for its determination, are dealt with in Section 1.5.3.

Furthermore, it has been suggested[37] that the difference in the martensite start temperature M_S between the weld metal and the parent steel HAZ influences the final

hydrogen distribution in the weldment. This, in turn, affects the hydrogen concentration and whether the cracks locate in the weld metal or in the HAZ. Since the M_S factor has both hydrogen and microstructure related characteristics, it is dealt separately with in Section 1.5.5.

1.2.2 Microstructure

Whist the general effects of hydrogen and hydrogen diffusion on weld metal cracking are relatively well established and understood, the same does not apply when it comes to the influence of WM chemical composition and microstructure[54].

In the case of the HAZ cracking, it is usually sufficient to know the maximum HAZ hardness, which is determined by the steel's chemical composition (mainly carbon) and the weld $t_{8/5}$ cooling time. Generally, the harder the microstructure, the greater the cracking susceptibility[13, 24, 25, 28–30]. For the weld metal the situation is more complicated, particularly in multipass welding. In general, the susceptibility of weld metal to hydrogen cracking appears to increase as the strength increases[2, 3, 12, 54, 74, 76, 100, 106], that is, the proportion of microstructures exhibiting greater hardenability, is increasing. Unlike for the HAZ, there is no consensus about any unified ‘critical hardness’ in the case of weld metal, although in the early works[56] one can find suggestions that WM cracking might occur when its hardness exceeds that of the HAZ. It was also claimed[54] that WM hardness has not proved to be a reliable indicator of weld metal cracking susceptibility, even though correlations do exist among WM hardness, strength and its alloy content. There exist also evidence[8, 9] that WM hydrogen cracking in multipass welds can occur in microstructures that are not essentially martensitic.

Previous experience has shown[3, 54, 55] that hydrogen cracking in multipass weld metal is often accompanied by an apparent high degree of plastic strain. Therefore, cracks tend to locate in such microstructural regions where intense plastic straining accumulates. A common feature is the presence of cracks in pro-eutectoid grain-boundary ferrite, GBF, at prior-austenite grain boundaries and solidification cell boundaries[54]. Cracking will generally occur in the filling layers and transverse to the welding direction, then growing either normal to the weld surface or at an angle orientation in the weld thickness direction. In the latter case, i.e., *Chevron cracking*, the high longitudinal tensile stress causes slip bands to form at 45° angle in the weld thickness direction. Microscopic observations have revealed[54, 98. 99] that concentration of plastic strain in the intergranular GBF, coupled with transport of hydrogen into these regions, leads to crack initiation. These staggered cracks then link up by a ductile shear mechanism assisted by hydrogen[54], see *Fig. 3*. Microcracks are seen to often grow into several directions to further link up to form transverse macrocracks[3b]. Apart from linking microcracks, sometimes parts of the crack do not link, but form a "staircase" pattern.

Examinations on WM crack locations had revealed[3b] that transverse cracks in multipass welds tend to appear in the as-welded dendritic microstructures, i.e., in the regions that remained unaffected by the reheat of the following passes and therefore usually contain proeutectoid GBF ferrite. Those parts of the Chevron crack locating in

the GBF have been found[54] to often show quasi-cleavage fracture surface, whilst cracks in other regions exhibit more ductile fracture appearance. Both intergranular and transgranular cracking modes have been recognised, the former usually running through the GBF phase[54]. Initiation of cracking in the as-deposited microstructures was clearly associated with the GBF, the internal microstructure being apparently of secondary importance[70]. Likewise, another study[121] reports that cracks appeared to be initiated essentially from the weld metal areas having columnar grain structure and composed of grain boundaries decorated with GBF, whilst equiaxed (reheated) grains provided better resistance to cracking. In reheated WM regions, the crack appears to have formed first, then widened as a result of re-heating due to successive passes[54]. A proposed[54, 98, 99] mechanism of Chevron crack formation in multipass welds is shown in *Fig. 3*.

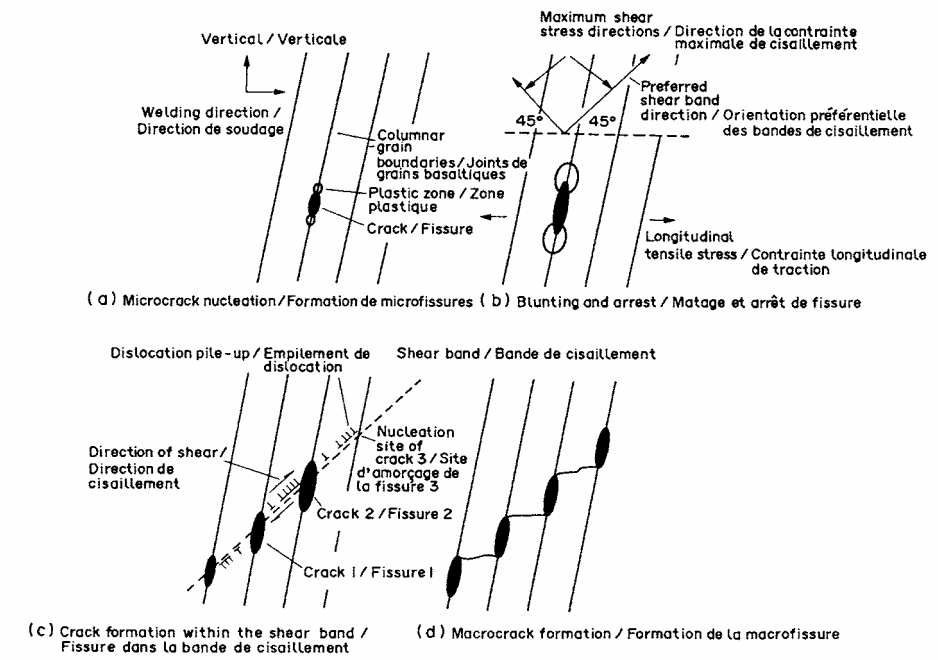

Fig. 3. Proposed mechanism of Chevron crack formation associated with dislocation shear bands: (a) microcrack nucleation, (b) blunting and arrest, (c) crack formation within the shear band, (d) macrocrack formation[54, 98, 99].

The harmful role of GBF phase is supported also by the recent findings[16–18] demonstrating a positive correlation between the volume fraction of GBF and WM hydrogen cracking susceptibility. The results implied that the cracking sensitivity of multipass WMs may, at low hydrogen levels less than 4.5 ml/100 g DM (IIW), essentially depend on the weld metal microstructure, particularly, the volume fraction of GBF. At high hydrogen contents the conditions seem to change, so that the hardness and tensile strength of weld metal will become increasingly important in controlling the hydrogen cracking behaviour[16–18].

With extra-high strength weld metals of $R_{p0.2} \geq 690$ MPa, hydrogen cracks have been observed, accordingly, within regions of intense plastic strain[54, 55]. Instead of GBF, cracking appeared at isolated locations in the weld metal and along slip bands parallel to laths of martensite, M, as well as along slip bands across M laths[55]. Microscopy (SEM) revealed fracture surface described as quasi-cleavage mode with several tiny shallow dimples. The later stages of crack growth showed wavy slip bands, again characteristic of intense plastic strain, and dimpled fracture surfaces. It was believed that the absence of intergranular cracking in this case can be explained by the very low weld metal oxygen level[54, 55], which is a characteristic feature of extra-high strength weld metals. Thus, cracking was usually transgranular and only occurred along solidification cell boundaries when cells were oriented normal to the strain. These were considered as initiation sites. When cells were at an angle to the strain, a mixed mode fracture along and across cells was observed.

In addition to weld metal strength, microphases and inclusion structure have been reported[21, 22] to have importance in determining the sensitivity of WM to hydrogen cracking. Microphases and inclusions affect the diffusion rate of hydrogen, available trapping sites, crack initiation conditions, all of which are considered as controlling factors in terms of WM cracking. As the morphology of inclusions affects the hydrogen diffusivity and trapping, it follows, for instance, that different types of weld metals can, in principle, possess different responses to cracking, even though they would exhibit relatively similar strength and hydrogen content[8, 9, 16–18].

It is known[54] that weld metal chemical composition has an effect also on the level of residual (retained) hydrogen. This could account in part for the higher susceptibility of higher strength weld metals to hydrogen cold-cracking[54], especially in multipass welding where part of retained hydrogen may become re-activated by the thermal effects of successive welding runs.

The attempts on defining the effects of specific alloying elements on WM cracking susceptibility have not been very revealing and do exist mainly for single-pass welds. A study[64] based on G-BOP tests reports, Nb levels of 0.06% in the weld metal increased the crack susceptibility significantly, whereas V (0.05%), Mo (0.2%) and Ni (1.2%) had minimal effect, and Mn appeared to have a mildly beneficial effect. The crack susceptibility was not related to the hardness and the effects of these alloying elements could not be characterised by any existing carbon equivalent formula[64].

Reported findings on the relationship between WM hardness and its hydrogen cracking susceptibility are somewhat conflicting and inconsistent. In terms of Implant rupture stress and at a given level of hydrogen, the susceptibility of WM to hydrogen cracking was found[71] to increase linearly with the hardness. As a general trend, this is consistent also with the findings made elsewhere[2, 3], although results of the Implant test are likely to apply to reheated weld metal, as the notch of the specimen inevitably locates there. With regard to hydrogen embrittlement, the reheated weld metal has been claimed[70] to behave in a similar manner to the parent steel HAZ. Indeed, an early study[56] has already suggested that WM cracking might occur when its hardness exceeds that of the HAZ. This, however, contrasts with the later findings[6, 7] demonstrating that in multipass welds with a low carbon content of 0.06%, the ‘critical hardness’ above which cracking tended to occur actually was different in the case of the weld metal and the HAZ. Whilst approximately 300 HV was found[6, 7] ‘safe’ for the HAZ according to the *y*-

groove Tekken test, cracking in the corresponding FCAW weld metals occurred, under similar welding conditions, at hardness levels of around 250–280 HV. Similar findings have been reported in another study[8] on SAW weldments revealing transverse hydrogen cracks in the weld metals of hardness no more than about 200 HV. A recent study[121] concluded that cracking in extra high-strength HSLA-100 welds was controlled by the weld overall strength and the local variation of WM microstructure, but was little affected by the microhardness variation.

As a consequence, the relationship between WM chemical composition, microstructure and cracking susceptibility seems to be less straightforward than for the HAZ. It is not only the hardness, but also the expression for the integrated hydrogen diffusion parameter-hydrogen dependence, i.e., $\beta\tau + \log H_D$, or, $H_{R100}/H_0 = f(\Sigma D \Delta t)$, that is found[72] to be a function of weld chemical composition. Whereas some studies have shown reasonable fits using the conventional IIW carbon equivalent formula CE_{IIW}[72], others seem to rely more on the P_{cm} formula[54]. Furthermore, WM hardness and microstructure are both influenced also by the number and nature of e.g. non-metallic inclusions that are not accounted for in any common carbon equivalent formula.

From the standpoint of prediction method, it hence appears essential to investigate to which extent hardness and strength are sufficient factors to describe the weld metal cracking sensitivity. Any predictive system will become complicated once it has to consider microstructural factors, such as weld metal oxygen and impurity content, inclusion morphology, volume fraction of GBF and/or retained austenite / M-A constituent.

1.2.3 Stresses

Stresses produced during the welding fabrication are either (i) residual welding stresses due to internal restraint or (ii) reaction stresses caused by external restraint[65]. Of these, the residual stresses are a result of the non-uniform temperature distribution. These stresses are in a short range equilibrium in the vicinity of the weld. Reaction stresses, in turn, are a consequence of the clamping effect, i.e., other structural members somehow prevent the free thermal shrinkage[65]. These long range stresses are deleterious in that the net stress is not reduced with cracking. Hydrogen cracking in welds is generally associated with residual welding stresses[68].

Phase transformations have shown a remarkable beneficial effect on residual and/or reaction stress development when the γ to α volume change is large and the γ–α phase transformation takes place at a comparatively low temperature[66]. This stress reducing effect, prominent in single-pass welding, is considered to attenuate in multipass welding due to the repetitive thermal cycles, consequently the effect would prevail only when welding the final weld run[67a].

Experience has shown[65], in single-pass welds the residual stresses play only a secondary role in hydrogen cracking of butt joints, whilst the reaction stresses predominate the risk of cracking. This does not, however, apply to multipass welds where

the residual and reaction stresses form a complicated system whose accurate solutions usually require thermal elastoplastic FEM analyses.

The effect of the geometry of a structural detail on residual stress (actually, reaction stress) development in butt welds under (external) restraint is described[66, 73] using a parameter named "restraint intensity", R_F. It is simply defined as the force per unit of weld length caused by the elastic change of a unit in root gap, uniform along a butt weld joint. In practice, R_F increases with the plate thickness h. Predominant stress component for hydrogen cold cracking is the one perpendicular to the crack orientation[2, 3]. In the case of HAZ underbead root cracking, what counts is the transverse net stress, σ_{net}, across the weld throat[13, 25, 63]. In the weld root these stresses can reach the critical level and finally, as plate thickness and hence restraint intensity, R_F, increase, even the level of the weld metal yield strength, $R_{e(WM)}$[13].

Whereas the transverse stresses are of decisive importance for the HAZ underbead/root cracking in butt welds, the situation with regard to the cracking in filling runs of multipass welds is just the reverse. Transverse hydrogen cold cracking in multipass WMs is essentially controlled by the longitudinal tensile residual stress in the welding direction, σ_{resL}, which is intensified in the presence of transverse notches or imperfections, such as an unspliced backing bar or a gap[54]. Unlike longitudinal hydrogen cracks, transverse cracks have been found to locate predominantly below the final weld layer[76, 100] or in the 2nd or 3rd last weld layer[3, 12], i.e., in the filling runs in the area where both longitudinal residual stress and hydrogen accumulation will concentrate the most[2, 3, 12, 19, 74, 76, 100].

A characteristic finding with respect to multipass welds is that the longitudinal tensile stress, while first remaining at a comparatively low level in the weld root, increases soon towards the filling layers and reaches its maximum, i.e., the true yield strength of weld metal[19, 23, 67b]. This can occur already after some 2 to 3 bead layers have been deposited, irrespective of the value of R_F[19, 23]. Any further increase in plate thickness therefore does not increase the level of weld longitudinal tensile stress in the filling runs anymore[19], as shown in *Fig. 4*.

As a result, intensity of restraint R_F due to structural rigidity is considered[19, 23] to contribute to the multipass WM cracking susceptibility to a lesser extent than is the case with HAZ root/underbead cracking. As far as heavy plates are concerned, the longitudinal residual stress in the filling layers of multipass weldment are expected practically equivalent to the weld metal true yield strength, provided the weld is long enough – preferably 300–500 mm or more[19, 23, 67b].

Apart from this, however, structural rigidity may influence the precise location of the cracks. There are indications[19, 20, 74] that hydrogen cracks in highly rigid structures and thick multipass welds may appear already in the mid-thickness of the weldment, whereas in small-scale tests[3, 12] they generally tend to locate under the 2nd–3rd latest filling bead layer closer to the weld surface.

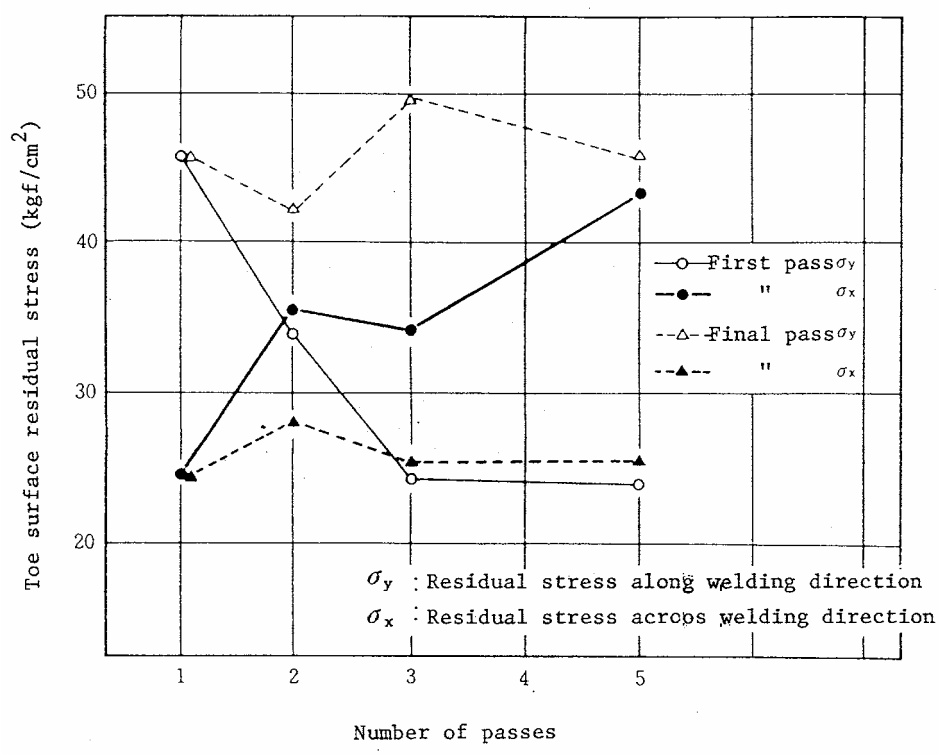

Fig. 4. Effect of number of welding passes on residual stresses in the toe of multipass weld[19].

It has been shown[23] that the critical hydrogen content H_{cr} for the occurrence of weld metal cracking decreases exponentially as the weld longitudinal residual tensile stress σ_{resL} elevates. This dependence obeys a decaying exponential function of a general form[23]:

$$H_{cr} = A * 10^{(-B * \sigma_{resL})} \quad (4)$$

where: A and B are constants.

As a consequence of Eq. (4), the use of higher strength weld metals yields a drastic decrease in the critical hydrogen content capable of causing cracks. The increase in the risk of WM hydrogen cracking with strength is thereby a result of (i) crack sensitive microstructure, in conjunction with (ii) remarkably elevated stress state. This is in agreement with the previous experimental findings[3, 12] that have documented transverse hydrogen cracks in weld metals with no more than ≈ 4 ml/100 g DM (IIW) diffusible hydrogen in the cases where WM yield strengths were around 700 MPa or more.

The means to overcome the greater cracking risk in high-strength weld metals may differ between root pass and filling layer welding in the sense how to relax the stress rise via consumable selection. When welding root runs, it is often acceptable to use filler metals of undermatching strength, which results in desired reduction of the welding residual stress in the highly stressed root area[13, 24, 25]. In contrast to root runs, however,

the use of filler metals producing undermatching weld metal strength is often unacceptable for filling runs and surface layers.

Besides on weld metal strength, the longitudinal residual stresses have been found[74] to depend on the applied interpass temperature T_i during welding. In a previous work, residual stress measurements with strain gauge method revealed that while the tensile residual stresses reached the level of the WM yield strength under low T_i conditions (< 50°C), increasing T_i (> 120°C) was accompanied by a reduction of σ_{resL} so that the residual stresses remained less, about 75–85% of the WM yield strength[74].

The role of residual stress development and stress concentration aspects in multipass welds from the design viewpoint are dealt with in more detail in Section 1.5.1.

1.2.4 Welding process

The results of single-pass cracking tests, such as the G-BOP test, generally demonstrate[54, 72] that hydrogen cracking susceptibility is independent of welding process. This is usually the case when for example plots of diffusion integrated parameter, e.g., $\beta\tau$, against simple composition-hydrogen formulae of the form: $A\ (CE_{IIW}) + B\ (\log H_F)$ are made[72].

In the case of multipass weld cracking tests, the findings are not always as consistent. There exist evidence[8, 9] that, other factors being equivalent, hydrogen cracking risk can be greater for submerged-arc (SAW) weld metals than for shielded metal arc (SMAW) or flux-cored arc (FCAW) welds. This has been attributed[8, 9, 19–21] to differences in bead shape and size which, in turn, affect the hydrogen diffusion distances and, finally, the local hydrogen concentration H_{Rmax}. Even with equivalent levels of heat input, different welding methods tend to yield weld beads of different geometrical shape and size[8, 9]. Typically, SAW is known to produce comparatively narrow weld beads with high depth-to-width ratio[8, 32, 33], whilst beads with less penetration and wider shape are characteristic of FCAW[9].

The bead shape and size effects, especially from the standpoint of weld local hydrogen concentration, are dealt with in more detail in Sections 1.5.2 and 1.5.3. The effects of heat input on weld hydrogen content are discussed in Section 1.5.6.

1.3 Mechanisms of hydrogen induced and assisted cracking

Unlike many other damage mechanisms, such as e.g. creep failure at high temperatures, or brittle cleavage fracture at low temperatures, hydrogen cracking is not associated with any unified micromechanism[24, 25, 36, 42, 46, 50, 51, 54]. Besides in terms of fracture micromechanisms, the initiation and propagation events of hydrogen cracking can be investigated and elucidated via observations on those microscale processes that emerge at the crack tip and fracture process zone under the presence of hydrogen concentration. This approach puts the focus on surface effects, as well as on the hydrogen-dislocation

interactions. Some of these mechanisms are common to both hydrogen-induced and hydrogen-assisted cracking. According to this classification[75], the following three mechanisms are generally defined: (i) *hydrogen enhanced decohesion* (HEDE), (ii) *hydrogen enhanced localised plasticity* (HELP) and (iii) *adsorption induced dislocation emission* (AIDE).

All these processes involve a complex combination of a number of events: (i) hydrogen dissociation, adsorption and transport to the crack tip, (ii) dislocation emission and egress, (iii) hydrogen diffusion and movement of vacancies, (iv) transport of hydrogen to dislocations, (v) hydrogen effects on dislocation mobility and hydrogen trapping at particle-matrix interfaces[75]. Thus, controversies regarding the features how to distinguish between these three mechanisms, are not surprising. It has been postulated[75] that the appearance of a certain mechanism may depend also on the operating temperature in such a way that AIDE and HEDE mechanisms would dominate at lower temperatures, whereas HELP occurs predominantly at higher temperatures.

1.3.1 Hydrogen enhanced decohesion

Classical *hydrogen enhanced decohesion* (HEDE) was first discovered by Troiano in the 1960's, then subsequently re-discovered by Oriani in the 1970's and Gerberich et al. in the 1980's. This mechanism involves weakening of the interatomic bonds in the atomically sharp crack tip and the surrounding process zone as a consequence of absorbed hydrogen[75]. Decreases in electron charge density between metal atoms occurs due to (i) absorbed hydrogen at the atomically sharp crack tip, followed by diffusion and presence of hydrogen in (ii) interstitial sites and (iii) at the particle-matrix interfaces. These phenomena then result in final decohesion in terms of tensile separation of atoms[75].

Unlike the other two mechanisms, hydrogen enhanced decohesion (HEDE) is characterised by limited dislocation activity[75]. In the cases where HEDE predominates, fractographic investigation can reveal atomically flat fracture surfaces, which is considered a demonstration of negligible plasticity involved in this mechanism. These findings are consistent with the observations that HEDE is generally the predominant mechanism for *brittle-like intergranular fracture*[75].

Earlier work[7, 34] on hydrogen cracking in weldments demonstrates that intergranular fracture becomes a predominant form as the weld diffusible hydrogen content increases and/or segregation of impurities into prior-austenite grain boundaries is intensified. The latter occurs typically when welding conventional steel using comparatively high heat inputs. Accordingly, proportion of intergranular fracture is found[39] to diminish at the expense of transgranular fracture in the case of modern, low-impurity steels and weld metals.

1.3.2 Hydrogen enhanced localised plasticity

Hydrogen enhanced localised plasticity (HELP) was first introduced by Beachem in 1972 and re-introduced by Birnbaum et al. in the 1980's. This mechanism is characterised by a decrease in repulsive interactions between dislocations and obstacles due to reconfiguration of their hydrogen atmospheres. Hydrogen accumulates and concentrates around the voids over a certain volume ahead of the crack tip. As hydrogen concentration becomes highly localised, so is also the case with plasticity. This mechanism only operates in certain temperature and strain rate regime where hydrogen atmospheres can keep up with dislocations[75].

Direct evidence for HELP being a characteristic embrittlement mechanism has been reported[75], for example, from in-situ TEM observations. When fracture appearances in thin foils strained in a vacuum have been compared to those strained in hydrogen atmosphere, the presence of hydrogen was found to result in an increase in dislocation activity and facilitate fracture by localised shear mechanism. Localised microvoid coalescence coupled with enhanced dislocation activity in terms of extensive slip on planes intersecting cracks have been observed[75] directly by TEM when examining thin foils.

A distinct difference between HEDE and HELP is therefore the increased *dislocation activity* in the latter mechanism. Another difference is the *amount of plasticity involved* in the fracture process; whilst atomically flat fracture surfaces were associate with HEDE, observations of dimpled fracture surfaces in the regions of highly localised strains have been reported in the case of HELP. The latter findings are regarded as characteristic of ductile crack growth under the presence of substantial external stress which then transfers to internal localised strain. Owing to its nature, HELP is considered to contribute especially to *slip-band (induced) fractures* and hence promote fracture by *localised microvoid coalescence*[75].

Earlier work[6, 7, 53] has demonstrated that especially Implant specimens extracted from the weld metals can exhibit substantial plasticity in the hydrogen-induced fracture process. This usually manifests itself as a ductile fracture surface with large plastically deformed areas despite the presence of hydrogen, which totally contrasts to the typical brittle fracture surface characteristic to the hydrogen embrittled HAZ Implant specimens.

1.3.3 Adsorption induced dislocation emission

Adsorption induced dislocation emission (AIDE) has been proposed by Lynch at 1977. This mechanism encompasses similarities to both HEDE and HELP and hence incorporates some features from already existing theories and models.

In accordance with HEDE, the mechanism involves *weakening of the interatomic bonds* at the crack tip as a result of absorbed hydrogen. Crack surfaces (and sub-surfaces) are recognised to act as strong trapping sites for hydrogen. The presence of hydrogen at these surfaces leads to weakening of interatomic bonds (presumably metal-metal bonds, while the hydrogen-metal bonds are inherently weak) at crack tips, which further

enhances emission of dislocations. *Dislocation emission*, in turn, promotes and facilitates linking of cracks with voids ahead of the cracks and over a characteristic distance, Δa. This linking is recognised to occur along some low-index planes or grain boundaries, leaving shallow dimples on fracture surfaces as the fracture propagates further[75].

The decisive role of *dislocation emission* in the AIDE mechanism is, in turn, similar to HELP, except that strains can be even more localised than those for microvoid coalescence associated with HELP. As evidence supporting AIDE and the dislocation emission theory, this mechanism has been recognised[75] also under conditions where there was no time for any significant hydrogen diffusion ahead of cracks. Thus, it is not a prerequisite of AIDE for hydrogen atmospheres to keep up with dislocations, such as was the case with HELP[75].

In general, dislocations emit from the plastic zone ahead of the cracks, egressing at crack-tip surfaces. The influence of embrittling environment, such as absorbed hydrogen, is seen[75] particularly in that dislocations tend to emit predominantly from crack tips, which then results in crack advance and crack opening. Consequently, increasing proportion of dislocation emission from the crack tips manifests itself as greater crack growth Δa for a given crack opening displacement, i.e., COD. Accordingly, the strains required for fracture should lessen due to the embrittling effect of absorbed hydrogen at the crack tip. It has been reported[75] that in the case of cleavage or quasi-cleavage fracture, cracking occurs on {100} planes in <110> directions. This suggests that slip on planes intersecting the crack tips plays a critical role in the AIDE mechanism.

The characteristic features of AIDE that can be identified using electron microscopy are considered[75] as: (i) dimpled fracture surfaces due to high localised strains, (ii) extensive slip on planes intersecting cracks, and (iii) formation of localised microvoid coalescence coupled with intensified dislocation activity. In comparison to HEDE or HELP, the importance of crack surface effects in hydrogen cracking is regarded[75] more pronounced in AIDE and is, hence, given more attention. The findings supporting the role of surface effects in AIDE are given[75] as: (i) a high hydrogen concentration on and just beneath the crack tip surface, (ii) substantial effect of hydrogen adsorption on atomic bonding, (iii) cracking at very high velocities and (iv) abrupt ductile-to-brittle transitions on e.g. changing of temperature[75].

Owing to its complex nature, AIDE seems capable of contributing to *cleavage like fracture*, as well as to *dimple formation* associated with *ductile fracture*.

According to AIDE, degree of hydrogen embrittlement should increase with (i) increasing surface coverage of hydrogen on crack surfaces, (ii) increasing filling of sub-surface sites with hydrogen and (iii) increase in hydrogen absorption at internal crack or void tips[75]. Quantitative predictions are often problematic, because for instance the difficulties in modelling dislocation-emission process.

1.4 Hydrogen diffusion and its role in cracking of multiple-pass weld metals

Earlier work[2, 3, 21–23] have shown that hydrogen cold cracking in multiple-pass weld metals occurs when accumulating hydrogen exceeds a certain critical level, H_{cr}. This hydrogen accumulation via diffusion is thermally activated, continuing process that takes place throughout the welding until finishing of the final bead. For the analysis of the dynamic behaviour of diffusible hydrogen, diffusion needs to be described in terms of the *mass diffusion equation*, with the introduction of the *activity coefficient of the diffusing mass* into the diffusion equation[21, 22]. This enables diffusion and accumulation of hydrogen to be determined under conditions where the properties of the diffusion medium vary locally and under defined distributions of stresses and strains.

Diffusion of mass in a uniform medium is governed by the Fick's second law that relates the rate of composition with time to the concentration profile. A steel weld cannot, however, be regarded as uniform medium for hydrogen diffusion, since the weldment consists of regions composed of quite different microstructures. Whereas the HAZ of ferritic steel comprises mostly hardened, bainitic-martensitic transformation products with relatively high dislocation density, weld and base metals are often less hardened in nature, consisting of bainitic or ferritic microstructures[22]. Besides dislocation density, the number and morphology of inclusions and microphases acting as traps for diffusible hydrogen, are also different among the HAZ and weld metal[21, 22]. Hence, hydrogen diffusion is influenced by the diffusive media of a non-uniform nature, where hydrogen diffusion due to temperature dominates over mass diffusion[79].

A weld root with an acute notch is subjected to triaxial stresses (in the as-welded condition) that also cause lattice expansion. Hydrogen diffusion in welds is therefore not only affected by the gradient of microstructures and dislocation densities, but also the fields of stress and strain in the weld[22]. As, for instance, plastic strain and microstructure influence the diffusion coefficient of hydrogen, these interactions need to be evaluated[21, 22].

The equations for the analysis of dynamic behaviour of hydrogen in multipass welds are given.

1.4.1 General equation for the diffusion of mass

The diffusion of mass in a uniform medium is governed by the Fick's second law[22, 78] that relates the rate of composition with time to the concentration profile $c(x)$, as:

$$(\partial c/\partial t) = D(\partial^2 c/\partial x^2) = D\,\nabla^2 c \qquad (5)$$

where c is the concentration of the diffusing mass, t is the time and D is the diffusion coefficient.

Hydrogen diffusion in steel welds has been analytically solved mainly using Eq. (5) under the given initial condition and boundary conditions[22]. For these analyses, hydrogen diffusion in a butt and fillet weld is often approximated with diffusion in an infinite plate and an infinite cylindrical rod, respectively[40].

The general equation of *mass diffusion* in a heterogeneous medium is defined[21, 22] as:

$$(\partial c / \partial t) = -\nabla J \tag{6}$$

where c is the concentration of the diffusing mass, t is time and J is the *mass flux*. The flux of the diffusing mass J can further be defined in terms of a *chemical potential of diffusing mass* μ, as[21, 22]:

$$J = -[D * c /(RT)] \nabla \mu \tag{7}$$

where D, R and T are the diffusion coefficient, gas constant and the absolute temperature, respectively. The *chemical potential* μ applied in thermodynamics is defined as[21, 78]:

$$\mu = [\partial G' / (\partial n)] = G_0 + RT \ln(x) = \mu_0 + RT \ln (a) \tag{8}$$

$$a = \gamma c \tag{9}$$

where G' is the Gibbs free energy in a system, dn is the change in the quantity of atoms of a substance in a system, a is the activity of a diffusing mass, γ is the activity coefficient of the mass, and c is the concentration of the diffusing mass.

Combining Eqs (6), (7), (8) and (9), the general equation of *mass diffusion* becomes[21]:

$$(\partial c / \partial t) = \nabla * \{[(D / \gamma) \nabla (\gamma c)] + [(Dc / T) (\ln (\gamma c)) \nabla T]\} \tag{10}$$

In a welded joint at its cooling stage, mass transfer at a certain local point is assessed at a certain moment of time. Thus, the change in temperature over an increment of time can be considered very small in relation to the absolute temperature. Under these conditions, it can be assumed that the temperature gradient is very small, i.e., $\nabla T \approx 0$). This approximation allows for Eq. (10) to be simplified even further, as[21]:

$$(\partial c / \partial t) = \nabla * [(D / \gamma) \nabla (\gamma c)] \tag{11a}$$

or, alternatively, as[21]:

$$(\partial c / \partial t) = \nabla * (D \nabla c) + \nabla * [(Dc / \gamma) \nabla \gamma] \tag{11b}$$

If it is assumed that the diffusion coefficient D and the generalised activity coefficient γ are independent of the location, as is the case with a homogeneous diffusion medium, it follows[22] that: $\nabla D = 0$ and $\nabla \gamma = 0$. Considering these, and rewriting Eq. (11a) in terms of the activity of the diffusing mass a according to Eq. (9), leads to the following form[21]:

$$(\partial a / \partial t) = (a / \gamma) * (\partial \gamma / \partial t) + \gamma \nabla * [(D / \gamma) \nabla a] \tag{12}$$

At a certain moment of time t, any change in the temperature T leads to corresponding change in the concentration of the diffusing mass c and, hence, also its activity a. Assuming, however, that the activity coefficient γ is itself independent of time t, it follows that: $\partial \gamma / \partial t = 0$. Consequently, Eq. (12) reduces simply into the following form[21]:

$$(\partial a / \partial t) = \gamma \nabla * [(D / \gamma) \nabla a] \tag{13}$$

This equation expresses the mass diffusion in a system in terms of the *activity gradient* of the diffusing mass ∇a, in conjunction with the *activity coefficient* of the mass γ and the *diffusion coefficient* D. Of these, the diffusion and activity coefficients are strongly dependent on the temperature, and microstructure & stress, respectively, as discussed later in Section 1.4.3.

1.4.2 Effects of temperature and continuity conditions

Unlike general diffusion, hydrogen diffusion is influenced by the diffusive media of a non-uniform nature[79]. Therefore, Fick's second law in the form of Eq. (5) cannot satisfactorily describe hydrogen diffusion in welds. Owing to its chemical nature, hydrogen diffusion due to the abrupt temperature changes clearly dominates over mass diffusion[79]. Consequently, the local accumulation of hydrogen and delayed phenomena cannot be solved satisfactorily by conducting an analysis of hydrogen diffusion in a homogeneous medium in accordance with Eq. (5)[22].

On this basis, Eq. (5) can be modified to account for the effect of temperature T on the diffusion of hydrogen. Thereby, we obtain[79]:

$$(\partial T / \partial t) = \kappa (\partial^2 T / \partial x^2) \tag{14}$$

$$\kappa = \lambda / \rho C \tag{15}$$

where κ is the thermal diffusion coefficient, λ is thermal conductivity and ρC is the volume of specific heat of the material. For calculations, values of 0.14 (cm^2/sec), 0.12 (cal/cm sec°C), 8.0 (g/cm^3) and 0.10 (cal/g) have been proposed[79] for κ, λ, ρ and C, respectively.

Combining Eqs (14) and (15), the general equation of *diffusion due to temperature* becomes:

$$\rho C (\partial T / \partial t) = \lambda (\partial^2 T / \partial x^2) \tag{16}$$

In practice, it is particularly the gradient of potential μ that governs the diffusion of hydrogen at any medium[79]. The total chemical composition in a system remains always the same, only the temperature T and the local concentrations c_i do change[79]. Thus, the continuity condition over the A–B boundary between the two separate concentrations, c_1 and c_2, can be expressed in terms of the chemical potential of hydrogen μ, as[79]:

$$\mu_A = \mu_B \Rightarrow \mu_0 + RT \ln (\gamma_\alpha c_1) = \mu_0 + RT \ln (\gamma_\beta c_2) \tag{17a}$$

It thereby follows that:

$$\gamma_\alpha c_1 = \gamma_\beta c_2 \Rightarrow \gamma_\alpha = (c_2 / c_1) \gamma_\beta \Rightarrow \gamma_\beta = (c_1 / c_2) \gamma_\alpha \tag{17b}$$

If one now assumes that for example atom B is very active in solid α, which applies e.g., to hydrogen diffused in solid α iron, the activity coefficient of diluted solute can be much higher than unity. The gradient of its chemical potential, $\nabla\mu$, c.f. Eq. (7), thereby essentially determines the mass diffusion of hydrogen.

1.4.3 Activity coefficient of the diffusing mass

The flux of the mass J that diffuses in any system under the conditions of locally varying pressure P and chemical potential μ', can be expressed, in accordance with Eq. (7), as[21]:

$$J = -[D * c / (RT)] \nabla (-PV^* + \mu') \quad (18)$$

where V^* is the partial molar volume of the diffusing mass (i.e., hydrogen), and P is the hydrostatic pressure considered as a mean of negative stresses in the triaxial directions in solids, as[22]:

$$P = -(\sigma_x + \sigma_y + \sigma_z) / 3 \quad (19)$$

The *chemical potential* μ that is normally applied in thermodynamics[78], is given by Eqs (8) and (9) and can be re-written as:

$$\mu = \mu_0 + RT \ln (a) = \mu_0 + RT \ln (\gamma_m c) \quad (20)$$

where γ_m is the activity coefficient determined by the type of a given microstructure and the amount of plastic strain[22].

Comparing Eqs (7) and (18) gives the following relation that incorporates the effects of locally varying pressure and chemical potential into the flux of the diffusing mass. This relation is defined[22, 80] by introducing a new term: the *generalised potential of diffusing mass*, Φ, being:

$$\Phi = PV^* + \mu \quad (21)$$

Combining Eqs (20) and (21), the equation for the generalised potential Φ becomes:

$$\Phi = \mu_0 + RT \ln (\gamma_m c) + PV^* = \mu_0 + RT \ln (\gamma_m c) + RT \ln [\exp(PV^* / RT)] \quad (22a)$$

Let us now set the last term of Eq. (22a) as:

$$\exp (PV^* / RT) = \gamma_P \quad (22b)$$

Consequently, re-combining Eqs (22a) and (22b), the final equation of the generalised potential Φ can be expressed as[22]:

$$\Phi = \mu_0 + RT \ln (\gamma_m * \gamma_P * c) \quad (23)$$

Comparing Eqs (23) and (20), the activity coefficient can be written in the form of a *generalised activity coefficient* γ of the diffusing mass defined as[22]:

$$\gamma = \gamma_m * \gamma_P \quad (24)$$

where γ_m and γ_P are the *interactive activity coefficients* due to microstructure (and plastic strain) and stress, respectively[21, 22], c.f., Section 1.4.6.

When the activity coefficient γ in a system is locally decreasing, the potential or activity of the diffusing mass, a, becomes also reduced[22] in accordance with Eq. (9). As a consequence, a kind of potential difference, or "well", is formed. The diffusing mass thereby diffuses gradually into this potential well, resulting in local accumulation of the mass[22]. The triaxial stress effect[81, 82], c.f. Eqs (19) and (21) further enhances the accumulation of hydrogen.

1.4.4 Potential of hydrogen in structural steel weld metal

The activity coefficient γ and the diffusion coefficient D of hydrogen are both expected to vary sharply in welds, as the microstructures of the HAZ and the weld metal experience abrupt changes due to the temperature changes caused by successive thermal cycles[21, 22]. In addition, the stresses and plastic strains will vary greatly, especially near those weldment areas where the stresses concentrate, such as at the weld root or weld toe. Thus, the *potential for hydrogen*, μ, must be accounted for at any such boundaries where discontinuity exists[21].

The theories[21, 22, 79, 80] defining the hydrogen potential μ usually assume that the hydrogen responsible for cold cracking, i.e., the *diffusible (reversible) hydrogen* is in a temporarily trapped state (apart from residual hydrogen) and that no chemical reactions occur when lattice-diffusing hydrogen diffuses into a trapping site. Under these assumptions, two conditions can be defined[21] that must prevail at the α–β boundary between a lattice site and a trapping site: (i) *continuity condition* of the hydrogen potential μ meaning that the variation of μ across the boundary must be smooth, and (ii) *conservation condition* of the mass flux of hydrogen meaning that the mass of hydrogen J is conserved at the boundary.

According to the continuity condition of the hydrogen potential μ, it follows that[21]:

$$\mu_\alpha = \mu_\beta \tag{25}$$

where subscripts α and β denote to the lattice site and the trapping site of the boundary, respectively.

Combining Eq. (25) with Eqs (8) and (9), the equation for the continuity condition becomes[21]:

$$\gamma_\alpha c_\alpha = \gamma_\beta c_\beta \tag{26}$$

In addition, the condition that the hydrogen potential is smoothly continuous across the α-β boundary gives the following relation[21]:

$$\nabla\mu_\alpha = \nabla\mu_\beta \tag{27}$$

According to the condition of hydrogen conservation at the α-β boundary, it follows that[21]:

$$J_\alpha = J_\beta \tag{28}$$

where J is the mass flux of hydrogen, and subscripts α and β denote to the lattice site and the trapping site of the boundary, respectively.

Combining Eqs (28) and (7), the equation for the conservation condition becomes[21]:

$$[(D_\alpha c_\alpha) / (RT)] \nabla \mu_\alpha = [(D_\beta c_\beta) / (RT)] \nabla \mu_\beta \tag{29}$$

Substituting Eq. (27) into Eq. (29), the following relation can be written[21]:

$$D_\alpha c_\alpha = D_\beta c_\beta \tag{30a}$$

Combining Eqs (30a) and (26) allows an alternative expression to Eq. (30a) to be written as[21]:

$$D_\alpha / \gamma_\alpha = D_\beta / \gamma_\beta \quad (30b)$$

Under the conditions defined by Eqs (26), (27) and (29), the diffusion coefficient of hydrogen in the trapping site of the α–β boundary, D_β, depends on the ratio of the local equilibrium concentration (c_α/c_β) or, alternatively, the inverse ratio of the activity coefficient [$(1/\gamma_\alpha) / (1/\gamma_\beta)$], at each site of the α–β boundary. These relations have been verified[21] by demonstrating a satisfactory correspondence between the estimates of an apparent diffusion coefficient predicted according to the equations and the experimental results. Specifically, this correspondence has also involved[83] the temperature and plastic deformation dependencies of the diffusion coefficient of hydrogen in iron and steel.

Apart from the conditions defined by Eqs (25)–(30), an alternative approach[84] determines the hydrogen potential Φ on the basis of the hydrogen concentration c according to Sievert's law, as:

$$\Phi = (P_{H2} / P_0)^{0.5} = c / k \quad (31)$$

where P_{H2} is the partial pressure of hydrogen, P_0 is the total pressure, c is the concentration of hydrogen and k is the hydrogen solubility in steel calculated as a function of temperature T and obeying Eq. (32) of the form:

$$\log k = 1.677 - 1420 / T \quad (32)$$

Consequently, applying Eqs (31) and (32), the hydrogen diffusion in a weldment can be solved by the variation calculations using the hydrogen potential Φ [22, 84].

1.4.5 Determination of the diffusion coefficient of hydrogen

For the analytic (or numerical) solutions of hydrogen diffusion, it is necessary to determine the *diffusion coefficient of hydrogen*, D_H, in steel as a function of temperature[21, 22]. A number of reports[21, 40, 59, 84–88] have been published on the determination of apparent hydrogen diffusion coefficients applying techniques such as gas evaporation and electrolytic penetration. Selection of an appropriate D_H value is a complicated problem, since published values show wide scatter amounting to even three orders of magnitude in ferritic steels at room temperature, as shown in *Fig. 5* for example[40]. The scatter in apparent D_H values has been attributed[21, 22, 25, 40, 59] to factors such as microstructure, composition, reversible hydrogen traps and surface conditions of a specimen used for the determination. Reviews[108] considering the scatter bands for hydrogen diffusion coefficients have been published recently.

Generally, different analytic equations are given for the calculation of the apparent hydrogen diffusion coefficient D_H at different temperature regions[21, 22, 85–87]. At higher temperatures of about 200°C and above, D_H is shown[21, 22, 40] to lie quite close to the coefficient for lattice diffusion, D_α, whereas D_H at lower temperatures is significantly lower and shifted towards that for the trapped hydrogen as the temperature decreases[22].

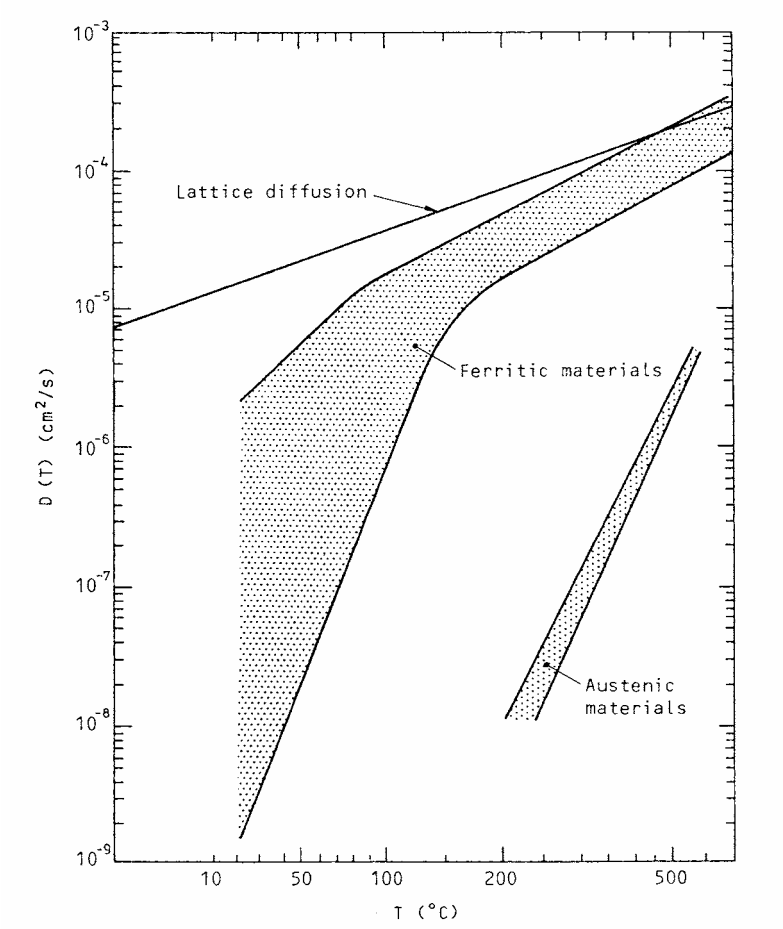

Fig. 5. Variation of apparent hydrogen diffusivity with temperature in steels[40].

According to the literature[21, 22, 85–87], the following equations have been proposed for the determination of the hydrogen diffusion coefficient D_H at a given temperature range θ (°C):

$$D_H = 1.51 * 10^{-2} * \exp[-11970 / (RT)] \quad ; \quad \theta \geq 500°C \tag{33a}$$

$$D_\alpha = 1.4 * 10^{-3} * \exp[-3200 / (RT)] \quad ; \quad 200 \leq \theta < 500°C \tag{33b}$$

$$D_H = 0.12 * \exp[-7820 / (RT)] \quad ; \quad \theta < 200°C \tag{33c}$$

where D_H (or D_α) is the apparent diffusion coefficient for hydrogen in steel (cm^2/sec), R is a gas constant (= 2 cal/mol ≈ 8.4 J/mol), T is the temperature (K) and θ is the temperature (°C).

Sometimes, hydrogen diffusion equations are used as an alternative to hydrogen potential based approach[22]. For instance, diffusion equations can be formulated[88] as sub-equations according to the degree of trapping, i.e., (i) hydrogen of lattice diffusion,

(ii) hydrogen trapped in voids, and (iii) hydrogen trapped permanently or irreversible hydrogen. To perform these kind of analyses, one does not need to introduce hydrogen potential to derive solutions for hydrogen diffusion in a heterogeneous medium[22].

Another approach[22, 84] to calculate hydrogen diffusion and concentration in welds directly without the use of the hydrogen potential, is to derive microstructure-dependent hydrogen diffusion coefficients for each weld region. For the temperature region from 20 to 200°C, Eqs (34a)–(34c) have been proposed[84] for parent steel, the HAZ and weld metal, respectively:

$$D_H = 0.89 * \exp[-8856 / (RT)] \quad ; \quad \text{parent steel} \tag{34a}$$

$$D_H = 0.31 * \exp[-7990 / (RT)] \quad ; \quad \text{HAZ} \tag{34b}$$

$$D_H = 1.22 * 10^{-2} * \exp[-5200 / (RT)] \quad ; \quad \text{weld metal} \tag{34c}$$

where D_H, R and T are as for Eqs 33a–33c.

This way, the apparent diffusion coefficients can be varied in their analysis depending on the particular local region of the weldment[22].

The consistency of the resulting hydrogen concentrations and the respective locations in a weld are dealt with in Section 1.4.7. Anyway, it can already be seen that differences do exist between the D_H estimates according to Eq. (33c) and Eqs (34a)–(34c), for instance. Nevertheless, the D_H values according to Eqs (34a)–(34c) seem to decrease as the locus shifts from the parent steel to the HAZ and weld metal, as expected.

1.4.6 Determination of the interactive and generalised activity coefficients

Experience[21, 22, 89–92] on the effects of plastic deformation and alloying elements on hydrogen occlusion have demonstrated that introduction of *interactive activity coefficients* enables to incorporate the effects of plastic strain and microstructure, and stress, into the analysis of hydrogen diffusion and accumulation.

Previous work[89, 90] that compare the recorded hydrogen occlusion with the hydrogen solubility in annealed pure α iron, allows for the determination of the *interactive activity coefficient* with respect to strain and microstructure, γ_m. This, coupled with results[21, 90] on plastically deformed steel leads to the derivation of the interactive activity coefficient γ_m of the form[21]:

$$(1 / \gamma_m) = 1 + 0.001228 * v_{pore} * \exp[6733 / (RT)] \tag{35}$$

where γ_m is the interactive activity coefficient due to microstructure and strain, R is the gas constant (= 2 cal/mol ≈ 8.4 J/mol), T is the temperature (K), and v_{pore} is a parameter for microvoid volume (%) relating to the available trapping sites for lattice hydrogen[91].

Values of v_{pore} have been determined[21] for iron, steel and weld metals applying cold-strained tensile bar specimens, some of which have been heat-treated to obtain microstructures characteristic to the HAZ. The diffusion and interactive activity coefficients of hydrogen, D_H, γ_m, have been determined experimentally from these bar

specimens by using gas-chromatography measurements of transient effusion of hydrogen with details described elsewhere[21]. Values of γ_m have then been calculated[21] applying Eq. (30b) that compares the measured diffusion coefficient D_β with that of unstrained and pure α-iron, D_α. Values of v_{pore}, in turn, have been determined[21] by substituting the calculated values of γ_m into Eq. (35).

The *interactive activity coefficient* with respect to hydrostatic pressure or compressive triaxial stress, γ_P, is generally determined[21, 22] as a function of pressure, P, gas constant R (= 2 cal/mol ≈ 8.4 J/mol), temperature T (K) and the partial molar volume of hydrogen, V^*, in accordance with Eq. (22b). The partial molar volume of hydrogen, V^*, represents the extent of the effect of pressure on hydrogen activity. Values of V^* = 2 ml/mole have been reported[92] according to the hydrogen penetration experiments for steel and iron under tensile stress.

Table 1 shows an example of the database[21] of collated values of D_H and v_{pore} for pure α iron, structural steel in different cold-strained and heat-treated conditions (simulating the HAZ microstructures), and weld metal.

Table 1. Hydrogen occlusion and diffusion coefficient D_H in steel at 20°C [21].

Steel specimen & condition	Total effusion (ml/100 g)	Diffusion coefficient D_H (cm^2/sec)	v_{pore} (%)
Pure α iron	–	$5.74 * 10^{-6}$	0
Structural steel SM50B			
– as-delivered	0.24	$1.8 * 10^{-6}$	0.0169
– 2% strained	0.26	$7.6 * 10^{-7}$	0.0506
– 4% strained	0.43	$5.6 * 10^{-7}$	0.0715
– 6% strained	0.50	$4.4 * 10^{-7}$	0.0932
– 7% strained	0.78	$4.0 * 10^{-7}$	0.1032
– restraint-free, heat-treated*)	–	$4.2 * 10^{-7}$	0.0982
– restrained & heat treated**)	–	$3.1 * 10^{-7}$	0.1350
Weld metal	0.22	$1.6 * 10^{-7}$	0.0213

*) : used for V_{pore} when considering only microstructural change in the analysis[21]

**) : used for V_{pore} when both microstructural change and strain distribution in the weld are considered[21].

An alternative approach[22] to analyse the hydrogen diffusion is to apply a *generalised activity coefficient*, γ_g, instead of interactive activity coefficients. The generalised activity coefficient is defined as[22]:

$$\gamma_g = \{\exp[PV_H^*/(RT)]\} / \{1 + 0.001228 * v_{pore} * \exp[6733/(RT)]\} \quad (36a)$$

$$v_{pore}(\%) = v_0 + 0.0123 * \varepsilon_p \quad (36b)$$

where ε_p is the equivalent plastic strain and v_0 is a microstructure dependent parameter associated with a particular region of the weld. Values of v_0 = 0.0169, 0.0982 and 0.0213% have been suggested[22] for the parent steel, the HAZ and the weld metal, respectively.

Distributions of the equivalent plastic strain ε_p of single- and multiple-pass weldments have been calculated[21], for instance, by *a finite element method* (FEM). As the hydrogen trapping effects are already incorporated into the generalised activity coefficient γ_g according to Eq. (36a), the corresponding diffusion coefficient of hydrogen used in numerical analyses should be that for the lattice diffusion, D_α [22].

1.4.7 Numerical analysis of hydrogen diffusion and accumulation effects

Numerical analysis enables solutions of *hydrogen diffusion* in welds having complex geometries and under the conditions where the diffusion coefficient of hydrogen varies depending on time, temperature and location[22]. For the numerical modelling of hydrogen diffusion, a two-dimensional (2D) *finite difference method* (FDM) is often applied[93–95], with hydrogen diffusion in a butt weld being approximated with diffusion in an infinite plate[40]. The 2D FDM analysis that uses a partial differential equation obeying the law of mass conservation is applicable for assessing hydrogen diffusion in both single and multiple-pass welds. For the analysis, Eq. (12) that gives the activity of the diffusing mass, is formulated and converted into a finite difference equation[21, 22]. This equation expresses the mass diffusion in a system in terms of the *activity gradient* of the diffusing mass ∇a, in conjunction with the *activity coefficient* of the mass γ and the *diffusion coefficient* of hydrogen D, with incorporated temperature dependencies.

Traditionally, numerical analyses are mostly concerned with single-pass welds and root runs. Accomplished FDM analyses[93–95] have shown, for instance, that hydrogen evolves more rapidly from a pipe girth weld than from the root beads of Lehigh or Tekken cold-cracking tests, simply because the root surface exposed to the atmosphere is wider in a pipe girth weld than in the cracking test welds[93]. Another FDM analysis on the distribution of hydrogen concentration in a multipass weld has revealed[94] that hydrogen concentrates beneath the final weld layer. Moreover, the maximum values of the local hydrogen concentration calculated by FDM were found consistent with the results of gas chromatographic measurements of hydrogen evolved from specimens sectioned at various thicknesses of a weld[94]. Accordingly, the calculations and experiments both demonstrated that this maximum value in multipass weld is close to the weld hydrogen content determined using a quenching method for a single-pass weld[94, 95].

Regarding *hydrogen accumulation*, a steel weld cannot be considered as a uniform medium for hydrogen diffusion, since the weld comprises a microstructural gradient with differences in dislocation densities and inclusions acting as traps[22]. Any geometrical discontinuities, such as weld root in a single-bevel groove, also cause stress concentration and/or the development of triaxial stresses[22]. For the analysis of hydrogen accumulation effects, additional factors therefore need to be encountered, namely, (i) the differences in microstructures in different weld regions, (ii) plastic strain distributions, as well as (iii) stresses and stress concentrations due to groove geometry and notch effects[21, 22]. A current practice thereby is that the stress and strain distributions, and sometimes also the heat conduction calculations, are solved by FEM[21, 22], in conjunction with the analysis of

the hydrogen diffusion patterns applying FDM. Alternatively, one can conduct a complete FEM analysis of all the relevant factors.

The documented FDM and/or FEM analyses[20–22, 100] providing quantitative data on hydrogen accumulation effects are mostly concerned with single-pass welds and root runs, only. The effects of (i) hydrogen diffusion, (ii) activity coefficients of hydrogen in strained and/or heat-treated steel and (iii) the stress and strain fields being incorporated, the results show that diffusible hydrogen accumulates at the weld root and the HAZ[21]. The transient hydrogen concentration at the root reaches its maximum some time after completion of welding[22]. Among microstructure, plastic strain and hydrostatic stress, the most influential factor on hydrogen accumulation was found the microstructural change associated with the γ–α phase transformation and the gradient of microstructures between parent steel, the HAZ and the weld metal, followed by the effects of equivalent strain and hydrostatic stress[21]. Accounting for all these factors, the maximum hydrogen accumulation was recorded[21] nearly five times as high as that resulting from hydrogen diffusion due to a concentration gradient, alone.

With respect to the HAZ in the middle of the weld throat depth, no stress nor strain concentration exist there, consequently, hydrogen accumulation is influenced essentially by the weld thermal cycle and the resulting microstructural changes[21]. This, in turn, manifests itself as a prolongation of time required for hydrogen diffusion. Whilst hydrogen concentration at the weld root was found to reach its maximum within 2 hours after welding[21, 84], the corresponding maximum in the hydrogen concentration in the middle of the throat depth was recognised nearly 5–7 hours after welding[21]. As far as the absence of stress concentration is concerned, these conditions apply also to multiple-pass weld metal. Consequently, hydrogen cracking in the filling layers of multipass weld metals is expected to require longer times to occur, than is the case with root/underbead cracking in the HAZ of single-pass welds.

In the case of single-run welds, applying preheating has been shown[13, 21, 25, 63, 77] very effective in reducing the maximum level of hydrogen accumulation. For example, preheating a weld up to 200°C, the maximum content of hydrogen accumulated at the weld root can become reduced to about one fifth of that attained without preheating[21]. This is essentially a consequence of substantial prolongation in the weld cooling time at low temperatures, e.g., t_{100}, due to preheating, with a subsequent increase in the thermal parameter of hydrogen diffusion, $\Sigma D\Delta t$, resulting in a remarkable reduction of the H_{R100}/H_0 ratio in accordance with Eq. (1)[13, 25, 63, 77].

With regard to multiple pass welding, the advantages of elevated preheat/interpass temperatures in reducing the concentration of accumulated hydrogen are documented to a lesser extent[8, 20], and are sometimes conflicting[8]. For instance, a Japanese work[20] reports a relatively small decrease in the H_{Rmax}/H_0 ratio with increasing preheat/interpass temperature θ_i, compared to that recorded for single-pass welds[13, 25, 63, 77], see *Fig. 6*. This is particularly true with higher heat inputs (and lesser beads), presumably because of accentuated weld bead penetration, overlapping and greater diffusion distances for hydrogen[20]. This contrasts to the single-pass welds that, from the viewpoint of hydrogen effusion, actually benefit from elevated heat inputs, c.f., Eq. (1).

The effects of preheating on hydrogen concentration in single and multiple-pass welds are dealt with in more detail in Section 1.5.3.

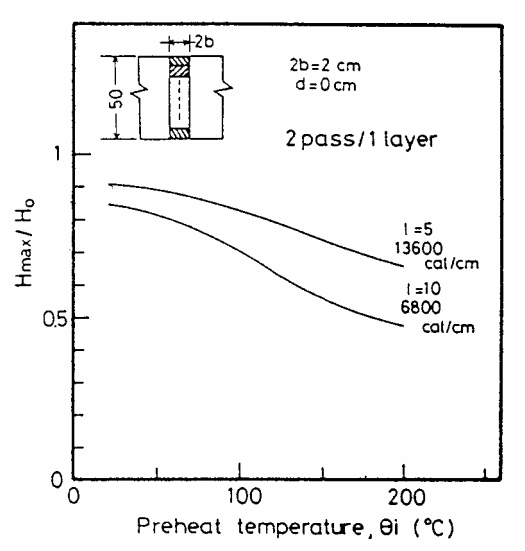

Fig. 6. The ratio of the final maximum hydrogen concentration to the initial hydrogen content, H_{max}/H_0, as a function of preheat/interpass temperature θ_i and for two different weld heat inputs and number of bead layers l – multipass welding[20].

1.5 Specific design factors affecting transverse hydrogen cracking in multipass weld metal

Earlier work[2–9, 12, 19–23, 26, 37] on hydrogen cracking in multipass weld metals have identified (i) factors whose influence differs from that traditionally experienced with HAZ root/underbead cracking in single-pass welds, as well as (ii) factors which needed not to be taken into account at all when assessing the HAZ cracking, but appear to become relevant for the weld metal cracking situations. These factors have been found[3, 19–23] to affect hydrogen accumulation towards the filling runs, as welding proceeds. Hydrogen accumulation, in turn, determines the *local (final) hydrogen concentration* H_{Rmax} in welds, which is the predominant hydrogen factor in hydrogen cold cracking of multipass weld metals.

The specific factors are: (i) the absence of *stress concentration* due to geometric discontinuities inside the weld metal, (ii) the influence of *individual bead layer thickness* h_w and *weld build-up thickness* a_w on hydrogen diffusion and accumulation, (iii) the influence of *weld bead penetration* and the resulting *weld bead overlapping* d/h_w on hydrogen accumulation and H_{Rmax} in the filling layers, and (iv) the influence of *interpass time* t_i and *interpass temperature* T_i on H_{Rmax} in welds. Additionally, the role of (v) the γ-α phase transformation and martensite start (M_s) temperature, as well as of (vi) welding heat input Q are given.

1.5.1 Welding residual stresses and stress concentration

Both numerical modelling[19–22] and direct measurements[20, 96, 97] using small sections extracted from actual welds have proven, in multipass welding the local hydrogen concentration, H_{Rmax}, increases in weldment thickness direction towards the filling runs as a result of diffusion and accumulation of hydrogen. Earlier work in Japan[19–23, 94, 95, 100], for example, clearly demonstrate that the local hydrogen concentration in multipass welds always tends to reach its maximum at the height of 0.75–0.90 of plate thickness from the plate bottom, irrespective of the actual plate thickness, c.f. *Fig. 2*. This coincides with the observation[3, 12, 20] that transverse hydrogen cracks tend to locate mostly beneath the weld surface below the 1st or 2nd last layer, where also the weld longitudinal residual tensile stress has been shown[19] to reach its maximum value, c.f. *Fig. 4*. This has led to the conclusion that transverse hydrogen cracking in multipass WM is a direct consequence of the combination of two essential factors: (i) a sufficiently high *local (final) hydrogen concentration* H_{Rmax} and (ii) the maximum peak in the weld *longitudinal tensile residual stress* σ_{resL}.

Experiments on multiple-pass welds carried out by WES[19] and NSC[3, 12, 20–23] have demonstrated that the weld longitudinal tensile stress, while being first reduced in the weld root as subsequent bead layers are being deposited, rise subsequently towards the filling layers as the number of subsequent passes increase and will finally reach its maximum, i.e., the level of weld metal true yield strength. The maximum of σ_{resL} under the final layer has been found to remain almost unchanged soon after about 2 bead layers have been deposited[19], as shown in *Figs 4* and *7*. The prerequisite to the development of the maximum σ_{resL} value is that the weld in a specimen is long enough, preferably at least 300–500 mm or more[19, 67]. Being the weld/specimen too small, the results, in terms of residual stress build up, cannot be expected to be descriptive of the real welded structure[67].

To attain the maximum peak in hydrogen accumulation, in turn, about 4 to 5 layers are generally required[19, 20], as shown in *Fig. 9*. As far as the longitudinal stress is concerned, and provided a crack-sensitive microstructure and sufficient amount of hydrogen are present, transverse WM hydrogen cracking is principally possible in a welded joint with no more than 2 bead layers.

There exist evidence[13, 24, 25, 66, 67b] that in single-pass welds, low temperature phase transformations may cause reduced residual stresses in localised regions at welds in low alloy steels, such as e.g. quenched & tempered extra-high strength Ni-Cr-Mo grades. This effect is accentuated further by applying sufficiently high preheating[67b]. In the case of multipass welds, however, this only concerns the final weld bead, since the stresses in previous bead layers have been shown to become elevated due to cycling to temperatures below the phase transformation temperature during subsequent weld passes[67b]. This thermal cycling of successive beads gives a "saw-tooth" stress distribution. With respect to the residual stress, the beneficial effects of low phase transformation temperature and preheat in low alloy steel welds hence only apply to the final weld bead[67b].

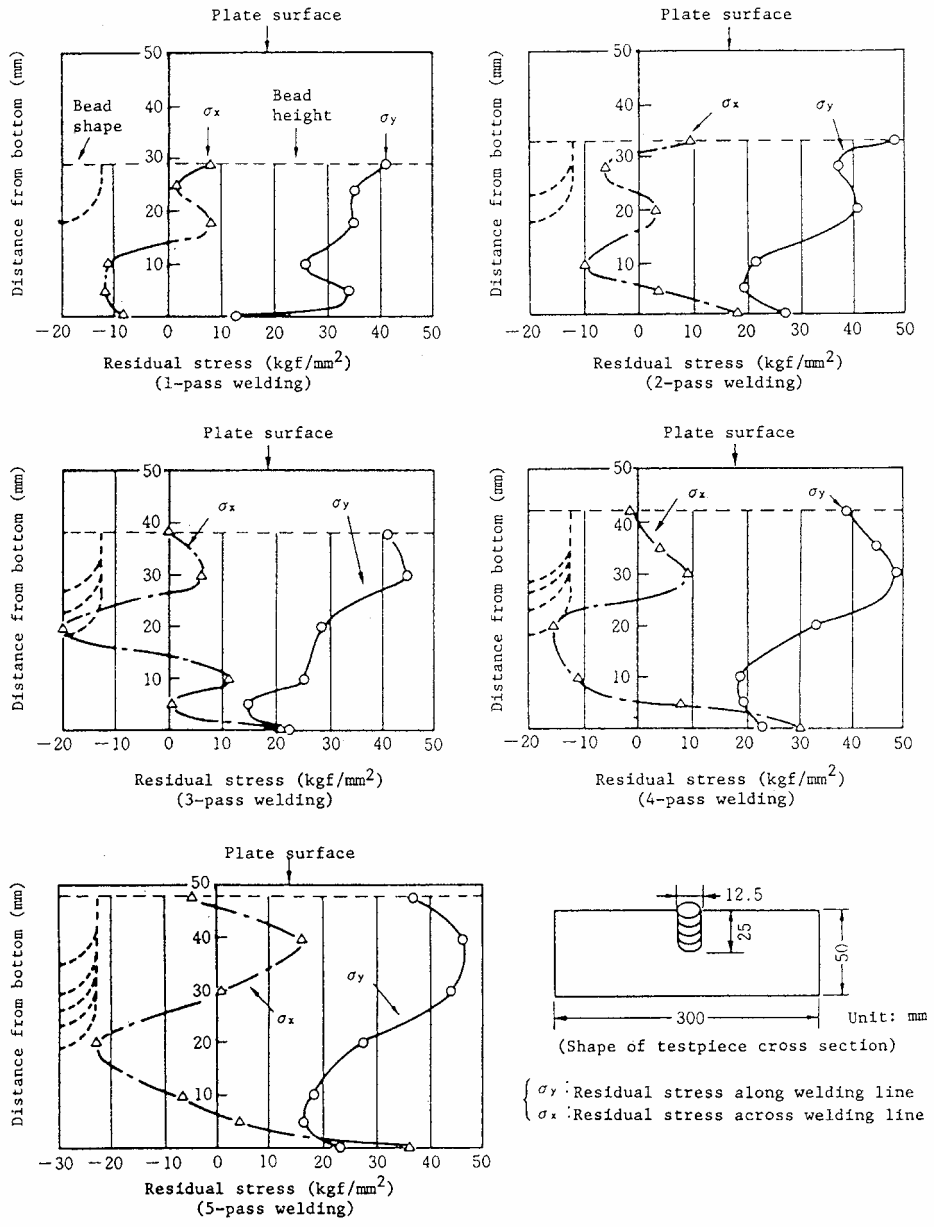

Fig. 7. Through-thickness distribution of residual stresses in multipass weld metals[19].

It is known[13, 21, 22, 25, 37] that diffusion of hydrogen in the weld root region is promoted and intensified by the tri-axial stress state due to geometrical discontinuity and the resulting stress concentration. This kind of stress-concentration is very effective in elevating the HAZ root cracking sensitivity of single-bevel groove welds, for instance[19, 21, 22]. Unlike the HAZ root cracking in single-pass welds, there is no such stress concentration arising from e.g. geometrical effects that could possibly act as local stress raiser inside the filling beads of multipass weld metal. Because of the absence of stress concentration, such cracking risk assessment methods that are based on the stress field or groove severity parameters[13, 25], the former being similar to K in fracture mechanics, have been traditionally considered difficult to apply.

As there is no apparent stress concentration, the accumulation of hydrogen in the weld metal is primarily governed by the weld thermal cycle and the associated microstructural change resulting from the γ-α phase transformation[21, 22]. Because of this, hydrogen cracking in the WMs may sometimes appear after substantial time passed after the completion of welding. The time of crack appearance is often 3 to 4 times longer than what is encountered with the HAZ root/underbead cracking[21, 22]. This may explain why unexpected WM hydrogen cracks have sometimes been recognised[76, 117] after several weeks (sometimes nearly 5 weeks) of the completion of welding.

As it comes to predictive systems assessing weld metal cracking risk, one has to content with estimates of overall level of weld longitudinal residual stress, in place of parameters such as the stress field/intensity parameter ΣI_{cr}, or the groove/specimen severity parameter, F_I[2, 3, 13, 25]. Thus, the effect of residual stress on the cracking risk of multipass weld metals is usually encountered using causal factors, i.e., critical threshold level of stress and applying regression analyses[2, 3], instead of sophisticated local approach-based numerical modelling capable of determining intrinsic local stresses and distributions at and near a crack tip[38].

1.5.2 Plate thickness/weld build-up thickness and bead layer thickness

Earlier work[19–22, 96, 97] have consistently demonstrated that the final local hydrogen concentration H_{Rmax} in multipass welds is governed by hydrogen diffusion and accumulation towards the filling runs throughout the welding until finishing of the final filling layer. Therefore, the H_{Rmax} in the filling runs can differ from both the remaining weld diffusible hydrogen content $H_{R100max}$ characteristic of single-pass welds, and the initial hydrogen content H_0 determined using a single-pass test according to IIW/ISO 3690[57]. It has been shown[8, 9, 19–23] that besides H_0, H_{Rmax} depends on weld thermal history and weld bead geometry and size, i.e., on (i) *the complete weld thermal cycle* that determines the hydrogen injection, accumulation and the conditions of subsequent hydrogen effusion, (ii) *weld bead size* affecting the diffusion distances of hydrogen, as well as on (iii) *weld bead overlapping* due to penetration of successive passes, which influences the volume of re-activated hydrogen available for subsequent accumulation.

The weld thermal cycle, weld bead size and weld bead overlap are defined[19–23] in terms of the *thermal factor of hydrogen diffusion*, $\Sigma D\Delta t$, an *individual bead layer*

thickness, h_w and *weld bead overlap ratio*, d/h_w, respectively. Of these, the overlapping effects are dealt with in Section 1.5.3. The thermal and geometrical conditions for hydrogen diffusion can be incorporated by describing them using a single parameter, the *integrated diffusion-distance parameter*, P_{D-D}, introduced[19, 20] according to Eq. (37) as:

$$P_{D-D} = \Sigma D\Delta t / h_w^2 \quad (37)$$

where h_w is the thickness of an individual weld bead layer (cm) and $\Sigma D\Delta t$ is the thermal factor of hydrogen diffusion (cm^2).

Theoretically, $\Sigma D\Delta t$ incorporates the diffusion coefficient of hydrogen, D, at a certain temperature and the time interval Δt to which the corresponding D value applies[19, 21–23]. Numerical solutions for $\Sigma D\Delta t$ are determined by integrating over the complete weld thermal history, i.e., from T_m to T_i acc. to Eqs (2a) and (2b). For analytic calculations, $\Sigma D\Delta t$ is usually written in an approximative form according to Eqs (3a)–(3c)[19, 21–23].

The effect of weld bead size on hydrogen diffusion is encountered[19, 20] via *individual bead layer thickness*, h_w. In Eq. (37), h_w^2 is merely proportional to the square of the diffusion distance from the middle of the bead to its outer surfaces. Alternatively, $h_w/2$ can be regarded as the distance that needs to be covered by the diffusing hydrogen. It has been shown[19–23] that the approximation of hydrogen diffusion through an 'element surface area', as one may picture the term h_w^2 to mean, by applying the square of the individual bead layer thickness, provides a realistic description of the effect of bead size on the diffusion of hydrogen under the thermal cycle of welding. The $\Sigma D\Delta t/h_w^2$ ratio as defined in Eq. (37), is thereby indicative of the loss of hydrogen from the element in the time available.

According to Eq. (37), the shorter the weld thermal cycle (i.e., fast cooling rate, short interpass time) and/or the greater the bead size, the smaller the corresponding P_{D-D} value, meaning that hydrogen diffusion becomes more difficult. Thus, the smaller the P_{D-D}, the greater is the final hydrogen concentration H_{Rmax} and hence the cracking risk, as shown in *Figs 8* and *10*. The thermal conditions for hydrogen diffusion are essentially enhanced with increasing the weld cooling time towards low temperatures, e.g., t_{100}, that is, by applying higher thermal inputs that yield an increase in $\Sigma D\Delta t$ in accordance with Eqs (3a)–(3c). An increase in bead size h_w, in turn, leads to greater diffusion distances, which further manifests itself as a reduction of the integrated diffusion-distance parameter P_{D-D} throughout the thermal input range.

It has been proven[19–23] that the maximum value of the remaining weld diffusible hydrogen content in the case of both single- and multiple-pass welds, denoted as $H_{R100max}$ and H_{Rmax}, respectively, depends essentially on diffusion conditions of hydrogen as defined by Eq. (37). This is comprehensively demonstrated in *Fig. 8* that shows the ratio between the *maximum remaining weld diffusible hydrogen* and the *weld initial hydrogen*, $H_{R100max}/H_0$, plotted against the hydrogen diffusion conditions, i.e., *the integrated diffusion-distance parameter*, $\Sigma D\Delta t/h_w^2$. Primary data in *Fig. 8* originate from Osaka University (OU) and Nippon Steel Corp. (NSC), Japan[20]; these data do not account for overlapping effects. Assuming that no weld overlapping occurs, i.e., $d = 0$, $H_{R100max}$ corresponds to $H_{max(d=0)}$.

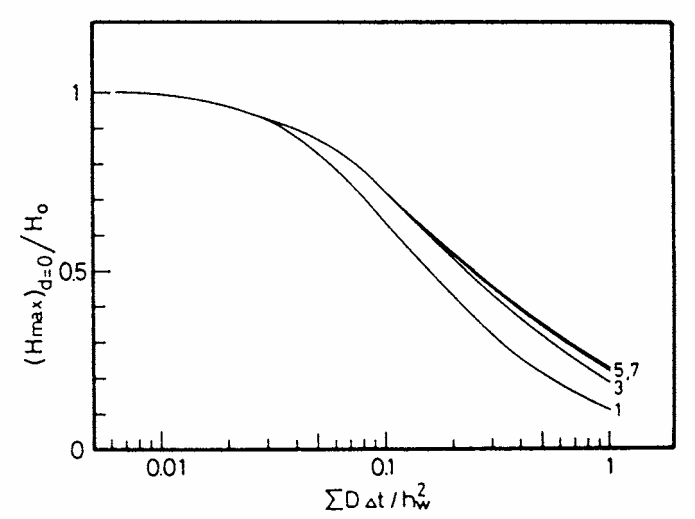

Fig. 8. The $H_{R100max}/H_0$ ratio as a function of the integrated diffusion-distance parameter $\Sigma D\Delta t/h_w^2$ – overlap not included. Primary data according to Osaka University and NSC[20], Nos 1, 3, 5 and 7: separate trials.

According to the data[20] in *Fig. 8* and looking one pass at a time, $H_{max(d=0)}$ (that corresponds to $H_{R100max}$ when assuming no weld overlap, i.e., $d = 0$) remains high and almost at the level of H_0 as long as $\Sigma D\Delta t/h_w^2$ is comparatively small, then decreasing as $\Sigma D\Delta t/h_w^2$ starts to increase. The data in *Fig. 8* suggests that the relationship between the $H_{R100max}/H_0$ ratio and the $\Sigma D\Delta t/h_w^2$ can be expressed using a decaying sigmoidal function incorporating positive first degree and negative second-degree polynomic terms. A general form of this expression is derived according to the primary data in *Fig. 8*, as:

$$H_{R100max(d=0)}/H_0 = \{e^{[-A\,P_{D-D}/(B^{PD-D})]}\} + C * P_{D-D} - D * (P_{D-D})^2 \qquad (38)$$

where *A, B, C* and *D* are constants and P_{D-D} is the integrated diffusion-distance parameter according to Eq. (37).

According to *Fig. 9*, with any given value of P_{D-D} the local hydrogen concentration H_{max} (that corresponds to $H_{R100max}$ when assuming no weld overlap, i.e., $d = 0$) seems to reach a constant, maximum level after a certain number of weld bead layers. As expected, under conditions allowing only limited diffusion of hydrogen (i.e., P_{D-D} values < 0.1) this maximum level is reached sooner, after about 2 to 4 layers[19, 20], whereas under favourable diffusion conditions (i.e., P_{D-D} values > 0.5), not until some 5 to 6 layers were deposited[19, 20]. This, in turn, coincides with the build-up of weld longitudinal residual stress σ_{resL} in multipass welds, c.f., *Fig. 4*.

The results of various types of multipass weld metal cracking tests[2, 3, 8, 9, 12, 76], as well as those of numerical modelling[20–23, 100] are consistently demonstrating that the occurrence of weld metal cracking appears to increase with the local maximum hydrogen concentration H_{max}. According to the modelling data[19–23], the influence of weld thermal history and bead size on diffusion and accumulation of hydrogen are satisfactorily described applying Eqs (37) and (38).

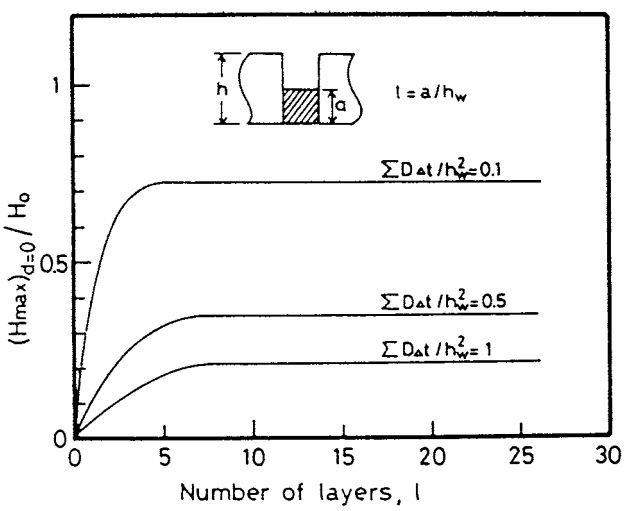

Fig. 9. $H_{max(d=0)}$ /H_0 ratio as a function of the number of bead layers l (l = a_w/h_w), at different levels of the diffusion-distance parameter $\Sigma D\Delta t/h_w^2$ [20] – overlap not included (d = 0).

Whilst the increase in H_{max} or h_w has been shown to affect adversely on cracking occurrence in multipass weld metals, the role of *plate thickness* h *or weld build-up thickness* a_w is less clear. Whilst some studies[2, 20] reveal practically no influence of plate thickness on required preheat/interpass temperature T_{cr}, others[3, 12, 76] show a significant trend of increasing T_{cr} as thickness increases, until the effect is usually offset above 50–60 mm. In general, the detrimental effects of increasing h and a_w have been attributed[3] either to elevated stress level or an increase in hydrogen accumulation, or both.

On the other hand, contrasting findings showing practically no effect of either h or a_w on weld metal cracking susceptibility have been documented[2]. In their experiments on extra-high strength SAW weld metals of $R_M \approx$ 755–1080 MPa, Okuda et al.[2] found the influence of weld build-up thickness a_w quite minimal and hence insignificant in the thickness range of 20 to 80 mm. Accordingly, a Japanese study[20] on SMAW weld metals reports, at the $R_M \approx$ 800 MPa strength level a H_{Rmax} value of 3.5 ppm was high enough to cause cracking in a wide thickness range from 25 to 150 mm. This implies, being a given level of weld metal strength (and hardenability) high enough to cause hydrogen cracking, the critical H_{Rmax} level appears to be fairly constant regardless of plate thickness[20].

Contrary to this, Yurioka et al. reported[3, 12] an approximately logarithmic dependence of the hydrogen cracking susceptibility on weld build-up thickness a_w in the thickness range from 20 to 50 mm, above which the effect gradually starts to level off as thickness increases further. Their study was concerned with SMAW and GMAW weld metals of $R_M \approx$ 590–885 MPa. In line with Yurioka's work, an Australian study[76] on high-strength basic and rutile FCAW weld metals of $R_M \approx$ 820–855 MPa reports that, other factors being constant, the occurrence of weld metal cracking in terms of number and density of cracks progressively decreased as plate/weld build-up thickness was reduced from 50 to 30 mm. Finally, no cracking was found in the 20 mm thick welded section[76].

A recent German work[11] suggests that the 'limit thickness', above which further increase in thickness does not lead to a subsequent rise in the required preheat temperature, is not constant but varies depending on the weld hydrogen content. With low weld hydrogen contents of 2–4 ml/100 g DM (IIW), the effect of thickness was recognised to offset not until above 65–70 mm, whereas with higher weld hydrogen contents of 8–10 ml/100 g DM (IIW), the effect of thickness seemed to become levelled off already above 45 mm. The experimental data of NSC[3, 12] is recognised to fall within these ranges of hydrogen and thickness.

As a result, presently there is no consensus about the effect of plate or weld build-up thickness on the hydrogen cracking susceptibility of multipass weld metals. Different views exist[2, 3, 11, 12, 76] on whether h or a_w should be considered as a relevant parameter into the predictive systems or not, and if so, what is the most appropriate mathematical description of their influence. Moreover, a possibility that plate or weld build-up thickness affects the hydrogen cracking risk differently, depending e.g., on the applied groove geometry of a test specimen, thermal history of welding, weld metal strength and conditions for hydrogen effusion and escape, must be taken into account.

1.5.3 Weld penetration and bead overlap – effects on final hydrogen concentration

Besides the thermal factor of hydrogen diffusion, $\Sigma D\Delta t$, and bead size in terms of individual bead layer thickness h_w, *weld bead penetration* and the resulting *bead overlapping* have been shown[19, 20] to affect hydrogen accumulation and hence the final local hydrogen concentration H_{Rmax} in multipass welds. This effect, characteristic to multiple-pass welds, is described[19, 20] by *weld bead overlapping*, d, or *weld overlap ratio*, d/h_w. Numerical modelling have shown[20] that increasing bead overlap leads to intensified hydrogen accumulation and hence elevated H_{Rmax} concentration.

As a result, the *final local hydrogen concentration* H_{Rmax}, here denoted as $H_{Rmax(d>0)}$ accounting for weld bead overlapping (i.e., $d > 0$) in multipass weld metals, depends essentially on (i) *weld thermal cycle* described using the thermal factor of diffusion, $\Sigma D\Delta t$, (ii) *individual bead layer thickness* h_w and (iii) bead penetration in terms of *weld overlap ratio* d/h_w, as shown in *Fig. 10*.

A direct consequence of overlapping is that the conditions of hydrogen accumulation will inevitably become different between single-pass and multiple-pass welds. In single-pass welds, the remaining maximum diffusible hydrogen content $H_{R100max}$ is always lower than the initial diffusible hydrogen content H_0[13, 25, 59, 63, 69]. Because of a decaying exponential dependence[13, 25, 63] of the $H_{R100max}/H_0$ ratio on $\Sigma D\Delta t$, as defined in Eq. (1a), $H_{R100max}$ decreases progressively as soon as $\Sigma D\Delta t$ starts to increase as a result of slowed cooling e.g., due to preheating. With prolonged cooling times in terms of e.g., t_{100}, $H_{R100max}$ can reduce down to values being remarkably less than H_0[101]. This is particularly the reason why preheating is so effective in reducing the root/underbead hydrogen cracking risk in the HAZ of single-pass welds[13, 25, 101].

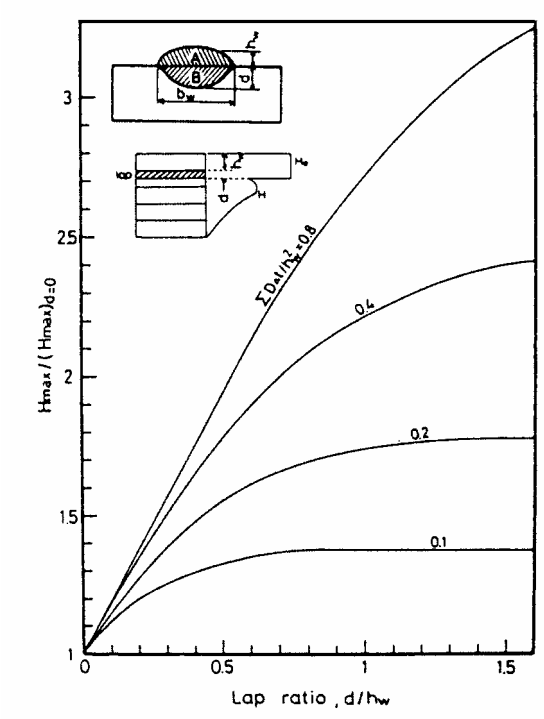

Fig. 10. Effect of the overlap ratio, d/h_w, on the maximum final hydrogen concentration-maximum remaining diffusible hydrogen content -ratio, $H_{Rmax(d>0)}/H_{Rmax(d=0)}$, at different levels of the integrated diffusion-distance parameter, $\Sigma D\Delta t/h_w^2$ [20] – overlap included ($d > 0$).

In multiple-pass welding, in turn, $H_{Rmax(d=0)}$ corresponding to the maximum remaining diffusible hydrogen content after the first pass being laid, has been shown[19, 20] to subsequently increase from the initial level of $H_{R100max}$ towards the filling layers, as welding proceeds. This is explained[19–23] by additional supply of hydrogen released from previously solidified passes as they are re-melted by subsequent pass as a result of weld penetration and bead overlapping. Released hydrogen is then transported further towards the filling layers due to enhanced diffusion caused by the repetitive thermal cycles of successive passes. Being accumulated into filling layers, this additional supply of hydrogen may compensate some of the hydrogen loss due to effusion from the weld during its cooling and interpass intervals.

A Japanese work[19, 20] have demonstrated that in the case where overlapping in terms of the d/h_w ratio is substantial and the conditions for diffusion of hydrogen are favourable (i.e., at high P_{D-D} values), the local hydrogen concentration in the filling runs, $H_{Rmax(d>0)}$, may be elevated nearly 3 times higher than in the absence of any overlap, $H_{Rmax(d=0)}$, as shown in *Fig. 10*. To obtain a realistic description of the H_{Rmax}/H_0 ratio in the case of multipass welds, the effect of weld overlap in terms of the weld bead overlap ratio, d/h_w, must therefore be included into the analysis. This requires $H_{Rmax(d=0)}$ to be replaced by $H_{Rmax(d>0)}$ in the applied calculation formulae.

Fig. 10 shows the effect of d/h_w ratio on the $H_{Rmax(d>0)}/H_{Rmax(d=0)}$ ratio at different values of the integrated diffusion-distance parameter of hydrogen, $\Sigma D\Delta t/h_w^2$. The primary data in *Fig. 10* is based on numerical modelling and weld-sectioning experiments, having its origin in the earlier work[20] made at Osaka University and Nippon Steel Corp., Japan. The $H_{Rmax(d>0)}/H_{Rmax(d=0)}$ ratio in *Fig. 10* expresses the local final hydrogen concentration under the influence of weld bead overlapping, in relation to the hydrogen content unaffected by any overlap. Here, $H_{Rmax(d=0)}$ denotes to hydrogen present in a weld before any overlapping occurs, which is the situation e.g. in the first pass of multiple-pass weldment. Thus, with respect to hydrogen level and other welding procedural factors being equivalent, $H_{Rmax(d=0)}$ in a first pass of a multiple-pass weld can be regarded to correspond to $H_{R100max}$ of a single-pass weld.

For the application of the diagrams in *Fig. 10* to the assessment of hydrogen accumulation, the effects of *weld thermal cycle*, *bead size* and *overlap* on H_{Rmax} are expressed in terms of $\Sigma D\Delta t$, h_w^2 and d/h_w, respectively. Under these premises, the data[20] in *Fig. 10* can be applied to describe the overlap effect using a relationship between the $H_{Rmax(d>0)}/H_{Rmax(d=0)}$ ratio and the d/h_w ratio at a given level of $\Sigma D\Delta t/h_w^2$.

According to *Fig. 10*, a general form[20] of the overlap equation thereby becomes:

$$H_{Rmax(d>0)} / H_{Rmax(d=0)} = 1 + A\,(d/h_w)^m \qquad (39)$$

where A and m are constants that depend on the particular $\Sigma D\Delta t/h_w^2$ value in question.

How steeply the $H_{Rmax(d>0)}/H_{Rmax(d=0)}$ ratio rises with greater d/h_w values, is seen to depend essentially on $\Sigma D\Delta t/h_w^2$ in question. *Fig. 10* shows that at high $\Sigma D\Delta t/h_w^2$ values, the behaviour of $H_{Rmax(d>0)}$ no longer obeys power-law dependence, but becomes nearly a linear function of the d/h_w ratio. For the cases where $\Sigma D\Delta t/h_w^2 >> 0.8$, constants A and m in Eq. (39) can hence be fixed as: $A = 2$ and $m = 1$.

In the case of single-pass welding, enhanced diffusion conditions of hydrogen in terms of greater $\Sigma D\Delta t$ are known[3b, 13, 25, 59, 63, 69] unambiguously beneficial in allowing for greater hydrogen effusion and escape as the weld cools down. Under the conditions of increasing weld bead overlap d/h_w and multipass welding, as presented in *Fig. 10*, intensive hydrogen diffusion in terms of greater $\Sigma D\Delta t/h_w^2$ appears[20] to turn detrimental in that it allows for a rapid increase of $H_{Rmax(d>0)}$ in the filling runs. According to *Fig. 10*, small overlap in terms of d/h_w only yields a 10–20% increase in the $H_{Rmax(d>0)}$, thus nearly corresponding to situation of no overlap. Contrary to this, high d/h_w ratios may, under favourable diffusion conditions, cause remarkably high local hydrogen concentrations of nearly 3 times higher than under conditions of no overlap[20].

Whether $H_{Rmax(d>0)}$ towards the filling runs can, under excessive overlap and intensified diffusion conditions, become even greater than the initial diffusible hydrogen content H_0 according to a single pass hydrogen test, has not been demonstrated experimentally. According to the modelling data[20] in *Fig. 10*, $H_{Rmax(d>0)}$ values exceeding H_0 seem possible, in theory, under conditions comprising small bead layer thickness h_w and provided that excessive weld bead penetration, d, takes place[20]. The theoretical and experimental work at Leeds University[96, 97] and TWI[31], however, give no reason to believe that H_0 could be exceeded in multipass welding under any circumstances. Presently, no experimental data exists[31, 96, 97] to verify that $H_{Rmax(d>0)}$ actually could ever exceed H_0, even though $H_{Rmax(d>0)}$ can well exceed the level of

remaining weld diffusible hydrogen content $H_{R100max}$ characteristic to single-pass welds[19, 20, 100].

In practice, inclusion of the overlap effect in terms of d/h_w into predictive systems requires some kind of metallographic examination. This can be done either from a polished macrosection of the actual weld or from a cross-section of a separate bead-on-plate trial weld macrosection according to *Fig. 11* and welded with the same parameters to be later used in actual production welding.

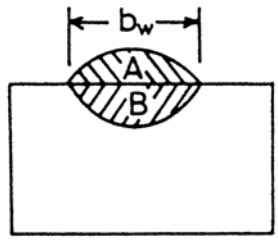

Fig. 11. A simple approximative methodology for determining the d/h_w ratio from a bead-on-plate test weld: $d/h_w \approx B/A$ [20].

Ignoring the effect of overlap d/h_w is likely to raise a possibility of underestimating the actual local hydrogen concentration $H_{Rmax(d>0)}$ in the filling passes of multiple-pass weld metals. Even with equivalent levels of heat input, different welding methods tend to yield weld beads of different shape. Typically, SAW produces narrow weld beads with quite high depth-to-width ratios[8, 32, 33], whilst beads with less penetration and wider shape are characteristic with FCAW[9]. Welding procedures that yield excessive penetration and overlapping may exhibit hydrogen cracking sensitivity greater than that concluded on the basis of single-pass cracking tests. In such cases, need of preheating may be underestimated, which results in potential danger of cracking in actual welding fabrication.

At present, there is no unified predictive system that would account for the effect of weld bead penetration and the resulting bead overlap on final (local) hydrogen concentration.

1.5.4 Interpass time and temperature

Because accumulation of hydrogen in multipass weld metals is a continuous, diffusion-controlled process, interpass temperature T_i and interpass time t_i are considered more important as controlling parameters, than in the case of the HAZ root/underbead cracking in single-pass welding. However, detailed experimental data on the combined effects of T_i and t_i in affecting WM hydrogen cracking in multipass welds are not available in the literature.

Multipass V-Groove cracking tests conducted previously at TWI[8, 9] implied that whilst higher T_i was needed as the weld diffusible hydrogen content and arc energy

increased, cracking can be prevented by raising the interpass temperature T_i also whenever the total welding time and/or the interpass time t_i remained too short[8, 9]. This was particularly the case with greater plate thickness. In practice, t_i can remain too short when welding e.g., short tack welds, at a high welding speed, or in the cases where weld cooling is deliberately intensified to shorten the total interpass time. The latter technique is sometimes used to compensate excessively long welding times resulting from the use of higher arc energies.

Consequently, other welding procedural factors being constant, longer interpass time in terms of t_i and Σt_i, or higher interpass temperature, are expected to lessen the risk of cracking in multipass weld metals, whereas shortening these time factors seems to induce an opposite effect[8, 9].

In practice welding fabrication, welding is usually not continued until a maximum allowed T_i has been reached. Thus, the higher the arc energy, the higher the interpass time t_i. Those TWI experiments[8] that employed intensified cooling to maintain constant interpass temperature as arc energy was raised, had therefore presumably overemphasised the severity of the applied test, as well as the effect of higher arc energies apparently increasing the cracking risk, in relation to the practice welding conditions.

Presently, there is no generally accepted expression for the effect of interpass time on the cracking risk in multiple-pass weld metals. Therefore, it is deemed necessary to somehow include a parameter describing the effect of interpass time into predictive systems[8, 102].

1.5.5 M_S temperature and hydrogen distribution

Traditionally, *martensite start temperature* M_S has been used as an indicator of the alloy's hardenability and austenite stability. For the higher strength steels, M_S can also indicate a transition during cooling between the slow and fast diffusion rates of hydrogen. In general, the higher the M_S, the larger will be the temperature range available for rapid hydrogen transport in the ferrite or martensite phase[37]. Because of the significant differences in the hydrogen diffusion coefficient and solubility in austenite, γ, and ferrite/martensite, α, the temperature at which the steel transforms from austenite to ferrite or martensite will affect the degree of hydrogen transport. Thus, the M_S temperature is both a measure of (i) the microstructure evolution and (ii) the ability to have available a phase (i.e., ferrite or martensite) for rapid hydrogen transport[37].

With respect to weldments, there exists evidence[37] that the difference in the M_S temperature between the weld metal and the parent steel HAZ influences the hydrogen distribution in multipass welds. This further affects the final hydrogen concentration and whether cracks will finally locate in the weld metal or in the HAZ.

During welding, the concentration of diffusible hydrogen in the weld/HAZ interface increases as a function of time. The driving force for the hydrogen accumulation and the resulting non-uniform distribution of hydrogen is the thermal diffusion process activated by the successive overlapping thermal cycles due to multiple-pass welding and assisted by localised stress gradients in the weldment due to tri-axial stress state or geometrical

discontinuities[21, 22, 37]. During weld cooling, the HAZ that has just experienced the γ–α phase transformation is capable of transporting hydrogen a significant distance into a parent metal due to high diffusivity of hydrogen in ferrite. The hydrogen transport cannot, however, proceed extensively, until the weld metal also transforms to ferrite. As austenitic, weld metal stores high hydrogen contents (due to high solubility of hydrogen in austenite) but can not move it fast enough to the fusion boundary due to slow diffusion rate of hydrogen in austenite[37].

One can determine the M_S temperature either experimentally by dilatometric measurements, or numerically using some of the existing formulae[37, 104] in the literature. Although there are formulae derived for both parent steels and weld metals[104], most of them suffer the shortcoming of disregarding the weld cooling rate, which makes their use somewhat approximative for welds.

Experimental measurements have shown[37] that when martensite transformation in the HAZ occurs at a higher temperature than in the WM, the resulting hydrogen concentration in WM is always higher than in the cases where the weld metal transforms before the HAZ. It follows, being the M_S temperature for the parent plate HAZ higher than that for the WM, excess hydrogen concentration may result in the WM instead of hydrogen diffusing into the HAZ, as shown in *Fig. 12*. This situation can promote WM hydrogen cracking. Its is known that current development in steel processing techniques have enabled high strength parent plate to be manufactured with considerably leaner alloying than is the case with the WMs. Thus, the way the M_S temperatures tend to differ between the parent plate and the weld metal is expected to favour cracking in WM, in particular.

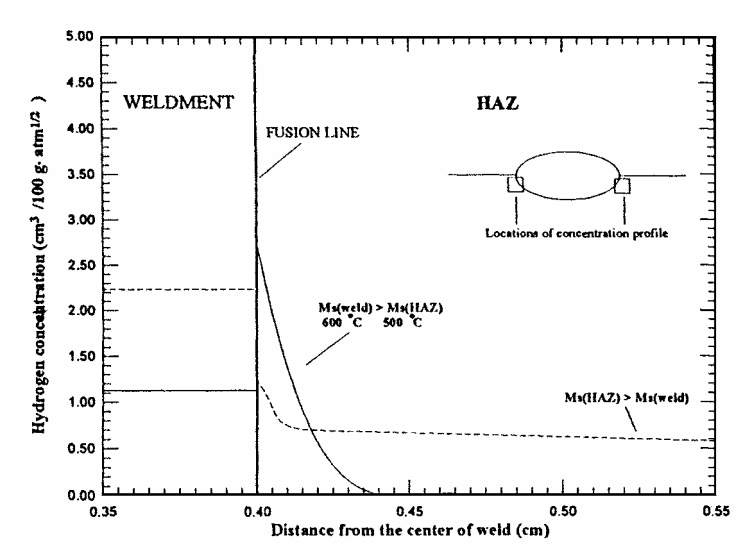

Fig. 12. Hydrogen distribution across the weldment fusion boundary for $M_{S(Weld)} > M_{S(HAZ)}$ and $M_{S(Weld)} < M_{S(HAZ)}$[37].

The recent experimental findings[26] based on WIC cracking tests and using different hydrogen levels have shown a relationship between the M_S temperature of the weld metal and its hydrogen cracking sensitivity. In this study, extra-high strength welds of $R_M \approx$ 890–1000 MPa were examined[26]. At a given hydrogen level, there existed a 'critical M_S temperature' below which cracking was systematically recorded[26, 37]. The higher the hydrogen content, the higher the critical M_S temperature, see *Fig. 13*.

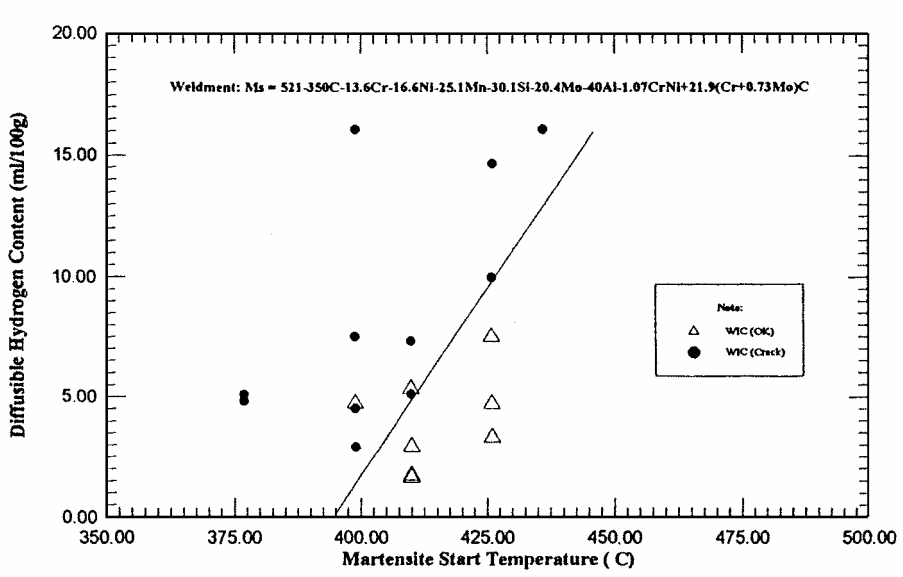

Fig. 13. Diagram of hydrogen cracking/non-cracking zones as a function of weld hydrogen content and weld metal M_S temperature[37].

The results[37] imply that weld metal M_S temperature, or the difference in M_S between WM and parent steel HAZ, ΔM_S, could serve as a kind of composition based hydrogen-cracking index. In many cases in practice, however, WM and HAZ microstructures are not essentially martensitic, which leads to thinking that temperatures such as A_{r3} or B_S might be more relevant temperatures than M_S. Such systematic comparisons of the different temperatures were, however, not found in the published literature. An M_S expression for weld metal, which incorporates the influence of the WM oxygen content, has been suggested[37] as a further improvement to better describe the effect of oxide inclusion on austenite decomposition kinetics.

1.5.6 Welding heat input

In order to reduce the risk of hydrogen cracking in the HAZ, increasing the heat input Q is unambiguously beneficial. This is ascribed to a decrease in weld cooling rate and hence

the hardenability effect, which reduces the volume fraction of martensitic transformation products, thus manifesting itself as lower HAZ hardness[6, 7, 13, 24, 25, 27–30, 34, 52, 53, 101].

In the case of multipass weld metals, there exist evidence that the effect of heat input on cracking can appear differently from the common experience for HAZ cracking. Experiments on CMn SAW weld metals of $R_{p0.2} \approx 355$–450 MPa, for instance, have demonstrated[8] an increased risk of weld metal cracking with increasing arc energy in the range 1–5 kJ/mm. Thus, raising the heat input can actually worsen the conditions for cracking in multipass welds, which is the reverse of common experience for HAZ cracking. This was attributed to *greater diffusion distances* as bead size in terms of h_w increases, which further results in elevation in the local final hydrogen concentration H_{Rmax}, more hydrogen being retained by larger weld beads[8]. Another consequence of elevated heat input is an *increased weld penetration* and *weld bead overlap* in terms of the d/h_w ratio, which intensifies the hydrogen accumulation towards the filling runs[19, 20].

Contradictory findings have also been reported. A previous work[53] on extra-high strength ($R_{p0.2} \approx 700$ MPa) multipass SAW welds found no difference in the weld metal cracking appearance between the 2.0 and 4.5 kJ/mm heat input welds. Regardless of heat input, the required preheat, about 180°C, was dictated by cracking sensitivity of the weld metal instead of the HAZ. Another set of experiments[5] made for extra-high strength ($R_{p0.2} \approx 745$ MPa) multipass SMAW weld metals failed to reveal any effect of arc energy on the cracking occurrence within the 1.5–5.0 kJ/ mm range. This was even though the bead size in terms of both a_b and h_w was found to increase with the arc energy. Since cracking did not appear in any of these weld metals, the lower than expected cracking sensitivity may have also prevented the appearance of arc energy effects, even if such existed. It is noteworthy that no intensified weld cooling was applied in any of these experiments, consequently, with higher arc energies the interpass time also tended to become higher, hence presumably accentuating the hydrogen effusion.

The effect of heat input on cracking risk of multipass weld metals has usually been explained[8, 19–21] by its influence on the *integrated diffusion-distance parameter* $\Sigma D\Delta t/h_w^2$ in accordance with Eq. (37). Even though the thermal factor of diffusion, $\Sigma D\Delta t$, increases with higher heat inputs[13, 25,19,20,63], the fact that bead size and hence the diffusion distance increase simultaneously in relation to the square of bead size, h_w, in the dominator[8, 19, 20], may result in an overall reduction of the final $\Sigma D\Delta t/h_w^2$ at higher heat inputs.

Another fact accounting for the deleterious effect of high heat inputs on weld metal cracking is that hardness of the weld metal is usually much less affected by the changes in heat input or weld cooling time, than in the case of the HAZ[6, 7]. Any attempts to reduce weld metal cracking risk via lowering its hardness by raising the heat input are therefore likely to be far less effective than what have been recognised e.g., for the HAZ root cracking. What remains is hence the effect of heat input on *weld bead geometry* in terms of h_w, weld penetration and bead overlap in terms of d/h_w and, consequently, on the conditions for *hydrogen diffusion and accumulation* described in terms of $\Sigma D\Delta t/h_w^2$.

This implies that inclusion of a heat input term into a predictive system should be accomplished via incorporating it to ‘hydrogen retention’ and the resulting final hydrogen concentration $H_{Rmax,}$ rather than to the weld $t_{8/5}$ cooling time or weld hardness HV.

1.6 Preheat assessment methods for the avoidance of hydrogen cracking in multipass weld metal

Only two of the reviewed[1–8, 11, 12, 23] calculation methods for predicting the necessary preheat for weld metals were based on experimental tests that actually involve multipass welding. All the other methods were mostly derived from the results of various types of single pass tests. The two prediction methods are those according to Okuda et al.[2] and Yurioka et al.[3].

1.6.1 Method according to Okuda et al.

Okuda's prediction method[2] is based on experiments using multipass SAW of 50 mm thick, heavily restrained 500 x 400 mm specimens with a single U-groove preparation welded from one side and having a 25° groove angle, no root face and a groove depth of 40 mm. This specimen geometry is reported[2] to have been chosen because the existing evidence[106] showed that the increase in welding residual stress in weld metal with increasing plate thickness tends to level off to a constant value with plate thickness of about 50 mm and above. Different consumables (i.e., electrodes and fluxes) were used to obtain various weld metal strength and hydrogen levels[2].

Most of the weld metal cracks observed in the tests were transverse cracks within a depth of 5 to 15 mm below the plate surface, i.e., the location where residual stresses and local hydrogen accumulation are both shown[2, 3, 19–22, 54, 76, 94, 95, 100] to reach their maximum in multipass welding. It is worth noticing that only extra-high strength weld metals (i.e., R_M = 755–1080 MPa) were used in these experiments[2]. The illustration of the test specimen preparation according to Okuda et al. is shown in *Fig. 14*.

Okuda found[2] that the required preheat temperature to prevent hydrogen cracking in weld metal depends on the weld metal ultimate tensile strength, R_M, and the logarithm of weld diffusible hydrogen, $\log(H_D)$, measured with the gas chromatography method. Despite the nearly constant level of residual stress above 50 mm plate thickness, the cracking susceptibility seemed to increase still further with the increase in weld build-up thickness a_w, as local hydrogen continued to accumulate. The influence of weld build-up thickness on WM hydrogen cracking susceptibility was found[2] quite minimal and hence insignificant in the 20–80 mm thickness range. Therefore, Okuda's model does not consider plate/weld build-up thickness as a variable, see *Appendix 1*. Anyway, Okuda's model is stated[2] to be applicable irrespective of plate thickness, provided it does not exceed 40 and 80 mm in the case of single-side and double-side groove joints, respectively.

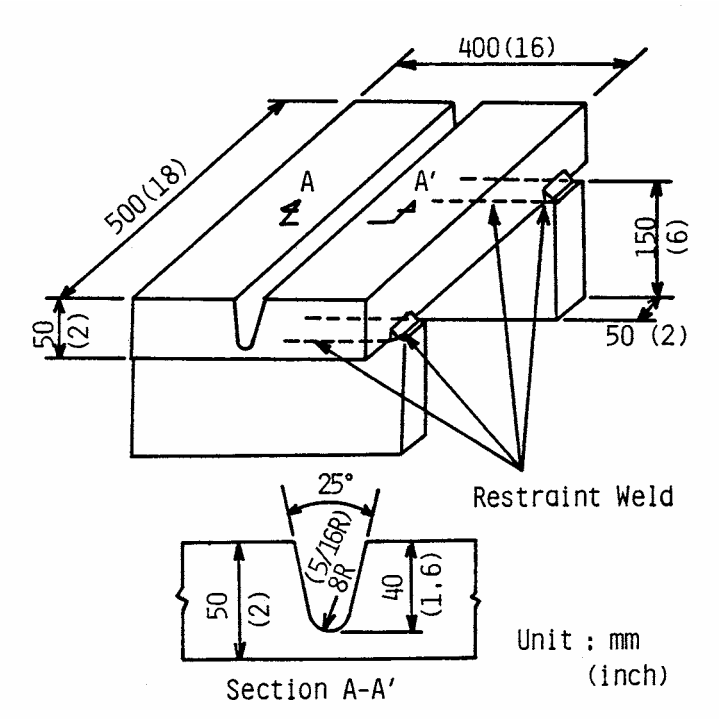

Fig. 14. Multipass weld metal U-Groove cracking test according to Okuda et al.[2a].

1.6.2 Method according to Yurioka et al.

Yurioka's prediction method[3] is based on experiments comprising multipass SMAW and GMAW of high-strength HT80 class plates of various weld build-up thicknesses and applying a 300 x 300 mm specimen. The specimen uses a symmetrical Y-groove preparation welded from one side and having a 60°-groove angle, small root gap (few mms) and a relatively large root face. In addition to weld metal tensile strength R_M and diffusible hydrogen, $\log(H_D)$, inclusion of the weld build-up thickness a_w as an input parameter can be regarded as an extension to Okuda's method. The illustration of the test specimen configuration according to Yurioka et al. is shown in *Fig. 15*.

In Yurioka's experiments, welds of somewhat lower strength (R_M = 580–885 MPa) were used[3], in comparison to Okuda's work[2]. Similarly to Okuda's findings, the observed WM cracks were mostly transverse to the weld direction and situated in the 2nd or 3rd last weld filling layer[3,12], i.e., the location where the longitudinal residual stress and local hydrogen in multipass welding are known[2, 3, 19–22, 54, 76, 94, 95, 100] to accumulate the most.

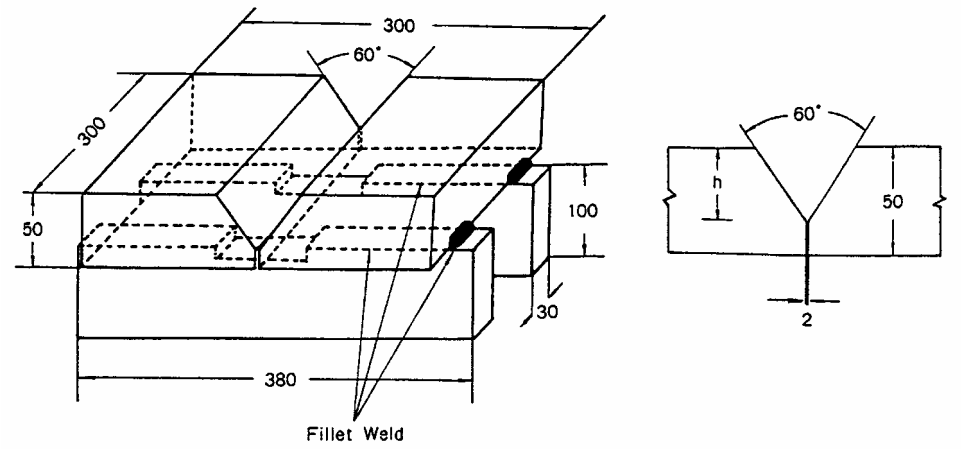

Fig. 15. Multipass weld metal Y-Groove cracking test according to Yurioka et al.[3b, 12].

Yurioka found[3,12] that the required preheat temperature to prevent hydrogen cracking in weld metal depends on the weld metal tensile strength R_M, the logarithm of the weld diffusible hydrogen, $\log(H_D)$ or $\log(H_0)$, measured with the JIS glycerine method, and the weld build-up thickness a_w. Instead of a single equation, Yurioka's method uses three sub-equations in accordance with the a_w range in question. These sub-equations are applicable for weld a_w ranges of 15–30 mm, 30–50 mm and over 50 mm, as shown in *Appendix 1*. In accordance with Okuda, Yurioka also considers the influence of a_w constant with plate thickness above 50 mm[3].

Yurioka et al.[3] regarded the diffusible hydrogen content the most important parameter governing cracking. Unfortunately, their hydrogen measurements are based on the glycerine method, which induces some inaccuracy into the prediction, as one has to use approximative equations to convert the JIS hydrogen values to the IIW values. A comparatively large number of conversion formulae can be found in the literature, each of them giving somewhat different result, see *Appendix 1*.

1.6.3 Small-scale cracking tests and their usability

Most of the small-scale hydrogen cracking tests for weld metals are designed for single-pass welds[54]. The principal experiments employed for single-pass weld metals are the (symmetrical) Y-Groove Tekken test, the tensile restraint cracking (TRC) test, the gapped bead on plate (G-BOP) test and the Welding Institute of Canada (WIC) test[8, 26]. Single pass weld tests, however, are of little assistance in the provision of procedural guidance for multipass welds, principally because of the hydrogen retention characteristics of a much larger volume of weld metal in multipass welds, and because such factors as interpass time and -temperature are not encountered with single pass welds[8].

With regard to multipass weld metal cracking tests, different researchers and institutes have been traditionally devoted to different types of cracking test specimens and/or

groove geometries. In their experiments, Okuda et al[2] used a 500 x 400 mm size U-Groove specimen of 40 mm groove depth and 50 mm plate thickness, c.f. *Fig. 14*. Yurioka et al.[3, 12], in turn, apply a 300 x 300 mm size symmetrical Y-Groove specimen where the plate thickness and weld build-up thickness can be varied independently on each other, c.f. *Fig. 15*. Both of these test specimens are heavily restrained by using welded strong-backs on the reverse side, to ensure adequate structural rigidity. At The Welding Institute, U.K. (TWI), an 800 x 400 mm size V-Groove full-thickness specimen configuration is applied, with restraining anchor welds on both ends[8, 9], as shown in *Fig. 16*.

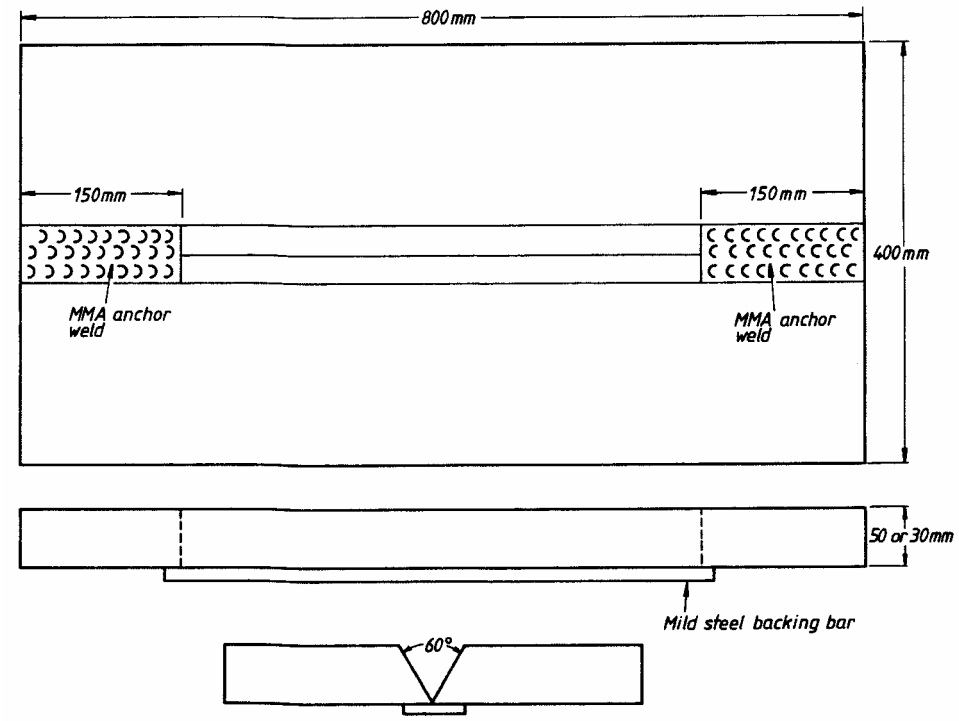

Fig. 16. Specimen configuration of the V-Groove cracking test for multipass weld metals applied by TWI[8].

According to the earlier work in Japan[19], the U-shaped groove appeared ideal particularly for the occurrence of weld metal transverse cracks in multiple-pass welding.

The outcome of the tests is interpreted differently among the tests. Okuda et al.[2a] propose a safety margin of 15%, principally because the average tensile properties are assumed used in the analysis instead of 'worst case' maximum values. Thus, his description of the 'safe' Crack – No Crack line derived from the experimental data[2] is multiplied with a safety factor of 1.15. Yurioka et al.[3], in turn, use the sub-equations derived from the Y-Groove experiments directly without any external safety factors. Since every single test is accounted for in the analysis and designated as cracked, if

cracks were found, his description is a kind of ‘lower bound’ safe line. Having compared the results of oblique *y*-groove and symmetrical Y-Groove tests for single-pass and multiple-pass welds, respectively, Yurioka concludes[3b] that hydrogen cracking in weld metal can be avoided by adopting a preheat temperature of about 25°C lower than that for preventing root cracking in the JIS *y*-groove Tekken test. This view, however, has not been fully shared by other researchers[107].

Overall, suitable cracking tests for multipass weld metals are sparse and not standardised within Europe. In Japan, Japanese Welding Association (JWA) has published a standard WES 1105-1985[19] entitled *"Cracking Test for Single-Bevel Groove Multi-layer Welds"*. This standard specifies a small-scale 300 x 600 x t mm^3 (where t = plate thickness and $t \geq 38$ mm) test specimen with single-bevel (i.e., ½-V) groove preparation having 45° groove angle, root face and restraining welds on both ends of the specimen, as shown in *Fig. 17*. The standard is intended primarily for SMAW welding, although also SAW and GMAW welding can be applied. The adoption of 45° single-bevel (½-V) groove is justified by stating that it is suitable for examining parent steel HAZ root cracks, underbead cracks and toe cracks, as well as enables the occurrence of transverse weld metal cracks to be confirmed[19]. The standard defines appropriate ranges of interpass temperatures, in relation to the applied preheat temperature. The standard also provides defined quantitative criteria for the acceptable crack size: it judges the test result as "cracked" in the case any cracks having a length of 0.5 mm or more are being detected[19].

For the assessment of the risk of hydrogen cracking in multipass welds, it is essential to gain information on the complete thermal history as the weld cools down to temperatures of 200–100°C, usually in terms of t_{200}, t_{150} or t_{100}[13, 19, 23, 25, 101]. This way, one can assure that a given specimen is large enough to be descriptive of real structures, as far as weld cooling is concerned. With respect to the t_{100} weld cooling time, there exist evidence[6, 7] demonstrating that the values measured from small-scale specimens, e.g. the JIS *y*-groove Tekken test, correlate reasonably well to the values measured from large-scale welded sections. Experiments carried out by JWA, Japan[19], ended up to a similar conclusion when comparing the $t_{8/5}$ and t_{150} cooling times between small-scale specimens and larger test panels corresponding to an actual structure. The outcome was that the heat cycle during multiple-pass welding of the 300 x 600 x t mm^3 ($t \geq 38$ mm) test specimen conforming to WES 1105-1985 (NSC)[19] differed very little from that of larger plates and panels corresponding to those used in real welded structures. According to the VTT experiments[7], at similar levels of arc energy and preheat/interpass temperature, there were no significant differences in the t_{100} values between butt welds and fillet welds, either.

Presently, there exists no systematic investigation on whether the differences in preheat estimates given by different cracking tests can be traced back to the differences in specimen groove geometries or specimen size.

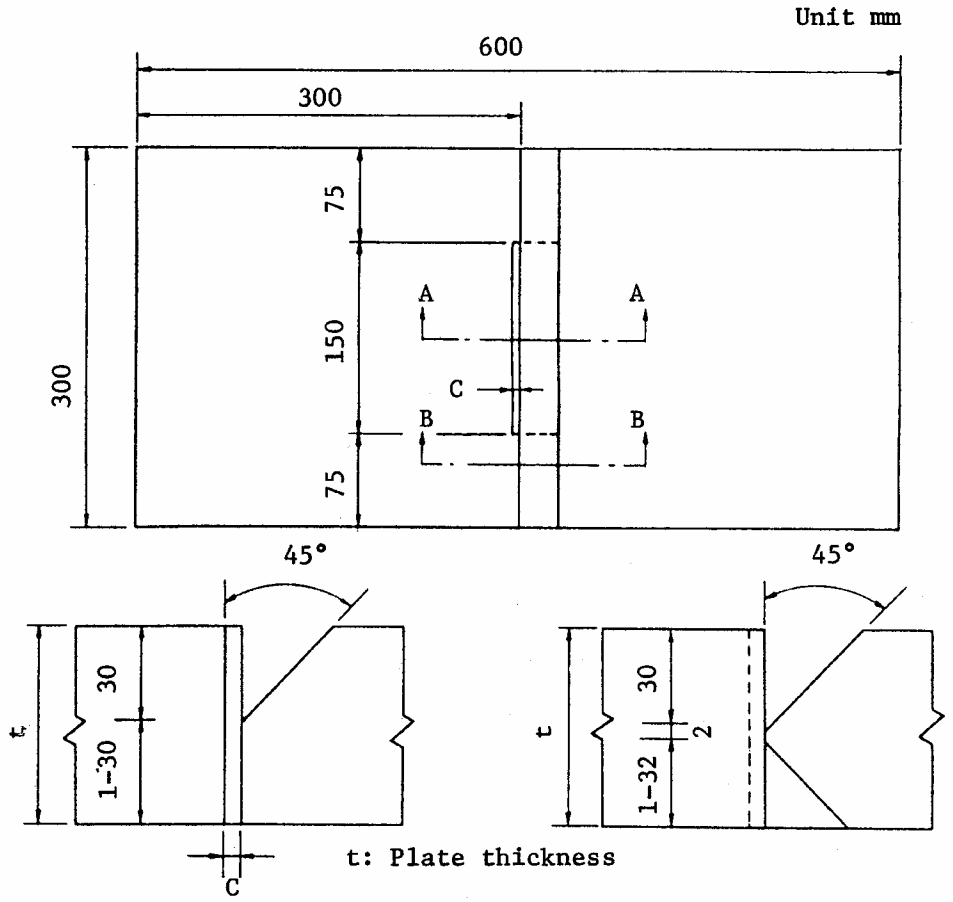

Fig. 17. Specimen configuration of the single-bevel (½-V) Groove multiple-pass weld cracking test according to WES 1105-1985 (JWA)[19].

1.7 Practical experiences of hydrogen cracking in multipass welds – overview

According to the previous work[6, 7] made at VTT, the risk of hydrogen cracking in multipass weld metals must be taken into account already in 460 MPa nominal yield strength grades when using consumables producing an overmatching weld metal strength. The risk was found[6, 7] evident for a 50 mm plate thickness in high rigidity structures containing rutile FCAW welds with the weld metal $R_{p0.2} \approx 600$ MPa, $R_M \approx 680$ MPa and the weld diffusible hydrogen content of ≈ 9 ml/100 g DM (IIW).

Earlier work at VTT[52, 53] also demonstrated that the required preheat in a 690 MPa nominal yield strength steel may be dominated by the cracking sensitivity of the multiple-pass weld metal instead of the HAZ. According to the weld metal Implant tests, instrumented Restraint tests and analytic calculations, in order to avoid weld metal cracking in a 40 mm thick 690 MPa yield strength DQT steel, a preheat of 180°C – higher than that for the HAZ – was found necessary[52, 53]. This was confirmed by the results of SAW multipass welding tests where WM transverse cracking in the filling runs could be eliminated only after raising the minimum preheat/interpass temperature up to 150°C. At 2.0 and 4.5 kJ/mm heat input, the occurrence of WM cracking appeared independent of the heat input[52, 53].

Apart from extra-high strength weld metal exhibiting predominantly martensitic microstructures, the possibility of hydrogen cracking in rutile FCAW weld metals of hardness no more than 250–280 HV was confirmed at VTT[6, 7], as well, at least in the case of thick plates and rigid structures. Therefore, as shown also by TWI[8, 9], a maximum hardness level in a given steel proved acceptable from the HAZ cracking viewpoint, say, 350 HV, is not necessarily 'safe' in terms of weld metal cracking. Despite of this, standards such as SFS-EN 288-3:1992[10a] and its very recent successor, Draft prEN ISO 15614-1[10b], categorically specify a 'permitted maximum hardness' of the *welded joint* according to steel group (i.e., strength class) and whether heat-treated or not, hence without distinguishing between the HAZ and the weld metal.

According to the earlier VTT data[6, 7], a single-pass K-Groove Tekken test is expected to give more reliable preheat estimates than an oblique *y*-groove JIS Tekken test for such weldment configurations and structural applications where weld metal root cracking is the predominant form of cracking. This is often the case with e.g. pipeline girth welds. The results[6, 7] of VTT are, in this sense, compatible with the earlier findings[107] made at TNO, The Netherlands. With respect to transverse cracking in multipass weld metals, the results[6, 7] do not provide sufficient evidence on the overall applicability of the K-Groove Tekken test in assessing hydrogen cracking susceptibility of multipass weld metals irrespective of the groove geometry (and F_I value) in question.

The analyses made at VTT[6, 7] at that time suggested, whenever transverse weld metal cracking in the filling layers is the predominant mode of cracking, both Okuda's and Yurioka's prediction methods can be applied. Unfortunately, the two methods were shown[4–7] to give greatly varying predictions. Okuda's model[2] considers low hydrogen more effective in lowering the required preheat/interpass temperature, thus putting more weight on penalising the increase in hydrogen. Yurioka[3], in turn, considers the weld build-up thickness a_w to affect substantially the preheat estimate, whereas this factor is completely omitted from Okuda's prediction. Neither of the two methods[2, 3] includes the effect of heat input. For the cases where there is a possibility of root cracking to become a predominant mode, e.g., line-pipe girth welds, neither of the models is suggested[4–7, 23] to be applied, but specific assessments instead.

A recent German work[11] reported good agreement between the EN 1011-2:2001 Method B estimates and the results of multipass V-Groove welding experiments. The work concludes that EN 1011-2:2001 Method B[1b] originally based on SEW 088 Merkblatt and derived from the results of single-pass HAZ cracking tests, e.g., *y*-groove Tekken tests, can be applied safely also for estimating relevant preheat temperatures for

multipass welds. One only has to replace the CET carbon equivalent of the parent steel with the corresponding value of the weld metal increased by 0.03%[1b].

This, however, contrasts with the earlier NSC data[12] on preheat estimates based on multipass Y-Groove tests, which differ substantially from those according to EN 1011-2 : 2001 Method B. The former NSC data[12] indicate that weld metal hydrogen cracking can occur with weld hydrogen as low as ≈ 4 ml/100 g DM (IIW), provided weld metal strength is high enough, i.e., $R_{p0.2} \geq$ 730–750 MPa and R_M in excess of ≈ 820 MPa. It was recognised[12] that a preheat/interpass temperature of 150–175°C was necessary to prevent cracking in $R_M \approx$ 820 MPa weld metals with 4 ml/100 g DM (IIW) hydrogen.

According to EN 1011-2 : 2001 Method B[1b], preheat temperatures considerably lower than those actually needed to eliminate cracking in the multipass Y-Groove tests would have been predicted as 'safe'. A comparison of T_0 predictions according to the Y-Groove cracking tests[12] and EN 1011-2 : 2001 Method B[1b] is presented in *Appendix 2*.

Overall, it is obvious that contrasting findings exist on the necessary preheat levels predicted by the currently available methods[1b, 2, 3, 11, 12] intended for the cracking risk assessments in multipass weld metals.

2 Aims of the current work

The overall aims of the Doctoral Thesis were (i) to identify causal factors that govern transverse hydrogen cracking in filling runs of high-strength multipass weld metals (WM), as well as (ii) to define the primary parameters to describe the cracking behaviour. This was to enable the development of an experimentally verified engineering methodology that allows reliable predictions of the necessary precautions for the prevention of WM hydrogen cracking.

The experimental working phase within the present work focused on multiple-pass weld metal cracking in shielded-metal arc (SMAW) and submerged-arc (SAW) welds. As a first stage of experiments, SMAW was chosen due to its feasibility in obtaining different levels of weld diffusible hydrogen in a controlled manner by re-drying and moisturing the electrodes. The use of SMAW to perform various types of Y- and U-Groove cracking tests hence allowed the necessary scaling of the critical limits of Crack – No Crack conditions according to weld metal strength and weld hydrogen. The work continued with sets of SAW multipass cracking tests and using a similar U-Groove test specimen configuration as was applied to the SMAW cracking tests. The data obtained for these two welding processes were then compared, in order to reveal any possible differences that may appear in the cracking susceptibility between SMAW and SAW weld metals of otherwise similar strength and initial hydrogen content.

Based on the experimental data, numerical calculations were made for analysing the interactions between the crack-controlling factors, in order to assess the critical boundary conditions for weld metal hydrogen cracking in SMAW and SAW multipass weldments. The interpretation of the findings was supported by the analyses of the results of all-weld metal tensile tests, all-weld metal hardness surveys, weld residual stress measurements, weld dilatometric measurements, bead size measurements and microstructural investigations.

The final deliverables of the Doctoral Thesis were: (i) predictive diagrams and equations for the assessment of WM hydrogen cracking risk by defining *the critical Crack – No Crack boundary conditions* in terms of ‘safe line’ description giving the desired lower-bound estimates, and (ii) predictive equations capable of giving reliable estimates of *the required preheat/interpass temperature* for the avoidance of weld metal hydrogen cracking in the Crack region.

To accomplish Item (i) it was deemed necessary to define the *weld critical hydrogen content* H_{cr} below which hydrogen cracking in multipass weld metals will not occur even under the most stringent conditions realistically met in practice welding fabrication. This was to serve as a ‘first line of defence’ against WM cracking.

Within Item (ii), engineering formulae are to be derived for predicting the required preheat/interpass temperatures for the avoidance of WM hydrogen cracking, once the other controlling factors are such that the ‘Crack region’ is inevitably entered. This is thought to serve as a ’second line of defence’ against WM cracking.

3 Experimental and analytical procedures

The experimental part of the thesis is concerned with multipass cracking tests on shielded-metal arc (SMAW) and submerged-arc (SAW) weld metals of various strengths and hydrogen levels. The outcome of the various cracking tests are analysed in order to reveal the primary crack controlling factors.

Materials for the cracking tests and the associated experiments comprise SMAW electrodes and SAW tubular wires & fluxes of different strengths and chemical compositions. The experiments consisted of (i) multipass WM cracking tests, (ii) analyses of weld chemical composition, (iii) all-weld metal tensile tests, (iv) weld hardness measurements, (v) weld residual stress measurements, (vi) measurements on hydrogen diffusion and diffusivity, (vii) weld dilatometric measurements, and (viii) metallographic and microscopic studies of the weld bead sizes, weld microstructures and phase fractions. Based on the experimental data, numerical calculations are made for analysing the interactions between the crack-controlling factors in order to assess the critical boundary conditions for hydrogen cold cracking in SMAW and SAW multipass weld metals.

Within the experimental programme of the present thesis, multipass SMAW cracking tests were performed at VTT Industrial Systems (formerly, VTT Manufacturing Technology), Finland, and at Nippon Steel Corp. (NSC), Japan. Multipass SAW cracking tests were made at ESAB, Finland, ESAB, United Kingdom and Mäntyluoto Works, Finland. Helsinki University of Technology, Finland, carried out the weld residual stress measurements, whilst University of Oulu, Finland, was responsible for the hydrogen permeation tests, diffusivity calculations and derivation of the diffusion coefficients of hydrogen, as well as for the all-weld metal tensile tests. Hardness surveys and metallographic studies of weld metals were carried out jointly at University of Oulu and VTT Industrial Systems.

3.1 Materials

For obtaining a sufficiently wide spectrum of weld metal strengths, electrodes representing six different classes were used for the cracking experiments of SMAW weld

metals. These were: (i) *ESAB OK 48.08* (AWS A/SFA 5.5: E 7018-G; EN 499: E 46 5 1Ni B 32 H5), (ii) *OK 74.78* (AWS A/SFA 5.5: E 9018-D1; EN 757: E 55 4 MnMo B 32), (iii) *OK 75.75* (AWS A/SFA 5.5: E 11018-G; EN 757: E 69 4 Mn2NiCrMo B 32 H5), (iv) *Nittetsu L-80* (IIS Z 3212 D 8016; AWS A5.5 E 11816-G), (v) *Atom Arc 12018* (AWS A/SFA 5.5: E12018-M) and (vi) *OK 75.78* (DIN 8529: HY 89 86 Mn3NiCrMo B H5). These electrodes aimed at covering all-weld metal yield strengths in the range of 480–920 MPa.

The 'average' chemical compositions of the experimental SMAW weld metals made using these six electrodes are given in *Table 2a*. The analysed weld chemical compositions and the corresponding weld metal strength values are given in *Appendix 7* and *Table 11*, respectively.

As a comparison, SAW tubular flux-cored wires representing four different strength classes were used for the multipass weld metal cracking experiments. These were: (i) *ESAB OK Tubrod 15.24S* (AWS A/SFA 5:23: F5A6-EC-G), (ii) *OK Tubrod 15.26S*, (iii) *OK Tubrod 15.27S* and (iv) *OK Tubrod 15.29S*. The flux used in all the SAW experiments was *ESAB OK Flux 10.62* (AWS A5.17: F6A4-EM12, F6P5-EM12). These filler wires & flux combinations aimed at covering all-weld metal yield strengths in the range of 480–900 MPa.

The analysed chemical compositions of the experimental SAW weld metals made using these four 4 tubular wires & flux are given in *Appendix 7* and *Table 2b*.

Table 2a. Average chemical composition of the SMAW weld metals made using the electrodes for the weld metal cracking experiments.

Electrode / w-% in weld metal	C	Si	Mn	Mo	Cr	Cu	V	Ni
OK 48.08	0.04	0.35	1.24	0.01	0.04	0.01	0.027	0.97
OK 74.78	0.05	0.31	1.48	0.38	0.03	0.02	0.018	0.04
OK 75.75	0.04	0.37	1.57	0.35	0.34	0.01	0.022	2.24
Nittetsu L-80	0.05	0.50	1.36	0.55	0.32	0.02	0.006	2.58
Atom Arc 12018	0.06	0.33	2.03	0.49	0.88	0.01	0.011	2.14
OK 75.78	0.05	0.25	2.18	0.67	0.42	0.01	0.023	3.10

Table 2b. Average chemical composition of the SAW weld metals made using the tubular filler wires for the weld metal cracking experiments. Flux: Esab OK Flux 10.62.

Electrode / w-% in weld metal	C	Si	Mn	Mo	Cr	Cu	V	Ni
OK Tubrod 15.24S	0.05	0.24	1.79	0.10	0.03	0.03	0.010	0.83
OK Tubrod 15.26S	0.08	0.17	1.80	0.52	0.02	0.03	0.013	0.86
OK Tubrod 15.27S	0.07	0.25	2.03	0.54	0.03	0.03	0.010	2.54
OK Tubrod 15.29S	0.07	0.23	2.00	0.50	0.25	0.03	0.016	3.10
OK Tubrod 15.27S[*)]	0.08	0.20	1.87	0.33	0.02	0.01	0.011	1.58

[*)] : thin plate weld (6 mm) made as a 2-pass weld, see Section 3.2

To ensure a sufficiently wide range of weld hydrogen for the cracking tests, SMAW electrodes were either re-dried according to the manufacturer's recommendations, or moistured by holding them in the humidity chamber over a period of time under controlled levels of moisture and temperature. The procedures are explained in detail in a previous report[4]. In most cases, humidity chamber conditions of 40°C temperature and 80% relative humidity were found appropriate for obtaining weld diffusible hydrogen levels of 8–11 ml/100 g DM (IIW). For some electrodes, more aggressive conditions of 40°C / 90% humidity were found necessary for obtaining the highest hydrogen levels of 12–19 ml/100 g DM (IIW).

With respect to SAW, the fluxes were first moistured at 1100°C, following by re-drying intervals at various temperatures according to a specific procedure designed and performed by ESAB, Gothenburg, Sweden. A more detailed description is given elsewhere[4, 5, 112].

Since it has been proven[3, 5a, 19] that transverse WM hydrogen cracking is controlled essentially by the weld longitudinal residual stress that, in turn, is dictated by the yield strength of the weld metal, parent plate is not considered as a variable in the present study. Consequently, fine-grained microalloyed structural steel with nominal $R_{p0.2} \approx 460$ MPa and 60 mm in thickness was applied throughout the basic testing programme, unless otherwise noted. Occasionally, a 6 mm thick fine-grained microalloyed thin plate with nominal $R_{p0.2} \approx 650$ MPa was used as a reference steel to assess the effect of plate/weld build-up thickness and weld bead size on the cracking risk.

3.2 Experiments and testing methods

The SMAW weld metals made with the six electrodes were subjected to (i) multipass weld metal cracking tests applying different Y- and U-groove geometries and various specimen sizes, (ii) hydrogen diffusion measurements for determining the diffusion coefficients for different weld metals, (iii) analyses of weld metal chemical composition, (iv) all-weld metal tensile tests, (v) weld hardness measurements, (vi) weld residual stress measurements, (vii) weld dilatometric measurements and (viii) metallographic and microscopic studies of the weld bead size, weld metal microstructures and phase fractions.

The SAW weld metals made with the four electrodes were subjected to (i) multipass weld metal cracking tests applying the U-groove configuration and fixed specimen size, (ii) analyses of weld metal chemical composition, (iii) weld hardness measurements and (iv) metallographic and microscopic studies of the weld bead size.

3.2.1 Welding processes and procedures

Welding was made as multipass SMAW and SAW using different arc energies depending on the purpose of the test. In the Y- and U-Groove SMAW cracking experiments made at VTT Industrial Systems, fixed arc energy and interpass temperature levels of 3.0 kJ/mm

and about 70–100°C, respectively, were constantly applied throughout the cracking test programme. This was to define lower bound estimates of the boundary curve between Crack-No Crack regions with respect to the two controlling factors assumed as being of primary importance[2,3]: strength R_M and hydrogen H_D. To attain this further necessitated limiting the number of additional variables.

In the U-Groove SAW experiments made at ESAB, Finland and ESAB, Waltham Cross, U.K., also the heat input Q was taken as a variable, consequently three levels: 2.0, 3.0 and 4.0 kJ/mm were used. For the Taguchi test matrix prescribed for the latter SAW tests, two additional variables were adopted besides Q, namely, preheat/interpass temperature T_0/T_i and weld diffusible hydrogen H_D. Apart from the test matrix, complementary SAW U-Groove tests were made at ESAB Waltham Cross, U.K. and Mäntyluoto Works Oy, Finland. In these experiments, heat input and weld hydrogen were kept constant and the tests aimed at defining 'safe' interpass temperatures for the two extra-high strength wires: *OK Tubrod 15.27S* and *OK Tubrod 15.29S*.

Additionally, multiple-pass welded SMAW pads were made for obtaining specimens for tensile tests and hardness measurements. In these cases, the arc energies were adjusted according to the ratio of the groove shape factor F for bead-on-plate and groove weld (with bevel preparation), with the intention to obtain equivalent $t_{8/5}$ weld cooling times.

The detailed welding parameters are given in the context of each experiment.

3.2.2 Weld hydrogen measurements

With the exception of the SMAW Y-Groove cracking tests made at NSC (c.f., *Table 3a*), the weld diffusible hydrogen content H_D of welds associated with all the SMAW and SAW cracking tests in the present thesis was measured using the Osaka University mercury method. The method has been shown[13, 25] to have a linear correlation to the IIW mercury method in accordance with ISO/IIW 3690[57].

The individual weld diffusible hydrogen contents measured for each consumable and condition are presented in the context of the corresponding multipass weld metal cracking test.

3.2.3 Weld cracking test programme

The cracking test programme comprised SMAW and SAW multipass weld metal cracking tests applying the Y- and U-Groove specimen configurations. Here, the aim was to define and design a test specimen that would be small enough to be easily weldable, but large enough for the cracking conditions to be descriptive of real multipass welded structures. Specimens of 300 x 300/250 x 50 /60 mm and 500 x 500 x 60/70 mm were used for the SMAW and SAW processes, respectively. The Y- and U-Groove specimen configurations are depicted in *Figs 15* and *18*, respectively.

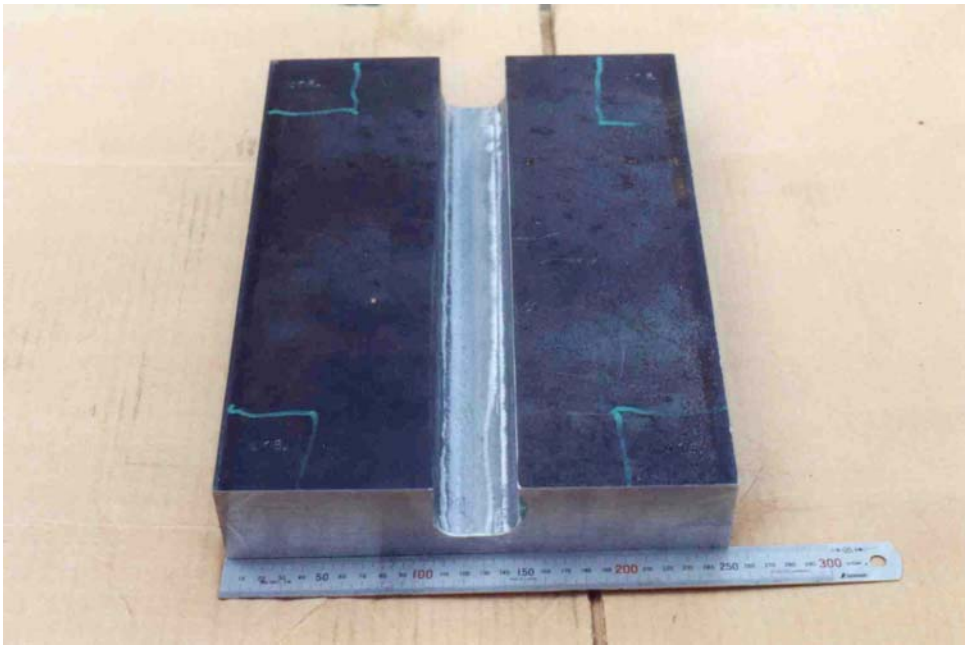

Fig. 18. The U-Groove multipass weld metal cracking test specimen designed by VTT Industrial Systems.

The SMAW experiments consisted of (i) symmetrical Y-Groove cracking tests identical with those made at Nippon Steel Corp. (NSC)[12], (ii) rectangular-shape U-Groove cracking tests designed by VTT and (iii) sc. double-welded large-scale Y-Groove cracking tests to verify the small-scale test results.

In these tests, both the interpass temperature and heat input were fixed. The interpass temperature T_i was constantly controlled down to about 70–100°C by applying forced cooling of the specimen, with the intention to define, at a given level of weld metal strength and hydrogen, the lower-bound Crack/No Crack boundary conditions giving the desired 'worst-case' estimates for weldability. Forced cooling conditions enabling the attainment of low interpass temperatures in conjunction with short interpass time, were thought to represent the most stringent conditions met in actual welding fabrication of large welded structural members.

For the SAW experiments, rectangular-shape U-Groove specimen configuration was employed. Besides strength and hydrogen, here, the interpass temperature T_i and heat input Q were also taken as variables. Consequently three levels of heat input and interpass temperature: 2.0, 3.0 and 4.0 kJ/mm and 100, 125 and 150°C, respectively, were applied in the Taguchi test matrix prescribed for the SAW cracking tests, as explained in Section 4.1.2.

The objective here was twofold. Firstly, the intention was to reveal any possible differences in the cracking sensitivity between SAW and SMAW weld metals at a similar level of strength and hydrogen. Secondly, the aim was to provide data for deriving mathematical description of the formula enabling the calculation of the required 'safe'

preheat/interpass temperature as a function of primary influential parameters, once the Crack-region was entered.

Additionally, some comparative experiments were made for thin V-Groove specimens of 6 mm in thickness and containing two weld passes, aiming at revealing any effects plate thickness might have on WM hydrogen cracking. All these specimens were fully restrained either by bolted clamps or welded strong-backs throughout the welding.

3.2.4 Analysis of weld chemical composition

The chemical composition of SMAW and SAW weld metals in the cracking tests was determined using *optical emission spectroscopy*. Analysis was performed for the last weld bead in the final filling layer, i.e., the location where most of the existing hydrogen cracks were recorded. In all the cracking test specimens, the last bead to be welded was in the middle of the final layer and the analyses were made from the centre of the weld bead in question, in order to avoid any dilution from the parent steel. Consequently, the analyses results correspond to all-weld metal chemical composition.

These data were used further in weld metal hardenability evaluation that was made to correlate weld chemical composition in terms of P_{cm} and CET carbon equivalents to hardness and, finally, ultimate tensile strength R_M.

3.2.5 Tensile tests

Tensile testing was carried out for the SMAW weld metals made using different electrodes and arc energy levels. The aim was simply to define true yield and tensile strength, $R_{p0.2}$ and $R_{M,}$ of all-weld metals for further analyses of cracking susceptibility and residual stress profiles, as well as to correlate strength with hardness. Thus, it was felt adequate to conduct these testing applying SMAW weld metals, only.

All the specimens were extracted longitudinally from the filling layers, aiming at characterising the weld region most prone to transverse WM hydrogen cracking. Testing was carried out at room temperature in accordance with SFS-EN 10002-1 using *round-bar specimens* (∅ 7 mm) according to SFS 3471.

3.2.6 Hardness survey

Weld hardness profiles were determined as *Vickers hardness* using HV_5 for all the SMAW and SAW weld metals. Again, measurements were concentrated to the surroundings of final weld beads in the filling runs.

The intention was primarily to define the average Vickers hardness HV_{ave} of as-welded and re-heated weld metal microstructures, separately. In each case, the corresponding individual maximum hardness HV_{max} of the weld metal was also recorded.

3.2.7 Weld residual stress measurements

Weld residual stress measurements were carried out for some of the SMAW weldments applying a sc. *Ring-Core drilling method*. The method uses a drilling tool that enables stresses below weld surface to be recorded in steps of ≈ 5 mm through the whole weld depth, if necessary. This option was regarded advantageous, since the weld longitudinal stress that was of primary interest here has been reported[2, 3, 19, 20, 23, 76, 100] to reach its maximum at the depth of about 10–30% from the top surface of the plate (and the weld).

To reveal any possible effects of specimen (and weld) length, measurements were made on two 40 mm thick Y-Groove cracking test specimens having (weld) lengths of 300 and 800 mm. The experiments were welded using *OK 74.78* electrode with 3.0 kJ/mm arc energy.

Additionally, to investigate the effect of plate thickness on residual stress build-up, comparative experiments were made using 6 mm thick, 2-pass welded thin plates of 500 mm in length and applying conventional *hole-drilling* method applicable for stress measurements in thin plate.

The principles of the Ring-Core test method are presented in *Appendix 3*.

3.2.8 Measurements of hydrogen diffusion coefficient

Hydrogen diffusion measurements were carried out using the *electrochemical hydrogen permeation test* under potentiostatic conditions to measure the hydrogen diffusion coefficient, D_H. A detailed description of the experiments and principles of the applied methodology are given in separate reports[5b, 36b]. A short introduction is given in *Appendix 4*.

The experiments were carried out using a potentiostatic voltage supply EG&G Model 263. With regard to the experiments, two kinds of traps are assumed to be present, deep and shallow ones[5b]. The double- or multiple-charging technique was therefore adopted for the hydrogen permeation tests carried out in the present study instead of a single charging stage, in order to eliminate the effect of deep traps.

A number of series of measurements were performed, with the aim at extending the number of chargings in each test to 3, 4 or more successive charging cycles. All the specimens studied here were pre-prepared according to the following procedure:(i) sawing the specimen down to a thickness of ≈1 mm, (ii) grinding the entry side of the specimen to 300 grid, (iii) grinding the exit side of the specimen to 1200 grid, polishing and nickel-coating under 3 mA/cm^2 for 3 minutes in Watt's bath (i.e., 250 g/l nickel

sulfate [$NiSO_4$-$6H_2O$], 45 g/l nickel sulphate [$NiCl_2$-$6H_2O$] and 40 g/l boric acid [H_3BO_3]), (iv) spot welding a metal wire on both the entry and the exit side, (v) pouring 0.1N NaOH solution into the exit side glass compartment and continuous bubbling with N_2 during the whole time, (vi) prior to charging, pouring 0.1N H_2SO_4 acid into the enter side glass compartment, continuous bubbling with N_2.

After these treatments, the experiments continued with the actual hydrogen charging and hydrogen permeation measurements for determining the hydrogen diffusion coefficients.

The measurements aimed at defining hydrogen diffusion coefficients for various SMAW, FCAW and SAW weld metals of different chemical compositions. The intention was to also compare the D_H values measured here to the published literature data. The measured D_H values were to be used further in numerical calculations evaluating the weld local hydrogen concentration H_{Rmax} as a function of weld thermal history and weld bead size.

3.2.9 Dilatometric measurements

Dilatometric measurements were made to determine the γ–α phase transformation temperatures of the SMAW weld metals, in relation to that of the microalloyed parent steel. Measurements were made using *Gleeble 1500 thermal simulator* and applying various weld $t_{8/5}$ cooling times to simulate the effect of arc energy on weld cooling and, hence, on the phase transformation temperature. The peak temperature and holding time of the thermal cycle were chosen as 1350°C and 1 sec, respectively. Four $t_{8/5}$ cooling times of 10, 20, 30 and 40 sec were set, coupled with 3D type cooling curve; these $t_{8/5}$ values roughly corresponded to the arc energy levels of 1.9, 3.7, 5.6 and 7.5 kJ/mm, respectively.

Cylinder shaped specimens of 10 mm in diameter and 75 mm in length were used for the experiments. The specimens were extracted longitudinally from the filling layers of multipass SMAW weldments.

The intention was to examine, whether differences in the γ–α phase transformation temperatures between the weld metal and the parent steel HAZ have had any influence on the cracking tendency of the differently alloyed weld metals. A detailed description of the measurements is given in a separate report[36a].

3.2.10 Weld bead size measurements

Weld bead size measurements were performed from transverse weld cross sections that were polished and etched before examining them under *optical microscope*. Height and widths of the final weld bead in the filling layer were determined by idealising its shape into a form of trapezium.

The aim here was to investigate any possible effect a welding process might have on bead size, especially, whether SMAW and SAW would yield different bead sizes at similar heat input range.

3.2.11 Metallographic examinations

Metallographic examination was performed as *optical microscopy* for the SMAW weld metals made using different electrodes and arc energies. The phase fractions were calculated from filling runs of the weld specimens and are given as mean values of all the measurements made from each specimen in question. Microstructures were characterised and classified to enable the calculation of the phase fractions of different microstructural constituents. For this purpose, all the specimens were polished to a 3 μm finish and etched in 4% Nital. Microstructural constituents were classified according to the IIW recommendations[13, 14] for the classification of weld metal microstructures using optical microscopy.

The intention here was to find a relationship between the weld metal cracking sensitivity and microstructure. The details of the examination and classification are explained in a separate report[36a].

3.3 Analytical calculations

On the basis of the experimental data of this study, numerical calculations were made for analysing the interactions between the crack-controlling factors, with the aim at assessing the critical Crack – No Crack boundary conditions for hydrogen cold cracking in SMAW and SAW multipass weld metals.

These calculations comprise: (i) analyses of the effects of weld thermal cycle in terms of $\Sigma D\Delta t$, weld bead size h_w and bead overlap d/h_w on final hydrogen concentration, (ii) derivation of hydrogen diffusion coefficients D_H for various types of weld metals, and (iii) calculations of preheat/interpass temperature estimates T_{cr} for the avoidance of hydrogen cracking in multipass weld metals.

3.3.1 Effects of thermal and geometrical factors on final local hydrogen concentration

In addition to weld initial diffusible hydrogen H_0, the local (final) hydrogen concentration H_{Rmax} in multipass welds has been shown[8, 9, 19–23] to depend on *complete weld thermal history*, *bead size* and *weld overlap* due to penetration of successive passes. As thermal gradient, bead size and overlap are welding process related, the present study investigates

their influence on H_{Rmax} in the case of arbitrary, yet typical, SMAW and SAW multipass welds. This is to evaluate whether H_{Rmax} could possibly differ between SMAW and SAW filling runs so significantly that this factor should be included into predictive systems assessing the weld metal cracking risk. For this purpose, measured data for SMAW welds are applied for the analysis. With respect to SAW, arbitrary weld geometry was defined using relevant literature data[32, 33].

For the analysis, the complete weld *thermal cycle* is expressed in terms of the *thermal factor of diffusion*, $\Sigma D\Delta t$, introduced in Section 1.2.1. In theoretical form, $\Sigma D\Delta t$ is defined in Eqs (2a) and (2b)[21–23]. For the comparative calculations made here, it is sufficient to consider the cracking conditions at a constant temperature, i.e., 100°C, consequently $\Sigma D\Delta t$ can be expressed using another factor, $\Sigma D\Delta t_{(100)}$, that has been shown[13, 23–25] to approximate Eq. (2) comparatively well. The use of $\Sigma D\Delta t_{(100)}$ in place of $\Sigma D\Delta t$, allows calculation of the $\Sigma D\Delta t_{(100)}$ factor within engineering accuracy directly from the recorded weld thermal history using the weld cooling time from the peak temperature down to 100°C, t_{100}. Therefore, empirical Eq. (3b) allowing for calculation of estimate of $\Sigma D\Delta t_{(100)}$ on the basis of the weld t_{100} data is applied in the present study.

For this purpose, a set of t_{100} cooling times were chosen which correspond to the 1.7 kJ/mm arc energy welding of a 50 mm thick plate at various preheat temperatures (i.e., 3-dimensional heat flow conditions), see *Appendix 10*.

The effect of *weld bead size* on hydrogen diffusion distance is described using the square of the individual bead layer thickness, h_w^2. The h_w^2 factor has been shown[19–23] to provide a realistic description of the effect of bead size on the diffusion of hydrogen in weld thickness direction and under the thermal cycle of welding, as explained in Section 1.5.2.

The thermal and geometrical conditions for hydrogen diffusion were incorporated by describing them using the *integrated diffusion-distance parameter*, $\Sigma D\Delta t/h_w^2$, as defined[19, 20] in Eq. (37). The $\Sigma D\Delta t/h_w^2$ ratio is considered indicative of the loss of hydrogen from a weld bead in the time available, this time depending on the thermal conditions of welding. Here, $\Sigma D\Delta t$ obeys Eq. (3b) and h_w is determined experimentally from a weld macrosection in question.

3.3.2 Derivation of values for hydrogen diffusion coefficient

A detailed description of the methodology for deriving diffusion coefficients of hydrogen, D_H, is given elsewhere[5b, 36b]. Principles of the applied procedure are explained in *Appendix 4* which shows determination of D_H from the potentiostatic curve that displays current on the exit side of the specimen, I_a, as a function of time t in the permeation test. Whilst I_c is the constant charging current applied to the entry side of the specimen, I_a is the recorded current from the reverse (exit) side of the specimen and is hence proportional to the extent and velocity hydrogen permeates through the specimen during the test. Thus, I_a is influenced by the hydrogen diffusion coefficient D_H of the given specimen. Consequently, it is I_a that shows correlation with D_H, not I_c.

The J/J_{max} in the y-axis in *Appendix 4* is directly proportional to the charging current $I_c/I_{c(max)}$ where I_c corresponds to C_0, i.e., the mean value of hydrogen concentration on the specimen entry side. As long as I_c is kept constant, the recorded I_a–t curve will be an exponential curve. Different D_H values in different materials then manifest themselves as different shapes of the corresponding I_a–t curve. Before deriving D_H from the I_a–t curve, the sc. onset point must be determined. In the present study, the time at which I_c was applied to the specimen entry side was set as the onset point. After applying I_c, the corresponding I_a–t curve can be recorded. The onset point in the I_a–t curve is then defined as the original zero: $t_0 = 0$, $I_0 = 0$, from which the previous part – being treated as an diffusion independent background, is omitted from the entire transient curve. Further, the relaxation time, i.e., the time regarded as being due to finite rate constant for transfer of hydrogen atoms from the surface into the metal phase[109], approximately equal to 10 sec on the basis of the present experiments, was applied in the analysis. Usually, the point of the first maximum I_a peak detected after the original zero was defined as the end point, see *Appendix 4*.

The recorded I_a–t curves were processed before they were applied for calculation of D_H according to the requirement of the Fourier's solution. Values of $D_{t(0.1)}$, $D_{t(0.2)}$ and $D_{t(0.25)}$ were calculated corresponding to the ratio of J/J_{max} to 0.1, 0.2 or 0.3, respectively[110]. These were found[109, 111] to be more reliable than the commonly determined values for the time lag, breakthrough time or half delay time.

Consequently, the hydrogen diffusion coefficients D_H were calculated for Armco iron, modern fine-grained high-strength structural steel, as well as for the SMAW, FCAW and SAW weld metals. It was thought that the experiments for Armco iron would serve as a reference test expected to give D_H values characteristic for clean metals practically free from hydrogen traps and hence exhibiting high hydrogen diffusivity. The D_H values for the modern fine-grained structural steel, in turn, were expected to be somewhat lower than those for Armco iron but, owing to the low impurity content of the parent steel, still remarkably higher than the values for the weld metals with a greater number of hydrogen traps.

3.3.3 Calculation of safe preheat/interpass temperature estimates for multipass weld metal

Analyses of the calculation methods for predicting safe preheat/interpass temperature estimates, T_{cr}, for multipass weld metals comprise to principal phases. These are: (i) re-analysis of the former data sets from the Y-Groove cracking tests[12] conducted by Nippon Steel Corp. (NSC), and (ii) derivation of an optimised T_{cr} prediction on the basis of the results from the SAW U-Groove experiments made in the present thesis.

The Y-Groove data set[12] from the former experiments made at NSC is given in *Appendix 5*. The data consist of SMAW and GMAW multipass experiments with two weld R_M levels of ≈ 820 and 750 MPa, weld build-up thicknesses a_w of 20, 30 and 40 mm and weld diffusible hydrogen in the range of about 2 to 11 ml/100 g DM (IIW). These

data[12] are re-analysed in the present thesis in order to derive alternative expressions that would enable the avoidance of the use of various sub-equations of the Yurioka-formula, c.f., *Appendix 1*.

Since both Okuda et al.[2] and Yurioka et al.[3] have demonstrated the vital role of weld metal tensile strength R_M and diffusible hydrogen H_D, R_M, and H_D were adopted as primary factors for the re-analysis of the NSC data[12]. As the true value of weld metal strength is not always known in practice, R_M is approximated for the present re-analysis using the actual weld metal chemical composition in terms of the CET carbon equivalent[1]. Despite the fact that Okuda et al.[2] – in contrast to Yurioka et al.[3] – found no significant effect of plate/weld build-up thickness a_w on cracking susceptibility, the inclusion of a_w is regarded imperative, because the cracking tests made in the present thesis comprise also thin plate two-pass welds as reference experiments.

According to present knowledge[1–3, 12, 54, 76, 100, 116, 117] on crack-controlling factors in multipass weld metals, a first attempt was made to estimate T_{cr} using the former NSC Y-Groove data set[12]. These NSC data were fitted by an empirical equation that describes T_{cr} as a function of weld metal CET, a_w and H_D. A general form of this expression is given as:

$$T_{cr} = A * CET + B * (a_w)^m + C * (H_D)^n - D \qquad (40a)$$

where *A, B, C* and *D* are constants, *m* and *n* are exponents (m, n < 1), CET is the carbon equivalent (%) calculated from the true weld metal chemical composition in accordance with EN 1011-2:2001[1b], a_w is weld build-up thickness (mm) and H_D is weld diffusible hydrogen content (ml/100 g DM) according to ISO/IIW 3690[57].

A second step was to investigate whether the over-conservatism in the T_{cr} estimates acc. to Eq. (40a) for moderate strength weld metals investigated here, could be reduced while still ensuring 'safe' and 'realistic' estimates for the extra-high strength welds. This was made by accentuating the logarithmic effect of hydrogen – a trendline that appears obvious when analysing the former NSC Y-Groove data set[12], as well as the results of Okuda et al.[2]. For this purpose, Eq. (40a) is rewritten with respect to the hydrogen term as:

$$T_{cr} = A * CET + B * (a_w)^m + \{[C * \ln(H_D)] / [D * (H_D)^n]\} - E \qquad (40b)$$

where *A, B, C, D* and *E* are constants, whereas exponents *m* and *n* and factors CET, a_w and H_D are in accordance with Eq. (40a).

Applying a form of Eq. (40b), the experimental data from the SAW U-Groove cracking tests made in the present study were analysed. These data are thereby fitted by a revised formula that: (i) puts more weight on the effect of weld metal strength by adjusting the $A * CET$ factor, and (ii) accentuates the logarithmic effect of hydrogen with a consequence of rewarding the attainment of low levels of weld hydrogen.

A third step was to evaluate the descriptive potential of parameters that could be related to weld metal strength, others than CET. It is realised that despite of its simplicity, any compositional based parameter, such as carbon equivalent, has debility that its disregards the effect of weld cooling on hardenability. Since the weld ultimate tensile strength R_M has been shown[6, 7, 23] a linear function of weld hardness, HV, and hardness, on the other hand, incorporates the effects of both the chemical composition

and the weld thermal cycle on hardenability, it was deemed imperative to test alternative expressions replacing CET in Eq. (40b) by weld metal hardness in terms of HV_{ave} and HV_{max}.

Consequently, Eq. (40b) is re-formulated as:

$$T_{cr} = A * HV + B * (a_w)^m + \{[C * \ln(H_D)] / [D * (H_D)^n]\} - E \quad (40c)$$

where HV is the actual weld metal Vickers hardness (HV_5) in terms of either average hardness HV_{ave} or the individual maximum hardness HV_{max}. Constants *A, B, C, D* and *E*, exponents *m* and *n* and factors CET, a_w and H_D are in accordance with Eq. (40b).

The aim here is to pursue optimisation of T_{cr} predictions in order to (i) accentuate the effect of weld metal strength on T_{cr}, (ii) accentuate the logarithmic effect of H_D on T_{cr} at low hydrogen levels, and (iii) introduce a strength based parameter that is more convenient to measure than R_M, but capable of incorporating the effects of chemical composition and weld thermal cycle on weld metal hardenability and, hence, its strength.

Finally, the applicability of alternative expressions for a_w and H_D were investigated. All the data were therefore re-fitted applying the following expressions for H_D and a_w, as:

$$T_{cr} = f\{[C * \ln(H_D)] / [D * (H_D)^n]\} \quad (41a)$$

$$T_{cr} = f[C * (H_D)^n] \quad (41b)$$

$$T_{cr} = f[C * \log(H_D)] \quad (41c)$$

$$T_{cr} = f[C * \tanh(H_D / D)] \quad (41d)$$

$$T_{cr} = f[B * (a_w)^m] \quad (42a)$$

$$T_{cr} = f[B * \tanh(a_w / C)] \quad (42b)$$

The intention of these final adjustments of the expression for H_D and a_w was to (i) describe more realistically the cracking occurrence in the case of thin plate welds and (ii) avoid overly conservative estimates at high H_D levels without a need to sacrifice the safety at low H_D levels. These data assessments were based on the comparisons to the most relevant literature data[2, 3, 12] and the experimental results of the present thesis.

4 Results

Results of the experimental programme of the thesis are presented, consisting of (i) multipass Y- and U-Groove cracking tests for SMAW and SAW weld metals, (ii) analyses of weld chemical composition, (iii) all-weld metal tensile tests, (iv) weld hardness measurements, (v) weld residual stress measurements, (vi) measurements on the diffusion and diffusivity of hydrogen, (vii) weld dilatometric measurements, and (viii) metallographic and microscopic studies of the weld bead sizes, weld microstructures and phase fractions.

4.1 Multipass weld metal cracking tests

The cracking test programme comprised (i) small-scale Y-Groove cracking tests on SMAW weld metals, (ii) large-scale double-welded Y-Groove tests on SMAW weld metals, (iii) small-scale U-Groove cracking tests on SMAW and SAW weld metals, and (iv) comparative V-Groove tests on thin plate SMAW and SAW welds.

4.1.1 Cracking tests for SMAW thick plate weld metals

The SMAW cracking test programme on thick plate weld metals consisted of (i) small-scale Y-Groove cracking tests made at Nippon Steel Corp. (NSC), Japan, and VTT, Finland, (ii) large-scale double-welded Y-Groove tests made at VTT, Finland, and (iii) small-scale U-Groove cracking tests made at VTT, Finland.

4.1.1.1 Small-scale Y-Groove tests

The first phase of the experimental programme revolving around SMAW weld metals composed of six Y-Groove cracking tests made at NSC, Japan, and using extra-high strength *Nittetsu L-80* electrode of $R_M \approx 810$ MPa. Earlier work[12] has shown, this electrode to produce weld diffusible hydrogen content $H_D \approx 4$ ml/100 g DM (IIW) in the as-received condition. For the electrodes used here, this was confirmed by measurements made at NSC, as shown in *Table 3a*. The chemical composition of *Nittetsu L-80* weld metal is given in *Table 2a*.

The dimensions of the Y-Groove specimen were 300 x 300 x 50 mm^3 with 60° -groove angle, 10 mm root face, 2 mm root gap and welded strong backs in the reverse side to restrain the specimen against any distortion. The weld build-up thickness a_w thereby becomes 40 mm. The applied specimen configuration hence complies with that denoted[3, 12] as the "NSC Y-Groove specimen", c.f., *Fig. 15*. The objective here was to evaluate the effect of heat input Q on cracking risk of multipass weld metals, since Q is presently not included either in the Yurioka's[3] or Okuda's[2] prediction method. Three levels of arc energy E: 1.5, 3.0 and 5.0 kJ/mm were therefore applied. With each arc energy, welding was made at two levels of interpass temperature T_i of 150 and 175°C chosen to produce cracked and crack-free weld metals, respectively. The required T_i values for cracked and crack free welds, at given levels of weld metal strength and hydrogen, were estimated according to the Yurioka-formula[3b] in *Appendix 1*.

The results of the Y-Groove cracking tests for SMAW welds made at NSC are shown in *Table 3a*. After welding was completed, a period of 48 h was waited before carrying out the metallographic examination. The possible existence and morphology of the cracks was confirmed from polished macrosamples of the longitudinally cut, full-thickness weld sections.

Post-test metallography revealed that none of the six test specimens showed any characteristic transverse weld metal hydrogen cracks. Thus, the results do not enable one to draw sound conclusions on the effect of heat input on WM hydrogen cracking susceptibility in the present case.

Table 3a. Y-Groove cracking tests for Nittetsu L-80 weld metals made at NSC, Japan, using elevated preheat/interpass temperatures.

Specimen	Weld Strength $R_{p0.2}/R_M$ (MPa)	Arc energy (kJ/mm)	Current (A)	Voltage (V)	Travel speed (cm/min)	H_D (ml/100 g DM IIW)	T_i (°C)	t_i (min ± min)	Total no of bead layers	Crack – No Crack
15-F	790/860	1.5	160	25	15.5	4.0	≥ 150	6 ± 6	43	NC
15-G		1.5	160	25	14.8	4.0	≥ 175	5 ± 5	43	NC
30-F	745/845	3.0	160	25	7.7	4.0	≥ 150	9 ± 4	24	NC
30-G		3.0	160	25	7.6	4.0	≥ 175	7 ± 2	24	NC
50-F	640/850	5.0	160	25	4.6	4.0	≥ 150	13 ± 4	15	NC
50-G		5.0	160	25	4.6	4.0	≥ 175	10 ± 3	15	NC

The second set of SMAW experiments comprised Y-Groove cracking tests made at VTT and using specimen dimensions identical to those of the NSC specimens[3, 12], c.f. *Fig. 15*. Again, the applied electrode was *Nittetsu L-80* which, according to the Osaka

University mercury method[13, 25], gave ≈ 3.8 ml/100 g DM (IIW) weld diffusible hydrogen in the as-received condition. Bead placement and welding sequence followed that undertaken at NSC. Constant arc energy of 3.0 kJ/mm was applied. The specimens were bolted tightly onto a table using clamps to ensure absolutely rigid conditions and negligible deformation during welding, as shown in *Fig. 19*.

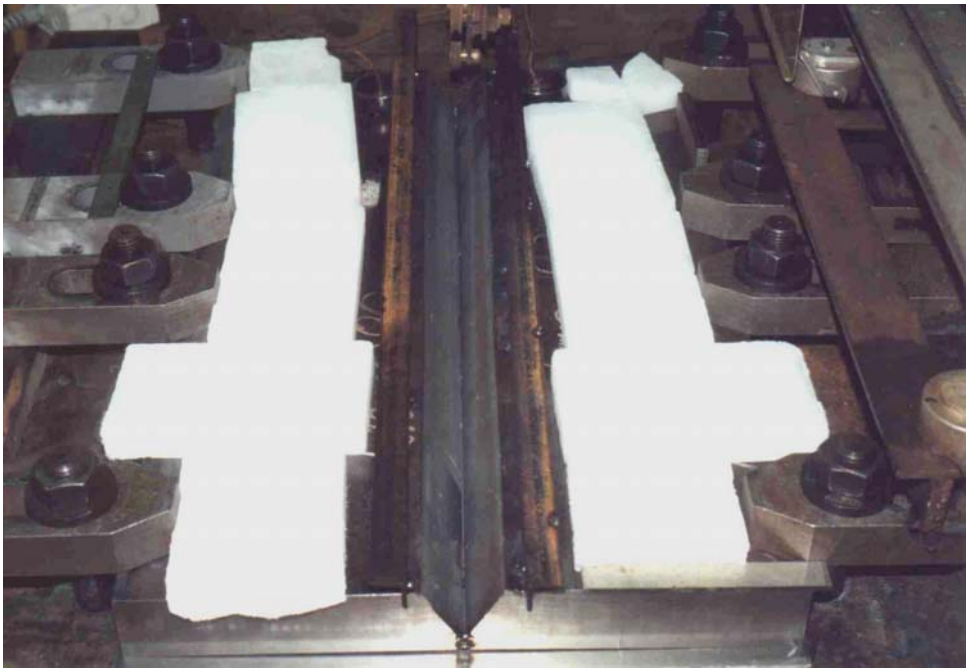

Fig. 19. Principles of specimen fixing and test conditions: bolted clamp fixtures and the arrangements for intensified cooling during welding using slices of solid CO_2.

Since none of the experiments at NSC and given in *Table 3a* revealed any characteristic WM hydrogen cracks, the testing conditions for the VTT Y-Groove cracking tests were deliberately made more severe by employing intensified cooling during welding. The use of intensified cooling during the time between each and every bead layer enabled to obtain low interpass temperatures T_i in conjunction with short interpass times t_i. Otherwise, this combination would have been impossible to achieve, e.g., under 'free' air-cooling conditions. Intensified cooling was done by coupling continuous blow of compressed air onto the specimen edges with crushes and slices of solid CO_2 placed onto the steel bars on the surface of the specimen. This enabled t_i values of around 3–4 min in the combination with $T_i \approx 70–100°C$ to be obtained The principles of fixing by bolted clamps and the cooling arrangements are shown in *Fig. 19*.

The results of the Y-Groove cracking tests for SMAW welds made at VTT are shown in *Table 3b*. After welding was completed, a period of 48 h was waited before carrying out the metallographic examination. The possible existence and morphology of the cracks

was confirmed from polished macrosamples of the longitudinally cut, full-thickness weld sections.

It can be seen that the experiments associated with the H_D levels of 3.8 and 10.9 ml/100 g DM (IIW) did not reveal any hydrogen cracks. This implies, in contrast to the earlier NSC data[12], SMAW multipass welds made using the *L-80* electrode and at weld hydrogen content of ≈ 4 ml/ 100 g DM (IIW) are not prone to hydrogen cracking, no matter how short is the interpass time t_i. The fact that *N2* did not reveal cracks is regarded surprising, as the earlier NSC Y-Groove tests have shown[12], the H_D contents of ≈ 6.7 and 10.4 ml/100 g DM (IIW) lead to hydrogen cracking of the *L-80* weld metal, see *Appendix 5*.

Table 3b. Y-Groove cracking tests for Nittetsu L-80 weld metals made at VTT using intensified cooling.

Specimen	L-80 Strength $R_{p0.2}/R_M$ (MPa)	Arc energy (kJ/mm)	Current (A)	Voltage (V)	Travel speed (cm/min)	H_D (ml/100 g DM IIW)	T_i (°C)	t_i (min ± sec)	Total no of bead layers	Crack / No Crack
N1	745/845	3.0	170	23–24	8	3.8	≤ 105	4 ± 25"	30	NC
N2	745/845	3.0	170	23–24	8	10.9	≤ 99	4 ± 31"	31	NC
N3	745/845	3.0	170	23–24	8	**13.2**	≤ 94	4 ± 05"	31	**C**

Next, weld hydrogen was raised further by performing moisturing of *Nittetsu L-80* under extreme conditions of 45°C / 95%. This eventually resulted in the appearance of characteristic transverse WM hydrogen cracks in *N3* associated with H_D of ≈13 ml/100 g DM (IIW), see *Table 3b*. Although being clearly visible in the X-ray examination, these cracks did not enter the weld surface, as did most of those cracks in the later experiments, see Sections 4.1.1.2 and 4.1.1.3. The morphology of the cracks was confirmed by metallographic examination of the longitudinally cut full-thickness weld sections. An example of transverse hydrogen crack recorded in the *N3* weld metal is presented in *Fig. 21*.

According to *Table 3b*, a weld H_D content as high as ≈ 13 ml/100 g DM (IIW) was required, before weld metal hydrogen cracking occurred in *Nittetsu L-80* weld metal of R_M ≈ 810 MPa.

4.1.1.2 Small-scale U-Groove tests

For the next stage of small-scale cracking tests, a rectangular-shape U-Groove specimen was designed at VTT Industrial Systems, acting as a modification of the NSC Y-Groove test. The intention of the U-Groove configuration was to reduce the total welding time, while maintaining the inherent severity of the test by ensuring sufficient rigidity of the specimen. The specimen size was 300 x 300/250 x 60 mm, the groove dimensions varying to some extent depending on the test. A U-groove having a depth of 25–30 mm and a width of 40–45 mm was adopted for specimens *U1–U11*, whilst for specimens *U12–U34* the depth and width both were 40 mm. The groove depth corresponds to the

weld build-up thickness a_w and could be varied independently of the specimen thickness. An example of the U-Groove specimen is shown in *Fig. 18*. The specimens were bolted tightly onto a table using clamps to ensure absolutely rigid conditions and negligible deformation during welding, c.f., *Fig. 19*.

Similarly to the VTT Y-Groove tests in Section 4.1.1.1, intensified cooling was used for the U-Groove experiments during the time between each and every bead layer, in order to deliberately raise severity of testing and to ensure low interpass temperature T_i and short interpass time t_i. Intensified cooling was done by coupling continuous blow of compressed air onto the specimen edges with crushes and slices of solid CO_2 placed onto the steel bars on the surface of the specimen. This enabled t_i values of around 3–4 min in the combination with $T_i \approx$ 70–100°C to be obtained The principles of fixing by bolted clamps and the cooling arrangements are shown in *Fig. 19*.

Measurements on the weld diffusible hydrogen content, H_D, applying the Osaka University mercury method[13, 25] confirmed that the use of re-dried, as-received and moistured electrodes produced weld H_D values in the range of 3 to19 ml/100 g DM (IIW).

After welding was completed, a period of 16 h was waited before carrying out the final NDT inspection to detect possible delayed hydrogen cracks. This time interval was in accordance with standard EN 1011-2 : 2001[1b]. Both ultrasonic examination and X-ray inspection were made. In the cases where NDT indications were found, the morphology of the cracks was confirmed by metallographic examination of the longitudinally cut full-thickness weld sections.

Additionally, occasional U-Groove cracking tests were conducted for the *OK 74.78* weld metals of $R_{p0.2} \approx$ 550 MPa otherwise as previously, but prolonging the period before the NDT inspection to 7 days (168 h) instead of the 16 h period. Since the cracking tendency of this particular weld metal appeared surprisingly low in the first phase of the programme[4], further testing was deemed necessary. This was to now ensure enough time for complete hydrogen diffusion, as the plate (and weld build-up) thickness were relatively great and the WM strength close to the lower end of the 'critical' range with respect to WM cracking risk.

The test matrix and the results of all the U-Groove cracking tests for the five SMAW weld metals made at VTT are given in *Table 4*. The U-series finally comprised 34 tests in total and was focused on *OK 48.08*, *OK 74.78*, *OK 75.75*, *Atom Arc 12018* and *OK 75.78* electrodes.

It can be seen that of the entire number of test welds in *Series U* associated with the 16–48 h period, only three sets of specimens exhibited characteristic transverse weld metal hydrogen cracks. These were: (i) *U11*, *U25*, *U26* and *U29* welded with *OK 75.75*, (ii) *U13*-*U17* & *U20* welded with *OK 75.78* and (iii) *U27*-*U30* welded with *Atom Arc 12018*. Thus, weld metal hydrogen cracking took place only in the case of the specimens welded with the electrodes of the highest strengths: *OK 75.75*, *OK 75.78* and *Atom Arc 12018* that produced weld metal strengths of $R_{p0.2} \approx$ 680, 880 and 890 MPa, respectively.

Table 4. U-*Groove cracking tests for SMAW weld metals made at VTT using intensified cooling.*

Specimen No	Filler Material	Arc energy (kJ/mm)	Current (A)	Voltage (V)	Travel speed (cm/min)	H_D (ml/100 g DM IIW)	T_i max. or range (°C)	t_i (min ± sec)	Total No of bead layers	Crack/ No Crack
	OK 48.08 : $R_{p0.2} \approx 455$ MPa, $R_M \approx 530$ MPa									
U6	OK 48.08	3.0	250	24	12	5.1	≤ 102	4 ± 02"	30	NC
U7	OK 48.08	3.0	250	24	12	6.8	≤ 97	4 ± 02"	24	NC
U9	OK 48.08	3.0	250	24	12	9.2	≤ 99	4 ± 01"	24	NC
U19	OK 48.08	3.0	250	24	12	10.8	≤ 97	3 ± 05"	39	NC
	OK 74.78 : $R_{p0.2} \approx 550$ MPa, $R_M \approx 650$ MPa									
U4	OK 74.78	3.0	250	24	12	5.4	≤ 108	4 ± 10"	27	NC
U5	OK74.78	3.0	250	24	12	5.5	≤ 101	4 ± 02"	24	NC
U12	OK74.78	3.0	250	24	12	13.5	≤ 108	3 ± 05"	39	NC
U8	OK74.78	3.0	250	24	12	15.1	≤ 100	4 ± 02"	24	NC
U34[*)]	OK74.78	2.0	250	23	17	15.5	57–74	4 ± 02"	56	NC
U33[*)]	OK74.78	3.0	250	24	12	**15.5**	90–107	4 ± 05"	37	**C**[*)]
U32[*)]	OK74.78	3.0	250	24	12	**17.6**	88–101	4 ± 05"	37	**C**[*)]
U31[*)]	OK74.78	3.0	250	24	12	**17.6**	91–107	4 ± 10"	39	**C**[*)]
U18	OK74.78	3.0	250	24	12	18.9	≤ 105	3 ± 05"	39	NC
	OK 75.75 : $R_{p0.2} \approx 680$ MPa, $R_M \approx 810$ MPa									
U1	OK 75.75	3.0	250	24	12	3.2	≤ 174	4 ± 40"	25	NC
U3	OK 75.75	3.0	250	24	12	3.2	≤ 105	4 ± 05"	30	NC
U2	OK 75.75	3.0	250	24	12	5.6	≤ 101	4 ± 15"	27	NC
U10	OK 75.75	3.0	250	24	12	6.2	77–105	10 ± 1"	27	NC
U29	**OK 75.75**	3.0	250	24	12	**10.1**	85–92	4 ± 02"	39	**C**
U11	**OK75.75**	3.0	250	24	12	**12.6**	≤ 97	4 ± 02"	27	**C**
U25	**OK75.75**	3.0	250	24	12	**14.3**	90–100	7 ± 10"	39	**C**
U26	**OK75.75**	3.0	250	24	12	**14.3**	100	15 ± 1"	39	**C**
	OK 75.78 : $R_{p0.2} \approx 885$ MPa, $R_M \approx 965$ MPa									
U21	OK 75.78	3.0	250	24	12	2.6	98–106	15 ± 1"	39	NC
U24	OK 75.78	3.0	250	24	12	2.8	70–83	10 ± 1"	39	NC
U23	OK 75.78	3.0	250	24	12	2.8	85–95	7 ± 10"	39	NC
U22	OK 75.78	3.0	250	24	12	3.3	101–110	15 ± 1"	39	NC
U20	**OK 75.78**	3.0	250	24	12	**4.3**	97–104	15 ± 1"	39	**C**
U13	**OK 75.78**	3.0	250	24	12	**5.1**	≤ 96	4 ± 02"	39	**C**
U14	**OK 75.78**	3.0	250	24	12	**5.1**	81–93	7 ± 10"	39	**C**
U15	**OK 75.78**	3.0	250	24	12	**5.1**	67–76	10 ± 1"	39	**C**
U17	**OK 75.78**	3.0	250	24	12	**5.1**	98–112	10 ± 1"	39	**C**
U16	**OK 75.78**	3.0	250	24	12	**5.1**	94–103	15 ± 1"	39	**C**
	Atom Arc 12018 : $R_{p0.2} \approx 890$ MPa, $R_M \approx 1020$ MPa									
U30	**Atom Arc**	3.0	250	23	12	**3.2**	95–101	4 + 2"	39	**C**
U28b	Atom Arc	3.0	250	24	12	3.4	80–94	4 ± 02"	39	NC
U28a	**Atom Arc**	3.0	250	24	12	**3.4**	80–94	4 ± 02"	39	**C**
U27	**Atom Arc**	3.0	250	24	12	**4.4**	83–96	4 ± 02"	39	**C**

[*)] : tests made applying a period of 168 h (7 days) before the final NDT inspection, otherwise 16 h period in accordance with EN 1011-2 : 2001[1b].

The results demonstrate that once a certain WM strength level is exceeded, the WM hydrogen cracking risk in multipass SMAW increases quite dramatically. For cracking to occur at the $R_{p0.2} \approx$ 680–690 MPa strength level, *OK 75.75* electrodes producing $H_D \geq 10$ ml/100 g DM (IIW) were required. To create cracking conditions for the extra-high strength *OK 75.78* and *Atom Arc 12018*, weld metals of $R_{p0.2} \approx$ 880–890 MPa exhibiting H_D of no more than 3–4 ml/100 g DM (IIW) were crack-sensitive enough. Not even re-drying of *Atom Arc 12018* did always guarantee crack-free welds at $H_D \approx 3.2$ ml/100 g DM (IIW), although it did so the case of *OK 75.78* welds. As an example, a photograph of characteristic transverse hydrogen crack found from the *U11* weld metal is shown in *Fig. 22*.

An interesting finding regarding the interpass time t_i was that whenever WM cracking took place, it did so irrespective of the interpass time t_i, even though t_i was varied over a range from 4 to 15 min. Accordingly, provided the other factors, i.e., strength and hydrogen, were not severe enough to provoke WM cracking, shortening t_i alone was not sufficient to create conditions for triggering the crack initiation event.

For the low strength *OK 48.08* weld metals of $R_{p0.2} \approx$ 480 MPa, it was impossible to create conditions severe enough to result in WM cracking with any practical hydrogen levels in the range of 5–11 ml/100 g DM (IIW).

In the case of *OK 74.48* welds of $R_{p0.2} \approx$ 550 MPa, the cracking behaviour was found to depend essentially on the applied period before the final NDT inspection. Using a period of 16 h, as required in EN 1011-2 : 2001[1b], it appeared impossible to create conditions severe enough to lead to WM hydrogen cracking at any of the applied hydrogen levels ranging from 3 to 19 ml/100 g DM (IIW). Contrary to this, all the experiments at 3.0 kJ/mm associated with a prolonged period of 168 h (7 days) resulted in WM Chevron c00racking, although not until at comparatively high weld hydrogen contents of 15.5–17.6 ml/100 g DM (IIW). Even in this series, however, a single cracking test, *U34*, otherwise similar to the others as regards to the electrode and weld hydrogen, but welded at 2.0 kJ/mm, appeared as crack-free despite a 7 days period and H_D of 15.5 ml/100 g DM (IIW), as shown in *Table 4*.

These plausible findings are perceived as indisputable evidence that the 16 h period, EN 1011-2 : 2001[1b] currently requires before final NDT inspection, does not always guarantee crack-free welds in the case of thick multiple-pass welds. In the present case, the 16 h period has obviously been inadequate to allow for complete hydrogen diffusion in the 550 MPa yield strength *OK 74.78* weld metals, hence resulting in WM hydrogen cracking after a remarkably long period of time.

4.1.1.3 Large-scale double-welded Y-Groove tests

To confirm the validity of small-scale tests in assessing the cracking risk of larger structures, a double-welded large-scale Y-Groove test specimen was specifically designed at VTT, pursuing to verify the small-scale test results. Groove geometry of the specimen was, as such, in accordance with the NSC Y-Groove experiments c.f. *Figs. 15* and *19*, except that the specimen was lengthened up to 800 mm. The weld build-up thickness a_w

and the plate thickness were 50 and 60 mm, respectively. Again, heavily bolted clamp fixtures were used to ensure structural rigidity, heavy restraint conditions and negligible distortion and deformations during welding.

The use of the *YDT* specimen allows the assessment of the cracking sensitivity of two different weld metals (made using two different consumables) in one single test specimen. To make the multipass test weld, about ½ of the groove length was deposited with the 1st electrode, whilst the remaining ½ specimen length was filled with another electrode. Besides the absolute cracking risk, this technique enabled also the assessment of the relative cracking risk between the two different weld metals under equivalent thermal and structural conditions. According to the literature[2, 3, 8, 12, 19, 67], the applied 800 mm specimen should provide sufficient weld length for the development of longitudinal residual stress σ_{resL} so as to finally achieve its maximum level, i.e., weld metal yield strength $R_{p0.2}$. The test matrix and the cracking test results for *Series YDT* are shown in *Table 5*.

Table 5. Double-welded Y-Groove cracking tests for SMAW weld metals made at VTT using intensified cooling.

Specimen	Filler Material 1st 2nd	Arc energy (kJ/mm)	Current (A)	Voltage (V)	Travel speed (cm/min)	H_D (ml/100 g DM IIW)	T_i (°C)	t_i (min ± sec)	Total No of bead layers	Crack / No Crack
Y-DT1	**OK75.75**	3.0	250	24	12	**13.5**	≤ 90	4 ± 02"	38	**C**
	OK74.78	3.0	250	24	12	13.5	≤ 90	4 ± 02"		NC
Y-DT2	OK74.78	3.0	250	24	12	18.9	≤ 81	3 ± 07"	38	NC
	OK48.08	3.0	250	24	12	8.8	≤ 81	3 ± 07"		NC

According to *Table 5*, the results of the double-welded Y-Groove cracking tests confirm the findings of the U-Groove tests shown in *Table 4*. Under similar weld hydrogen content and equivalent thermal and structural conditions, the extra-high strength Ni-Cr-Mo alloyed *OK 75.75* weld metal with $R_{p0.2} \approx 690$ MPa exhibited remarkably higher WM hydrogen cracking sensitivity than the lower-strength Mo-alloyed *OK 74.78* weld metal with $R_{p0.2} \approx 550$ MPa. As an example, a photograph of characteristic transverse hydrogen crack found from the *OK 75.75* weld metal in specimen *YDT1* is shown in *Fig. 20*.

Table 5 shows that even under most stringent conditions of $H_D = 18.9$ ml/100 g DM (IIW) and $t_i \approx 3$ min, hydrogen cracking did not occur in the *OK 74.78* weld metal, provided a 16 h period conforming to EN 1011-2 : 2001[1b] was applied. The results of double-welded large-scale Y-Groove tests are hence in accordance with the small-scale cracking test data.

Consequently, it is perceived, all the specimen and groove configurations studied in the present thesis yielded compatible results in terms of WM cracking sensitivity.

Fig. 20. Characteristic transverse weld metal hydrogen cracks found from the OK 75.75 weld metal side in specimen YDT1 (large-scale Y-Groove test, upper 2/3rds: electrode OK 75.75., lower 1/3rd: electrode OK 74.78).

4.1.1.4 Metallographic examination of crack morphologies

Metallographic investigation revealed that the extra-high strength weld metals: *Nittetsu L-80*, *OK 75.75*, *OK 75.78* and *Atom Arc 12018* with $R_{p0.2} \geq 690$ MPa exhibited transverse, or slightly curved, crack morphologies characteristic to hydrogen cold cracks associated[2, 3, 12, 19, 54, 74, 76, 100, 106] with high-strength multipass weld metals. As an example, a photograph of weld metal hydrogen cracks found from weld *N3* is shown in *Fig. 21*.

The cracks were found to having been initiated below the final weld bead layer. In most cases, they had entered the weld surface. Simultaneously, cracks had been propagating normal to the weld surface and grown vertically downwards into the approximately 1/3–1/2-depth of the weld build-up thickness a_w. As examples, photographs of WM hydrogen cracks found from welds *U11* and *YDT1* are shown in *Figs 20* and *22*, respectively.

Unlike in extra-high strength SMAW welds, transverse WM hydrogen cracks recorded from high-strength *OK 74.78* weld metals of $R_{p0.2} \approx 550$ MPa, did not enter the weld surface, even though they – as those in the extra-high strength WMs – had been initiated below the final weld layer. Instead of propagating normal to the weld surface in the weld thickness direction, these cracks tended to propagate at angle of about 45° downwards into the approximately 1/3–1/2-depth of the weld build-up thickness a_w. These cracks thereby exhibited a characteristic Chevron-type[54] morphology, see *Fig. 20*. As an example, a photograph of WM cracks found from weld *U31* and associated with the prolonged period of 168 h (7 days) before the NDT, is shown in *Fig. 23*.

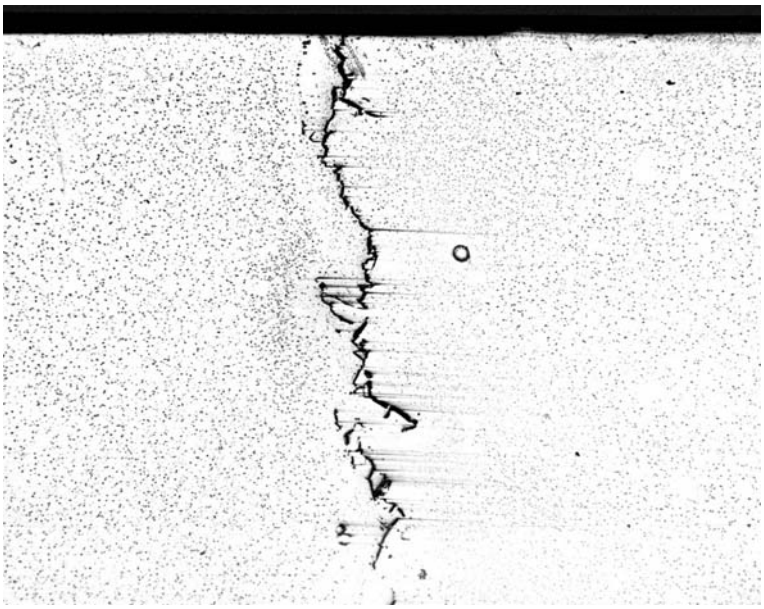

Fig. 21. Example of the morphology of transverse hydrogen crack recorded from the L-80 weld metal in specimen N3 (Y-Groove test, electrode: Nittetsu L-80) (25 x).

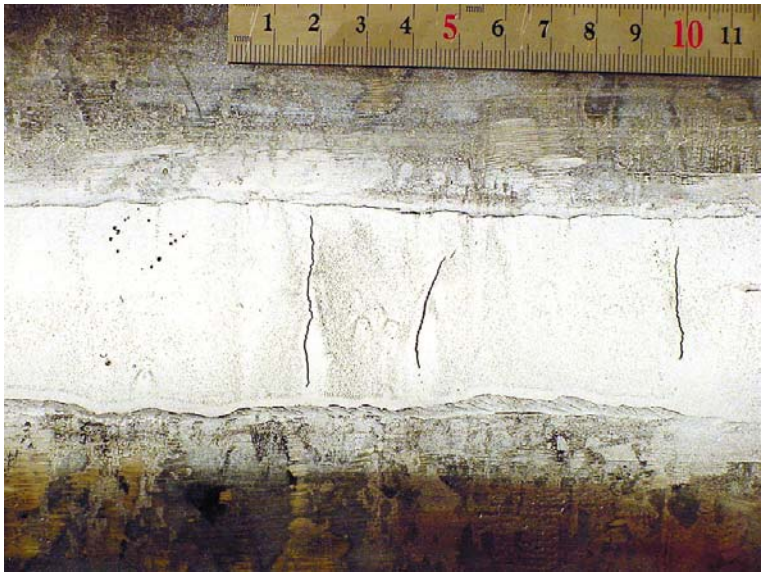

Fig. 22. Characteristic transverse weld metal hydrogen cracks recorded from the OK 75.75 weld metal in specimen U11 (U-Groove test, electrode: OK 75.75).

Fig. 23. Characteristic weld metal Chevron crack recorded from the OK 74.78 weld metal in specimen U31 associated with the period of 168 h (U-Groove test, electrode: OK 74.78).

4.1.2 Cracking tests for SAW thick plate weld metals

The SAW cracking test programme on thick plate weld metals consisted of (i) preliminary small-scale U-Groove cracking tests made at ESAB, Finland, (ii) a comparatively large set of small-scale U-Groove cracking tests made at ESAB, U.K., denoted as 'final test series' and designed according to the principles of the statistical Taguchi analysis, and (iii) complementary small-scale U-Groove cracking tests made at ESAB, U.K. and Mäntyluoto Works, Finland.

Of these, the preliminary SAW cracking tests in Item (i) were made under intensified cooling conditions similar to those for the SMAW experiments, aiming at defining lower-bound estimates of the boundary curve between Crack – No Crack regions with respect to strength and hydrogen. All the other cracking tests according to Items (ii) and (iii), in turn, employed elevated preheat/interpass temperatures, with the intention to determine 'safe' T_{cr} estimates.

4.1.2.1 Small-scale U-Groove tests

The SMAW cracking test data in *Tables 3–5* showed that all groove configurations and specimen types yielded practically compatible results in terms of the weld metal cracking sensitivity. One of the applied variants, i.e., the U-Groove test was therefore chosen for the entire SAW cracking experiments of the present study.

In the cases of preliminary SAW cracking experiments, the final SAW cracking test series, the complementary tests at ESAB, U.K. and the complementary tests at Mäntyluoto Works, Finland, the U-Groove specimen sizes were 500 x 500 x 60 mm, 500 x 500 x 70 mm, 500 x 500 x 70 mm and 510 x 800 x 60 mm, respectively, c.f. *Fig. 18* on page 76. A rectangular U-groove having a depth and width of 40 mm was used constantly, apart from the specimen thickness and size. The fixing arrangements of specimens, as well as the NDT inspections and routines were similar to those applied for the SMAW U-Groove tests and described in Section 4.1.1.2. The minimum period before final NDT inspection was 16 h in accordance with EN 1011-2 : 2001[1b].

Table 6. Preliminary U-Groove cracking tests for SAW weld metals at ESAB, Finland, using intensified cooling.

Specimen No	SAW wire/ OK Flux 10.62	Arc energy (kJ/mm)	Current (DC+) (A)	Voltage (V)	Travel speed (cm/min)	H_D (ml/100 g DM IIW)	T_i range (°C)	t_i (min ± sec)	Total no of layers	Crack / No Crack
	$R_{p0.2} \approx 530$ MPa, $R_M \approx 620$ MPa									
SU1	OK 15.24S	5.0	570	32	22	6.2	125–155	4 ± 05	20	NC
	$R_{p0.2} \approx 580$ MPa, $R_M \approx 670$ MPa									
SU4	**OK 15.26S**	4.0	610	37.5	34	**13.6**	93–105	7 ± 05	31	**C**
	$R_{p0.2} \approx 760$ MPa, $R_M \approx 825$ MPa									
SU2	**OK 15.27S**	4.0	620	37.5	35	**7.2**	71–82	7 ± 05	30	**C**
SU3	**OK 15.27S**	4.0	620	37.5	35	**9.1**	71–96	7 ± 05	30	**C**

The test matrix and results of preliminary SAW U-Groove cracking tests are shown in *Table 6*. Of the experiments, specimens *SU4*, and *SU2* and *SU3*, welded with high-strength *OK Tubrod 15.26S* and extra-high strength *OK Tubrod 15.27S* tubular wires, respectively, exhibited characteristic transverse WM hydrogen cracks. The cracks in *SU4*, *SU2* and *SU3* were associated with weld diffusible H_D of 13.6, 7.2 and 9.1 ml/100 g DM (IIW), respectively. Contrary to these, specimen *SU1* welded with a lower strength *OK Tubrod 15.24S* tubular wire was found crack-free.

Test matrix and results of the final SAW U-Groove cracking test series made at ESAB, U.K., are shown in *Table 7*. The objective here was to design a test matrix according to the principles of a statistical Taguchi analysis. Consequently, for each of the three weld metal strength classes, 3 variables (i) arc energy, (ii) preheat/interpass temperature and (iii) weld hydrogen content, were taken, all them at three separate levels, as shown in *Table 7*.

Table 7. Final U-Groove cracking tests for SAW weld metals at ESAB, U.K. and using elevated preheat/interpass temperatures.

Specimen No	SAW wire/ OK Flux 10.62	Arc energy (kJ/mm)	Current (DC+) (A)	Voltage (V)	Travel speed (cm/min)	H_D (ml/100 g DM IIW)	T_i range (°C)	t_i (min ± min)	Total no of layers	Crack / No Crack
	$R_{p0.2} \approx 580$ MPa, $R_M \approx 670$ MPa									
395	OK 15.26S	2.0	550	30	50	4.9	100–115	5	42	NC
593	OK 15.26S	2.0	550	30	50	4.9	93–109	5 ± 2	46	NC
396	OK 15.26S	3.0	550	30	33	6.1	125–132	5 + 4	31	NC
397	OK 15.26S	4.7	550	30	21	8.4	133–152	7 ± 1	20	NC
	$R_{p0.2} \approx 760$ MPa, $R_M \approx 825$ MPa									
398	**OK 15.27S**	2.0	550	30	50	**6.1**	144–157	5	45	**C**
399	**OK 15.27S**	3.4	550	30	29	**8.4**	82–111	7 – 2	28	**C**
400	**OK 15.27S**	4.0	550	30	25	**4.9**	124–135	7 + 1	21	**C**
594	**OK 15.27S**	5.0	550	30	20	**4.9**	121–138	7 + 6	20	**C**
	$R_{p0.2} \approx 890$ MPa, $R_M \approx 960$ MPa									
401	**OK 15.29S**	2.0	550	30	50	**8.4**	105–129	5 + 1	44	**C**
402	**OK 15.29S**	3.0	550	30	33	**4.9**	143–160	5 + 4	28	**C**
403	**OK 15.29S**	4.0	550	30	25	**6.1**	93–116	7 + 2	20	**C**

According to *Table 7*, two essential observations are perceived. Firstly, the risk of transverse weld metal hydrogen cracking is seen to increase dramatically with WM strength, particularly for welds made with *OK Tubrod 15.27S* and *OK Tubrod 15.29S* exhibiting nominal yield strengths of $R_{p0.2} \geq 700$ MPa. This is in line with the results of the SMAW U-Groove and preliminary SAW U-Groove experiments, compare *Tables 4*, *6* and *7*. Overall, the results demonstrate that for the extra-high strength weld metals of $R_{p0.2} \geq 700$ MPa, H_D levels of about 5 ml/100 g DM (IIW) and above are high enough to provoke cracking, even though moderate interpass temperatures of 125–150°C are employed. At lower WM yield strengths of $R_{p0.2} \leq 580$ MPa, weld H_D levels above 10 ml/100 g DM (IIW) seem to be necessary in order to create critical conditions for inducing WM cracking.

What is more surprising is that whilst all the 7 specimens welded with *OK Tubrod 15.27S* and *OK Tubrod 15.29S* displayed characteristic WM transverse hydrogen cracks, none of the 4 specimens welded with *OK Tubrod 15.26S* revealed any cracks. Consequently, whether WM cracking did, or did not, occur, both these phenomena took

place totally irrespective of the other parameters: weld hydrogen, arc energy and preheat/interpass temperature.

For quantitative assessment of the cracking tendency, sc. 'severity grading' was defined for each weldment on the basis of NDT magnetic inspection, ultrasonic inspection and X-ray examination, all performed at Rautaruukki Oyj, Finland. These grades are given in *Table 8*.

According to *Table 8*, 'cracking severity grading' seems not to have any unified relation to the WM cracking conditions in terms of weld hydrogen or preheat/interpass temperature. For instance, test *No 5* (weld 399) with the highest H_D content and the lowest T_i level among the *OK Tubrod 15.27S* weld metals, did not display the correspondingly high severity grading, but rather the opposite. The only noticeable trend is that, in general, *OK Tubrod 15.29S* weld metals show higher severity grading than *OK 15.27S* weld metals. Thus, the WM strength is, again, found to affect the cracking susceptibility, whilst the severity grading seemed practically insensitive to hydrogen, interpass temperature and heat input.

Table 8. Final SAW U-Groove cracking tests at ESAB, U.K., using intensified cooling.

Test	Weld No	SAW Filler Wire / OK Flux 10.62	Weld hydrogen level*) (ml/100 g DM IIW)	Arc energy (kJ/mm)	Interpass temperature (°C)	Crack – No Crack	Cracking Severity Grading**)
1	U395	OK Tubrod 15.26S	4.9 (7)	2.0	100	NC	0
2	U396	OK Tubrod 15.26S	6.1 (10)	3.0	125	NC	0
3	U397	OK Tubrod 15.26S	8.4 (15)	4.0	150	NC	0
4	**U398**	**OK Tubrod 15.27S**	**6.1** (10)	2.0	150	**C**	5 ; 8
5	**U399**	**OK Tubrod 15.27S**	**8.4** (15)	3.0	100	**C**	4 ; 5
6	**U400**	**OK Tubrod 15.27S**	**4.9** (7)	4.0	125	**C**	2 ; 8
7	**U401**	**OK Tubrod 15.29S**	**8.4** (15)	2.0	125	**C**	6 ; 8
8	**U402**	**OK Tubrod 15.29S**	**4.9** (7)	3.0	150	**C**	7 ; 9
9	**U403**	**OK Tubrod 15.29S**	**6.1** (10)	4.0	100	**C**	3 ; 9
10	U593	OK Tubrod 15.26S	4.9 (7)	2.0	100	NC	0
11	**U594**	**OK Tubrod 15.27S**	**4.9** (7)	4.0	125	**C**	5 ; 9

*) : measured values confirmed; target levels defined according to flux humidity and given in brackets ()

**) : 1st value: defect density index, 2nd value: defect depth index; scale from 1 (least severe) to 10 (most severe)

Table 9 shows the results of complementary SAW U-Groove cracking tests for *OK Tubrod 15.27S* and *Tubrod 15.29S* weld metals made at ESAB, U.K. and Mäntyluoto Works, Finland, respectively. As the cracking sensitivity of these two weld metals appeared particularly intense, the complementary experiments aimed at finding 'safe' preheat/interpass temperatures for both grades at a constant weld hydrogen level. Here, it was felt realistic to choose hydrogen levels commonly faced with SAW in practice welding fabrication, i.e., ≈ 4–7 ml/100 g DM (IIW).

Table 9. Complementary U*-Groove cracking tests for SAW weld metals at ESAB, U.K. & Mäntyluoto Works, Finland, and using elevated preheat/interpass temperatures.*

Specimen No	SAW wire/ OK Flux 10.62	Arc energy (kJ/mm)	Current (DC+) (A)	Voltage (V)	Travel speed (cm/min)	H_D (ml/100 g DM IIW)	T_i range (°C)	t_i (min ± min)	Total no of layers	Crack – No Crack
	$R_{p0.2} \approx 760$ MPa, $R_M \approx 825$ MPa									
U907	**OK 15.27S**	2.0	550	30	50	**6.5**	114–132	5 + 0.5	46	**C**
U908	**OK 15.27S**	2.0	550	30	50	**6.5**	168–183	5 + 2	42	**C**
U905	**OK 15.27S**	2.0	550	30	50	**6.5**	189–203	4 ± 2	45	**C**
U906	**OK 15.27S**	2.0	550	30	50	**6.5**	218–233	4 + 0.5	45	**C**
U144	**OK 15.27S**	2.0	550	30	50	**6.5**	243–254	3 + 1	45	**C**
	$R_{p0.2} \approx 890$ MPa, $R_M \approx 960$ MPa									
MW1	**OK 15.29S**	4.0	550	30	25	**6.0**	250–253	7 ± 2	23	**C**
MW3	**OK 15.29S**	4.0	550	30	25	**6.0**	275–278	6 ± 3	25	**C**
MW4	OK 15.29S	4.0	550	30	25	6.0	285–288	6 ± 3	25	NC
MW2	OK15.29S	4.0	550	30	25	6.0	300–305	6 ± 3	24	NC

It can be seen that, at the applied weld H_D of 6.0–6.5 ml/100 g DM (IIW), the levels of 'safe' preheat/interpass temperature for the *OK Tubrod 15.27S* and *Tubrod 15.29S* weld metals lie above 250°C and around 285–300°C, respectively. Even considering the comparatively high strength of these two SAW weld metals, the recorded preheat/interpass temperatures required for crack-free welds appeared somewhat higher than anticipated previously.

4.1.2.2 Metallographic examination of crack morphologies

In accordance with SMAW, metallographic investigation revealed that the extra-high strength SAW weld metals: *OK Tubrod 15.27S and OK Tubrod 15.29S* with $R_{p0.2} \geq 760$ MPa exhibited transverse, or slightly curved, crack morphologies characteristic to hydrogen cold cracks associated[2, 3, 12, 19, 54, 74, 76, 100, 106] with high-strength multipass weld metals.

As in the case of SMAW, the cracks in the SAW weld metals were found to initiate below the final weld bead layer. In the majority of the examined SAW welds that revealed hydrogen cracks, they had grown towards, and were finally entering, the weld surface. Simultaneously, these cracks had been propagating normal to the weld surface in the weld thickness direction and finally grown vertically into the approximately ½-depth of the weld build-up thickness a_w.

For the welds associated with the lowest H_D of 4.9 ml/100 g DM (IIW), however, this was not the case and the cracks tended to be sub-surface cracks, either remaining immediately beneath the final filling layer, or growing downwards into the approximately ½-depth of the weld build-up thickness a_w.

As examples, photographs of transverse WM hydrogen cracks exhibiting the crack orientation of 'straight vertical propagation in the weld thickness direction' are shown for *OK Tubrod 15.27S and OK Tubrod 15.29S* weld metals in *Figs 24a* and *24b*,

respectively. Example photographs of transverse WM hydrogen cracks exhibiting a ‘staircase patter’ along its path of propagation into the weld thickness direction are shown for *OK Tubrod 15.27S and OK Tubrod 15.29S* weld metals in *Figs 25a* and *25b*, respectively. Example photographs of transverse WM hydrogen cracks locating immediately below the final filling layer as sub-surface cracks and associated with low weld hydrogen contents are shown for *OK Tubrod 15.27S and OK Tubrod 15.29S* weld metals in *Figs 26a* and *26b*, respectively.

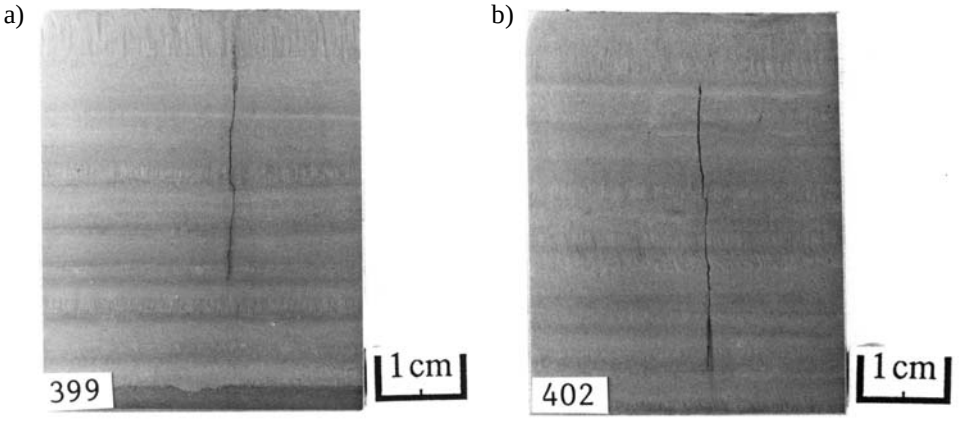

Fig. 24. Examples of characteristic transverse weld metal hydrogen cracks exhibiting the morphology of ‘straight vertical propagation into weld thickness direction’, recorded from (a) OK Tubrod 15.27S and (b) OK Tubrod 15.29S weld metals in specimens U399 and U402, respectively (U-Groove test).

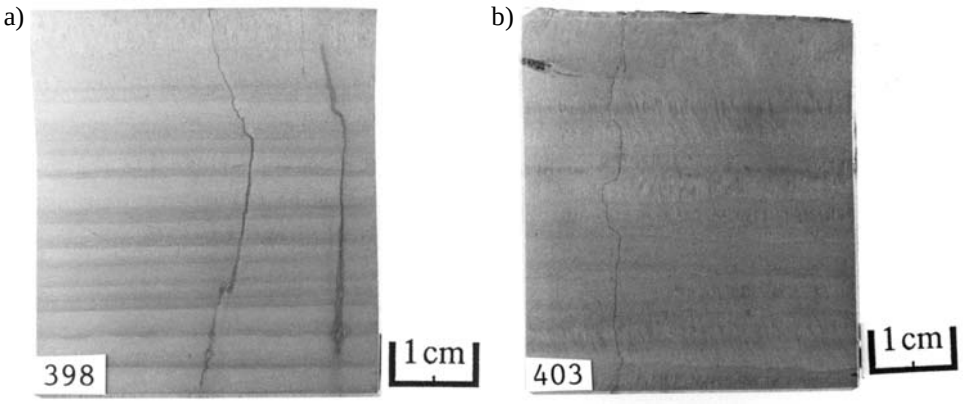

Fig. 25. Examples of characteristic transverse weld metal hydrogen cracks exhibiting the morphology of a ‘staircase patter’ along its path of propagation into weld thickness direction, recorded from (a) OK Tubrod 15.27S and (b) OK Tubrod 15.29S weld metals in specimens U398 and U403, respectively (U-Groove test).

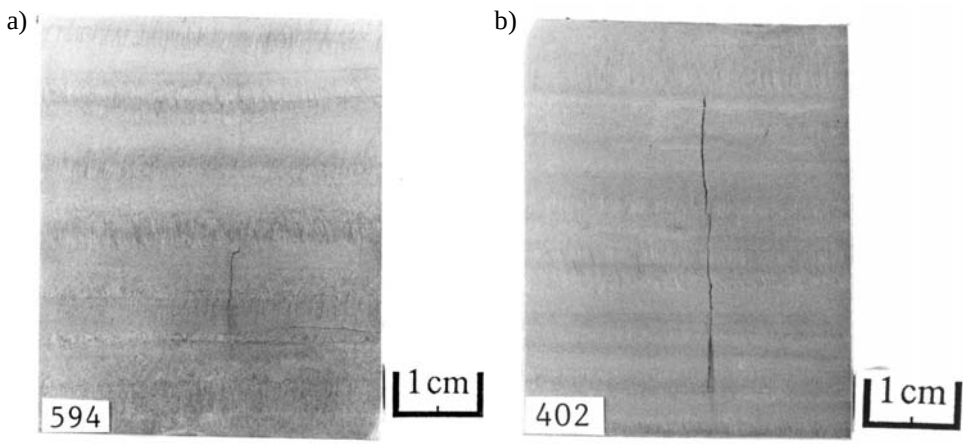

Fig. 26. Examples of transverse weld metal hydrogen cracks exhibiting a sub-surface appearance, i.e., cracks locating immediately below the final filling layer as sub-surface cracks and associated with low weld hydrogen contents, recorded from (a) OK Tubrod 15.27S and (b) OK Tubrod 15.29S weld metals in specimens U594 and U402, respectively (U-Groove test).

In one case, transverse WM hydrogen cracks were recorded also from the 'moderate strength' *OK Tubrod 15.26S* weld metals of $R_{p0.2} \approx 580$ MPa, however, this was associated with high weld H_D of 13.6 ml/100 g DM (IIW) in specimen *SU4*, see *Table 6*. Unlike in extra-high strength SAW welds, cracks in the *OK Tubrod 15.26* weld metal in *SU4* did not enter the weld surface, although they were revealed to having been initiated below the final filling layer. Instead of propagating normal to the weld surface, these cracks had propagated at angle of 45° in the weld thickness direction and into the approximately ½-depth of the weld build-up thickness a_w. These cracks were hence similar to those found from the SMAW in the case of *OK 74.78* weld metal having $R_{p0.2} \approx 550$ MPa, and exhibited a Chevron-type[54] morphology. As an example, photographs of WM cracks found from the weld *SU4* are shown in *Figs 27a* and *27b*.

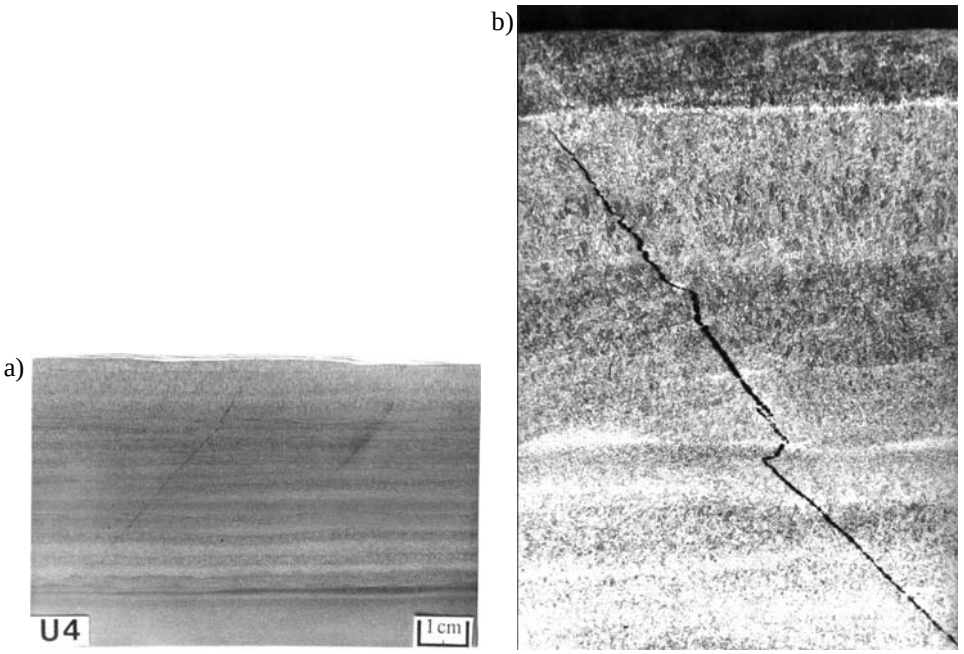

Fig. 27. Characteristic weld metal Chevron crack recorded from the OK Tubrod 15.26S weld metal in specimen SU4 and associated with high weld hydrogen (a) macrograph, (b) microstructure (U-Groove test).

4.1.3 Comparative cracking tests for welds in thin plate

As comparative tests to heavy plate multiple-pass welds, a separate set of V-Groove cracking tests were conducted for two-pass weld metals in a thin plate. The experiments were made on SMAW and SAW weld metals using *OK Tubrod 15.27S* tubular wire and *OK 75.75* electrode, respectively, in accordance with the consumable characteristics in *Table 2* on p. 73.

For the V-Groove cracking tests, 6 mm thick plate specimens were applied. The specimen size was 500 x 500 x 6 mm. The V-Groove preparation employed here had 60°-groove angle and no root face, which made the adoption of a separate root backing necessary. Welding was done as one-side welding using 2 passes, one pass per layer. Intensified cooling similar to that in the case of thick plate experiments was applied for the SMAW experiments, however, in the case of SAW experiments the hydraulic fixtures of the SAW equipment prevented the appropriate placement of any slices of CO_2 ice onto test specimens.

The intention here was to examine the dependency of the WM cracking risk on plate and weld build-up thickness a_w under equivalent strength and hydrogen in relation to

thick multipass welds. The results of the V-Groove cracking experiments are summarised in *Table 10*.

Table 10. Comparative SAW and SMAW V-Groove cracking tests for 6 mm thick specimens made at VTT and HUT, using intensified cooling and air cooling in the case of SMAW and SAW experiments, respectively.

Specimen No	SAW wire / OK Flux 10.62	Arc energy (kJ/mm)	Current (A)	Voltage (V)	Travel speed (cm/min)	H_D (ml/100 g DM IIW)	T_i max (°C)	t_i (min ± sec)	Total no of layers	Crack – No Crack
SMAW	$R_{p0.2}$ ≈ 680 MPa, R_M ≈ 810 MPa									
T-1	OK 75.75	1.3	108	23	12	14.4	68–74	4 ± 02"	2	NC
T-2	OK 75.75	1.3	108	23	12	9.2	69–76	4 ± 02"	2	NC
SAW	$R_{p0.2}$ ≈ 700 MPa, R_M ≈ 820 MPa									
S-1	OK 15.27S	1.9	580	28	50	16.0	60–65	4 ± 15"	2	NC
S-2	OK 15.27S	1.9	580	28	50	16.0	63–66	4 ± 15"	2	NC

It can be seen that none of the SMAW or SAW experiments made using thin plate two-pass welded V-Groove specimens resulted in transverse WM hydrogen cracks at any of the applied weld hydrogen contents ranging from H_D ≈ 9.2–16.0 ml/100 g DM (IIW).

In this respect, the risk of WM hydrogen cracking, at a comparable level of weld metal strength and weld hydrogen, is found significantly less for the 6 mm weld build-up thickness in thin plate than in the case of a 40 mm weld build-up thickness in heavy plate multiple-pass welds, compare *Table 10* to *Tables 2–9*.

4.2 All-weld metal tensile properties

Tensile testing was carried out for the SMAW multipass weld metals at room temperature in accordance with SFS-EN 10002-1. The intention was to measure the all-weld metal properties; consequently, round-bar specimens (∅ 7 mm) according to SFS 3471 were used. The specimens were extracted from the final weld beads of the filling layers. Summary data of the tensile test results for all the SMAW specimens are given in *Table 11*.

All welds were made using an 'equivalent' arc energy level of 3.0 kJ/mm[4], meaning that the actual arc energy values for multiple-pass weld metal pads and bevel groove butt welds were adjusted to yield equable weld cooling conditions in terms of weld $t_{8/5}$. Thus, 2.4 kJ/mm arc energy in the *OU* experiments accrues from the bead-on-plate like conditions for the weld metal pads, whereas 3.0 kJ/mm was applied in the *VTT* experiments that were made using a bevel groove preparation. A lower arc energy was used to compensate a somewhat lower weld cooling rate $t_{8/5}$ in bead-on-plate like welding (shape factor: $F \approx 1.0$) of multiple-pass pads, compared with welding into a bevel V-groove (shape factor: $F \approx 0.8$). All the test results are therefore regarded comparable in this sense. A more detailed description has been given elsewhere[4].

Table 11. Summary of the tensile test data for the experimental SMAW multipass weld metals.

Specimen code	Filler material (Electrode)	Arc energy E (kJ/mm)	Yield strength $R_{p0.2}$ (MPa)	Tensile strength R_M (MPa)	Elongation A_5 (%)
OU1	OK 48.08 (Ni)	2.4	455	525	27.9
OU1.1		2.4	456	530	33.4
VTT3-5		2.4–3.2	503	578	30.5
VTT1	OK 74.78 (Mo)	3.0	550	650	18.1
OU2		2.4	470	590	22.3
OU2.1		2.4	541	624	30.1
VTT6-8		2.4–3.2	552	640	30.1
VTT2	OK 75.75 (Ni-Cr-Mo)	3.0	680	810	14.6
OU3		2.4	680	780	17.4
OU3.1		2.4	718	818	22.3
NSC15	Nittetsu L-80 (Ni-Cr-Mo)	1.5	790	860	17.7
NSC30		3.0	745	845	19.9
NSC50		5.0	640	850	17.5
OU4	OK 75.78 (Ni-Cr-Mo)	2.4	883	963	19.6
VTT9-11	Atom Arc 12018 (Ni-Cr-Mo)	1.6–3.2	890	1022	19.2

4.3 Weld metal hardness and chemical composition

Weld metal hardness survey was carried out for (i) SMAW weld metals representing the cracking test welds, (ii) a set of SMAW multiple-pass weld metal pads made with different arc energies, (iii) preliminary SAW cracking test welds associated with high arc energies, and (iv) the final SAW cracking test series made using different arc energies and elevated preheat/interpass temperatures.

The *NSC* and *VTT* specimens[4, 5b] were extracted from the actual SMAW Y- and U-groove cracking test welds, respectively, made at 3.0 kJ/mm arc energy. The *OU* specimens[4, 5b] were made as bead-on-plate like SMAW multiple-pass pads ($F \approx 1.0$) using 2.4 kJ/mm arc energy adjusted to yield weld $t_{8/5}$ cooling time equivalent to that associated with the bevel groove preparation ($F \approx 0.8$) in the *NSC* and *VTT* experiments[4, 5b]. In addition, SMAW pads were made using three arc energy levels: 1.6, 2.4 and 3.2 kJ/mm, to reveal the influence of arc energy on weld metal hardness.

The *SU* and *U* specimens were extracted from the preliminary and final SAW U-groove multipass cracking tests welds, respectively, made at various arc energies and, in the case of the latter test series, using also different preheat/interpass temperatures. The preliminary SAW cracking test welds were associated with high arc energies of 4.0–5.0 kJ/mm and were made applying a constant preheat/interpass temperature, see *Table 6*. The final SAW U-groove cracking test welds, in turn, were associated with three different levels of arc energy: 2.0, 3.0 and 4.0 kJ/mm and under preheat/interpass temperatures of 100, 125 and 150°C.

Table 12. Summary of weldability indexes, P_{cm}, CET, *and weld metal Vickers hardness values* HV_5 *for the SMAW weld metals at different arc energy levels.*

Specimen No	SMAW Electrode	Arc energy (kJ/mm)	P_{cm} (%)	CET (%)	HV_{ave} as-welded/ reheated	HV_{max} (HV)
NSC15	Nittetsu L-80	*1.5*	0.233	0.325	*317*	*342*
VTT1.6		1.6	0.201	0.294	286 / 296	303
VTT2.4		2.4	–	–	269 / 270	290
NSC30		*3.0*	0.235	0.325	*304*	*319*
VTT3.2		3.2	0.215	0.313	261 / 260	268
NSC50		*5.0*	0.232	0.321	*291*	*301*
VTT1/1.6	OK 74.78	1.6	0.156	0.232	235 / 216	239
VTT1/2.4		2.4	0.155	0.232	234 / 218	237
VTT-U20		3.0	0.160	0.225	–	–
OU2		2.4	0.165	0.237	215	230
VTT1		3.0	0.163	0.238	217	232
VTT1/3.2		3.2	0.155	0.232	219 / 191	225
VTT2/1.6	OK 75.75	1.6	0.222	0.324	295 / 287	308
VTT2/2.4		2.4	0.221	0.322	292 / 281	299
OU3		2.4	0.222	0.321	271	281
VTT2		3.0	0.214	0.308	269	279
VTT2/3.2		3.2	0.216	0.316	276 / 273	280
T-1		1.3	0.180	0.254	273	280
VTT3/1.6	OK 48.08	1.6	0.136	0.192	208 / 185	216
VTT3/2.4		2.4	0.131	0.186	215 / 185	221
VTT-U7		3.0	0.129	0.182	–	–
OU1		2.4	0.132	0.183	189	209
VTT3		3.0	–	–	–	–
VTT3/3.2		3.2	0.127	0.182	198 / 179	204
VTT4/1.6	Atom Arc	1.6	0.286	0.410	353 / 353	362
VTT4/2.4	12018	2.4	0.281	0.402	337 / 358	365
VTT4		3.0	0.294	0.416	–	–
VTT4/3.2		3.2	0.275	0.399	325 / 326	338
VTT5/1.6	OK75.78	1.6	0.287	0.434	(256) / 330	351
VTT5/2.4		2.4	0.277	0.411	335 / 342	351
OU4		3.0	0.273	0.408	–	–
VTT5/3.2		3.2	0.256	0.390	326 / 332	338

* specimens VTT1-VTT5 : VTT Y-groove cracking tests: 3.0 kJ/mm
* specimens VTT-U7, VTT-U20 : VTT U-groove cracking tests: 3.0 kJ/mm
* specimens OU1-OU5 : OU multiple-pass welded pads: 2.4 kJ/mm
* specimens NSC15, NSC30 and NSC50 : NSC Y-groove cracking tests: 1.5, 3.0 and 5.0 kJ/mm
* specimens VTT1/1.6-VTT5/1.6 : VTT multiple-pass welded pads: 1.6 kJ/mm
* specimens VTT1/2.4-VTT5/2.4 : VTT multiple-pass welded pads: 2.4 kJ/mm
* specimens VTT1/3.2-VTT5/3.2 : VTT multiple-pass welded pads: 3.2 kJ/mm
* specimen T-1 : VTT V-groove cracking tests: 2-pass welded thin plate

Tables 12 and *13* summarise the results of Vickers hardness traverses (HV_5) and associated weldability indexes (P_{cm}, CET) for the SMAW and SAW multipass weld metals, respectively. The Vickers hardness profiles were measured from the filling layers

of the SMAW and SAW welds. Both as-welded and re-heated weld metal microstructures were examined in order to reveal possible differences in their hardenability. The chemical composition of all-weld metals was determined using *optical emission spectroscopy*. Using these analysis data, P_{cm} and CET were calculated for the SMAW and SAW weld metals applying the following formulae:

$$P_{cm} = C + Si/30 + (Mn + Cu + Cr)/20 + Ni/60 + Mo/15 + V/10 + 5 \quad (43a)$$

$$CET = C + (Mn + Mo)/10 + (Cr + Cu)/20 + Ni/40 \quad (43b)$$

Table 13. Summary of weldability indexes, P_{cm}, CET, *and weld metal Vickers hardness values* HV_5 *for the SAW weld metals at different arc energy levels.*

Specimen No	SAW tubular wire/ Flux OK 10.62	Arc energy (kJ/mm)	P_{cm} (%)	CET (%)	HV_{ave} (HV) As-welded/ Re-heated	HV_{ave} (HV) All regions	HV_{max} (HV)
SU1	OK Tubrod 15.24S	5.0	0.172	0.263	225	225	235
SU4	OK Tubrod 15.26S	4.0	0.205	0.302	237 / 235	234	241
SU2	OK Tubrod 15.27S	4.0	0.256	0.382	–	313	334
SU3	OK Tubrod 15.27S	4.0	0.258	0.383	–	312	335
U395	OK Tubrod 15.26S	2.0	0.227	0.333	273 / 258	265	277
U593	OK Tubrod 15.26S	2.0	0.238	0.345	265 / 262	264	277
U396	OK Tubrod 15.26S	3.0	0.226	0.334	252 / 256	251	262
U397	OK Tubrod 15.26S	4.7	0.216	0.322	251 / 254	249	262
U398	OK Tubrod 15.27S	2.0	0.264	0.396	313 / 310	315	336
U399	OK Tubrod 15.27S	3.4	0.258	0.388	328 / 333	313	367
U400	OK Tubrod 15.27S	4.0	0.271	0.402	303 / 326	315	345
U594	OK Tubrod 15.27S	5.0	0.265	0.387	334 / 353	348	362
S-1	OK Tubrod 15.27S	1.9	0.210	0.341	–	257	266
U401	OK Tubrod 15.29S	2.0	0.271	0.399	348 / 341	345	367
U402	OK Tubrod 15.29S	3.0	0.273	0.402	347 / 331	339	362
U403	OK Tubrod 15.29S	4.0	0.283	0.419	336 / 373	354	376

* specimens No SU1-SU4 : preliminary SAW U-groove cracking tests at ESAB, Finland
* specimens No U395-U403 and U593-U594 : final SAW U-Groove cracking tests at ESAB, U.K.
* specimen No S-1 : SAW V-Groove cracking tests: 2-pass welded thin plate made at HUT & VTT, Finland

Comparing the data in *Tables 12* and *13* reveals that the SAW *Tubrod 15.27S* weld metals having nominal yield strength $R_{p0.2} \approx$ 690–700 MPa exhibit somewhat higher hardness, as well as greater P_{cm} and CET values than, for instance, the SMAW *OK 75.75* weld metals of true $R_{p0.2} \approx$ 690 MPa. Presumably, this explains why, at the similar level of apparent strength, the SAW weld metals are seen to exhibit WM hydrogen cracking at considerably lower weld hydrogen contents than the corresponding SMAW welds, as shown in *Tables 4*, *5*, *6* and *7*.

4.4 Residual stresses in weld metal

Weld residual stress measurements were carried out for multipass SMAW thick welds applying a *Ring-Core method.* The method uses a drilling tool that enables stresses below the weld surface to be recorded in steps of ≈ 5 mm through the whole weld depth, if necessary. The stresses are measured using strain gauges placed into a drilled hole in a way that the relaxation of stresses caused by material removal, as the hole is machined, is recorded as micro-strains and converted to stresses applying mathematical algorithms. The Ring-Core method was regarded advantageous in view that the weld longitudinal tensile residual stress that was of primary interest here, have been shown[19,20,23] to reach its maximum at a depth of about 10–25% from the plate surface.

The principles of the Ring-Core method are shown in *Appendix 3*. The measurements were made on two 40 mm thick Y-*Groove* cracking test specimens *HL40* and *HL402*, c.f., *Figs 15* and *22*, having the weld lengths of 300 and 800 mm, respectively. The specimen length in the Y-Groove test corresponds to the weld length. Both specimens had the width of 300 mm, weld thickness a_w of 30 mm and were welded at 3.0 kJ/mm using *OK 74.78* electrode. The specimens were checked using NDT to ensure they did not contain any cracks.

To investigate any possible effects plate thickness might have on residual stress development, comparative measurements were made for 6 mm thick, two-pass welded thin plates of 500 mm in length. Here, the weld build-up thickness a_w was 6 mm. The SAW and SMAW experiments were welded using *OK Tubrod 15.27S* tubular wire and *OK 75.75* electrode, respectively. For thin plate specimens, two restraining methods were applied: bolted clamps similarly to SMAW heavy plates, and welded strong backs. Because of small plate thickness, conventional *hole-drilling method* was applied.

The results of the residual stress measurements applying the Ring Core and the hole-drilling methods are presented in *Appendix 3*. The residual stress components are given to the weld longitudinal direction (S_a), weld transverse direction (S_c) and to the angle orientation of 45° between them (S_b). All stresses are plotted against the actual weld depth. The stress analyses were made using two calculation functions developed at Helsinki University of Technology (HUT) and Siemens KWU.

4.4.1 Ring-Core measurements for thick plate multipass welds

In the case of thick multipass welds, the results demonstrate that for both specimens, the first maximum peak of the weld <u>longitudinal</u> residual stress, $\sigma_{resL} \equiv S_a$, is recorded at the depth of about 6–10 mm from the weld surface. This location corresponds comparatively well to that below the final, or the 2nd last, weld bead layer, which is in line with the findings reported elsewhere[3, 5, 12, 19, 23, 54, 76].

Comparing the maximum peak stress for the 300 mm long *OK 74.78* weld in *Appendix 3* to its true yield strength (i.e., $R_{p0.2}$ for specimen *VTT1*) in *Table 11*, shows that the recorded maximum σ_{resL} of 510–520 MPa is only about 30–40 MPa lower than the weld

metal $R_{p0.2}$ of 550 MPa. This implies that even with a specimen (and weld) of no more than 300 mm in length, structural conditions in terms of longitudinal residual stress development are fairly representative of that in real welded structures.

A similar comparison between σ_{resL} and $R_{p0.2}$ in the case of the 800 mm long weld revealed the σ_{resL} level practically equivalent to the weld metal $R_{p0.2}$. This is consistent with the fact that the weld longitudinal residual stress have been shown[19, 23, 67] to increase towards its theoretical maximum, that is, the true weld metal $R_{p0.2}$, as the specimen and weld length increase enough.

4.4.2 Hole drilling measurements for thin plate welds

The results for thin plates demonstrate that the way the specimen are being fixed and restrained, affects essentially the residual stress development, see *Appendix 3*.

In the case of SMAW and SAW specimens attached by bolting them onto the welding table using clamps, longitudinal residual stress σ_{resL} remains considerably lower than that recorded for thick multipass welds, i.e., only about 0.35–0.56% of the true WM yield strength. For the SAW specimens restrained by strong-backs welded on the bottom side, the σ_{resL} was found clearly higher than in the case of bolt-attached specimens, i.e., about 0.71–0.94% of the true WM yield strength.

As expected, transverse σ_{res} remained in all these cases practically nil, or even compressive. This can be attributed[25, 49, 65, 66] to low restraint of thin plate against weld transverse shrinkage.

It is noteworthy that owing to inaccuracies of hole drilling as a method, the true longitudinal σ_{resL} can be about 10–40% lower[5c] than the measurements indicate.

The difference in residual stress level between the two restraining methods can presumably be explained by differences is deformation pattern of the welded plates. For a thin two-pass welded plate specimen, the welding residual stresses seem to become partly relieved when the bolts and clamps have been removed after welding, even though the plate was rigidly attached during the whole welding operation. In the case of thick multipass welded specimens, even such a minor stress relaxation could not have occurred because of higher structural restraint of a thick multipass weldment after welding was finished.

In contrast to the attachment by bolted clamps, restraining accomplished via welded strong-backs did not allow for any specimen deformation, neither during nor after welding.

4.5 Hydrogen diffusion measurements

The aim of *electrochemical hydrogen permeation tests* carried out[5b, 36b] for the present study under potentiostatic conditions was to define diffusion coefficients of hydrogen,

D_H, for different types of weld metals. The examined SMAW and SAW weld metals were in accordance with *Table 2a* and *2b*, respectively, whereas the FCAW welds represented typical high-strength welds obtained with rutile tubular wires. The intention was to also compare the D_H values measured here to those data sets available internally at NSC, Japan[79], and to openly published data[21, 22].

To eliminate the effect of deep traps, double- or multiple-charging techniques were adopted[5b, 36b] instead of a single charging stage. The experiments, however, demonstrated that even deep traps could be filled completely already during the first charging stage, so they no longer induce any effect in subsequent chargings. As a result, relatively stable and constant D_H values were obtained in the repeated (i.e., parallel) tests. As hydrogen diffusion during the electrochemical permeation test obeys Fick's law and the test itself meets the boundary conditions of this law, applied experimental techniques and analyses of the recorded data[5b] enabled the development of an accurate way for calculating the hydrogen diffusion coefficients.

Consequently, D_H values were determined for Armco iron, modern fine-grained high-strength structural steel, as well as for the SMAW, FCAW and SAW weld metals. It was thought, the experiments for Armco iron would serve as a reference test expected to give D_H values characteristic for clean metals practically free from hydrogen traps and hence exhibiting high hydrogen diffusivity. The D_H values for the modern fine-grained structural steel, in turn, were expected to be somewhat lower than those for Armco iron but, owing to the low impurity content of the parent steel, still remarkably higher than the values for the weld metals with a greater number of hydrogen traps.

4.5.1 Hydrogen permeation tests for parent steel

The chemical composition of Armco iron used for the experiments is given in *Table 14a*. The specimens were annealed at 950°C for 30 min, then cooled in a furnace to room temperature before measuring the hydrogen diffusivity.

The mean value of hydrogen diffusion coefficient D_H for Armco iron at room temperature was found approximately 70 (± 5) $* 10^{-6}$ cm^2/sec.

Table 14a. The chemical composition of Armco iron (wt-%).

C	Mn	P	S	Impurity
0.0012	0.017	0.005	0.025	< 0.1

The chemical composition of the microalloyed high-strength low-impurity structural steel used for the D_H experiments is given in *Table 14b*.

Table 14b. The chemical composition of the high-strength base material (wt-%).

C	Si	Mn	Ni	V	S	P	Nb	Al
0.16	0.5	1.7	0.45	0.12	0.01	0.025	0.05	0.02

The measured hydrogen diffusion coefficients D_H for the parent steel at room temperature are presented together with the results for the SMAW weld metals in *Table 17*, see Section 4.5.2.

4.5.2 Hydrogen permeation tests for SMAW multipass weld metals

In the first set of experiments, multipass weld metals made with *OK 74.78* and *OK 75.75* electrodes were used. The chemical composition of the electrodes is given in *Table 15*. The applied welding parameters and procedures are given in *Table 16*.

Table 15. Chemical composition of the SMAW electrodes used for D_H experiments.

SMAW electrode/ Composition wt-%	C	Si	Mn	Mo	Cr	Ni
OK 74.78	0.06	0.35	1.5	0.4	–	–
OK 75.75	0.06	0.35	1.5	0.4	0.4	2.3

Assuming, hydrogen diffusion changes only slightly once the deep traps in weld metal have been filled with hydrogen, no more than, say, 2 or 3 hydrogen charging treatments in the test are needed to calculate the hydrogen diffusion coefficients. Here, several cycles were used in each test with an increasing charging current I_c, and the first ones were neglected in the analysis[5b, 36b]. Tests were repeated a few times (codes: I#–IV#).

The conditions where all deep traps in weld metal become filled with hydrogen before measuring the actual D_H value are thought justified by the fact that these conditions represent multipass welding quite realistically. In the case of single-pass welds, in turn, one can expect D_H values associated with conditions where traps are not filled yet, to be more descriptive.

Table 16. Welding procedure data for the SMAW weld metals used for D_H experiments.

SMAW electrode / Welding procedure data	OK 74.78 (∅ 5 mm)	OK 75.75 (∅ 5 mm)
Electrode condition	70% / 40°C / 18 h	70% / 40°C / 18 h
Weld (initial) diffusible hydrogen content (ml/100 g DM IIW)	10.0	9.7
Welding current (A)	250	250
Arc voltage (V)	23	23
Travel speed (cm/min)	12	12
Preheat temperature (°C)	100	100
Interpass temperature (°C)	125	125
Number of passes	14	14

The results of D_H measurements made at room temperature for the two examined SMAW weld metals are summarised together with the fine-grained microalloyed parent steel values in *Table 17*. The D_H values are seen to vary according to the location from

which the specimens were extracted. This stems from the slight differences in chemical composition and microstructure in different locations within the weld.

Table 17. The values of hydrogen diffusion coefficient D_H *for the examined SMAW weld metal specimens (at room temperature, RT).*

No of charging / D_H value (cm^2/sec)	Weld Metal OK 74.78	Weld Metal OK 75.75	Microalloyed high-strength base material
D_H (I#)	$5.5 (\pm 0.5) * 10^{-6}$	$4.0 (\pm 0.5) * 10^{-6}$	$25 (\pm 1) * 10^{-6}$
D_H (II#)	$10.0 (\pm 0.5) * 10^{-6}$	$10.0 (\pm 0.5) * 10^{-6}$	$25 (\pm 5) * 10^{-6}$
D_H (III#)	$8.0 (\pm 0.5) * 10^{-6}$	$3.5 (\pm 0.5) * 10^{-6}$	–
D_H (IV#)	$15.5 (\pm 0.5) * 10^{-6}$	–	–

Table 18. The values for hydrogen diffusion coefficients D_H *collated from literature and NSC databases.*

D_H value / Temperature	D_H : RT (cm^2/sec)	D_H : 100°C (cm^2/sec)	D_H : 300°C (cm^2/sec)
Base Material			
1.4E-3 exp (-3200/RT)	$5.9 * 10^{-6}$	$19 * 10^{-6}$	$86 * 10^{-6}$
1.3E-3 exp (-3200/RT)	$5.6 * 10^{-6}$	$18 * 10^{-6}$	$79 * 10^{-6}$
0.12 exp (-7820/RT)	$0.19 * 10^{-6}$	$3.4 * 10^{-6}$	–
0.89 exp (-8856/RT)	$0.24 * 10^{-6}$	$6.2 * 10^{-6}$	–
NSC experiments	$5.7 * 10^{-6}$	–	–
TWI experiments	–	$3.3 * 10^{-6}$	$65 * 10^{-6}$
Heat-Affected Zone (HAZ)			
0.31 exp (-7990/RT)	$0.37 * 10^{-6}$	$6.9 * 10^{-6}$	$290 * 10^{-6}$
NSC experiments	$0.31–0.42 * 10^{-6}$	–	–
SMAW Weld Metals			
1.22E-2 exp (-5200/RT)	$1.7 * 10^{-6}$	$11 * 10^{-6}$	$130 * 10^{-6}$
NSC experiments	$0.16 * 10^{-6}$	–	–

According to *Table 17*, there are no significant differences in the values of D_H between *OK 74.78* and *OK 75.75* weld metals. As expected, the D_H values for weld metal are somewhat lower than those for the parent steel, presumably due to greater number of traps available in the weld metal, compared to relatively clean microalloyed fine-grained steel.

For the comparison purposes, a number of hydrogen diffusion coefficient values collated from the literature[21, 22] and NSC databases[79] for weld metals, HAZs and base metals are presented in *Table 18.*

The data in *Table 18* demonstrate substantial scatter in the individual D_H values collated from different sources. The scatter is, in fact, greater among the values summarised from various investigations even for the same welded region, than it is among the values associated with entirely different weld regions (i.e., weld, HAZ or parent steel).

4.5.3 Hydrogen permeation tests for SAW and FCAW multipass weld metals

The second stage of experiments comprised electrochemical permeation tests for SAW and FCAW multipass weld metals. Rutile type FCAW wire *Filarc PZ 6138* and basic type SAW wire & flux combination of *OK Autrod 13.27* & *OK Flux 10.62* were used to weld the multipass experiments. The applied welding parameters and procedures are given in *Table 19.*

Table 19. Welding procedure data for the FCAW and SAW weld metals used for D_H *experiments.*

Consumable / Welding procedure data	Filarc PZ 6138 (∅ 1.2 mm)	OK Autrod 13.27 (∅ 4 mm) / OK Flux 10.62
Electrode condition	as-received	as-received
Weld (initial) diffusible hydrogen content (ml/100 g DM IIW)	not measured	not measured
Welding current (A)	216	700
Arc voltage (V)	25	30
Travel speed (cm/min)	46	25
Arc energy (kJ/mm)	0.7	5.0
Preheat temperature (°C)	115	115
Interpass temperature (°C)	< 150	< 150

For the measurements, each welded sample was cut in thickness direction into three separate sections representing (i) the weld upper-area (i.e., filling runs), (ii) the mid-thickness area and (iii) the weld root area. The average values of the hydrogen diffusion coefficient D_H for the examined SAW and FCAW weld metals are presented in *Figs 28a* and *28b*, respectively. All measurements were made at room temperature.

According to *Fig. 28a*, there is a systematic tendency in all the examined SAW specimens *S10–S113* for their D_H values to increase in weld thickness direction when going from the weld upper-area towards the weld root area. Possible reasons for this phenomenon that was not recognised in the case of the FCAW weld metals, c.f., *Fig. 28b*, are discussed in Chapter 5.9.

Fig. 28b shows that in contrast to the SAW welds, the examined FCAW weld metals display no corresponding change in D_H as a function of weldment thickness. The variation of D_H in weld thickness direction is found not systematic, but relatively random, between the examined FCAW specimens *F9–F13*.

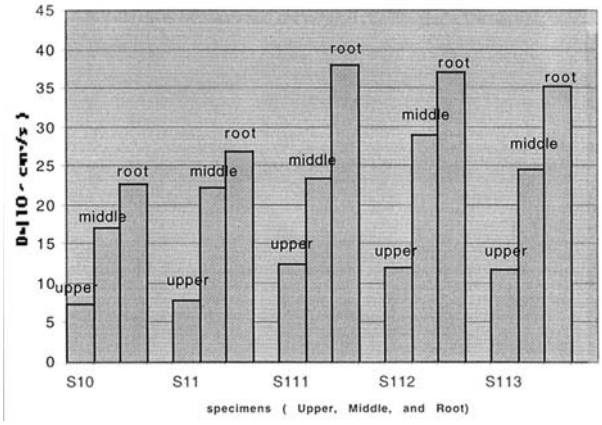

Fig. 28a. The average values of hydrogen diffusion coefficient D_H in the filling runs (upper), mid-thickness layers (middle) and root runs (root) for the SAW specimens.

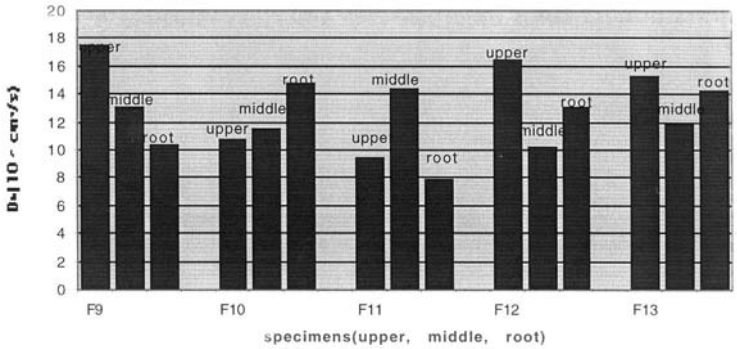

Fig. 28b. The average values of hydrogen diffusion coefficient D_H in the filling runs (upper), mid-thickness layers (middle) and root runs (root) for the FCAW specimens.

For the comparison purposes, the typical ranges of the D_H values for all the examined SMAW, SAW and FCAW weld metals, as well as those for Armco iron and microalloyed fine-grained high-strength steel are collated in *Table 20*.

According to *Table 20*, the measured D_H values all decrease in the order of Armco iron, fine-grained structural steel and the weld metals, as expected. This can be attributed to the greater number of hydrogen traps available in the weld metals than in the low-impurity fine-grained structural steel, or in the annealing heat-treated Armco iron that represents D_H values nearly characteristic of pure α-iron.

With respect to weld metals in *Table 20*, the D_H values do not differ significantly between SMAW and FCAW welds. The D_H values recorded for the SAW filling layers also lie relatively close to those for FCAW and SMAW weld metals, whereas those for the SAW mid-thickness and root runs are seen to approach those for the fine-grained structural steel.

Table 20. Summary of the D_H data for SMAW, SAW and FCAW weld metals, together with the values for Armco iron and fine-grained structural steel (at room temperature).

Weld / Steel / Range of D_H values (at RT)	Average D_H range (cm^2/sec)	D_H range in weld filling layers (cm^2/sec)	D_H range in weld mid-layers (cm^2/sec)	D_H range in weld root layers (cm^2/sec)
Armco iron	$70\ (\pm 5) * 10^{-6}$	–	–	–
fine-grained steel	$25\ (\pm 5) * 10^{-6}$	–	–	–
SMAW OK 74.78	$5.5–15.5 * 10^{-6}$	–	–	–
SMAW OK 75.75	$3.5–10.0 * 10^{-6}$	–	–	–
FCAW PZ 6138	$7.9–17.5 * 10^{-6}$	$9.4–17.5 * 10^{-6}$	$10.3–14.4 * 10^{-6}$	$7.9–14.7 * 10^{-6}$
SAW OK Autrod 13.27 / OK 10.62	$7.0–38.0 * 10^{-6}$	$7.0–12.5 * 10^{-6}$	$17.0–29.0 * 10^{-6}$	$22.5–38.0 * 10^{-6}$

4.6 Phase transformation temperature

Dilatometric measurements were made to determine the γ–α phase transformation temperatures for the SMAW weld metals and, as a reference, for microalloyed parent steel. The techniques and results are explained in detail elsewhere[36a].

Measurements were made for *OK 48.08*, *OK 74.78*, *OK 75.75* and *OK 75.78* multipass weld metals, as well as for the RAEX 460ML parent steel using Gleeble 1500 thermal simulator and four different thermal cycles in terms of weld $t_{8/5}$ cooling time. The peak temperature and holding time of the thermal cycle were chosen as 1350°C and 1 sec, respectively. Four $t_{8/5}$ cooling times of 10, 20, 30 and 40 sec were set, coupled with 3D type cooling curve; these $t_{8/5}$ values roughly corresponded to the arc energy levels of 1.9, 3.7, 5.6 and 7.5 kJ/mm, respectively.

The summary of the phase transformation experiments subjected to dilatometric measurements is given in *Table 21*.

Table 21. Results of the dilatometric measurements with Gleeble 1500 – parent steel RAEX 460 ML and the SMAW weld metals.

Cooling time $t_{8/5}$ (sec)	$t_{8/5}$ = 10 s		$t_{8/5}$ = 20 s		$t_{8/5}$ = 30 s		$t_{8/5}$ = 40 s	
Temperature (°C) / Specimen	A_{r1} (°C)	A_{r3} (°C)	A_{r1} (°C)	A_{r3} (°C)	A_{r1} (°C)	A_{r3} (°C)	A_{r1} (°C)	A_{r3} (°C)
OK 48.08	570	720	590	730	605	740	610	750
OK 74.78	540	690	570	710	580	740	585	750
RAEX 460 ML	440	610	510	630	525	645	540	665
OK 75.75	370	540	440	575	460	580	465	590
OK 75.78	290	455	300	490	360	500	380	505

The results show that with all weld $t_{8/5}$ cooling times, the γ–α phase transformation temperature in the higher alloyed Ni-Cr-Mo bearing *OK 75.75* and *OK 75.78* weld metals starts and ends at a lower temperature than in the microalloyed parent steel. The phase

transformation temperature in the leaner-alloyed Mo bearing *OK 74.78* and Ni bearing *OK 48.08* weld metals, in turn, starts and ends at a higher temperature than in the parent steel. For all weld metals and the parent steel, the transformation temperature raised as the $t_{8/5}$ increased.

The relevance of these findings with a view of explaining the pronounced cracking tendency of the higher alloyed Mi-Cr-Mo bearing weld metals, in relation to the leaner alloyed Mo bearing weld metals, is discussed in Section 5.8.

4.7 Weld bead size

Table 22 shows the results of the weld bead size measurements made under optical microscopy for a range of various SAW and SMAW welds. Both heavy multipass welds with 40 mm weld build-up thickness and two-pass thin plate welds of 6 mm build-up thickness were included. All measurements were concerned with the final weld bead of the last deposited filling layer.

Table 22. Results of the bead size measurements for SAW multipass thick welds – comparison to SMAW and SAW thin plate two-pass welds.

Weld / Dimension (mm)	SU1 SAW thick multirun weld	SU2 SAW thick multirun weld	SMAW thick multirun welds	T1 SMAW thin plate weld	S1 SAW thin plate weld
a_b	10.0	10.0	3.4–8.1	5.0	9.5
b_2	29.0	24.0	10.2–16.8	10.0	16.5
b_1	4.0	6.0	4–8	3	6
b_{ave}	20.0	15.0	7.5–15.5	7.0	12.0
Heat input (kJ/mm)	5.0	4.0	1.2–4.0	1.04	1.9
Arc energy (kJ/mm)	5.0	4.0	1.5–5.0	1.3	1.9

a_b : weld bead height

b_2 : weld bead 'maximum' width close to the weld surface at the upper-part of the bead

b_1 : weld bead 'minimum' width close to the weld root

b_{ave} : weld bead average width measured at a location of ½-bead height

The results in *Table 22* reveal that the differences in the final bead size are mostly heat input related and not so much welding process or plate thickness related. Therefore, within the same welding process and similar heat input range, the bead size is not expected to differ essentially e.g. between two-pass welded thin plate and multipass welded heavy plate.

This implies that the bead size effect, alone, may not be responsible for the lower WM cracking risk in thin plates, compared with thick multipass welds of similar strength and hydrogen. These findings are discussed in more detail in Chapter 5.

4.8 Microstructures of multiple-pass weld metals

Metallographic studies were carried out for all the SMAW weld metals in *Table 23*. Optical microscopy was used to visually examine the transverse sections cut from the specimens. All samples were polished to a 3 μm finish and etched in 4% Nital. Weld metal microstructures were classified according to the IIW recommendations[14, 15] for the classification of weld metal microstructures using optical microscopy. The phase fractions were calculated from the weld filling runs. In total, about 1000 number of points were calculated. For each specimen, fractions of different microstructural phases are given as average values of all the measurements made for a given specimen, without distinguishing specifically between as-welded and reheated weld metal microstructures. Since, however, the measurements were directed on filling runs, the presence and proportion of as-welded microstructures dominate the results in *Table 23*. Some examples of typical SMAW weld metal microstructures are shown in *Appendix 6*.

Table 23 summarises the proportions of each microstructural constituent. It can be seen that all the examined SMAW weld metals consist predominantly of acicular ferrite, AF. Among the *L-80* weld metals (*NSC*) where arc energy was varied[4, 5b], the highest amount of grain-boundary ferrite, GBF, is found to be associated with the 5.0 kJ/mm arc energy welds. This is in line with the corresponding reduction in hardness with a rise in the arc energy, see *Table 12*.

Table 23. Phase fractions of the experimental SMAW weld metals (%).

Specimen Code	Electrode / Alloying concept	Arc energy (kJ/mm)	Acicular ferrite (AF)	Polygonal ferrite (PF)	Ferrite with second phase (FS)	Grain boundary ferrite (GBF)
NSC15	L-80 (Ni-Cr-Mo)	1.5	90	2	3	5
NSC30	L-80 (Ni-Cr-Mo)	3.0	87	1	3	9
NSC50	L-80 (Ni-Cr-Mo)	5.0	85	1	2	12
VTT3	OK 48.08 (Ni)	3.0	66	5	5	24
VTT1	OK 74.78 (Mo)	3.0	75	1	5	19
VTT2	OK 75.75 (Ni-Cr-Mo)	3.0	84	2	6	8
VTT4	Atom Arc 12018 (Ni-Cr-Mo)	3.0	91	2	2	5
OU1	OK 48.08 (Ni)	2.4	63	8	3	26
OU2	OK 74.78 (Mo)	2.4	71	2	5	22
OU3	OK 75.75 (Ni-Cr-Mo)	2.4	81	5	4	10
OU4	OK 75.78 (Ni-Cr-Mo)	2.4	86	3	3	8

Besides arc energy, chemical composition and, hence, strength of a weld metal in question also affects the amount of GBF. It can be seen that the Ni-Cr-Mo bearing *L-80*, *OK 75.75*, *OK 75.78* and *Atom Arc 12018* weld metals with the highest strengths have also the highest AF contents, and much less GBF than, e.g., the Mn-Mo bearing *OK 74.78* welds. The amount of GBF is the greatest – and the amount of AF the lowest – in the Mn-Ni bearing *OK 48.08* welds of the lowest strength.

In all welds, the amounts of PF and FS are found very minor and more or less constant. Only in the *OK 48.08* welds, the amounts of FS and GBF are seen to have increased at the expense of AF.

It is noteworthy that the *OK 48.08* and *OK 74.78* welds that exhibited the greatest amounts of GBF did not reveal WM hydrogen cracks in any of the experiments made applying the standard 16 h period[1b], not even in those associated with the highest weld H_D of ≈ 18.9 ml/100 g DM (IIW), see *Tables 4* and *5*. In the case of *OK 74.78* weld metal, hydrogen cracks did not appear until the period before the NDT inspection was prolonged to 168 h (7 days). Furthermore, for the *OK 48.08* weld metals it was totally impossible to create conditions severe enough to result in WM hydrogen cracking.

It has been reported[3, 16–18] that the presence of GBF can be detrimental in that it promotes WM hydrogen cracking. This has been ascribed to the ability of GBF to act as a transport path to diffusing hydrogen, as well as to a microstructural mismatch, i.e., low strength (softness) of GBF in relation to the surrounding matrix. Provided that the presence of GBF in the examined welds had truly reduced the critical hydrogen content H_{cr} for WM hydrogen cracking, this effect was obviously far too small to become notable in the corresponding U- and Y-Groove cracking tests, see *Tables 4* and *5*.

5 Discussion

Based on the experiments of the present thesis, calculations are made to analyse the interactions between the primary crack-controlling factors in SMAW and SAW weld metals. These include dependencies between (i) WM chemical composition and hardness, (ii) WM hardness and strength, and (iii) weld critical hydrogen content-hardness-chemical composition-residual stress -interactions. Comparative calculations on the H_{Rmax}/H_0 relationships between SAW and SMAW were performed, supplemented with an analysis on the differences in the H_{Rmax}/H_0 relationship between single-pass and multiple-pass welds. The role of secondary factors, such as bead size, plate thickness, heat input, phase transformation temperature and local strength mismatch within multipass weld metals are discussed.

These analyses firstly aimed at defining the Crack-No Crack boundary conditions for the weld metal hydrogen cold cracking in multiple-pass welds. This was accomplished applying the Y- and U-Groove cracking data on SMAW multipass welds, to define the critical hydrogen content H_{cr} as a function of weld metal strength.

In the second stage, the former NSC Y-Groove data set[12] was re-analysed to derive a first-step engineering formula for the estimation of the required critical preheat temperature T_{cr}. Then, applying the final and complementary SAW U-Groove data sets, new formulae were derived for optimised prediction of safe T_{cr} estimates for the avoidance of hydrogen cracking in multipass weld metals.

5.1 Weld metal chemical composition – hardness relationships

Figs 29a and *29b* show all-weld metal Vickers hardness HV_5 for the SMAW multipass welds plotted as a function of the corresponding all-weld metal chemical composition in terms of P_{cm} and CET. The P_{cm} weldability index and CET carbon equivalent are in accordance with Eqs (43a) and (43b), respectively. The primary data on weld hardness and composition, consisting of the Y- and U-Groove cracking test welds and multiple-pass-welded pads, are given in *Table 12*.

Fig. 29a expresses the hardness-composition relationships in terms of weld metal maximum hardness $HV_{5(max)}$ recorded from the cracking tests and plotted as a linear

function of WM chemical composition. This expression hence represents a 'worst-case' upper-bound curve.

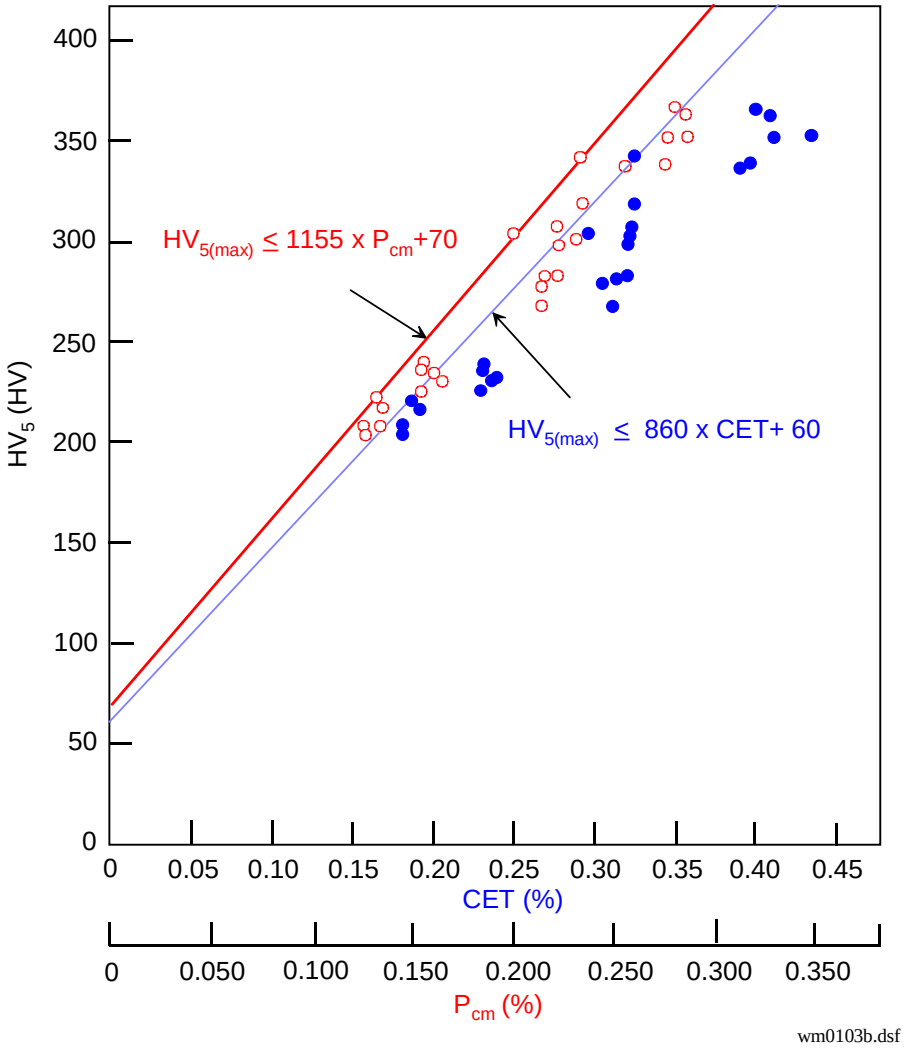

Fig. 29a. All-weld metal Vickers hardness $HV_{5(max)}$ as a function of weld P_{cm} and CET using the SMAW <u>maximum</u> hardness data.

The upper bound curves for the hardness-composition relationship in *Fig. 29a* can be expressed using individual maximum HV_5 values. Consequently, the $HV_{5(max)}$ data were fitted by linear functions of all-weld metal P_{cm} and CET, as:

$$HV_{5(max)} = 1155 * P_{cm} + 70 \quad (44a)$$

$$HV_{5(max)} = 860 * CET + 60 \quad (44b)$$

Fig. 29b, in turn, uses WM average hardness measured from the SMAW multiple-pass pads and covering an arc energy range from E = 1.6 to 3.2 kJ/mm. For the purposes of comparison, the preliminary SAW data from the U-Groove cracking test weldments and given in *Table 13* have been added into *Fig. 29b*. The description of the data in *Fig. 29b* has been derived using the SMAW data for the lowest E, i.e., 1.6 kJ/mm, in order to fully demonstrate any WM hardness increase as a result of rapid cooling cycle. The SMAW and SAW data enabled a separate hardness adjustment function to be derived to display the hardness reduction from the 1.6 kJ/mm reference level, with increasing arc energies.

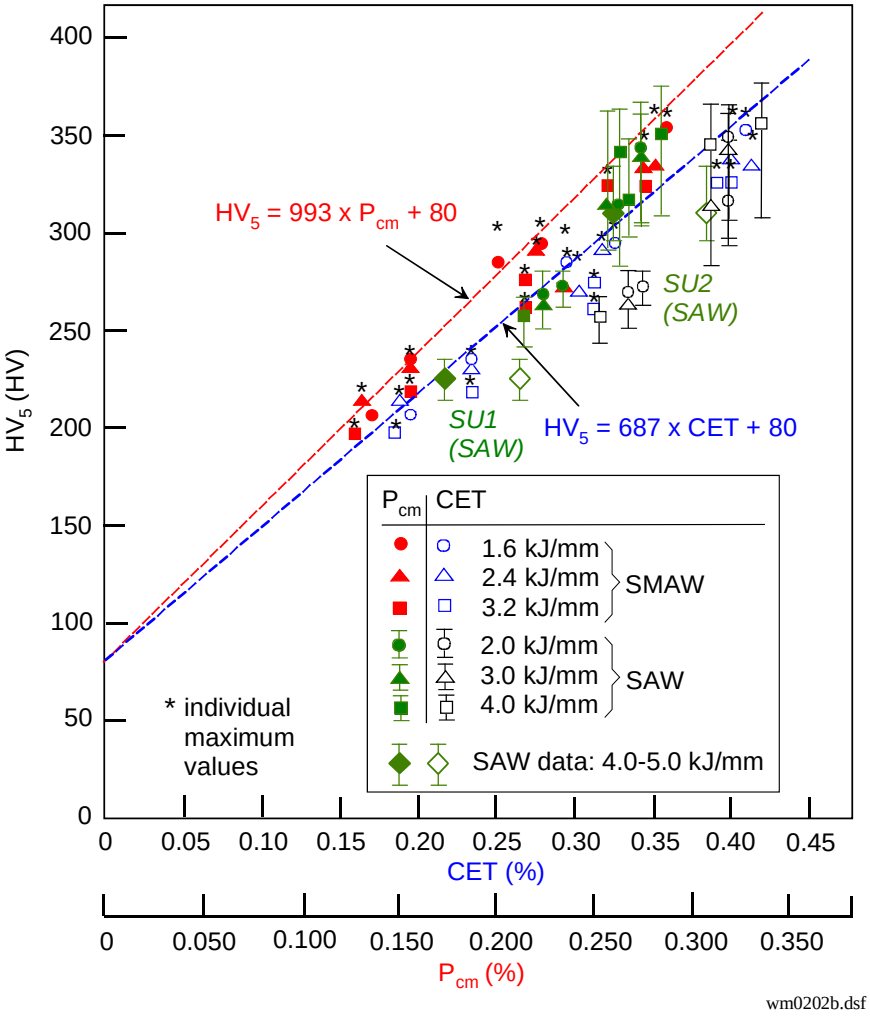

Fig. 29b. All-weld metal Vickers hardness $HV_{5(ave)}$ as a function of weld P_{cm} and CET using the SMAW average hardness data fitted according to the 1.6 kJ/mm arc energy data points. SAW hardness data from the U-Groove tests is added.

The ‘best-estimate’ curves shown in *Fig. 29b* were derived assuming a constant hardness of ≈ 70–100 HV that should still remain as P_{cm} and CET approach to nil. It was reasonable to adopt a unified, constant hardness value apart from whatever was the weldability index. This results in linear fittings that use the 1.6 kJ/mm arc energy data points of HV_{ave} data set, and are of the form:

$$HV_{5(ave)} = 993 * P_{cm} + 80 \quad (45a)$$

$$HV_{5(ave)} = 687 * CET + 80 \quad (45b)$$

These equations fulfil the theoretical limit conditions of $HV \rightarrow 80$ HV when $CET \rightarrow 0$ and $P_{cm} \rightarrow 0$. To comply with the currently available data, the validity range for Eqs (44) and (45) should be set as follows:

$$\begin{aligned} 195 &\le HV \le 365 \quad (HV_5) \\ 0.12 &\le P_{cm} \le 0.30 \quad (\%) \\ 0.18 &\le CET \le 0.45 \quad (\%) \\ 1.0 &\le E \le 4.0 \quad (kJ/mm) \end{aligned}$$

Theoretically, the ultimate maximum hardness a microstructure can reach is that of the 100% martensitic structure, whose hardness depends practically entirely on its C content. Provided the weld cooling cycle is rapid enough to yield maximum hardenability at a given weld C content, the ‘cut-off ’ value, HV_{limit}, for the weld maximum hardness HV_{max} and corresponding to that of the 100% martensitic structure can be expressed[113, 119] as:

$$HV \le HV_{max(1)} = 802 * C + 305 \quad (46a)$$

$$HV \le HV_{max(2)} = 884 * C * (1 - 0.3\,C^2) + 294 \quad (46b)$$

$$HV_{limit} = \max\{HV_{max(1)}, HV_{max(2)}\} \quad (46c)$$

Fig. 30 shows all-weld metal hardness HV_5 of the SMAW welds, c.f., *Table 12* as a function of arc energy E. In the range of E = 1.6 to 3.2 kJ/mm, the overall effect of arc energy on the HV_5 is found relatively small. In most cases, the change in HV_5 remained within the statistical scatter band of Vickers hardness, i.e., ≈ ± 30 HV units. Unlike in the case of the parent steel HAZ[13, 23–25, 28–30], inclusion of a separate cooling time parameter into composition-hardness formulae for weld metals was therefore felt unnecessary.

In the case of the two lean-alloyed weld metals, Ni bearing *OK 48.08* and Mo bearing *OK 74.78*, hardness is seen to remain virtually unchanged in the range of E = 1.6–2.4 kJ/mm. For the high-alloyed Ni-Cr-Mo bearing *OK 75.75*, *Atom Arc 12018* and *OK 75.78* welds, a reduction in hardness is found more evident and seems to occur in a relatively linear manner when the arc energy raises from 1.6 to 3.2 kJ/mm, see *Fig. 30*. The influence of arc energy on hardness is, in this respect, very similar between the three Ni-Cr-Mo alloyed SMAW weld metals.

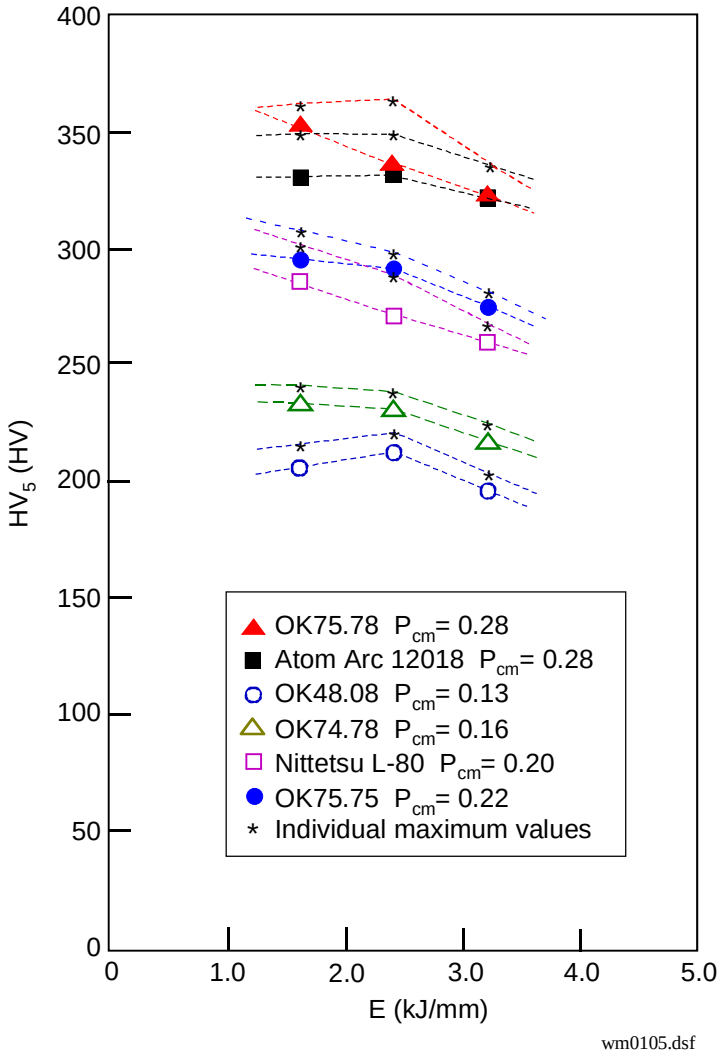

Fig. 30. All-weld metal Vickers hardness HV_5 as a function of arc energy E (or, in terms of heat input Q when replacing E by (Q / k) – for SMAW: k = 0.8 [1al]).

According to *Fig. 30*, simple linear adjustment formulae can be written to account for the change in hardness HV_5 as a function of heat input Q. The formulae use the 1.6 kJ/mm arc energy as the reference level, which ensures its compatibility with Eq. (45). Thus, these formulae can be used to obtain heat input adjusted hardness estimates, provided the weld chemical composition and E, or Q, are known. Due to the different hardness responses of the leaner- and higher-alloyed weld metals, as the heat input is varied, the formulae are constructed in a manner that relates them to the WM chemical composition in question, in terms of P_{cm} and CET, as follows:

$$HV_{5(ave)} = 993 * P_{cm} + 80 - \{[11 * ((Q / k) - 1.6)] * (3.1 * P_{cm})\} \quad (47a)$$

$$HV_{5(ave)} = 687 * CET + 80 - \{[11 * ((Q / k) - 1.6)] * (2.7 * CET)\} \quad (47b)$$

The validity limits given for Eqs (44) and (45) apply also to Eqs (47a) and (47b). What comes to hardness adjustment at arc energies lower than the 1.6 kJ/mm reference level, it should be borne in mind that the HV_{max} limit values according to Eq. (46) apply to Eqs (47a) and (47b).

These differences in the hardness responses between the Ni or Mo bearing and Ni-Cr-Mo bearing SMAW welds can be explained by the differences in their hardenability. Whether the change in hardness occurs over a certain P_{cm} or CET range, or not, depends on the capability of a particular weld metal to form the full spectrum of microstructural constituents from comparatively soft ferritic structures to hardened martensitic transformation products through the applied heat input range. This is illuminated in *Table 24* that presents a comparison between the measured individual WM maximum hardness of the SMAW and SAW weld metals together with the theoretical maximum hardness of 100% martensite microstructure.

Table 24. Comparison of hardness HV_5 between the measured maximum values of the SMAW and SAW welds, HV_{max}, and the theoretical maximum values corresponding to fully hardened 100% martensite structure, $HV_{max(M)}$, calculated according to Eqs (46b) and (46a).

SMAW Electrode / SAW tubular wire & OK Flux 10.62	WM carbon content (%)	Measured WM max. hardness HV_{max} (as-welded)	Calculated WM max. hardness $HV_{max(M)}$ (≡ 100% martensite) Eqs (46b)–(46a)	Difference between measured and calculated max. hardness $HV_{5(max)}$
OK 48.08	0.04	221	329–337	–108...–116
OK 74.78	0.04	239	329–337	–90...–98
Nittetsu L-80 (VTT)	0.03	303	320–329	–17...–26
OK 75.75	0.04	308	329–337	–21...–29
Atom Arc 12018	0.06	362	347–353	+9
OK 75.78	0.05	347	338–345	+2
OK Tubrod 15.26S	0.08	277	364–369	–87...–92
OK Tubrod 15.27S	0.07	362	356–361	+1...6
OK Tubrod 15.29S	0.07	376	356–361	+15...20

Table 12 clearly reveals how great is the difference between the measured $HV_{5(max)}$ values for the majority of the examined welds and the maximum hardness this weld metal can theoretically reach under the most stringent (i.e., rapid) cooling conditions. The smaller the difference, the greater the hardenability and hence the spectrum of those microstructural constituents the weld metal can display over the applied arc energy range from 1.6 to 3.2 kJ/mm and 2.0 to 4.0 kJ/mm for SMAW and SAW, respectively.

It can be seen that the measured HV_{max} values of the high-alloyed Ni-Cr-Mo bearing *OK 75.75, Atom Arc 12018, OK 75.78, OK Tubrod 15.27S* and *OK Tubrod 15.29S* weld

metals approach to, and finally reach, their theoretical maximum level $HV_{max(M)}$, i.e., that of a fully hardened microstructure corresponding to 100% martensite. Contrary to this, the measured HV_{max} values for the lean-alloyed *OK 48.08*, *OK 74.78* and *OK Tubrod 15.26S* welds remain – even with the shortest applied weld cooling time associated with the lowest E of 1.6 kJ/mm – considerably less than their calculated theoretical $HV_{max(M)}$.

It follows that, as the arc energy is raised from 1.6 to 3.2 kJ/mm, the Ni-Cr-Mo alloyed SMAW welds, for example, can display the full spectrum of microstructural phases from small amounts of martensite plus acicular ferrite to acicular ferrite and, finally, acicular ferrite plus grain boundary ferrite. The Ni and Mo alloyed welds, in turn, exhibit predominantly acicular ferrite plus grain-boundary ferrite microstructures over the whole arc energy range, but no notable amounts of martensite even with the lowest applied arc energy of 1.6 kJ/mm.

Overall, it can be concluded that variations in heat input have a much lesser influence on the hardness of the examined multiple-pass weld metals, than is usually the case for the parent steel HAZ in ferritic high-strength structural steels whose hardness-weld cooling time dependencies obey[13, 23–25, 28–30] the classical, steeply decaying S-curve.

5.2 Weld metal hardness – strength dependence

Earlier works at VTT[6, 7] and NSC[23, 113] have unambiguously shown that a linear relationship exists between all-weld metal hardness HV and its ultimate tensile strength R_M in the case of multipass welds. The same does not, however, apply to yield strength $R_{p0.2}$, as the $R_{p0.2}$ values for different weld metals showed[6, 7] no compatible correlation with their hardness. At a given level of weld hardness, rutile weld metals were found[6,7] to always exhibit higher yield strength than basic welds, presumably due to differences in their yield-to-tensile ratios and the resulting stress-strain characteristics.

Since these work at VTT[6, 7] and NSC[23, 113] contained data primarily from FCAW and SAW weld metals, respectively, it was necessary to examine whether the SMAW weld metals of the present thesis followed these hardness-strength dependencies. For this purpose, the WM tensile data in *Table 11* were plotted against the corresponding WM average hardness HV_5 values given in *Table 12*. These data are shown in *Fig. 31*, together with a linear relationship derived experimentally from the earlier FCAW data obtained at VTT (dotted line) and expressed[6, 7] as:

$$R_M = 2.5 * HV + 93 \tag{48a}$$

Fig. 31 shows that the SMAW experiments of the present study accord very well with the earlier FCAW data[7] obeying Eq. (48a). Unlike yield strength $R_{p0.2}$, the ultimate tensile strength R_M can hence be reliably expressed as a function of weld metal hardness HV, irrespective of the type of weld metal, i.e., whether rutile FCAW or basic SMAW.

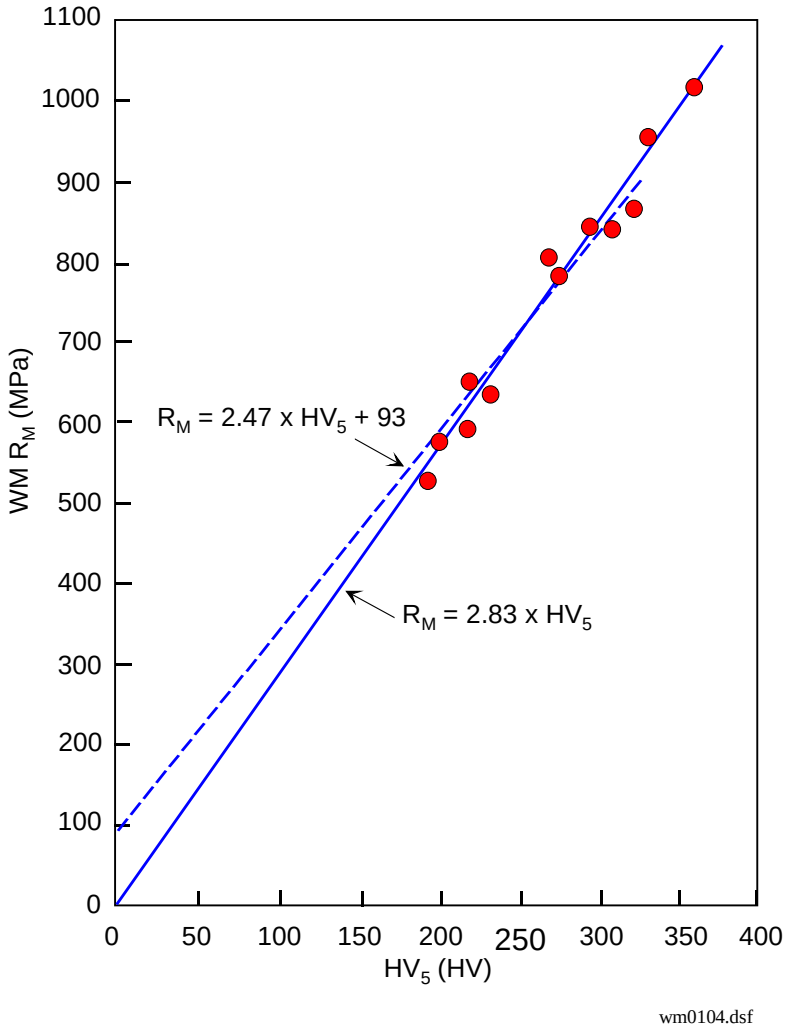

Fig. 31. All-weld metal tensile strength R_M as a function of weld metal hardness HV_5 – the present SMAW data, together with a dotted line according to the former[7] FCAW data.

If one follows the theory according to which $R_M \approx 0$ when $HV \approx 0$, inclusion of the present SMAW data into the analysis allows for re-writing of Eq. (48a) into more theoretically justified form that is expressed according to Eq. (48b) simply as:

$$R_M = 2.85 * HV_5 \qquad (48b)$$

This new linear expression obeying Eq. (48b) has been added into *Fig. 31* (solid line). It shows good agreement with the present SMAW data, as well as with the former[7] FCAW data (dotted line).

The present expression according to Eq. (48b) differs slightly from that proposed by Yurioka et al.[23] and based on the data[113] from high heat input SAW weld metals. A

comparison shows that at a given weld metal HV level, the R_M estimates according to Yurioka et al.[23] tend to become somewhat higher than those calculated in accordance with Eq. (48b). In the 100–360 HV range, for example, the difference in R_M estimates given by these two expressions remains no more than about 6–11%. Still, the fact that of these two formulae, it is Yurioka's expression[23] that gives higher R_M estimates, can be regarded as somewhat surprising. As the Yurioka-formula is based essentially on high heat input SAW data[113], whereas Eq. (48b) is derived predominantly from SMAW[5a,5b] and FCAW[6, 7] data associated with low and moderate heat inputs, one would expect the difference to be the reverse.

Alternatively, an estimate for weld metal R_M can be obtained also in the cases where only weld metal chemical composition is known, by applying Eq. (44) or Eq. (45) in conjunction with Eq. (48). An example of such an estimation of R_M values for extra-high strength *Y-80C*, *L-80*, *L-74* and *L-60* weld metals from the NSC experiments[12] is given in *Table 25* that compares measured R_M data to estimates of R_M calculated on the basis of weld chemical composition in terms of CET.

Table 25. Calculated R_M estimates for extra-high strength Y-80C, L-80, L-74 and L-60 weld metals from the former NSC experiments[12] – comparison of the measured NSC tensile test data[12] with the calculated R_M estimates according to Eqs (44b), (45b) and (48).

Filler material	Weld metal chemical composition CET[(1)] (%)	Weld metal tensile strength R_M[(2)] (MPa)	Calculated estimates of weld metal R_M (MPa)			
			'Worst case' R_M estimate acc. to Eqs (44b) and (48b)	'Worst case' R_M estimate acc. to Eqs (44b) and (48a)	'Best estimate' of R_M acc. to Eqs (45b) and (48b)	'Best estimate' of R_M acc. to Eqs (45b) and (48a)
Y-80C	0.321	852	958	923	**856**	835
L-80-1	0.312	825	935	904	**839**	820
L-80-2	0.300	814	906	878	**815**	800
L-80-3	0.293	807	889	863	**802**	788
L-74-1	0.278	744	852	831	**772**	762
L-74-2	0.248	745	778	768	**714**	711
L-74-3	0.280	733	857	835	**776**	766
L-60-1	0.223	643	717	714	**664**	669
L-60-2	0.186	618	626	636	**592**	606

(1) calculated acc. to Eq. (43b) applying analyses of WM chemical compositions given in Ref.[12]
(2) measured NSC tensile test data acc. to Ref.[12]

Analysis of the NSC data set[12] in *Table 25* is seen to support the applicability of Eqs (44), (45) and (48) in providing realistic estimates of weld metal R_M even when knowing only the weld metal chemical composition. Considering that the estimation here was made in two steps, firstly, applying weld chemical composition to derive estimates of weld hardness HV and, secondly, using these HV data to derive estimates of weld R_M, the estimates in *Table 25* agree surprisingly well with the measured NSC data[12]. The 'worst

case estimates' of R_M calculated according to Eq. (44b) in conjunction with either Eq. (48a) or (48b), are seen to overestimate the 'true' weld metal strength, as they in fact should, since these estimates were derived applying a 'maximum hardness data based fit' c.f. Eq. (44b) and are therefore expected to yield overly conservative estimates of weld hardness. However, the 'best estimates' of R_M calculated using Eq. (48b) in conjunction with Eq. (45b) that obeys an 'average hardness data based fit', are seen to accord very well with the measured[12] values. Applying Eq. (48a) in place of Eq. (48b) is seen to yield estimates that slightly underrate the 'true' weld strength. Therefore, Eq. (48b) that is based on a larger data set than Eq. (48a), should be preferred whenever 'best estimates' of R_M are required and calculated applying Eq. (45b) based on the 'average hardness data based fit'.

Consistently, comparison of weld metal P_{cm} – R_M relationship between a recent investigation[118] on extra-high strength SMAW multipass welds carried out by ELGA and the outcome of Eqs (45a) and (48b) of the present thesis demonstrates good agreement between the two approaches, as shown in *Appendix 9*. At a given weld P_{cm}, the present approach yields slightly greater values of weld metal R_M and is hence considered 'safe' as it comes to the assessment of WM hydrogen cracking risk. The difference in R_M estimates given by these two approaches is, however, minuscule, remaining less than about 5%.

Analyses of these separate NSC[12] and ELGA data sets[118] are hence regarded to validate the applicability of Eq. (48b) in conjunction with Eqs (44b) and (45b) in providing conservative but 'safe', and 'realistic', estimates of weld metal R_M, respectively, on the basis of weld metal chemical composition P_{cm}, or weld metal average hardness HV_{5ave}.

Overall, the possibility to calculate an estimate to all-weld metal tensile strength directly from Vickers hardness data HV_5 applying Eq. (48b) simplifies the 'engineering assessment' of WM cracking susceptibility, as it is not mandatory to carry out all-weld metal longitudinal tensile tests as a part of the cracking risk assessment. Sometimes, standards may require tensile testing of the welded joint anyway, albeit more often transverse than longitudinal to the weld. Unlike strength, hardness can be measured by relatively simple means e.g., from weld cross section or, by using appropriate devices, even from a polished weld metal surface without a need for sectioning or breaking the actual weldment.

A comparison of weld yield-to-tensile ratios, $R_{p0.2}/R_M$, between the *actual values* in accordance with $R_{p0.2}$ and R_M measured in the tensile test and *nominal values* calculated according to manufacturer's information on nominal weld $R_{p0.2}$ and R_M is summarised in *Appendix 8*. Despite the substantial differences in weld $R_{p0.2}$ and R_M between measured and nominal values for a range of differently alloyed weld metals associated with varying welding procedures, the corresponding $R_{p0.2}/R_M$ ratios are always found very similar, whether based on the actual or the nominal values of weld $R_{p0.2}$ and R_M. The $R_{p0.2}/R_M$ values reported in a recent work[118] on SMAW multipass weld metals of strengths ranging from $R_M \approx 550$ to 950 MPa were found to comply relatively well with the results of the present thesis, the only difference being that the values measured here on extra-high strength welds tended to be not that high as those reported in Ref.[118].

Overall, a comparatively accurate estimate to weld metal $R_{p0.2}$ can be obtained applying the weld metal $R_{p0.2}/R_M$ ratio that is calculated according to manufacturer's information on nominal weld $R_{p0.2}$ and R_M, as shown in *Appendix 8*.

5.3 Effect of weld thermal cycle, bead size and overlap on final hydrogen concentration in multipass welds according to analytic calculations

It is widely reported[2, 3, 8, 9, 12, 19–23, 54, 74, 76, 79, 94, 100, 106] that hydrogen concentration profile in multipass welds in thickness direction is non-uniform, since the maximum peak of final local concentration H_{Rmax} is governed by hydrogen diffusion and accumulation throughout the welding until finishing of the final layer. Therefore, H_{Rmax} in the filling runs can differ from both the remaining weld diffusible hydrogen $H_{R100max}$ characteristic of single-run welds, and the initial weld diffusible hydrogen H_0 according to ISO/IIW 3690[57]. Earlier work has shown[8,19–23] that in addition to H_0, H_{Rmax} depends on *complete weld thermal history*, *bead size* and *weld overlap* due to penetration of successive passes resulting in re-melting of previously solidified weld metal.

As thermal gradient, bead size and overlap all are welding process related, an attempt is made in the present thesis to investigate their influence on H_{Rmax} in the case of actual and arbitrary, yet typical, SMAW and SAW multipass welds. This was to evaluate whether H_{Rmax} could differ between SMAW and SAW filling runs so essentially that this factor should be included into predictive systems assessing the WM cracking risk. For this purpose, available data[5a, 5b] for SMAW welds was applied for the analysis. With respect to SAW, arbitrary weld geometry was defined using relevant literature data[32, 33].

For the present analysis, the (i) weld thermal cycle, (ii) weld bead size and (iii) weld bead overlap are defined[19–23] in terms of the *thermal factor of diffusion*, $\Sigma D\Delta t$, an *individual bead layer thickness*, h_w, and *weld bead overlap ratio*, d/h_w, respectively.

The weld *thermal cycle* in terms of $\Sigma D\Delta t$ incorporates the diffusion coefficient of hydrogen D at a certain temperature and the time interval Δt to which D applies. Integration over the complete weld thermal history from T_m to T_i has been shown[21–23] to obey Eq. (2), as described in Section 1.2.1.

Assuming it is sufficient to consider the hydrogen cracking conditions at a constant temperature, the description of hydrogen diffusion over the complete weld thermal history can be simplified. Consequently, $\Sigma D\Delta t$ is expressed here using $\Sigma D\Delta t_{(100)}$, a parameter shown[13, 23–25] to approximate Eq. (2) comparatively well, hence only one parameter, weld cooling time t_{100}, is needed. This allowed calculation of $\Sigma D\Delta t$ directly from the recorded weld thermal history using the t_{100} data. One of the empirical formulae presented in Section 1.2.1, Eq. (3b), was applied for calculating the estimates of $\Sigma D\Delta t_{(100)}$ on the basis of the available weld cooling data at low temperatures, t_{100}, given in *Appendix 10*.

For this, a set of t_{100} cooling times were chosen which corresponded to welding of a 50 mm thick plate at 1.7 kJ/mm arc energy and at different preheat temperatures, all

representing essentially 3-dimensional heat flow conditions, see *Appendix 10*. These t_{100} values for the analysis are given in *Table 25*, together with the corresponding $\Sigma D\Delta t_{(100)}$ values calculated according to Eq. (3b).

It is worth pointing out that of the formulae (3a)–(3c) given in Section 1.2.1 for calculating $\Sigma D\Delta t_{(100)}$ from weld cooling time, Eq. (3a) is stated[25] to generally yield the most accurate approximations of $\Sigma D\Delta t$. However, as Eq. (3a) requires weld cooling time data to temperatures also other than 100°C, and since such data is seldom available, it was concluded that for the purposes of comparisons between different welding processes and parameters, Eq. (3b) that is based solely on t_{100} data can be satisfactorily used within reasonable accuracy, consequently Eq. (3b) was chosen to be applied here.

Table 26. Effect of weld thermal history on the thermal factor of hydrogen diffusion $\Sigma D\Delta t_{(100)}$; conditions) equivalent to 50 mm plate and 1.7 kJ/mm arc energy at different levels of preheat temperature T_0, in accordance with the diagram given in Appendix 10.*

Preheat temperature T_0 (°C)	Weld cooling time t_{100} *) (sec)	Thermal factor of hydrogen diffusion $\Sigma D\Delta t_{(100)}$ (cm^2)
25	45	0.001793
50	70	0.002318
75	180	0.004447
100	800	0.016505
125	1600	0.034148
150	2200	0.048899
175	2500	0.056732
200	3000	0.070430

The effect of *weld bead size* on hydrogen diffusion distance was then treated using the square of the *individual bead layer thickness*, h_w^2, i.e., the square of the distance that needs to be covered by the diffusing hydrogen from the middle of the bead to its outer surfaces. This was regarded relevant, since it has been widely shown[19–23] that the approximation of hydrogen diffusion through an 'element surface area', as one may also picture the term h_w^2 to mean, by applying the square of the individual bead layer thickness provides a realistic description of the effect of bead size on the diffusion of hydrogen under the thermal cycle of welding. The $\Sigma D\Delta t/h_w^2$ ratio is thereby indicative of the loss of hydrogen from the element in the time available, this time depending on the nature of the weld thermal cycle.

This way, it was possible to incorporate the thermal and geometrical conditions for hydrogen diffusion by describing them using a single, *integrated diffusion-distance parameter*, $\Sigma D\Delta t/h_w^2$. This parameter has been described in Section 1.5.2 and defined[19, 20] in Eq. (37). For the present analysis, the dependence of $\Sigma D\Delta t$ on weld thermal cycle was taken in accordance with Eq. (3b) and h_w was determined experimentally from extracted macrosections of SMAW and SAW welds in question.

According to *Table 26*, thermal conditions for hydrogen diffusion are essentially enhanced with increasing weld cooling time t_{100}. The increase in t_{100} being a consequence of higher preheat temperatures, or, higher heat inputs, this means that higher thermal inputs in welding manifest themselves as an increase in the $\Sigma D\Delta t$ factor.

5.3.1 Thermal cycle and bead size effects – weld overlap excluded

It has been proven[19–23] that the remaining weld diffusible hydrogen content in the case of single- and multipass welds, denoted as $H_{R100max}$ and H_{Rmax}, respectively, depends essentially on diffusion conditions for hydrogen. These conditions have been shown[19–23] to obey Eq. (37), as explained in Section 1.5.2.

This is comprehensively demonstrated in *Fig. 32* that shows the ratio between the *maximum remaining weld diffusible hydrogen* and the *weld initial hydrogen*, $H_{R100max}/H_0$, plotted against hydrogen diffusion conditions in terms of *the integrated diffusion-distance parameter*, $\Sigma D\Delta t/h_w^2$. The primary data in *Fig. 32*, created[20] at Osaka University and NSC, Japan, do not account for the weld overlap effects, i.e., $d = 0$. In the absence of any weld overlap and looking one pass at a time, $H_{R100max}$ corresponds to H_{max} which hence applies to both single-pass and multiple pass welding situations, i.e., $H_{max} = H_{max(d=0)}$; $H_{R100max} = H_{R100max(d=0)}$ and $H_{max} \equiv H_{R100max(d=0)}$.

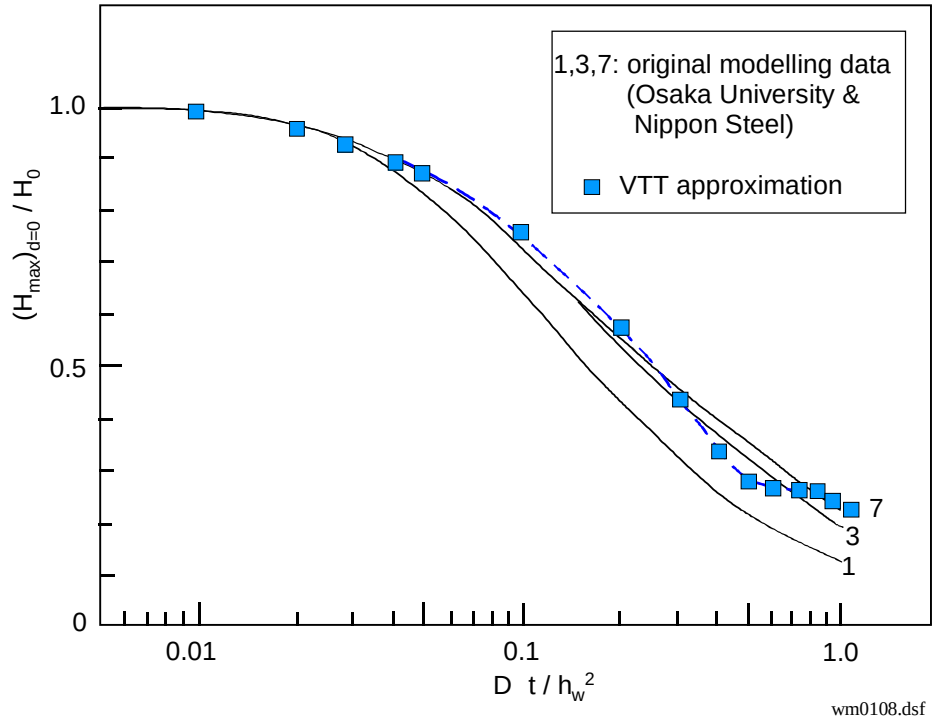

Fig. 32. The ratio between the maximum remaining weld diffusible hydrogen and weld initial hydrogen content, $H_{R100max(d=0)}/H_0$, as a function of the diffusion-distance parameter $\Sigma D\Delta t/h_w^2$ – overlap not included. Primary data according to Osaka University & NSC[20], calculated approximation according to VTT.

According to *Fig. 32* and looking one pass at a time, H_{max} remains high and almost at a level of H_0 as long as $\Sigma D\Delta t/h_w^2$ is low, then decreasing as $\Sigma D\Delta t/h_w^2$ starts to increase.

As the data in *Fig. 32* implied, the relationship between the $H_{R100max(d=0)}/H_0$ ratio and $\Sigma D\Delta t/h_w^2$ can be written using decaying sigmoidal dependence, a general form of this expression was derived according to the primary data in *Fig. 32*. The general equation incorporating positive first degree and negative second-degree polynomic terms of the form of Eq. (38) was given in Section 1.5.2.

In order to validate the general form of Eq. (38), a numerical fitting into the primary modelling data in *Fig. 32* was made in the present thesis. This fit obeying the form of Eq. (38) gave an experimental expression of the polynomic form, denoted as (■) in *Fig. 32*, as:

$$H_{R100max(d=0)}/H_0 = \{e^{[(-2.8 * \Sigma D\Delta t/h_w^2)/(0.18(\Sigma D\Delta t/h_w^2))]}\} + \\ + 0.70 * (\Sigma D\Delta t/h_w^2) - 0.45 * (\Sigma D\Delta t/h_w^2)^2 \quad (49)$$

Fig. 32 shows that in general, Eq. (49) gives estimates that are on the safe side in relation to the modelling data, that is, Eq. (49) proposes equal to or slightly higher values of the H_{max}/H_0 ratio than the modelling data. At high values of $\Sigma D\Delta t/h_w^2$ approaching unity, the accuracy of Eq. (49) is likely to weaken to some extent (presumably it would require a third-order term), however, in this $\Sigma D\Delta t/h_w^2$ range also the original modelling data exhibits comparatively great variations, as shown in *Fig. 32*. Consequently, it is concluded that Eq. (49) derived in the present thesis is an appropriate description of the dependence of the H_{max}/H_0 ratio on diffusion of hydrogen, with the effects of the weld thermal cycle and bead size being realistically accounted.

Eq. (49) was then applied to calculate the $H_{R100max(d=0)}/H_0$ ratio as a function of weld thermal conditions, $\Sigma D\Delta t$, and bead size in terms of h_w. For the analysis, three different bead layer thicknesses: 3, 4 and 8 mm were applied, as shown in *Table 27*. The calculated values of the $H_{R100max(d=0)}/H_0$ ratio are also given in *Table 27*. An increase in bead size in terms of h_w leads to longer diffusion distances in accordance with Eq. (37), which will further manifest itself as a dramatic reduction of $\Sigma D\Delta t/h_w^2$ throughout the thermal input range, as shown in *Table 27*.

5.3.2 Thermal cycle and bead size effects under the influence of weld overlap

In multipass welding hydrogen accumulation is influenced by the extent a successive pass penetrates to and re-melts the previous pass(es). This *overlapping* is described by the *weld bead overlap ratio*, d/h_w. Section 1.5.3 discusses findings from numerical modelling showing[19, 20] that increasing overlap leads to intensified hydrogen accumulation and hence elevated final local hydrogen concentration H_{Rmax}. This was explained[19–23] by additional supply of hydrogen released from previously solidified passes as they are re-melted by the subsequent pass. Hydrogen is further transported towards the filling runs due to enhanced diffusion caused by repetitive thermal cycles of successive passes.

For the analysis made here, it was presumed that the final local hydrogen concentration accounting for overlap effects, $H_{Rmax(d>0)}$, depends on *weld thermal cycle*,

bead size and the *weld bead overlap ratio*. To obtain a realistic description of the H_{Rmax}/H_0 ratio in the case of multiple-pass welds, the effect of weld bead overlap in terms of the d/h_w ratio must therefore be included into the analysis. This requires $H_{Rmax(d=0)}$ given in Eq. (49) to be replaced by $H_{Rmax(d>0)}$ in the calculation formulae to be further applied in the present analysis.

Fig. 33 shows the effect of the *weld bead overlap ratio*, d/h_w, on the maximum final hydrogen concentration – maximum remaining diffusible hydrogen content ratio, $H_{Rmax(d>0)}/H_{Rmax(d=0)}$, for different values of the integrated diffusion-distance parameter $\Sigma D\Delta t/h_w^2$. Here, $H_{Rmax(d>0)}$ refers to the maximum final local hydrogen concentration in the filling layers in multipass weld under the influence of the effects of weld bead overlapping. $H_{Rmax(d=0)}$, in turn, refers to the maximum weld diffusible hydrogen content that is remained in an individual pass after hydrogen effusion as the weld pass has cooled down to the working temperature, without any overlapping effects and hence no matter whether the weld bead in question is a single-pass weld, or a last solidified pass of multipass weld at the moment of the analysis. The primary data in *Fig. 33* has its origin in the earlier work[20] made at Osaka University and NSC, Japan. The $H_{Rmax(d>0)}/H_{Rmax(d=0)}$ ratio in *Fig. 33* thereby expresses the local (final) hydrogen concentration with the effects of hydrogen accumulation and weld overlapping included, in relation to the weld diffusible hydrogen content affected by hydrogen effusion, but unaffected by any overlap.

Let the effects of *weld thermal cycle*, *bead size* and *overlapping* on H_{Rmax} be expressed in terms of $\Sigma D\Delta t$, h_w^2 and d/h_w, respectively. The data[20] on hydrogen accumulation in *Fig. 33* can then be applied to describe the overlap effect using a relationship between the $H_{Rmax(d>0)}/H_{Rmax(d=0)}$ ratio and the d/h_w ratio, at a given $\Sigma D\Delta t/h_w^2$ level. Eq. (39) in Section 1.5.3 gives a general form of the overlap equation based on the primary data[20] in *Fig. 33*.

The results in *Table 27* reveal that all the $\Sigma D\Delta t/h_w^2$ values calculated according to Eq. (37) remain, in the present case, less than 0.8. *Fig. 33*, in turn, shows that the dependence of the $H_{Rmax(d>0)}/H_{Rmax(d=0)}$ ratio on the weld d/h_w ratio obeys a logarithmic, or power-law, dependence at $\Sigma D\Delta t/h_w^2$ values less than 0.8. For the analysis made here, four approximative sub-equations, each one corresponding to a different $\Sigma D\Delta t/h_w^2$ level, were hence derived from the primary data in *Fig. 33*. These fittings resulted in 4 power-law functions of the form:

$$H_{Rmax(d>0)}/H_{Rmax(d=0)} = 1 + 1.70 * (d/h_w)^{0.80} \quad (50a)$$

$$H_{Rmax(d>0)}/H_{Rmax(d=0)} = 1 + 1.25 * (d/h_w)^{0.60} \quad (50b)$$

$$H_{Rmax(d>0)}/H_{Rmax(d=0)} = 1 + 0.75 * (d/h_w)^{0.40} \quad (50c)$$

$$H_{Rmax(d>0)}/H_{Rmax(d=0)} = 1 + 0.45 * (d/h_w)^{0.35} \quad (50d)$$

Eqs (50a)–(50d) hence correspond to the $\Sigma D\Delta t/h_w^2$ values of 0.8, 0.4, 0.2 and 0.1, respectively, see *Fig. 33*. These sub-equations were then applied to calculate values of the $H_{Rmax(d>0)}/H_{Rmax(d=0)}$ ratio given in *Table 27*.

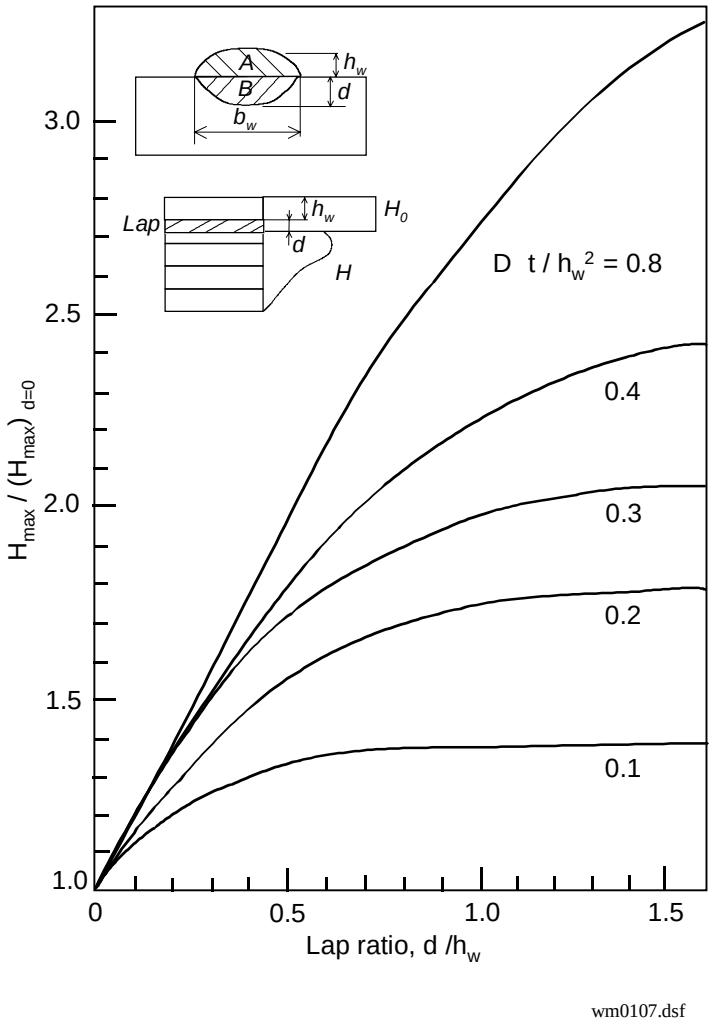

Fig. 33. Effect of weld bead overlap ratio d/h_w on maximum final hydrogen concentration – maximum remaining diffusible hydrogen content -ratio, $H_{Rmax(d>0)}$ /$H_{Rmax(d=0)}$, for different values of diffusion-distance parameter $\Sigma D\Delta t/h_w^2$ – overlap included. Primary modelling data acc. to Osaka University & NSC[20].

Table 27 shows the effect of weld thermal cycle in terms of weld t_{100} cooling time, on the thermal factor of diffusion, $\Sigma D\Delta t$, and the integrated diffusion-distance parameter $\Sigma D\Delta t/h_w^2$, calculated using different arbitrary, yet typical, bead sizes a_b of 5, 8 and 16 mm. According to VTT's earlier investigations[24, 25, 34, 53] on SMAW and SAW welds, these a_b values should roughly correspond to the individual weld bead layer thicknesses of $h_w \approx 3$, 4 and 8 mm, respectively. Of the h_w values, 3 mm corresponds quite well to the measured SMAW bead size data[5b], as well as to the bead reinforcement data for SAW reported elsewhere[32, 33]. The latter two, 4 and 8 mm, are thought to represent extreme

values for high-heat input SMAW and SAW weld metals, respectively. Values of $\Sigma D\Delta t$ and $\Sigma D\Delta t/h_w^2$ have been calculated according to Eqs (3b) and (37), respectively.

Table 27. Effect of integrated diffusion-distance parameter $\Sigma D\Delta t/h_w^2$ *on the remaining weld diffusible hydrogen content – initial weld hydrogen content -ratio* $H_{Rmax(d=0)}/H_0$ *(assuming no overlap) and on the final local maximum hydrogen concentration – initial weld hydrogen content -ratio* $H_{Rmax(d>0)}/H_0$ *when accounting for weld bead overlapping.*

Weld cooling time t_{100} (sec)	Welding method SMAW/SAW	Weld bead layer thickness h_w (mm)	Diffusion – distance parameter[1] $\Sigma D\Delta t/h_w^2$	Remaining diffusible hydrogen / initial hydrogen -ratio[2] $H_{Rmax(d=0)}/H_0$	$H_{Rmax(d>0)}$ / $H_{Rmax(d=0)}$ -hydrogen multiplier[3] as a function of d/h_w -ratio[4]	Final local maximum hydrogen / initial hydrogen - ratio $H_{Rmax(d>0)}/H_0$	
						SMAW	SAW
45	SMAW/SAW	3	0.020	0.96	1.10 / 1.15	1.06	1.10
	SMAW	4	0.011	0.98	1.10	1.08	–
	SAW	8	0.003	0.99	1.05	–	1.04
800	SMAW/SAW	3	0.183	0.60	1.55 / 1.70	0.93	1.02
	SMAW	4	0.103	0.77	1.35	1.04	–
	SAW	8	0.026	0.94	1.15	–	1.08
2200	SMAW/SAW	3	0.543	0.28	1.90 / 2.65	0.53	0.74
	SMAW	4	0.306	0.41	1.80	0.74	–
	SAW	8	0.076	0.83	1.25	–	1.04
3000	SMAW/SAW	3	0.783	0.27	2.10 / 3.20	0.57	0.86
	SMAW	4	0.440	0.30	1.90	0.57	–
	SAW	8	0.110	0.76	1.40	–	1.06

1) calculated acc. to Eq. (37), see *Table 25*
2) calculated acc. to Eq. (49), or determined from *Fig. 32*
3) calculated acc. to Eqs (50a)–(50d) or determined from *Fig. 33* using $\Sigma D\Delta t/h_w^2$ as defined in Eq. (49)
4) estimated values for the weld overlap ratio: d/h_w = **0.6** for SMAW and d/h_w = **1.5** for SAW, c.f., Refs[32, 33]

For *Table 27*, equivalent thermal welding conditions in terms of $\Sigma D\Delta t$ were adopted, i.e., it was assumed[5b, 24, 25, 32, 33] that an equivalent thermal heat input results in weld beads having greater d/h_w ratios in the case of SAW than SMAW. Thus, any differences in hydrogen diffusion are solely due to geometry-associated factors: weld bead penetration (overlap) and bead size, and not due to thermal cycle itself. According to the published data, values for the d/h_w ratio were set as 1.5 and 0.6 for the SAW[32, 33] and the SMAW[5b, 24, 25] welds, respectively.

In *Table 27*, the $H_{R100max(d=0)}/H_0$ ratio that assumes no overlap and hence refers, in that sense, to single-pass welding conditions, is then multiplied with the corresponding $H_{Rmax(d>0)}/H_{Rmax(d=0)}$ ratio which does account for the effect of weld overlapping. This calculation finally gives, at each level of $\Sigma D\Delta t/h_w^2$, the desired values of the $H_{Rmax(d>0)}/H_0$, that is, the maximum final local hydrogen concentration in multipass weld, in relation to the initial weld diffusible hydrogen content measured in a single-pass welding test. The thereby calculated $H_{Rmax(d>0)}/H_0$ values are given in *Table 27* over a

comparatively wide $\Sigma D\Delta t/h_w^2$ range and for the three arbitrary, yet typical, bead layer thicknesses of h_w = 3, 4 and 8 mm.

This allows for comparisons of the critical local hydrogen concentration in multipass welds in relation to the initial weld diffusible hydrogen, between different welding processes, as well as for evaluation of the influence of welding procedural factors on weld hydrogen. These are discussed further in Section 5.3.3.

5.3.3 Differences in final hydrogen concentration between SMAW and SAW welds

According to *Table 27*, omitting the effect of weld bead overlap, i.e., $d = 0$, the *final local hydrogen concentration* H_{Rmax} both in the case of SMAW and SAW remains always lower than the *initial weld diffusible hydrogen* H_0. Considering that $d = 0$ corresponds to the conditions in single-pass welds, it is not surprising that this finding is in agreement with the existing knowledge[3b, 13, 24, 25, 40, 59, 63] on the decaying exponential dependence of the $H_{R100max(d=0)}/H_0$ ratio on $\Sigma D\Delta t$ in the case of single-pass welds as defined in Eq. (1a), see Section 1.2.1.

Inclusion of the overlap effect, i.e., $d > 0$, allows one to conclude that overlapping will eventually raise the H_{Rmax} in the filling runs of multiple-pass welds, as shown in *Fig. 33*. Under these conditions, hydrogen accumulation is found different between the SMAW and SAW processes, see *Table 27*.

In SMAW welds, $H_{Rmax(d>0)}$ remains equal to or lower than H_0, even though the effect of weld bead overlapping in increasing the hydrogen accumulation is taken into account in accordance with Eqs (50a)–(50d). *Table 27* shows, this accrues from: (i) small bead layer thickness h_w that allows substantial amounts of hydrogen to escape in the weld cooling stage before subsequent weld beads were laid. This is seen as a drastic reduction in the $H_{R100max(d=0)}/H_0$ ratio with increasing $\Sigma D\Delta t/h_w^2$ in *Table 27*. Another reason attributes to (ii) low degree of weld overlapping (d/h_w = 0.6) characteristic of SMAW process because of the weld beads exhibiting relatively low depth-to-width ratios. A such low d/h_w in SMAW cannot induce any significant rise in the $H_{Rmax(d>0)}/H_0$ values as a result of overlapping, in contrast to SAW associated with higher d/h_w, as shown in *Table 27*.

The lower the weld cooling rate in SMAW, the greater becomes the difference between $H_{Rmax(d>0)}$ and H_0. With prolonged weld t_{100} cooling times and hence greater $\Sigma D\Delta t/h_w^2$ values, $H_{Rmax(d>0)}$ is seen to remain considerably lower than H_0, see *Table 27*. Thus, provided weld cooling can be effectively retarded by means other than raising the heat input (that would simultaneously increase h_w), the risk of WM hydrogen cracking in SMAW multipass welds should lessen along a decrease in $H_{Rmax(d>0)}$, even when H_0 remains unchanged. In practice, these means would include e.g. higher preheat/interpass temperatures, longer interpass times and/or retarded post-weld cooling.

In SAW welds, $H_{Rmax(d>0)}$ tends to become equivalent to H_0 over a wide heat input range. According to *Table 27*, this can be ascribed to high degree of weld overlapping

owing to the d/h_w ratios of 1.5–2.0 reported[32,33] typical to SAW process that generally produces weld beads of high depth-to-width ratios, hence accentuating the re-melting effect of previously solidified weld beads. Provided that SAW beads are also larger in size than SMAW beads, as is the case in general[5b, 24, 25, 32, 22], the size effect in conjunction with prolonged weld t_{100} cooling time is seen to accentuate the retention of hydrogen still further. This stems from larger bead layer thickness h_w and hence greater diffusion distances that do not permit any remarkable hydrogen release during the weld cooling stage before subsequent weld beads are laid. This is finally seen as a relatively small reduction in the $H_{R100max(d=0)}/H_0$ ratio with increasing $\Sigma D\Delta t/h_w^2$, c.f., *Table 27*.

Table 27 shows that irrespective of the weld t_{100} cooling time or the thermal factor of diffusion $\Sigma D\Delta t$, the $H_{Rmax(d>0)}/H_0$ ratio in SAW tends to always range around unity, except for very tiny bead size of h_w = 3 mm (which are rarely encountered in practice SA welding). This demonstrates that a combination of (i) large weld beads and (ii) high degree of weld overlapping in SAW can result in conditions where the effusion and release of hydrogen during the weld cooling stage actually become counterbalanced by the subsequent additional hydrogen supply due to pronounced weld overlapping and associated re-melting of previous beads. Therefore, instead of becoming reduced as in the case of SMAW, $H_{Rmax(d>0)}$ in SAW can eventually reach the level of H_0, as shown in *Table 27*. For SMAW, these conditions can also prevail, but only in the case of low thermal heat inputs and hence short t_{100} cooling times, see *Table 27*.

Consequently, the analysis made here allows to conclude, under equivalent thermal conditions and weld initial diffusible hydrogen in terms of $\Sigma D\Delta t$ (or t_{100}) and H_0, respectively, the final local hydrogen concentration H_{Rmax} can become higher in SAW multipass welds than is the case with SMAW. This is in line with some of the previously reported[8] cases where intense occurrence of WM hydrogen cracking was associated with high heat input SAW, in particular.

It is noteworthy that although low $\Sigma D\Delta t/h_w^2$ values are seen to yield high $H_{Rmax(d=0)}$ contents during the weld cooling stage, low $\Sigma D\Delta t/h_w^2$ also retards further accumulation of hydrogen in subsequent stages of weld overlapping by lowering the 'thermal driving force' $\Sigma D\Delta t$ for the diffusion of hydrogen. This is seen in *Figs 32* and *33*, as well as in *Table 27*. That low values of $\Sigma D\Delta t/h_w^2$ reduce hydrogen accumulation during weld overlapping stages, leads in most cases to lower multipliers of the $H_{Rmax(d>0)}/H_{Rmax(d=0)}$ ratio in the case of SAW than SMAW, as shown in *Table 27*. This, in turn, will balance to some extent the differences in the final hydrogen concentration $H_{Rmax(d>0)}$ between the two welding processes.

Overall, according to the analysis in *Table 27* it seems unlikely that H_{Rmax} could exceed the H_0 by more than ≈ 10%, neither in the case of SAW nor SMAW process. This is consistent with the views[67a] of the TWI that it should be physically impossible for H_{Rmax} to exceed H_0, no matter whether it is some intermediate or the final weld bead layer one is concerned with. Contrary to this, the Japanese modelling data[20] in *Figs 10* and *33* indicate that $H_{Rmax(d>0)}$ values exceeding H_0 seem possible in principle, under conditions comprising small bead layer thickness h_w and provided that excessive weld bead penetration, d, takes place[20]. In the absence of sound experimental evidence, and based on the present calculations for the welds studied here, it feels reasonable to conclude that $H_{Rmax} \approx H_0$ can be taken as a general approximation for the predictive

formulae assessing the hydrogen cracking risk of multipass weld metals. For SAW welds in thick plate, setting $H_{Rmax} \approx 1.1 * H_0$ might be more appropriate.

5.4 Derivation of the 'safe-line' for critical hydrogen content in multipass welds

According to the objectives of the present thesis, the first step was to define the *weld critical hydrogen content* H_{cr} below which hydrogen cracking in multipass weld metals will not occur even under the most stringent conditions realistically met in practice welding fabrication. This approach was to serve as a 'first line of defence' against WM cracking.

This chapter provides experimentally verified numerical formulae for calculating the estimates for the weld critical hydrogen content H_{cr} with respect to hydrogen cracking in multiple-pass weld metals. As candidates, those parameters appearing most promising according to the experiments of the present thesis, as well as to the literature data[2–9, 11, 12, 16–23, 26, 35, 37, 50, 51, 53, 54, 62, 67, 74, 76, 79, 94, 96, 97, 100, 102, 106], were chosen. These are based on (i) *weld longitudinal residual stress* σ_{resL} and assumed equivalent to the true yield strength of the weld metal $R_{p0.2(WM)}$, (ii) *weld chemical composition* in terms of either P_{cm} or CET, and (iii) *weld metal maximum Vickers hardness* in terms of HV_{5max}.

The aim here is to form a fundamental basis for the evaluation of the descriptive potential of these parameters for 'safe', yet, not overly conservative, predictions of the H_{cr} in the case of multipass welds.

5.4.1 Dependence of weld critical hydrogen content on longitudinal residual stress

According to the earlier theoretical and experimental work[2, 3, 13, 19, 23–25], the critical hydrogen content with respect to cracking, H_{cr}, decreases exponentially as the longitudinal residual stress σ_{resL} in a weldment increases. This can be regarded as analogous to the conditions in the Implant hydrogen cold-cracking test where the critical fracture stress σ_{crit} in a notched specimen and under axial tensile loading has been shown[13, 24, 25, 63] to depend on the microstructural hardness HV_{max} and the weld diffusible hydrogen content H_D. The general form of this dependence is given[24] according to Eq. (51), as:

$$\sigma_{crit} = A - B * HV_{max} - C * \log(H_D) \tag{51}$$

where *A*, *B* and *C* are constants. From Eq. (51), stress σ is seen to depend on a negative logarithm of hydrogen H, which is expressed in a general form as:

$$\sigma \equiv -C * \log(H) \tag{52}$$

Writing Eq. (52) in another form that expresses the weld critical hydrogen content H_{cr} as a function of weld residual stress σ_{res}, we obtain:

$$H_{cr} = A * 10^{(-B * \sigma_{res})} \quad (53)$$

It can be noted that the thereby derived Eq. (53) complies well with a corresponding expression of H_{cr} as defined in Eq. (4) and given by Yurioka[23].

The Ring-Core measurements in Section 4.4 confirmed that the weld longitudinal residual tensile stress σ_{resL} in the filling runs of thick multipass weldments is equivalent to the actual weld metal yield stress $R_{p0.2}$, see *Appendix 3*. This applies to welds that are long enough, i.e., ≥ 300 mm and under the most stringent restraint conditions that can be met in rigid large-scale welded constructions. Thus, Eq. (53) is considered to represent the 'worst-case' scenario with respect to weld metal cracking risk. The present results that prove $\sigma_{resL(max)} \approx R_{p0.2(WM)}$ to prevail are regarded to justify the transferability of the Implant test philosophy into the present WM cracking scheme. Provided an Implant specimen extracted from all-weld metal is loaded axially up to the level of the all-weld metal $R_{p0.2}$, the test itself should, in this sense, be descriptive of the stress-strain conditions in heavily restrained multipass welded joint.

Evaluation in Section 5.3 that was based on analytical calculations showed, it is reasonable to conclude that $H_{Rmax} \approx H_0$ describes the hydrogen factor characteristic of multipass welds. Since it is particularly H_{Rmax} that is considered[19, 20] as the actual local maximum hydrogen concentration being responsible for the occurrence of WM cracking, we can conclude that $H_{Rmax} \equiv H_{cr}$ in the case of multipass welds. On the other hand, H_0 represents the initial weld diffusible hydrogen content determined using a single-pass test according to IIW/ISO 3690[57]. It hence follows that for the analyses of the present study, it is justified to postulate, $H_{cr} = H_0$ can be adopted to ensure 'safe' estimates of H_{cr}. As H_0 can be determined using a single-pass test, this means that a link between the outcome of the Y- and U-Groove cracking tests given in Section 4.1 and the associated weld hydrogen content measured using single-pass tests conforming to ISO/IIW 3690[57], can be established by setting $H_{cr} = H_0$.

Thus, in the present thesis H_{cr} denotes to 'standard' weld initial hydrogen content determined using single-pass test, i.e., Osaka University mercury method and gas chromatography method for the SMAW and SAW weld metals, respectively.

The values of H_{cr} being known on the basis of the Y- and U-Groove test results and the associated weld hydrogen measurements, and setting $\sigma_{resL} = R_{p0.2(WM)}$, constants *A* and *B* in Eq. (53) can be determined according to the SMAW cracking test results in *Tables 3–5*. Consequently, a decaying exponential function obeying Eq. (53) was fitted into the experimental SMAW cracking test data available at those weld $R_{p0.2}$ strength levels that revealed WM hydrogen cracks in the corresponding cracking tests.

According to earlier experience[23, 24], the dependence of H_{cr} on σ_{resL} should obey exponential function of a form of Eq. (53). Fitting according to the SMAW cracking test data in *Tables 3–5* and in *Fig. 34* gives the following approximative expression for calculating best estimates for H_{cr} as a decaying exponential function of weldment longitudinal residual stress σ_{resL}:

$$H_{cr} = 275 * 10^{(-0.00235 * \sigma_{resL})} \quad (54a)$$

Fig. 34 shows that Eq. (54a) fitted according to the present SMAW cracking test data, gives a 'realistic' description of the dependence of H_{cr} on σ_{resL} also with respect to the SAW cracking experiments in *Tables 6–7*. For deriving a lower-bound of the 'safe' description of H_{cr}, a slightly modified expression is proposed as:

$$H_{cr} = 250 * 10^{(-0.00235 * \sigma_{resL})} \quad (54b)$$

It should be realised that applying Eq. (54) errors may arise at low σ_{res} values, since for the weld metal $R_{p0.2}$ levels below 550 MPa, only No Crack data exists, see *Tables 3–7*. Consequently, weld $R_{p0.2} \geq 550$ MPa should be set as a validity limit to Eq. (54).

Fig. 34 shows the weld critical hydrogen content H_{cr} as a function of weld longitudinal residual stress σ_{resL}, together with the Crack – No Crack boundary curve defined according to the multipass SMAW Y- and U-Groove cracking experiments and obeying Eq. (54a). As a reference, data from the U-Groove cracking tests for the SAW weld metals c.f. *Tables 6* and *7*, as well as from the two-pass V-Groove cracking tests for thin 6 mm plates c.f. *Table 10*, have been added.

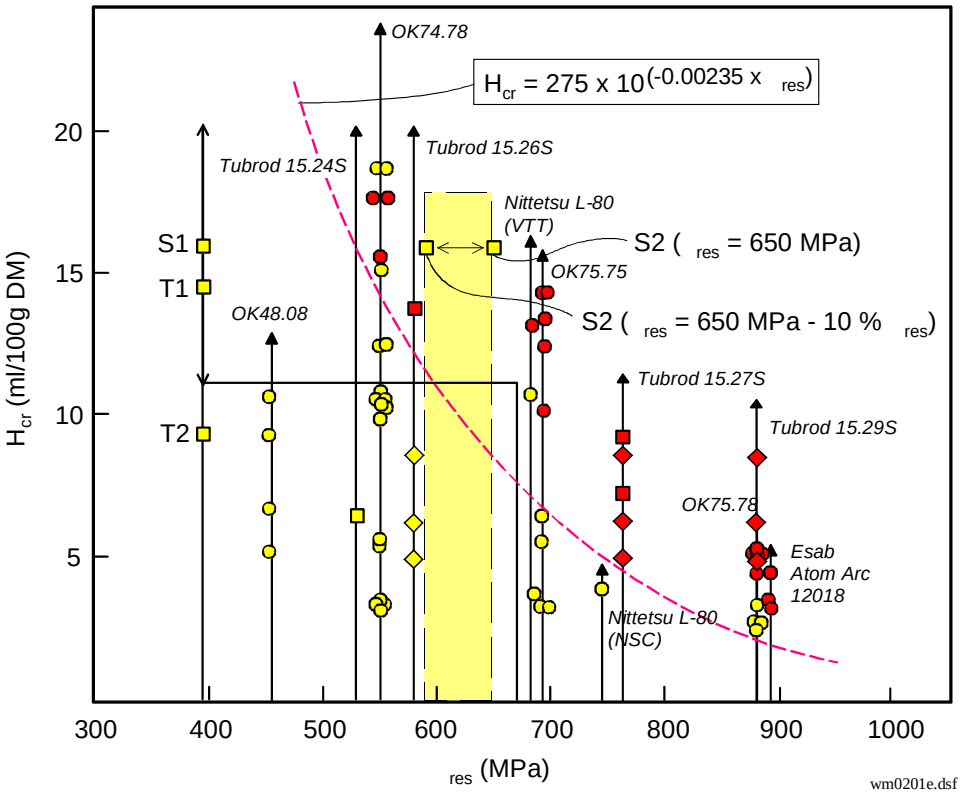

Fig. 34. Weld critical hydrogen content H_{cr} as a function of weld longitudinal residual stress σ_{resL}. The Crack – No Crack safe line fitted according to the SMAW Y- and U-Groove cracking tests (T_i = 70–100°C). Data from SAW U-Groove cracking tests and thin plate V-Groove cracking tests added, together with the scatter band associated with hole-drilling measurements.

According to *Fig. 34* it can be explained, for instance, why the cracking sensitivity of the extra-high strength $R_{p0.2} \approx 680$ MPa weld metals in thin plate V-Groove cracking tests was such low as demonstrated in *Table 10*. For the V-Groove specimens fixed by bolted clamps, relaxation of the σ_{resL} from the level of WM yield strength down to around 400 MPa that was recorded in hole-drilling measurements, c.f., *Appendix 3*, results in a corresponding shift of the data points to the left along the x-axis. The influence of this stress relaxation in terms of tolerated hydrogen content can then be read from the y-axis: the required H_{cr} to cause cracking in this case becomes so high that WM hydrogen cracking is considered totally impossible in practice welding fabrication. In the case of V-Groove specimens restrained with welded strong-backs, the level of σ_{resL} would, in principle, have remained sufficiently high to cause WM cracking, as shown in *Fig. 34*. That no cracks were recorded in this case either, is regarded as an indirect evidence that some other factor apart from σ_{resL} must have been responsible for the negligible WM cracking risk in the case of thin plate two-pass welds, see *Table 10*.

Analysing a recently reported[76] multipass cracking test data set on extra-high strength FCAW weld metals applying Eq. (54) yields contradictory findings. These experiments[76] comprise multipass welding tests on fully restrained plate specimens with a 60° V-groove preparation and using both basic and rutile type tubular wires designated as E110T-5 K4 and E111-T1 K3, respectively. Values of $R_{p0.2}$ for the corresponding basic and rutile weld metals are reported[76] as 700 and 755 MPa, respectively, whilst those of R_M were 855 and 825 MPa, respectively. It is evident that these welds become ranked differently with respect to their cracking susceptibility, depending on whether ranking is based on weld metal's $R_{p0.2}$ or R_M. Adopting $R_{p0.2}$ as a controlling factor in accordance with *Fig. 34*, neither Eq. (54a) nor (54b) would predict an individual test result[76] with the most critical combination of weld metal $R_{p0.2} = 700$ MPa and weld $H_D = 4.3$ ml/100 g DM (IIIW) to locate within the Cracking region. This, in turn, contrasts to the reported[76] NDT indications where hydrogen cracks were recorded from this particular weld. Setting $R_{p0.2}$ as 700 MPa and applying Eq. (54b) gives, in this case, the H_{cr} level of 5.6 ml/100 g DM (IIW), whilst cracking was recorded[76] at the 4.3 ml/100 g weld hydrogen, see *Table 28*.

Since the R_M of these weld metals, rather than $R_{p0.2}$, is found to comply with weld P_{cm}, these FCAW results[76] are discussed further in the context of the P_{cm} based approach in Section 5.4.2.

Table 28 compares the calculated values of weld critical hydrogen content H_{cr} applying Eq. (54) to those values derived from the results of the Y- and U-Groove cracking experiments in *Tables 3–7*. Values of H_{cr} are given as a function of weld residual stress σ_{resL} for the examined SMAW and SAW weld metals. *Table 28* shows, in all the cases where cracking did occur in the SAW weld metals, estimation of the H_{cr} according to Eq. (54b) fitted by the SMAW data would have indicated these test results to locate in the Cracking region, c.f., *Fig. 34*, thereby leading to 'safe' H_{cr} estimates for the SAW welds, as well. It should be realised, however, that only in the case of *OK Tubrod 15.26S* welds, both cracked and non cracked data were available, the rest of the SAW welds made with *OK Tubrod 15.24S*, *OK Tubrod 15.27S* and *OK Tubrod 15.29S* displaying either only cracked, or only non-cracked, results. This inevitably leaves us

with some uncertainty of the absolute safety of the H_{cr} estimates even according to Eq. (54b) in the case of SAW welds.

However, accounting for the presumed difference in the actual H_{Rmax} between SAW and SMAW welds as discussed in Section 5.3.3 and shown in *Table 27*, the level of 'true' H_{Rmax} for SAW welds can be assumed 10–40% higher than for SMAW welds. Considering this elevation, the experimental SAW data in *Table 28* and *Fig. 34* imply, the corresponding adjustment of the H_{cr} values obeying Eq. (54b) would have yielded 'safe' H_{cr} estimates also in the case of the SAW welds in *Table 28*.

Table 28. Weld critical hydrogen content H_{cr} at different WM strengths as a function of weld longitudinal residual stress σ_{resL} and assuming weld $\sigma_{resL} = R_{p0.2}$.

Weld longitudinal residual stress: σ_{resL} (MPa)	Weld critical hydrogen H_{cr} (ml/100 g DM IIW) calc.(*)	calc.(**)	experim.(***)	Nature of result: – experimental – interpolated – extrapolated – literature	SMAW / SAW Filler material Electrode or consumable
920	1.9	1.7	3.3–4.3	semi-experimental	OK 75.78 (nominal)
890	2.2	2.0	< 3.2	experimental	Atom Arc 12018 (true)
890	2.2	2.0	<< 4.9	experimental	OK Tubrod 15.29S / OK Flux 10.62
885	2.3	2.1	3.3–4.3	experimental	OK 75.78 (true)
835	3.0	2.7	< 3.2	semi-experimental	Atom Arc 12018 (nominal)
820	3.2	3.0	–	interpolated	
765	4.4	4.0	< 4.9	experimental	OK Tubrod 15.27S / OK Flux 10.62
755	4.6	4.2	< 8.5	literature[76]	FCAW E111T-1 K3
745	4.9	4.3	> 4.0	experimental	Nittetsu L-80 (NSC)
700	**6.2**	5.6	**< 4.3**	literature[76]	FCAW E110T-5 K4
690	6.6	6.0	6.2–10.1	experimental	OK 75.75
680	6.9	6.3	10.9–13.2	semi-experimental	Nittetsu L-80 (VTT)
620	9.6	8.7	–	extrapolated	
585	11.6	10.5	8.4–13.6	experimental	OK Tubrod 15.26S / OK Flux 10.62
550	14.0	12.7	15.1–15.5	experimental	OK 74.78
530	(15.6)	14.2	> 8.4	experimental	OK Tubrod 15.24S / OK Flux 10.62
480	(20)	18.6	> 10.8	extrapolated	OK 48.08

*) first sub-column: exponential best fit calculated acc. to Eq. (54a)

**) second sub-column: exponential lower-bound safe fit calculated acc. to Eq. (54b)

***) third sub-column: range of highest safe value-lowest unsafe value, or the highest individual safe value (>), or the lowest individual unsafe value (<) according to the experimental cracking test data

According to *Table 28*, an individual FCAW test result[76] with the combination of weld metal $R_{p0.2}$ = 700 MPa and weld H_D = 4.3 ml/100 g DM (IIW) is the only single test result whose cracking risk prediction applying Eq. (54b) appeared unconservative. It can

be seen that this particular test result is also the only one that contrasts radically with the rest of the SMAW, SAW and FCAW data. Anyway, this implies that the $\sigma_{resL} = R_{p0.2}$ based approach may not guarantee safe description of the H_{cr} for weld metals with comparatively low yield-to-tensile ratios and high strain hardening characteristics.

In Section 1.2.3, results are quoted from a former NSC study[12] where hydrogen cracking in multipass weld metal *L-80* with $R_{p0.2} \approx 745$ MPa has been reported at weld $H_D \approx 4$ ml/100 g DM (IIW). According to *Fig. 34*, such a situation would appear unlikely. *Table 28* shows, the critical H_{cr} corresponding to the 745–750 MPa yield strength level would lie around 4.3 ml/100 g DM (IIW). It should be borne in mind, however, that the former NSC experiments[12] at that time, exhibited constantly greater cracking risk than the experiments of the present thesis, as shown in *Appendix 2*. Also any attempts to reproduce the former NSC test results in the experimental phase of the present thesis appeared unsuccessful. This discrepancy has been addressed also in Chapter 1.7 and possible explanations discussed in more detail in Section 5.12.2.

Microscopic investigation in Section 4.8 revealed that significant amounts of grain-boundary ferrite GBF were present in the *OK 48.08* and *OK 74.78* weld metals, as shown in *Table 23*. None of these SMAW weld metals, however, revealed any transverse hydrogen cracks in the Y- or U-Groove cracking tests after a 'standard' 16 h period[1] before the NDT inspection, see *Tables 4* and *5*. Provided the presence of GBF in these welds had truly reduced the critical hydrogen content for WM cracking, this effect had obviously been too small to be noticed in the present cracking tests. Another explanation is that GBF affects WM cracking sensitivity only at low weld hydrogen levels of less than ≈ 4 ml/100 g DM (IIW)[16–18], i.e., at levels considerably lower than those associated with the cracked *OK 74.78* welds studied here.

It is therefore obvious that WM hydrogen cracking in the lower strength weld metals of $R_{p0.2} \leq 550$ MPa requires some other detrimental factor apart from σ_{resL} to provoke cracking. Indeed, a significant detrimental factor other than σ_{resL} was, according to the data in *Table 4*, obviously the *holding period before the NDT* was made, since prolonging the period up till 168 h eventually resulted in the occurrence of WM hydrogen cracking in some of the *OK 74.78* weld metals. It is noteworthy that some of the cracks associated with this prolonged holding time appeared at slightly lower weld H_D contents than those still producing sound welds in the case of the 16 h holding time, c.f. *Table 4* and *Figs 34–36*. Whether the prolonged holding period was necessary for hydrogen to diffuse and accumulate to sufficient extent to trigger hydrogen-induced crack initiation, or for an already initiated microcrack to grow further into a critical size, cannot be solely concluded.

5.4.2 Dependence of weld critical hydrogen content on weld chemical composition

In order to investigate compositional effects, a comparatively large WM cracking test data set by Wong et al.[26] was taken as a basis for the assessment of cracking risk of the

SMAW and SAW weld metals studied in the present thesis. These data are presented in *Fig. 35* and comprise results of Modified Cruciform (MC) and WIC cracking tests for both single- and multiple-pass welds. The data are considered useful for the present study, since the MC cracking test was described[26] as multipass WM cracking test that provides the combination of high structural restraint and thermal severity due to specimen geometry in conjunction with rapid weld cooling cycle.

Fig. 35 presents the 'No Cracking Region' of the original diagram (grey area) defined according to the results of the WIC and MC experiments[26]. The diagram plots weld critical hydrogen content H_{cr} against weld metal chemical composition in terms of P_{cm}. Besides the severity of the MC test specimen, the experimental data applied to derive the Cracking – No Cracking boundary was reported[26] to consist of extra high-strength weld metals with $R_M \approx 890–1000$ MPa. Thus, the original diagram is, in this respect, considered as representative of high structural rigidity and residual stress development characteristic to the Y- and U-Groove tests of the present thesis.

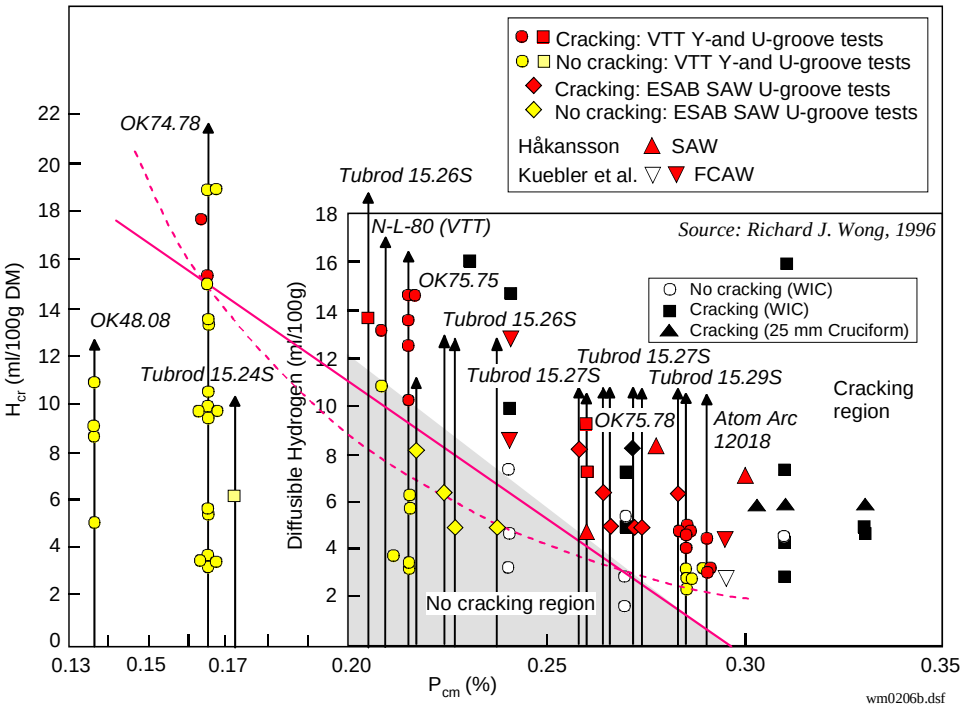

Fig. 35. 'Weld metal Cracking – No Cracking' Diagram according to Wong et al.[26]: grey area. Weld critical hydrogen content H_{cr} as a function of weld metal P_{cm}. Safe line according to VTT's SMAW Y- and U-Groove cracking tests (T_i = 70–100°C) (spots): cracked: red (black); non-cracked: yellow (grey). Data from SAW U-Groove cracking tests added (diamonds & squares).

Next, the results of the SMAW Y- and U-Groove multipass cracking tests in *Tables 3–5* were added into *Fig. 35* by plotting them against their P_{cm} values calculated for the

weld metal using Eq. (43a). For the reasons described in Section 5.4.1, H_{cr} denotes to 'standard' weld diffusible hydrogen content according to single-pass test, such as gas chromatography or IIW/Osaka University mercury method. The red (black) and yellow (grey) spots denote to Crack and No–Crack results, respectively. *Fig 35* shows that in general, the results of the Y- and U-Groove experiments made at VTT comply quite well with the original results[26] of the WIC and MC cracking tests.

It can be seen that the original No Crack area according to Wong et al.[26] and given in *Fig. 35* has been expressed in the form of a triangle, thereby implying a decaying linear dependency of weld H_{cr} on its P_{cm}. Therefore, the Y- and U-Groove cracking test data for the SMAW weld metals of the present study and given in *Tables 3–5* are firstly fitted with a linear expression of the form:

$$H_{cr} = 116 * (0.295 - P_{cm}) \tag{55}$$

On the basis of the present SMAW cracking test data, Eq. (55) is valid in the P_{cm} and H_{cr} ranges of: $0.13\% \leq P_{cm} \leq 0.30\%$ and $3.0 \leq H_{cr} \leq 19.0$ ml/100 g DM (IIW).

As a step further, the SAW U-Groove cracking test data from *Tables 6* and *7* have been added into the original diagram in *Fig. 35*. It is noteworthy that all the U-Groove cracking test results for the SAW multipass weld metals agree very well with the Y- and U-Groove cracking test data base consisting of the SMAW welds.

Following the theory on microstructure-hydrogen-stress interrelations according to Eq. (51), it is relevant to assume that the weld metal H_{cr}–P_{cm} relationship should, in fact, be exponential, just as was the case for the weld H_{cr}–σ_{resL} relationship according to Eq. (53). The SMAW Y- and U-Groove test results were therefore fitted by a decaying exponential expression of the form:

$$H_{cr} = 175 * 10^{(-6.460 * P_{cm})} \tag{56}$$

The validity limits for Eq. (56) are as those for Eq. (55).

Again, the U-Groove cracking test results for the SAW multipass weld metals are seen to accord comparatively well with the Crack – No Crack boundary curve obeying Eq. (56), as shown in *Fig. 35*. In one case only, an individual test result associated with the *OK Tubrod 15.26S* weld metal, would have been predicted as crack-susceptible according to Eq. (56), although it was actually crack-free as were also the other *OK Tubrod 15.26S* weld metals, see *Fig. 35*. *Table 7* shows, this individual SAW cracking test was welded applying the T_i of 150°C, consequently the conditions were, in this respect, somewhat less severe than in the SMAW U-Groove cracking experiments c.f., *Table 4*. Should this particular SAW experiment made applying $T_i \leq 100$°C, as was the case with the SMAW U-Groove tests where the T_i = 70–100°C was applied, the associated cracking risk would, accordingly, have been accentuated.

In general, the exponential expression obeying Eq. (56) is seen to shift the Crack–No Crack boundary line slightly downwards, i.e., towards lower critical H_{cr} values, compared to the linear expression according to Eq. (55), see *Fig. 35*. In this respect, Eq. (56) is expected to yield safer predictions of weld H_{cr} than Eq. (55) in the intermediate weld P_{cm} range of 0.18–0.28%, in particular. At low P_{cm} levels of less than 0.16%, Eq. (55) may, in turn, be safer owing to its linearity, whilst the exponential expression c.f. Eq. (56)

allows somewhat higher H_{cr} levels. It should be borne in mind, however, that for lower strength weld metals with $R_{p0.2} \leq 500$ MPa, there exists only No Crack data.

As a comparison, a recently reported[76] multipass cracking test data set on extra-high strength FCAW weld metals was analysed using the present diagram in *Fig. 35*. These data[76] comprised multipass welding tests on fully restrained, 400 x 370 x 50 mm plate specimens with 60° V-groove preparation and using basic and rutile type tubular wires designated as E110T-5 K4 and E111-T1 K3, respectively. The reported[76] values of $R_{p0.2}$ for the corresponding basic and rutile FCAW weld metals were 700 and 755 MPa, respectively, whilst those of R_M were 855 and 825 MPa, respectively. For the cracking tests, two levels of weld hydrogen H_D were chosen: 4.3, 2.5 and 12.8, 8.0 ml/100 g DM (IIW) for the basic and rutile consumables, respectively[76]. All welds were made under a maximum T_i of 140°C and using comparatively low heat inputs of about 1.6 and 0.95 kJ/mm[76]. Ultrasonic and visual NDT, confirmed with examinations of extracted macrosections, revealed[76] the occurrence of transverse WM hydrogen cracks in all the other welds except in one: the basic weld metal associated with the lowest weld H_D of 2.5 ml/100 g DM (IIW). It is noteworthy that whilst most cracks did appear already soon after welding, some of them had appeared only after 5–34 days after the completion of welding[76].

The reported[76] chemical compositions of the FCAW welds allowed calculation of their corresponding P_{cm} values according to Eq. (43a), which resulted in values of 0.29 and 0.24% for the basic and rutile FCAW weld metals, respectively. Plotting these P_{cm} values coupled with the corresponding weld H_D (i.e., 0.29%: 2.5, 4.3 ml/100 g; 0.24%: 8.5, 12.8 ml/100 g) into *Fig. 35* reveals that the application of the present Cracking – No Cracking diagram would have predicted the cracking behaviour correctly, i.e., consistently with that recorded in the NDT examination[76] for all the four weld metals. It can be seen that, with the exception of the weld associated with the lowest H_D content of 2.5 ml/100 g, all the other welds locate clearly in the Cracking region of the diagram in *Fig 35*. Even the one with the lowest weld H_D appears to locate quite close to the Crack region and the 'safe line', so the applied T_i of 140°C in the cracking tests has presumably contributed to the crack-free outcome.

A recently published[117] data set consisting of cracking tests on extra-high strength SAW welds offered another occasion to validate the present diagram in *Fig. 35*. These data[117] comprised multipass welding tests on rigidly restrained, 800 x 150 x 50 mm plate specimens with 70° Y-groove preparation and 28 mm weld build-up thickness. Three combinations of solid and tubular wires were used, designated as: (i) *SPOOLARC 120 + SPOOLARC 140 (OK Flux 10.63)*, (ii) *OK Tubrod 15.29S (OK Flux 10.47)* and (iii) *OK Tubrod 15.29S + SPOOLARC 140 (OK Flux 10.47)*. The true weld metal strength was not given, however, reported[117] chemical compositions of the SAW weld metals allowed calculation of their corresponding P_{cm} and CET values acc. to Eqs (43a) and (43b), respectively. This resulted in P_{cm} and CET values of 0.26, 0.28 and 0.30% and 0.36, 0.40 and 0.42% for the three SAW weld metals, respectively. Each of them displayed an individual weld hydrogen H_D content, which were recorded as: 4.5, 8.3 and 7.0 ml/100 g DM (IIW), respectively[117]. For each weld metal, the experiments were made under three different T_0/T_i of 80, 140 and 200°C and using moderate heat inputs in the 2.3–2.7 kJ/mm range[117]. Post test examination of the fracture surfaces revealed[76] that out of the total of

nine experiments, only one test weld did not exhibit any transverse WM hydrogen cracks: the one with weld H_D of 4.5 ml/100 g DM (IIW) and associated with the lowest CET of 0.36% in conjunction with the highest T_0/T_i of 200°C. It is, again, noteworthy that in several welds cracks appeared only after 3 to 5 days after the completion of welding[117]. Elevating T_0/T_i, or lowering the weld CET, in particular, were found to result in longer fracture times[117].

The fact that one of the applied levels of T_0/T_i was 80°C enables comparison between those particular data[117] and the SMAW data of the present thesis and made under T_i of around 70–100°C, c.f. *Table 4*. Plotting the P_{cm} values for the three SAW weld metals[117] coupled with the corresponding weld H_D (i.e., 0.26%: 4.5 ml/100 g; 0.28%: 8.3 ml/100 g; 0.30%: 7.0 ml/100 g), into *Fig. 35* reveals that the application of the present Cracking – No Cracking diagram would have, again, predicted the cracking behaviour correctly for all the three SAW weld metals. It can be seen that, with the exception of the weld associated with the lowest H_D of 4.5 ml/100 g and P_{cm} of 0.26%, the other welds locate clearly in the Cracking region of the diagram in *Fig 35*. The one with the lowest weld H_D and P_{cm} appears to locate nearly within the No Cracking region and thereby extremely close to the 'safe line' according to Eq. (55). This implies that the more conservative, exponential description for the 'safe line' obeying Eq. (56) is likely to provide better assurance against weld metal cracking.

Overall, it can be concluded that the present H_{cr}–P_{cm} diagram according to *Fig. 35*, in conjunction with Eq. (56), seems a viable 'engineering tool' in predicting safe, crack free welding conditions for different types of multipass weld metals, once the WM's true P_{cm} and weld hydrogen H_D are known. The applicability of composition based parameters, such as P_{cm}, in indicating weld metal's hydrogen cracking risk has been demonstrated experimentally also in a recent study[118] on high strength multipass SMAW weld metals.

It is interesting to note that the present P_{cm} based approach studied here provided a better description of safe H_{cr} also for the FCAW welds in Ref.[76], in comparison with the $\sigma_{resL} = R_{p0.2}$ based approach in Section 5.4.1. As for these FCAW welds, P_{cm} is found to coincide with weld metal R_M and not with $R_{p0.2}$, and since R_M relates to hardness HV, this suggests that weld metal HV would be more appropriate as a controlling factor, than either P_{cm} or $R_{p0.2}$ alone.

5.4.3 Dependence of weld critical hydrogen content on weld metal hardness

There exist evidence[6–9, 52, 53] showing that transverse hydrogen cracking in multipass weld metals is often associated with microstructures exhibiting lower hardness than in the case of the HAZ underbead/root cracking. Thus, any hardness level proven 'safe' against HAZ cracking is not necessarily safe for weld metal. Current standards for specification and qualification of welding procedures, such as EN 288-3 : 1992[10a], or its recent successor, Draft prEN ISO 15614-1[10b], however, treat the welded joint as an entity and do not thereby recognise the possibility of having hydrogen cracks in weld metal at lower

hardness levels than those specified as permitted maximum values for a corresponding parent steel group.

Earlier findings[27–30] have demonstrated that critical hardness with respect to hydrogen cracking is not constant, but decreases as steel's carbon content and hence CE_{IIW} are reduced. Following this, one may await lower critical hardness for weld metals with typically no more than 0.04–0.05% C, in comparison with high-strength structural steel with C ≈ 0.07–0.15%. Furthermore, as the recent cracking test results[76] for extra-high strength FCAW multipass welds in Section 5.4.1 showed, basic and rutile welds may exhibit quite different yield-to-tensile characteristics, resulting sometimes into situations where it is the weld metal R_M that seems to coincide with its cracking susceptibility, rather than $R_{p0.2}$. Therefore, it is deemed necessary to investigate whether weld metal's cracking susceptibility could be expressed in terms of a relationship between weld metal hardness HV_5 and weld critical hydrogen content H_{cr}. For the reasons already described in Section 5.4.1, H_{cr} denotes to 'standard' weld diffusible hydrogen content according to a single-pass test, such as e.g. gas chromatography or IIW/Osaka University mercury method.

Consequently, the Y- and U-Groove multipass cracking test data for the SMAW weld metals in *Tables 3–5* were analysed in terms of weld diffusible hydrogen H_D and weld metal's maximum hardness $HV_{5(max)}$ given in *Tables 3–5* and *12*, respectively. *Fig. 36* shows the weld critical hydrogen content H_{cr} plotted as a function of the associated all-weld metal maximum hardness $HV_{5(max)}$ for the experimental welds in accordance with their Crack – No Crack results given in *Tables 3–5*. The cracked and non-cracked specimens are denoted as red (black) and yellow (grey) spots, respectively. As supplementary data, the SAW U-Groove cracking test data from *Tables 6* and *7* have been added into *Fig. 35*.

Weld critical hydrogen content with respect to cracking, H_{cr}, has been shown[2, 3, 13, 19, 23–25] to decrease exponentially in accordance with Eqs (4) and (53) as the longitudinal residual stress σ_{resL} in a weldment increases. The weld residual stress measurements in Section 4.4, in turn, revealed σ_{resL} peak values comparable to weld metal $R_{p0.2}$, as shown in *Appendix 3*. On the other hand, *Fig. 31* shows how the weld metal hardness HV_5 increases with the tensile strength R_M and, hence, with $R_{p0.2}$. These findings result in a conclusion that the weld H_{cr} should, in principle, decrease in a similar manner to Eq. (53), as the weld metal hardness HV_{max} increases.

The Implant cold cracking test has been shown[13, 24, 25] to describe the critical fracture stress σ_{crit} in axial tensile loading of a round-bar specimen as a function of microstructural hardness HV_{max} and weld diffusible hydrogen H_D in a specimen. Thus, Eq. (51) giving a general expression of the dependence of σ_{crit} on HV_{max} and H_D, can be converted into the form:

$$B * HV \equiv C * [-\log(H_D)] \tag{57}$$

Resolving Eq. (57) to obtain a general expression for weld critical hydrogen, gives:

$$H_{cr} = C' * 10^{(-B * HV_{max})} \tag{58}$$

The values of H_{cr} and HV_{max} being known on the basis of the SMAW Y- and U-Groove test results and the associated hydrogen measurements in *Tables 3–5*, and the

corresponding weld hardness data being available in *Table 12*, constants *C'* and *B* in Eq. (58) can be determined according to the SMAW cracking test data c.f. *Tables 3–5*. The SMAW Y- and U-Groove cracking test data in *Fig. 36* were thereby fitted by a decaying exponential expression obeying Eq. (58), being of the form:

$$H_{cr} = 280 * 10^{(-0.00585 * HV_{max})} \quad (59)$$

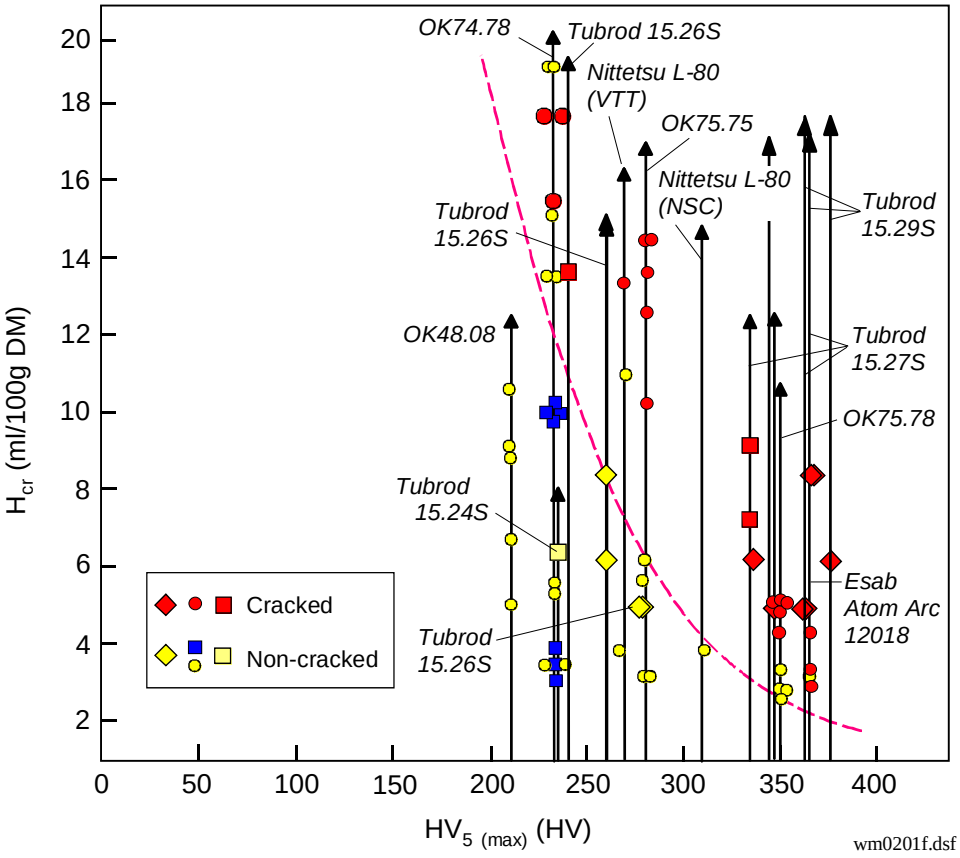

Fig. 36. Weld critical hydrogen content H_{cr} as a function of weld metal maximum hardness $HV_{5(max)}$. Safe line according to VTT's SMAW Y- and U-Groove cracking tests (T_i = 70–100°C) (spots): Cracked: red (black); non-cracked: yellow (grey). Data from SAW experiments added (diamonds).

The Crack – No Crack boundary curve obeying Eq. (59) is presented in *Fig. 36*. It can be seen that also in terms of the H_{cr}–$HV_{5(max)}$ relationship, the present U-Groove test results for the SAW multipass weld metals in *Tables 6* and *7* comply very well with the SMAW data from the Y- and U-Groove cracking experiments given in *Tables 3–5*. According to *Fig. 36*, in all the cases where cracking did occur in the SAW weld metals, estimation of the H_{cr} applying Eq. (59) fitted by the SMAW data would have indicated,

these test results will locate in the Cracking region c.f., *Fig. 36*, thereby leading to safe H_{cr} estimates for the SAW welds, as well. Accordingly, in all the cases where cracking did not occur in the SAW weld metals, Eq. (59) would also have predicted these test results as crack-free, i.e., the H_{cr} for these HV_{max}–H_D combinations were predicted higher than the actual weld H_D content of a given specimen. As supplementary data, the Crack – No Crack data points of the SAW cracking tests have been added into *Fig. 36*.

Since the two recent investigations on FCAW[76] and SAW[117] welds did not report any weld metal hardness data, such validation of the present HV_{max} based approach that was accomplished in the case of the P_{cm} based compositional diagram, could not be made here. However, a previous investigation[122] concluded that for a weld metal hydrogen level of H_D = 5 ml/100 g, the WM hardness must be kept below 300 HV to avoid hydrogen cracking. This is very well in line with the outcome of the present H_{cr}–$HV_{5(max)}$ diagram c.f. *Fig. 36*, as it was also pointed out in a recent review[123] on consumable development and the associated effects on hydrogen cracking.

On the basis of the present cracking test data as a whole, the validity limits to Eq. (59) should be set approximately as: $210 > HV_{5(max)} \geq 370$ HV and $2.0 \leq H_{cr} \leq 19.0$ ml/100 g DM (IIW).

In Section 1.2.2, results are quoted from a study[8] where hydrogen cracking in SAW multipass weld metals with a hardness of about 200 HV was recognised. According to the results of the present thesis, such a situation would not have been expected, until at the weld H_D amounting 18–19 ml/100 g DM (IIW), see *Fig. 34*. This implies that the descriptive potential of the weld HV_{max} as a parameter predicting the WM cracking risk, may weaken towards lower WM hardness. On the other hand, hardness such as 200 HV is situated at the lower tail of the whole data set of the present study and is therefore, strictly speaking, outside the validity limits of Eq. (59). This is by no means to state that the outcome of the quoted study[8], itself, would be insignificant or irrelevant to consider, but only to address that factors others than weld hardness may become increasingly dominant at low hardness welds. Investigation on such factors in low strength weld metals was not the scope of the present thesis. The applicability aspects are discussed in more detail in Section 5.12.7.

It feels reasonable to conclude that Eq. (59) is a safe description of the H_{cr}–HV_{max} dependence in the case of multipass WMs, at least for the majority of the present $HV_{5(max)}$ data in the examined HV range. With respect to the lower tail of the data, i.e., $HV_{5(max)} \leq 230$ HV, one cannot, however, be fully convinced of the safety of Eq. (59), since only non-cracked data are available, as shown in *Fig. 36*. Therefore, the precise level for the lowest H_D value that will be high enough to cause WM cracking at these low weld metal HV levels, cannot be established.

5.5 Comparison of the descriptive potential of approaches based on stress, composition and hardness related estimates

Table 29 compares the H_{cr} estimates for the SMAW and SAW weld metals calculated according to the weld longitudinal residual stress (= yield stress), weld metal chemical composition and weld metal hardness based approaches discussed in Sections 5.4.1, 5.4.2 and 5.4.3, respectively.

The estimates according to σ_{resL} (= $R_{p0.2}$), P_{cm} and $HV_{5(max)}$ based approaches have been calculated applying Eqs (54a) & (54b), Eqs (55) & (56) and Eq. (59), respectively.

5.5.1 Descriptive potential for the SMAW weld metals

For the SMAW welds the three approaches are all seen to yield essentially the same results and similar ranking of the examined weld metals in terms of their cracking susceptibility, thereby indicating good descriptive potential of the applied parameters: σ_{resL} = $R_{p0.2}$, P_{cm} and $HV_{5(max)}$ in assessing hydrogen cracking risk of multiple-pass weld metals.

Looking the three approaches individually in the case of SMAW, the P_{cm} approach acc. to Eqs (55) and (56) is constantly found to predict somewhat higher H_{cr} estimates than the other two approaches; this is particularly so for the linear P_{cm} fitting acc. to Eq. (55). The differences in the H_{cr} estimates between the exponential P_{cm} based fit acc. to Eq. (56) and the other two approaches, however, is comparatively small. The linear P_{cm} based fit that resembles closely the original treatise of the H_{cr}–P_{cm} diagram by Wong et al.[26] c.f. *Fig. 35*, is seen to deviate quite a lot from the other two approaches in that the H_{cr} estimates tend to become higher than those predicted by the other approaches. This raises some suspicion that the linear P_{cm} based fit acc. to Eq. (55), as well as the Wong diagram[26], may not always yield safe estimates of the weld H_{cr} content.

The use of the $HV_{5(max)}$ approach acc. to Eq. (59), in turn, is seen to yield in most cases the lowest H_{cr} estimates among the three approaches, whereas those predicted by the σ_{resL} = $R_{p0.2}$ approach acc. to Eq. (54) seem to fall in between those of the $HV_{5(max)}$ and P_{cm} based approaches.

From the standpoint of safety, the outcome of the σ_{resL} = $R_{p0.2}$, P_{cm} and $HV_{5(max)}$ based approaches was evaluated with respect to the range between the highest, but still safe, and lowest unsafe, weld H_D content in the cases of crack free and cracked SMAW Y- and U-Groove experiments, respectively. It is found that the $HV_{5(max)}$ approach yields safe H_{cr} estimates in every single case, as shown in *Fig. 36* and *Table 29*. The lower-bound σ_{resL} = $R_{p0.2}$ approach acc. to Eq. (54b) did so in all cases except one, i.e., *Nittetsu L80* (NSC) where the lowest 'critical' weld H_D content that would cause cracking is not known, because only one weld hydrogen level was attained, see *Table 3a*. The P_{cm} approach with the exponential fit acc. to Eq. (55) is likely to yield accordingly safe H_{cr} estimates, as it would not have predicted any of the cracked SMAW Y- or U-Groove experiments to

locate within the No Cracking region, and neither did any of the three approaches, compare *Figs 34*, *35* and *36*.

Addressing one example, namely, the relative WM cracking risk between *OK 75.78* and *Atom Arc 12018* weld metals, illuminates the importance of knowing true weld metal strength. In view of nominal $R_{p0.2}$, *OK 75.78* welds should be somewhat more crack-sensitive and correspondingly exhibit slightly lower weld H_{cr} content than *Atom Arc 12018* welds, see *Table 28*. Contrary to this, weld H_D values in the U-Groove cracking tests c.f., *Table 4*, plotted against the weld P_{cm}, indicate slightly higher cracking sensitivity for the *Atom Arc 12018* than *OK 75.78* welds, as shown in *Fig. 35*. The actual U-Groove cracking test results also demonstrate this relative ranking between the two weld metals, see *Table 4*.

Table 29. Comparison of the H_{cr} *estimates for the examined SMAW and SAW weld metals calculated according to the weld longitudinal residual stress* σ_{resL} (= $R_{p0.2}$), *weld metal chemical composition* P_{cm} *and all-weld metal hardness* $HV_{5(max)}$ *based approaches.*

Consumable / Approach	WM $R_{p0.2}$ (nom) *) (MPa)	WM R_M (nom) *) (MPa)	WM P_{cm} (%)	WM HV_{max} (HV_5)	Weld critical hydrogen content H_{cr} (ml/100 g DM (IIW))		
					σ_{resL} (=$R_{p0.2}$) Eq. (54a) 1) *Eq. (54b)* 2)	P_{cm} Eq. (*56*) 3) *Eq. (55)* 4)	HV_{max} Eq. (59) 5)
OK 48.08	480	530	0.136	210	(20)–(*18.6*)	(23) ; (*18.1*)	(16.5)
OK Tubrod 15.24S	530*)	620*)	0.172	235	(15.6)–(*14.2*)	(13.5) ; (*14.3*)	(11.8)
OK 74.78	550	650	0.165	230	14.0–*12.7*	15.0 ; *15.1*	12.6
OK Tubrod 15.26S	580*)	670*)	0.220	262	11.9–*10.8*	6.6 ; *9.4*	8.2
OK Tubrod 15.26S	580*)	670*)	0.232	277	11.9–*10.8*	5.6 ; *8.1*	6.7
Nittetsu L80 (VTT)	680	810	0.210	270	6.9–*6.3*	7.7 ; *10.4*	7.3
OK 75.75	690	810	0.215	281	6.6–*6.0*	7.1 ; *9.9*	6.4
OK 75.75	690	810	0.222	299	6.6–*6.0*	6.4 ; *9.1*	5.0
Nittetsu L80 (NSC)	745	845	0.235	319	4.9–*4.4*	5.3 ; *7.8*	3.8
OK Tubrod 15.27S	765	825	0.267	340	4.4–*4.0*	3.3 ; *4.4*	2.9
OK Tubrod 15.27S	765	825	0.261	365	4.4–*4.0*	3.6 ; *5.1*	2.1
OK 75.78	880	965	0.275	335	2.4–*2.1*	2.9 ; *3.6*	3.1
OK 75.78	885	965	0.285	350	2.3–*2.1*	2.5 ; *2.6*	2.5
OK Tubrod 15.29S	890*)	960*)	0.272	365	2.2–*2.0*	3.0 ; *3.9*	2.1
OK Tubrod 15.29S	890*)	960*)	0.283	376	2.2–*2.0*	2.6 ; *2.8*	1.8
Atom Arc 12018	890	1020	0.290	365	2.2–*2.0*	2.3 ; *2.1*	2.1

1) Exponential best fit calculated acc. to Eq. (54a)
2) Exponential lower-bound safe fit calculated acc. to Eq. (54b) (italic)
3) Exponential lower-bound safe fit calculated acc. to Eq. (56)
4) Linear simple fit calculated acc. to Eq. (55) (italic)
5) Exponential lower-bound safe fit calculated acc. to Eq. (59)
*) Nominal strength not confirmed by tensile testing
Values in brackets (): outside the validity limits of the particular equation.

This is also the case when plotting the weld H_D values from the U-Groove cracking tests against the measured all-weld metal maximum hardness $HV_{5(max)}$. According to *Fig. 36* one can realise why *Atom Arc 12018* welds should exhibit higher R_M than *OK 75.78* weld metals – that is because of the higher hardness $HV_{5(max)}$ recorded for the *Atom Arc*

12018 weld metal. In terms of nominal strengths of these two SMAW weld metals, however, an opposite ranking would have been expected. According to *Table 11*, the measured all-weld metal strength for *Atom Arc 12018* welds appears notably higher than the nominal values given by the manufacturer. Thus, the actual R_M of *Atom Arc 12018* welds was, within the arc energy range applied here, indeed higher than that of the *OK 75.78* welds. The discrepancies in the relative WM cracking sensitivity between the *OK 75.78* and *Atom Arc 12018* welds are hence attributed to the different levels of their true weld metal strength, in relation to the nominal strength.

Overall, analyses in *Table 29* demonstrate that the $HV_{5(max)}$ approach will unambiguously predict safe, yet realistic, H_{cr} estimates, hence being a potential approach of guaranteeing crack-free weld metals. The P_{cm} approach, however, inevitably leaves us with some uncertainty in those cases the H_{cr} estimates locate above the highest safe weld H_D content, while the lowest unsafe H_D content remaining unknown, see *Table 29* and *Fig. 35*.

5.5.2 Descriptive potential for the SAW weld metals

As far as the SAW weld metals are concerned, comparison between *Figs 35* and *36* reveals that the $\sigma_{resL} = R_{p0.2}$, P_{cm} and $HV_{5(max)}$ based approaches all rank these weld metals 'correctly', i.e., relative to their actual cracking sensitivity recorded in the U-Groove tests, compare *Table 4* to *Table 29*.

Certain differences in the predicted H_{cr} estimates between the approaches, however, are evidently seen. For instance, the P_{cm} and $HV_{5(max)}$ based approaches acc. to Eqs (56) and (59), respectively, tend to constantly yield lower H_{cr} estimates than the $\sigma_{resL} = R_{p0.2}$ based approach, as shown in *Table 29*. The only exception, as in the case of SMAW weld metals, is the linear P_{cm} based fit acc. to Eq. (55) that is seen to always predict somewhat higher H_{cr} estimates than the exponential P_{cm} based or the $HV_{5(max)}$ based approaches, see *Table 29*. That the H_{cr} estimates predicted by the $\sigma_{resL} = R_{p0.2}$ based approach tend to become suspiciously high, may accrue from the fact that the strength values of the SAW weld metals c.f., *Table 29* and given by the consumable manufacturer do not accurately correspond to those in the present U-Groove cracking experiments (here, it is worth highlighting that tensile testing in the present study was conducted to the SMAW weld metals only). Being so, the fact that the SAW weld metals studied here seem to be more crack sensitive according to the P_{cm} and $HV_{5(max)}$ based approaches than the $\sigma_{resL} = R_{p0.2}$ based approach, implies that either (i) the true weld metal $R_{p0.2}$ in the SAW U-Groove experiments have actually been higher than the values in *Table 29*, or (ii) the tubular SAW consumables produce weld metals that are more crack sensitive than what would be awaited according to their strength.

As the SAW welds in the U-Groove experiments were, unlike the SMAW experiments, welded using three levels of arc energy: 2.0, 3.0 and 4.0 kJ/mm, one would expect the effect of Q to appear in the cracking test results, as well as in the comparisons of the cracking occurrence between SMAW and SAW welds. *Figs 34*, *35* and *36* prove, however, that irrespective of generally higher heat inputs associated with SAW in

comparison to SMAW, all the SAW U-Groove cracking test results still fell realistically within the Crack–No Crack regions derived according to the SMAW cracking data.

Thus, the higher heat input in the case of SAW welds did not lead to such low hardness weld metals, that this would have manifested itself as lower weld H_{cr} according to the $HV_{5(max)}$ based than the P_{cm} based approach. In fact, the situation is rather the reverse, that is, for the SAW weld metals studied here the weld H_{cr} is always predicted lower according to the $HV_{5(max)}$ based than the $\sigma_{resL} = R_{p0.2}$ based approach. That the weld H_{cr} is predicted lower according to the $HV_{5(max)}$ based than the P_{cm} based approach, applies to the extra-high strength *OK Tubrod 15.27S* and *OK Tubrod 15.29S* weld metals. This means that the alloying content of these weld metals had been sufficiently high to retard any overall WM softening caused by high heat inputs. This is in line with the hardenability analysis and weld hardness measurements given in *Tables 24* and *13*, respectively, which show that these two weld metals have the alloying levels high enough to attain their maximum hardenability and sustain it throughout the applied Q range. For the high strength *OK Tubrod 15.26S* weld metals, the P_{cm} based approach yields the lowest H_{cr} estimates among the three approaches, hence indicating that this leaner alloyed weld metal has became softened to some extent as a result of high Q level, as shown in *Tables 13* and *24*.

This can be regarded a demonstration of a diminutive effect of the arc energy on WM hardness in the case of extra-high strength SAW multipass weld metals. Whilst the effect of arc energy on weld cooling time and, hence, hardenability is incorporated, or actually built-in, into the $HV_{5(max)}$ based approach, the P_{cm} based approach is a plain description of weld chemical composition effects. Should the heat input induce a notable effect on weld hardness, one would expect this effect to appear as notable differences in the SAW cracking test result plots between the exponentially fitted P_{cm} and the $HV_{5(max)}$ based approaches acc. to Eqs (56) and (59) and c.f. *Figs 35* and *36*. According to *Table 29*, no such differences are recognised.

5.5.3 Descriptive potential for the combined data sets of SMAW and SAW welds

Analysing the SMAW and SAW cracking test results in *Tables 3–7* as a combined data set, certain differences can be found regarding the descriptive potential of the $\sigma_{resL} = R_{p0.2}$, P_{cm} and $HV_{5(max)}$ based approaches in predicting estimates of the weld H_{cr}. The data in *Table 29* reveal differences in the relative ranking between the SMAW and SAW weld metals with respect to their cracking behaviour, depending on the applied approach.

Looking the 890 MPa yield strength level, the predicted H_{cr} estimates for the SMAW and SAW weld metals are comparatively similar irrespective of the applied approach. However, when comparing the 765 MPa yield strength SAW welds to the 880 MPa yield strength SMAW welds, it can be seen that the weld H_{cr} estimate according to the $\sigma_{resL} = R_{p0.2}$ based approach is allowed nearly twice as high for the *OK Tubrod 15.27S* weld metal ($R_{p0.2} \approx 765$ MPa) than for the *OK 75.78* welds ($R_{p0.2} \approx 880$–885 MPa), whereas

the $HV_{5(max)}$ based approach predicts almost similar H_{cr} for both SMAW and SAW weld metals, regardless of the over 100 MPa difference in their yield strengths.

This controversy between the SAW and SMAW welds applies more or less also to lower yield strengths in the 580–690 MPa range. For instance, a comparison between the *OK Tubrod 15.26S* SAW weld metals ($R_{p0.2} \approx$ 580 MPa) and the *Nittetsu L-80* & *OK 75.75* SMAW welds ($R_{p0.2} \approx$ 680–690 MPa) reveals, again, that whilst the $\sigma_{resL} = R_{p0.2}$ based approach predicts the weld H_{cr} estimate for the *OK 75.75* and *Nittetsu L-80* to remain no more than half of that permitted for the *OK Tubrod 15.26S* weld metal ($R_{p0.2} \approx$ 765 MPa), the P_{cm} and $HV_{5(max)}$ based approaches predict nearly similar weld H_{cr} for both weld metals, regardless of the about 100 MPa difference in their yield strengths.

Should this difference in the yield strengths between the present SAW and SMAW weld metals appear accordingly also in the U-Groove experiments given in *Tables 4*, *6* and *7*, leads inevitably to the conclusion that the tubular SAW consumables c.f. *Table 2b* produce weld metals that, in relation to their strength, are more crack sensitive than the SMAW weld metals c.f. *Table 2a* at the corresponding, or even higher, strength. Therefore, evaluating the descriptive potential of the three approaches for the entire spectrum of the SMAW and SAW welds studied in the present thesis, the $HV_{5(max)}$ based approach seems to accommodate the actual cracking susceptibility of different weld metal grades and strengths most realistically. The $HV_{5(max)}$ based approach is demonstrated to predict safe, yet realistic, weld H_{cr} estimates for all the examined cases of the SMAW and SAW multipass weld metals, as shown in *Table 29*.

The SAW data also emphasise the danger of obtaining unrealistic, or even unconservative, weld H_{cr} estimates in such cases where the $\sigma_{resL} = R_{p0.2}$ based approach is applied to weld metal whose actual strength properties e.g., in the cracking test differ essentially from the nominal weld metal strength of a particular consumable.

From the fundamental viewpoint, certain differences in physical characteristics of the investigated parameters, σ_{resL}, P_{cm} and HV, can be endorsed. Theoretically, it can be stated that the σ_{resL} based approach is based on actual physical properties of the material, i.e., yield strength, and is in this sense both scientifically relevant and theoretically justified. Weld residual stresses, in particular, relate to the weld metal yield strength, and not the ultimate tensile strength. The P_{cm} based approach, in turn, ignores the influence of weld thermal cycle and weld residual stress on the cracking behaviour. As far as hardness is concerned, it is considered merely an indication, or indirect measure, of a property called ‘tensile strength’, as shown in *Fig. 31*. A practical advantage of using the HV_{max} based approach is, however, that hardness combines conveniently the influence of both weld chemical composition and welding thermal cycle on weld metal's hardenability. Besides, weld hardness is still relatively simple to measure in practice and these measurements are required, anyway, in standards for specification and qualification of welding procedures, such as EN 288-3:1992[10a] and Draft prEN ISO 15614-1[10b]. If necessary, hardness can be measured even without breaking the specimen by using devices for surface measurements.

The P_{cm} and $HV_{5(max)}$ based approaches acc. to Eqs (56) and (59) are, in this sense, perceived as ‘engineering tools’ which are handy to use in practice, whereas the difficulties in applying $\sigma_{resL} = R_{p0.2}$ based approach acc. to Eq. (54) lie on its accurate quantification under situations where no directly measured data exist.

5.6 Role of weld build-up thickness and residual stress in weld metal hydrogen cracking

Presently, different views exist[2, 3, 76] on whether plate or, actually, weld build-up thickness should be considered, or not, as an influential factor affecting the risk of hydrogen cracking in multipass weld metals. Okuda et al.[2] found the influence of weld build-up thickness a_w quite minimal and hence insignificant in the 20–80 mm thickness range. Contrary to this, Yurioka et al. reported[3, 12] an increase of the hydrogen cracking susceptibility with the weld build-up thickness a_w in the 20–50 mm thickness range, above which the effect gradually starts to level off as thickness increases further.

The V-Groove experiments in *Table 10* demonstrate that none of the SMAW or SAW cracking tests made using thin plate two-pass welded specimens of 6 mm thickness resulted in transverse WM hydrogen cracks at any of the applied weld hydrogen contents in the range of $H_D \approx 9.2$–16.0 ml/100 g DM (IIW), despite the applied extra-high strength weld metal of $R_{p0.2} \approx 680$ MPa. In this respect, risk to WM hydrogen cracking, at a comparable level of weld metal strength and weld hydrogen, is found considerably less for the 6 mm weld build-up thickness a_w in thin plate, than in the case of heavy plate multipass welds of $a_w = 40$ mm.

Analysis of weld residual stresses in thin plate indicate, for the specimens restrained by bolted clamps relaxation of longitudinal σ_{resL} from the WM yield strength level down to around 400 MPa took place after the clamps were removed, see *Appendix 3*. According to *Fig. 34*, this relaxation would be enough to shift the cracking test data points from the Crack-region into the No Crack-region. With respect to the specimens restrained by welded strong-backs, such stress relaxation did not occur, consequently, some other factor apart from longitudinal residual stress is responsible for the fact that these experiments did not reveal any cracks either, see *Fig 34*.

It is hence concluded that for the majority of thin plate structures, the σ_{resL} can be expected to remain substantially lower than in the case of heavy plates, unless the structural configuration is so extremely rigid that it can prevent any possible deformations both during and after welding.

The residual stress measurements for multipass welds in thick plate, in turn, demonstrated that the weld longitudinal tensile residual stress σ_{resL} approaches the level of weld metal true yield strength $R_{p0.2(WM)}$, provided the weld is long enough, i.e., ≥ 300 mm. Raising the weld (and specimen) length up to 800 mm was shown to elevate the σ_{resL} still further, consequently σ_{resL} met a level equivalent to the true weld metal $R_{p0.2}$. The absolute rise in σ_{resL} with increasing weld length from 300 to 800 mm is, however, regarded as minuscule, as shown in *Appendix 3*.

Fig. 37 plots the weld H_{cr} for thin plate SMAW and SAW welds as a function of weld metal P_{cm}. These SMAW and SAW welds were made using *OK 75.75* and *OK Tubrod 15.27S*, respectively, whereas the TM parent steel was of a leaner chemical composition. Comparing *Figs 35* and *37* clearly shows how the welding of thin plate using two passes has lead to substantial dilution of weld chemical composition, in relation to the corresponding weld metals in multiple-pass welded thick plate. The corresponding P_{cm} values for the *OK 75.75* and *OK Tubrod 15.27S* weld metals in thin plate have descended

from 0.22 to 0.18% and from 0.26 to 0.21%, respectively. In the case of the *OK 75.75* weld metal *T1*, the intensified cooling conditions employed in SMAW have obviously compensated part of this reduction in hardenability due to leaner alloying, since the WM hardnesses for thin and thick plate welds were nearly identical. The corresponding HV_{ave} and HV_{max} values in these cases were ≈ 270 and 280 HV, respectively, see *Table 12*. Because of the absence of intensified cooling arrangements in the case of SAW, the leaner weld metal chemistry coupled with prolonged weld $t_{8/5}$ cooling time due to a two-dimensional heat flow in thin plate, have resulted in a marked decrease of WM hardness, and hence strength, in thin plate weld metal *S1* from the values of the corresponding *OK Tubrod 15.27S* thick plate welds. The corresponding HV_{ave} and HV_{max} values for the thin and thick plate *OK Tubrod 15.27S* welds were ≈ 257 and 266 HV and 313–315 and 336–367 HV, respectively, *Table 13*. This, in turn, manifests itself as an additional reduction in the risk of hydrogen cracking in the SAW thin plate welds studied here. Despite this, however, those SMAW and SAW welds associated with the highest weld hydrogen contents still locate within the Crack-region as it is defined for the multipass thick plate welds, see *Fig 37*.

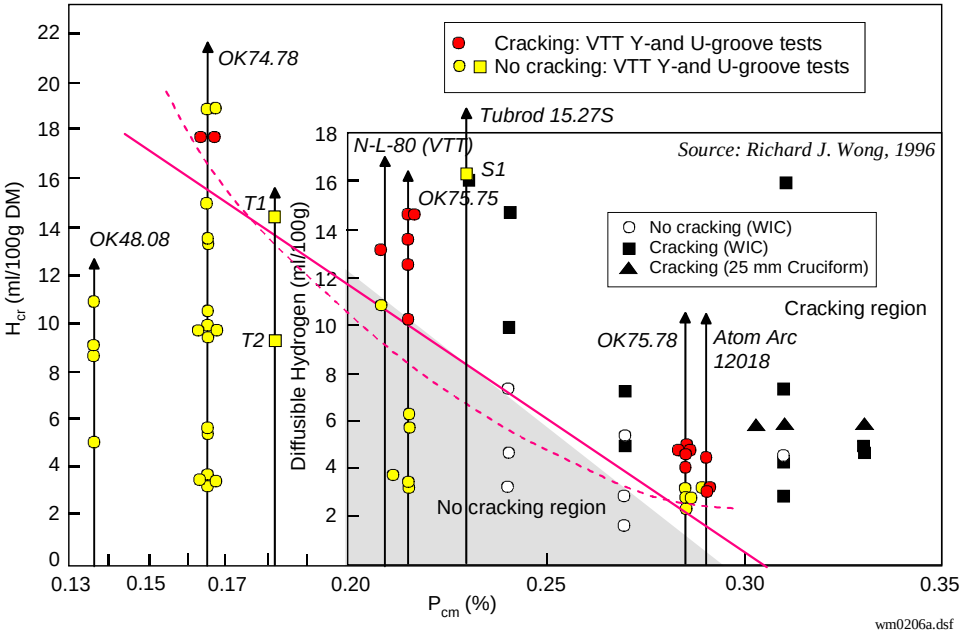

Fig. 37. Weld critical hydrogen content H_{cr} as a function of weld metal P_{cm}. Safe line according to VTT's SMAW experiments (T_i = 70–100°C) (spots): cracked: red (black); non-cracked: yellow (grey). Data from thin plate SMAW and SAW experiments added (squares).

Structures made of thin plate, but simultaneously rigid enough to prevent any weld residual stress relaxation via deformation, are regarded extremely rare. Overall, it is therefore concluded that in the case of thin plate (< 10 mm) transverse WM hydrogen cracking is precluded, provided weld metal $R_{p0.2} \leq 700$ MPa and weld $H_D \leq 16$ ml/100 g

DM (IIW). In relation to heavy plate welds of similar strength and hydrogen, the absence of transverse WM cracks in thin plate welds is thereby attributed to (i) lower weld longitudinal residual stress, negligible transverse stress and stress triaxiality, coupled with (ii) enhanced hydrogen effusion and escape due to less weld metal volume beneath the final bead.

A recently reported[76] work on multipass V-Groove cracking tests of extra-high strength FCAW weld metals comprise experiments aimed at determining the effect of weld build-up thickness a_w on the occurrence and presence of weld metal hydrogen cracks. Multipass weld metal cracking tests were made as 50, 40, 30 and 20 mm thick welds on fully restrained 400 x 370 x 50 mm plate specimens with 60° V-groove preparation and using rutile tubular wire designated as E111-T1 K3. Welding was made at 1.6 kJ/mm arc energy using the T_0/T_i of 140°C. The weld diffusible hydrogen was measured as 8.0 ml/100 g. Subsequent NDT and destructive examinations revealed, a 50 mm thick weld exhibited high crack density of uniformly distributed transverse sub-surface cracks distributed through the top half of the weld cross section. A 40 mm thick weld showed substantially less cracking, with lower crack density, whereas the 30 mm thick weld accordingly revealed cracks, but again the cracking density had decreased. Finally, no cracking was found in the 20 mm thick weld.

These very recent findings[76], in conjunction with the results of the present study seem to support the findings of Yurioka et al.[3, 12] in that reducing weld build-up thickness a_w will influence the WM hydrogen cracking risk by progressively reducing it. All the reviewed studies[2, 3, 12, 76] consistently report that the effect of weld build-up thickness on cracking is most prominent in the 20–50 mm a_w range. In fact, no data was available for a_w below 20 mm[4]. The results of the present thesis demonstrate that the WM cracking risk is progressively reduced with the a_w and becomes insignificant at weld build-up thicknesses below 10 mm, regardless of high weld metal strength and hydrogen content.

5.7 Effect of weld bead size on hydrogen diffusion distance and cracking risk

Earlier work[8] on SAW multipass welding of thick plate have shown that contrary to the HAZ, hydrogen cracking risk in SAW multipass weld metals is accentuated as the heat input increases. This was ascribed to greater diffusion distances of hydrogen as bead size increases, which results in higher local concentrations of hydrogen within the weld metal[8,9].

Microscopic examination of the experiments made in the present thesis revealed that bead size in the filling layers of the SMAW welds was not essentially different between the two-pass thin plate welds and thick plate multipass welds, provided they were welded with comparatively similar heat inputs, see *Table 22*. Only in the cases where the thick plate welds were made using clearly higher heat inputs than for the thin plate welds, the bead size both in terms of bead height, a_b, and bead width, b_2, b_1 and $b_{ave,}$ became accordingly greater.

With respect to SAW, bead height a_b appears relatively constant between thick and thin plate welds, irrespective of the higher heat input that was used consistently for thick plate welds, see *Table 22*. Bead width b_2, however, tends to become greater in thick multipass welds as a consequence of higher heat input, compared with the two-pass thin plate welds. This accrues from relatively similar welding current in SAW welding of both two-pass thin plate welds and multipass thick welds, as different heat inputs were attained by adjusting the torch travel speed, compare *Tables 7* and *10*. As a result, weld bead penetration and hence a_b and h_w become relatively similar, regardless of plate thickness. Contrary to this, arc voltage was higher for the multipass welds, with associated widening of weld bead width b_2, as shown in *Table 22*.

Consequently, the differences in bead size of the final filling layers are mostly heat input related and not so much welding process or plate thickness related. Realising that the weld bead height a_b and individual bead layer thickness h_w, in particular, relate to hydrogen diffusion distances in accordance with Eq. (37), one cannot expect significant differences in the final local hydrogen concentration H_{Rmax} between SAW and SMAW that would only arise from the reason that they are two different welding processes. With regard to the possibility of having higher weld bead overlap ratio d/h_w in the case of SAW, its effects on hydrogen accumulation and hence on the H_{Rmax} cannot be confirmed by the experiments performed in the present thesis. It is therefore thought that numerical modelling using FDM and/or FEM would be viable of elucidating this phenomenon.

According to *Table 4*, in one case two arc energy levels of 3.0 an 2.0 kJ/mm were adopted for the *OK 74.78* electrode at an equivalent weld hydrogen content of H_D = 15.5 ml/100 g DM (IIW), the corresponding specimens being *U33* and *U34*, respectively. The outcome was that *U33* exhibited cracks (after 7 days from the completion of welding), whereas *U34* did not. This could be regarded as a demonstration that weld metal in *U34* associated with lower arc energy and hence displaying smaller bead size than its counterpart *U33*, was less prone to WM cracking due to the bead size effect, in particular. *Table 22* shows that arc energy in the 1.5–5.0 kJ/mm range affects notably the bead size in the examined SMAW welds. These findings imply, bead size may induce a secondary effect on cracking occurrence, once the other crucial factors, i.e., strength and hydrogen are such to place the weld metal in question sufficiently close to its Crack – No Crack boundary line. This would explain why the bead size effect seems to become indiscernible for the majority of the data locating essentially either in the No Crack or the Crack region, c.f. *Figs 34–36*. Anyway, as only one test per arc energy level is available at a comparable hydrogen level for this comparison, one cannot draw any generalised conclusions concerning the bead size effect.

According to the majority of the U-Groove experiments made in the present thesis, the possibility of bead size affecting weld metal hydrogen cracking susceptibility as an underlying mechanism, could not be confirmed nor excluded, see *Tables 3–7* and *Figs 35* and *36*. What the cracking experiments indisputably demonstrate is that, eventually, the SMAW and SAW cracking test results were practically congruent with each other, as shown in *Figs 34*, *35* and *36*, provided that the results were normalised with the corresponding values of the true weld metal hardness $HV_{5(max)}$ and the actual weld metal chemical composition P_{cm}.

As a result, whatever the effects of bead size on WM cracking sensitivity might have been – since the bead size in terms of width b_2 was unambiguously greater in the case of SAW – these effects are obviously still of a second order of magnitude, in relation to weld metal strength and weld hydrogen.

5.8 Effect of weld metal chemical composition and local microstructural mismatch on cracking sensitivity

Earlier work[37] on high strength welds suggests that those extra-high strength weld metals which transform from austenite into ferrite at a lower temperature than the surrounding parent steel HAZ may be more prone to WM hydrogen cracking than weld metals displaying the reverse transformation sequence in relation to the parent steel HAZ. Lower γ–α phase transformation temperature in the weld metal means that a greater part of the weld cooling period will be spent with the weld metal being austenitic. As austenitic, weld metal has lower hydrogen diffusion coefficients and higher hydrogen solubilities than in the ferritic state, consequently, an austenitic weld metal can store high hydrogen contents that cannot move fast enough to the fusion boundary due to slow diffusion rate of hydrogen in austenite. This eventually results in elevated hydrogen concentration in the weld metal[37].

Should this be the case, besides weld metal, parent steel grade in question may also induce an indirect effect on WM cracking sensitivity. According to *Table 21*, those two Ni-Cr-Mo bearing SMAW weld metals, *OK 75.75* and *OK 75.78*, that had their γ–α phase transformation temperatures lower than that of the parent steel were recognised to exhibit extensive hydrogen cracking, whereas the other two leaner-alloyed *OK 74.78* and *OK 48.08* weld metals associated with higher phase transformation temperatures than the parent steel tended to be crack-free over a wide range of weld hydrogen. Since only one parent steel grade was used in the present work, one, however, cannot reliably verify whether this outcome in the cracking tests c.f. *Tables 3–5* is a plain coincidence, or a consequence of differences in the γ–α phase transformation temperature that had further contributed to cracking behaviour of the examined SMAW weld metals.

In many cases in practice, weld metal and HAZ microstructures are not essentially martensitic, which leads to thinking that temperatures such as A_{r3} or B_S might in these cases be more relevant temperatures than M_S. The way one study[37] equates martensite with ferrite in distinguishing between microstructures with slow (austenite) or high (ferrite/martensite) hydrogen diffusion rates implies that, as far as diffusion of hydrogen is concerned, M_S temperature would be a relevant description irrespective whether phase transformation from austenite eventually results in a ferrite, or martensite, microstructure. Any systematic comparisons of relevant temperatures in such cases, however, were not reported in the literature. An M_S temperature expression for weld metal, which incorporates the influence of the WM oxygen content, has been proposed[37] as further improvement to better describe the effect of oxide inclusion on austenite decomposition

kinetics. This suggests that modified M_S temperature expressions of that kind would more realistically take account of weld metals that are not essentially martensitic.

Nevertheless, the rise in the WM cracking occurrence when moving from the 480–580 MPa yield strengths up to the 680–890 MPa yield strengths is found quite dramatic for the investigated SMAW and SAW weld metals, as shown in *Tables 3–7* and *Figs 34–36*. Whilst *Fig. 34* implies, this phenomenon could be explained solely by the residual stress σ_{resL} effect, the rapid jump from the No Crack region into the Cracking region in the case of SAW weld metals when transferring from *OK Tubrod 15.26S* to *OK Tubrod 15.27S* leaves some doubt that the lower γ–α phase transformation temperature in the case of the extra-high strength *OK Tubrod 15.27S* weld metal could have contributed to its unambiguously higher crack sensitivity, compared to high strength *OK Tubrod 15.26S* weld metal, see *Tables 6–9* and *Figs 35–36*.

Overall, the present experimental results thereby demonstrate that the occurrence of transverse hydrogen cracking in multipass WMs is associated with the development of elevated residual stresses approaching the weld metal yield strength. Otherwise, critical conditions can hardly be met within a multipass weldment that lacks any geometrical discontinuity, such as a groove bevel acting as stress raiser in the case of single-pass root or HAZ underbead cracking. Conversely, should the residual stresses become relieved, as in the case of, e.g., thin plate welds and/or under conditions of low structural rigidity, it is found nearly impossible to create cracks under any combination of strength and hydrogen, as shown in *Fig. 37* and *Table 10*.

It is widely demonstrated[2, 3, 16–18, 54, 98, 99, 114, 115] that intensive accumulation of plastic strain in softer microstructures such as grain-boundary ferrite GBF is often a prerequisite for WM hydrogen cracking in thick multipass welds. Metallographic examination conducted in the present thesis, however, revealed that even the presence of high volume fractions of GBF, alone, did not lead to crack formation. According to *Table 23*, the highest amounts of GBF were associated with the *OK 74.78* and *OK 48.08* weld metals, i.e., particularly those that tended to be crack-free, unless subjected to very long periods before the NDT in the case of *OK 74.78*.

Assuming that the role of GBF acting as a path for diffusing hydrogen is conclusive, it is not easy to explain why particularly those weld metals with the highest amounts of GBF either did not crack at all, or required extreme conditions, i.e., the combination of a 7 days period and 15.5–17.5 ml/100 g DM (IIW) hydrogen, to reveal cracks. Meanwhile, the 16 h period was found perfectly sufficient for cracking to appear in the extra-high strength weld metals having much less GBF than the lower strength ones, see *Table 23*. One explanation may be that all those recent cases where the presence of GBF was found to indisputably contribute to WM hydrogen cracking, are reportedly[116] associated with comparatively low weld hydrogen of $H_D \leq 4.5$ ml/100 g DM (IIW) and with experiments using externally loaded hydrogen charged specimens[16–18]. In the Y- and U-Groove cracking experiments of self-restraining nature, being applied in the present thesis, such low weld H_D is found absolutely inadequate to cause weld metal cracking in those 480–550 MPa yield strength weld metals that contained the largest amounts of GBF.

Therefore, it is concluded that the cracking experiments applied in the present thesis have been, in any case, unable to asses these microstructural effects due to GBF, whether such effect existed or not. On the other hand, as most structural conditions in reality are

of self-restraining nature, the occurrence of WM hydrogen cracking provoked by the combination of $H_D \leq 4.5$ ml/100 g DM (IIW) and large fractions of GBF in the weld metal appears somewhat unrealistic in the light of the present experimental data, compare *Tables 3–7* and *Table 23*.

Hardness traverses summarised in *Table 30* reveal that an increase in SAW weld metal $R_{p0.2}$ when transferring from 550–630 to 690–900 MPa yield strength level is accompanied by a pronounced increase in local hardness mismatch within the multipass weld metals. This manifests itself as an approx. 50–80 HV difference in hardness between the individual maximum and minimum value in the case of *OK Tubrod 15.27S* weld metal, whereas the corresponding difference for *OK Tubrod 15.26S* weld metal is only about 20–25 HV.

Table 30. Local weld hardness mismatch ΔHV (= HV_{max}–HV_{min}) *in the multipass SAW weld metals at different levels of strength and arc energy.*

Specimen No	SAW tubular wire / Flux OK 10.62	Arc energy (kJ/mm)	P_{cm} (%)	CET (%)	HV_{max}–HV_{min} difference (HV)	HV_{ave} (HV) All regions	ΔHV (HV)
U395	OK Tubrod 15.26S	2.0	0.227	0.333	251–277	265	26
U396	OK Tubrod 15.26S	3.0	0.226	0.334	241–262	251	21
U397	OK Tubrod 15.26S	4.0	0.216	0.313	241–262	249	21
U593	OK Tubrod 15.26S	2.0	0.238	0.345	257–277	264	20
U398	OK Tubrod 15.27S	2.0	0.264	0.396	289–336	315	47
U399	OK Tubrod 15.27S	3.0	0.258	0.388	286–367	313	81
U400	OK Tubrod 15.27S	4.0	0.271	0.402	295–345	315	50
U594	OK Tubrod 15.27S	4.0	0.265	0.387	280–362	348	82
U401	OK Tubrod 15.29S	2.0	0.271	0.399	303–367	345	64
U402	OK Tubrod 15.29S	3.0	0.273	0.402	299–362	339	63
U403	OK Tubrod 15.29S	4.0	0.283	0.419	306–376	354	70

* specimens No U395–U403 and U593–U594 : final SAW U-Groove cracking tests at ESAB, U.K.

It should be highlighted that the hardness survey performed in the present thesis did not comprise any microhardness measurements, consequently the measurements cannot reveal the nature of very narrow phase interfaces. Hence, there is no direct evidence that such steep gradient of mismatching strength would have existed also across the phase interface. The results are therefore considered merely an indication of plausible differences in local hardness – and hence strength – properties of different microstructural regions of multipass weld metal, and that these local differences were emphasised with the increase in WM strength.

That local microstructural variations within multipass weld metal can affect the occurrence of hydrogen cracking, is demonstrated in a recent study[121] on SAW welding of extra-high strength HSLA-100 steel. The study reports that most of the appeared transverse WM cracks were densely populated in the weld region in which the microhardness increased gradually from the minimum hardness of a tempered band to the

maximum hardness in the recrystallised region. As the former region had essentially columnar grain structure, whereas the latter composed of equiaxed grains, this means that intensive cracking took place particularly in locations exhibiting both hardness gradient and microstructural gradient. The study[121] concluded that the location of hydrogen cracks formed in the WM was mainly controlled by the local variation in microstructure but was little affected by the initial microhardness of a single microphase itself. This means that a steep gradient in microstructures (and hence in hardness) is more determinant from the standpoint of hydrogen cracking occurrence than an individual microhardness of local microstructural phase. Consequently, cracking was not necessarily related to that WM microphase exhibiting the highest microhardness[121]. These findings are regarded consistent with the present thesis in that steep, local variations in weld microstructures that, for instance, manifests themselves as marked difference in the HV_{min} and HV_{max} of the given local microstructure, can accentuate the sensitivity of the weld metal to hydrogen cracking.

Apart from microhardness, it should be stressed that the results of the present thesis, in accordance with a number of works made elsewhere[2, 3, 12, 23, 26, 52, 53, 76, 107, 117] clearly demonstrate that WM hydrogen cracking sensitivity, and the need of elevated T_0/T_i, increase abruptly with the increase in WM tensile strength R_M, accompanied by an increase in *macrohardness*, $HV_{5(ave)}$ or $HV_{5(max)}$, as shown in *Figs 36* and *39*.

It has been shown[38] that for bimetallic welds, accentuated local strength mismatch incorporating softened local microstructural regions adjacent to coexisting microstructures of higher strength, can, under external loading, create conditions that favour elevation of linear-elastic stress in the high strength microstructures, whilst accumulation of plastic strain occurs in the softened regions. Should such a steep strength gradient exist across the phase interface in the present case, while the simultaneous transport and accumulation of hydrogen happens to result in microcrack formation at the phase interface, conditions for unstable crack growth may, under high residual tensile stress, be met at the interface of the two regions, of which one exhibits plastic behaviour while the other still behaves practically linear-elastically.

Anyway, metallography made here is yet too deficient to draw any firm conclusions on the mechanism principally described here. Moreover, in practice, overall weld metal overmatching strength is likely to ‘shield’ the weld against such kind of unstable crack propagation, anyway.

5.9 Comparison of hydrogen diffusivity between SMAW, SAW and FCAW multipass weld metals

In general, the measured D_H values were found to decrease in the order of Armco iron, fine-grained structural steel and the weld metal, as one would expected, see *Table 20*. This is attributed to the greater number of hydrogen traps available in the weld metal than in the low-impurity fine-grained structural steel, or in the annealing heat-treated Armco iron that represents D_H values nearly characteristic of pure α-iron.

Regarding weld metal it was found that the D_H values do not differ significantly between SMAW and FCAW welds. The D_H values recorded for the SAW filling layers also lie relatively close to those for the FCAW and SMAW weld metals, whereas those for the SAW mid-thickness and root runs are seen to approach those for the fine-grained structural steel, as shown in *Table 20*.

The measurements of the present thesis revealed a systematic tendency in all the examined SAW specimens for their D_H values to increase in weld thickness direction when transferring from the weld upper-area to the weld root area. This phenomenon, however, was not recognised in the case of the FCAW weld metals, compare *Figs 28a* and *28b*. It seems obvious that the weld chemical composition in the SAW filling layers and the root runs is not identical, because of the dilution that is always more pronounced in the weld root and is, overall, a characteristic feature of the SAW process. However, considering only the effect of chemical composition, it is still difficult to explain the observed differences in D_H between the filling runs and the weld central part, as the chemical composition in these weld metal regions should be more or less similar.

An explanation[5b, 36b] for the observed differences in the D_H values associated with different SAW weld depths could lie in the nature of weld thermal cycle. The high heat input Q of 5 kJ/mm in SAW welds results in pronounced re-heating of the previously solidified weld layers by the subsequent welding runs. This, in turn, causes significant microstructural changes over a wide distance in the weldment thickness direction. The higher the Q and the greater the number of successive thermal cycles, the lesser also becomes the number of hydrogen traps available in the weld metal. It could also be postulated that the smaller bead size of the FCAW welds allows the inclusion of all types of microstructures in all the diffusion samples, whereas the SAW bead size means that the diffusion specimens from near the surface only contain as-welded microstructures as opposed to more reheated microstructures towards the weldment root.

These phenomena are likely to explain the higher D_H values in the root area of the SAW welds, compared to the filling layers, as well as why the examined FCAW weld metals, unlike the SAW welds, display no corresponding change in D_H as a function of weldment thickness, see *Fig. 28b*. The variation of D_H in weld thickness direction is found not systematic, but relatively random between the examined FCAW specimens.

Overall, the scatter in measured D_H values appears greater among the values summarised from various investigations even for the same welded region, than it is among the values associated with entirely different weld regions, i.e., weld metal, HAZ, or parent steel, as shown in *Table 18*.

5.10 Comparison of cracking sensitivity between SMAW and SAW multipass weld metals

In the first instance and according to nominal yield strength $R_{p0.2}$, the SAW *OK Tubrod 15.27S* weld metals seem to exhibit cracks at lower weld H_D contents than the SMAW *OK 75.75* weld metals, compare *Tables 4* and *7*. This would imply, at similar levels of

nominal strength and hydrogen, SAW process is likely to represent greater risk to weld metal hydrogen cracking than the SMAW process.

A comparison of the SMAW and SAW U-Groove experiments in terms of their cracking risk according to *Tables 4* and *7* reveals that in the case of the SMAW welds of $R_{p0.2} \approx 680–700$ MPa, hydrogen contents of $H_D \approx 10$ ml/100 g DM (IIW) were necessary to induce cracks. For cracking to occur in the SAW welds of 700 MPa nominal yield strength, the corresponding critical H_D was only about 5 ml/100 g DM (IIW). These findings are in line with the preliminary SAW U-Groove test results c.f. *Table 6*, thereby suggesting that, at a comparable level of WM yield strength, SAW multipass weld metals would be more susceptible to WM hydrogen cracking than the SMAW welds. As a result, one would conclude that the tubular SAW consumables c.f. *Table 2b* produce weld metals that, in relation to their strength, are more crack sensitive than the SMAW weld metals c.f. *Table 2a*.

Sorting all the examined SMAW and SAW U-Groove cracking tests according to their actual weld metal chemical composition and measured weld metal hardness, the differences in WM cracking sensitivity between the SAW and SMAW experiments are seen to attenuate, as shown in *Figs 35* and *36*. Consequently, in terms of weld metal P_{cm} and $HV_{5(max)}$, all the SAW U-Groove cracking test results are found to agree nicely with the Crack – No Crack boundaries in *Figs 35* and *36*, i.e., the boundaries that were originally derived according to the SMAW Y- and U-Groove data c.f. *Tables 3–5*.

It follows that both in terms of $H_{cr}–P_{cm}$ and $H_{cr}–HV_{5(max)}$ relationships, the present SAW U-Groove cracking test results in *Tables 6* and *7* comply satisfactorily well with the corresponding SMAW Y- and U-Groove cracking test data, as shown in *Table 29*. The SAW U-Groove test results obtained in the present thesis do not, therefore, assign any need to modify the original Crack – No Crack boundaries derived from the SMAW cracking test data and expressed in terms of the $H_{cr}–P_{cm}$ and $H_{cr}–HV_{5(max)}$ relationships in *Figs 35* and *36*.

With regard to the $H_{cr}–\sigma_{resL}$ ($= R_{p0.2}$) relationship, the question of general validity is less clear, as shown in *Table 29* and *Fig 34*. Assuming the WM strength values given for the examined SAW welds according to *Table 29* by the consumable manufacturer prevailed also in the U-Groove cracking tests, leads to the conclusion that the examined SAW multipass weld metals would be more crack sensitive than awaited on the basis of their strength. Nevertheless, *Figs 35* and *36* show that the P_{cm} and HV_{max} based approaches provide a realistic description of WM cracking sensitivity of both the SAW and SMAW multipass weld metals examined in the present thesis.

It is interesting to notify that all the SAW U-Groove cracking test results fell realistically within the Crack – No Crack regions derived according to the SMAW data, regardless of the greater heat input range of $Q = 2.0–5.0$ kJ/mm associated with the SAW process, in comparison with the 2.4 kJ/mm for the SMAW process. At a comparable level of WM strength, one would have expected the higher Q in the case of SAW to yield weld metals of lower hardness than for the SMAW welds. Should this occur, it would have manifested itself as corresponding differences in the weld H_{cr} levels between the $H_{cr}–P_{cm}$ and $H_{cr}–HV_{5(max)}$ based diagrams, since the effects of Q are incorporated into the $HV_{5(max)}$ based approach, but not accounted for in the P_{cm} based approach. *Figs 35* and

36, however, do not reveal any those kind of systematic differences in the cracking test results, as shown also in *Table 29*.

It can hence be concluded that the effect of Q on WM hydrogen cracking occurrence in multiple-pass welds either (i) does not exist, or simply (ii) was too small to become notable in the present SAW cracking tests c.f. *Tables 6–8*. Since higher heat inputs have been previously reported[8] to accentuate WM cracking risk in multipass welding, the latter explanation seems more likely. Should, for instance, the local hydrogen concentration H_{Rmax} become higher in SAW than SMAW as a result of pronounced weld bead overlapping and somewhat greater bead width, could not be fully confirmed in the experimental cracking tests of the present thesis. The analytic calculations in Sections 5.3.2 and 5.3.3 suggest, this might well have been the case.

Presumably, *heat input* affects cracking sensitivity of weld metal within only a narrow region in the immediate vicinity of the Crack – No Crack boundary of a certain weld metal strength – weld hydrogen -combination. Therefore, the effect of Q seldom becomes notable and is hence difficult to reveal intentionally in the experimental cracking tests. According to *Figs 34–36*, only few of the data points actually lie so very close to the Crack – No Crack boundary line, whilst the vast majority of the data locates entirely either deep within the Cracking, or the No Crack, region. The same explanation probably applies also to *interpass time* t_i. Otherwise, it would be difficult to consider theoretical reasons why no effect of t_i on hydrogen cracking was apparent in the SMAW cracking experiments c.f. *Table 4*. A nearly fivefold reduction in t_i from 15 to 4 sec should lead to a corresponding reduction in thermal factor of diffusion $\Sigma D\Delta t$ during the time between two successive passes and throughout the welding operation. That the effect of t_i would be so effete it only becomes notable for those data points locating immediately adjacent to the Crack – No Crack boundary line, would thereby explain why the changes in t_i did not affect the final outcome of the cracking tests c.f. *Table 4*.

Nevertheless, the conclusion on the basis of the experiments made here is that, relative to the WM strength and weld hydrogen, heat input Q and interpass time t_i are of a secondary importance as crack controlling factors, as regards to hydrogen cracking in multipass weld metals.

5.11 Differences in final hydrogen content between single-pass and multiple-pass welds

The SAW U-Groove cracking tests for the extra-high strength *OK Tubrod 15.27S* and *OK Tubrod 15.29S* multipass weld metals c.f. *Table 9* demonstrated that exceptionally high interpass temperature T_i was necessary to prevent WM hydrogen cracking, once the other crack controlling factors: weld metal strength and hydrogen were such that the Cracking region was indisputably entered. This contrasts with the present knowledge[3b, 13, 22–25, 40, 59, 63, 69, 77, 101] on single-pass welds that, in this sense, do benefit remarkably from the use of elevated preheat temperature T_0. This has been attributed to intensified diffusion and effusion of hydrogen that progressively lower the H_{R100}/H_0

values as soon as T_0 reaches 75–100°C, the consequence being that weld t_{100} cooling time and hence $\Sigma D\Delta t_{(100)}$ start to increase sharply according to Eqs (1)–(3), respectively, see *Appendix 10*.

Therefore, analysis was made to evaluate the differences in the final hydrogen content H_{Rmax} between single-pass and multipass welds in terms of their $H_{R100(d=0)}/H_0$ and $H_{Rmax(d>0)}/H_0$ values, respectively.

With regard to the distribution of hydrogen concentration in multipass weld, it is known[21, 22, 94] that hydrogen concentrates beneath the final weld bead layer where the maximum values of the local hydrogen concentration were found[94] consistent with the results of gas chromatographic measurements of hydrogen evolved from specimens sectioned at various thicknesses of a weld. The calculations and experiments both demonstrate[94, 95] that the H_{Rmax} in multipass weld is close to the weld hydrogen content determined using a quenching method for a single-pass weld, that is, the weld initial diffusible hydrogen, H_0.

Assuming the difference in the H_{Rmax}/H_0 ration between single- and multiple-pass welds was responsible for the insensitivity of the multipass SAW welds to elevations of the T_i in the actual U-Groove experiments c.f. *Table 9*, analytic calculations were made to derive a set of $H_{R100(d=0)}/H_0$ and $H_{Rmax(d>0)}/H_0$ values for single- and multiple-pass welds, respectively, over a range of weld thermal conditions. These calculations are presented in *Table 31* that defines the weld thermal cycle in terms of T_0–t_{100} combinations corresponding to 1.7 kJ/mm arc energy welding of a 50 mm thick plate in accordance with *Appendix 10*.

In general, *Table 31* shows that, at a given level of T_0 and t_{100} which transfer further to $\Sigma D\Delta t_{(100)}$ according to Eq. (3b), single-pass welds are rewarded for applying elevated T_0 in that the H_{Rmax}/H_0 ratio tends to always become lower in single-pass weld than multipass weld. This trend is seen to accentuate towards higher thermal heat inputs, i.e., greater values of $\Sigma D\Delta t_{(100)}$, which means that, at an equivalent level of H_0, elevating the T_0/T_i is much less beneficial in lowering the H_{Rmax} in the case of multiple-pass welds than for single-pass welds. This finding is in agreement with the outcome from the SAW U-Groove experiments c.f. *Table 9* and may hence explain, why it was necessary to elevate T_i so remarkably once the Cracking region was entered, despite a comparatively low weld H_0 content. This is demonstrated also in *Fig. 39*.

It can hence be concluded that for multipass welds, going for strength – hydrogen combinations readily locating in the No Crack region is much more effective and desirable for preventing WM hydrogen cracking than the enhancement of hydrogen effusion by elevating the T_0/T_i under conditions that inevitably attribute to Cracking region at a given weld metal strength – hydrogen combination. In this respect, effective ways and means to control hydrogen cracking behaviour of multipass welds do differ from those suffusing single-pass welds.

Looking *Table 31* in more detail, it can be seen that for single-pass welds, Eq. (1a) that is a plain description of the thermal driving force for hydrogen diffusion and hence does not include any bead size effects, predicts lower $H_{R100(d=0)}/H_0$ values than Eq. (49) incorporating the bead size and thermal driving force, compare (2) and (3) in *Table 31*. This is particularly so with high thermal heat inputs, where $H_{R100(d=0)}/H_0$ acc. to Eq. (1a) become unrealistically low, compared to the corresponding values acc. to Eq. (49). It is

also evident that large beads (i.e., h_w = 8 mm) retain much greater amount of hydrogen than small beads (h_w = 3 mm) do, which further manifests itself as a wide range in the calculated $H_{R100(d=0)}/H_0$ values in accordance with Eq. (49), see *Table 31*. Even then, the $H_{R100(d=0)}/H_0$ values for single-pass welds and associated with h_w = 3–8 mm tend to go under the corresponding range of the $H_{Rmax(d>0)}/H_0$ values for multipass welds acc. to Eqs (49)–(50), compare [3] and [5] in *Table 31*.

Table 31. Comparison of the H_{Rmax}/H_0 ratio[*] between single- and multiple-pass welds over a range of weld thermal conditions.

Preheat temperature T_0 (°C)	Weld cooling time t_{100} (sec)	Thermal factor of diffusion [1] $\Sigma D\Delta t_{(100)}$ (cm^2)	Remaining diffusible hydrogen / initial hydrogen -ratio in single-pass weld $H_{R100(d=0)}/H_0$		Final local maximum hydrogen / initial hydrogen -ratio in multipass weld $H_{Rmax(d>0)}/H_0$	
			thermal[2]	geom. incl.[3]	graphic sol.[4]	analytical sol.[5]
25	45	0.001793	0.88	0.96–0.99	0.85–0.90	1.04–1.10
50	70	0.002318	0.85	–	0.85–0.90	–
75	180	0.004447	0.73	–	0.80–0.90	–
100	800	0.016505	0.32	0.60–0.94	0.70–0.85	0.93–1.08
125	1600	0.034148	0.10	–	0.65–0.85	–
150	2200	0.048899	0.03	0.28–0.83	0.60–0.80	0.53–1.04
175	2500	0.056732	0.02	–	0.55–0.70	–
200	3000	0.070430	0.01	0.27–0.76	0.50–0.70	0.57–1.06

*) for single- and multiple-pass welds, H_{Rmax} refers to $H_{R100(d=0)}$ and $H_{Rmax(d>0)}$, respectively

1) calculated acc. to Eq. (3b)

2) calculated acc. to Eq. (1a) excluding the bead size effects, applying $\Sigma D\Delta t_{(100)}$ in accordance with Eq. (3b) and assuming A = 70

3) calculated acc. to Eq. (49) accounting for bead size effects (h_w = 3 and 8 mm correspond to the lower and higher value of the given range), or determined from *Fig. 32*

4) graphic solution acc. to Osaka University & Nippon Steel Corp. c.f. *Fig. 6* originally presented in Ref.[20]

5) analytical solution c.f. *Table 27* and calculated acc. to Eqs. (49)–(50) using $\Sigma D\Delta t/h_w^2$ values acc. to Eq. (49) and estimated values for the weld overlap ratio d/h_w c.f. Refs[32,33] (applied range: bead sizes 3–8 mm)

For multipass welds, the graphic and analytic solutions of the $H_{Rmax(d>0)}/H_0$ are seen to agree comparatively well in that both expressions show accordingly, the $H_{Rmax(d>0)}/H_0$ decreases with increasing thermal heat inputs in terms of T_0 and t_{100} and, hence, $\Sigma D\Delta t_{(100)}$, compare [4] and [5] in *Table 31*. It is noteworthy that the range of variation for these two expressions originates from different sources. In the case of the analytic expression [5], the range of variation is caused by the bead size related effects, the minimum and maximum values corresponding to h_w of 3 and 8 mm, respectively, whereas for the graphic expression [4] the range is attributed[20] merely to the differences in the number of weld bead layers, *l*, and heat input Q, as shown in *Fig. 6*. Anyway, both these expressions show consistently that the $H_{Rmax(d>0)}/H_0$ associated with multipass welding declines to a lesser degree than the corresponding $H_{R100(d=0)}/H_0$ for single-pass welds, compare [4] and [5] with [3] in *Table 31*. This means that hydrogen effusion as a result of elevated T_0 occurs more efficaciously in single-pass welding, whereas multiple-

pass welds, particularly those with greater bead size, tend to retain hydrogen even when thermal heat inputs increase due to elevated T_0/T_i, as shown in *Table 31*.

This finding is in line with the outcome from the SAW U-Groove experiments c.f. *Table 9* and *Fig. 39*. It suggests that, besides increasing WM strength, the described difference in the responses between the $H_{Rmax(d>0)}/H_0$ and $H_{R100(d=0)}/H_0$ to the elevation of T_0/T_i might explain, why the need to elevate the T_i temperature for the extra-high strength *OK Tubrod 15.27S* and *15.29S* weld metals is so abrupt in multipass welding, once the WM strength and hydrogen are such that the weldment in question inevitably falls within the Cracking region.

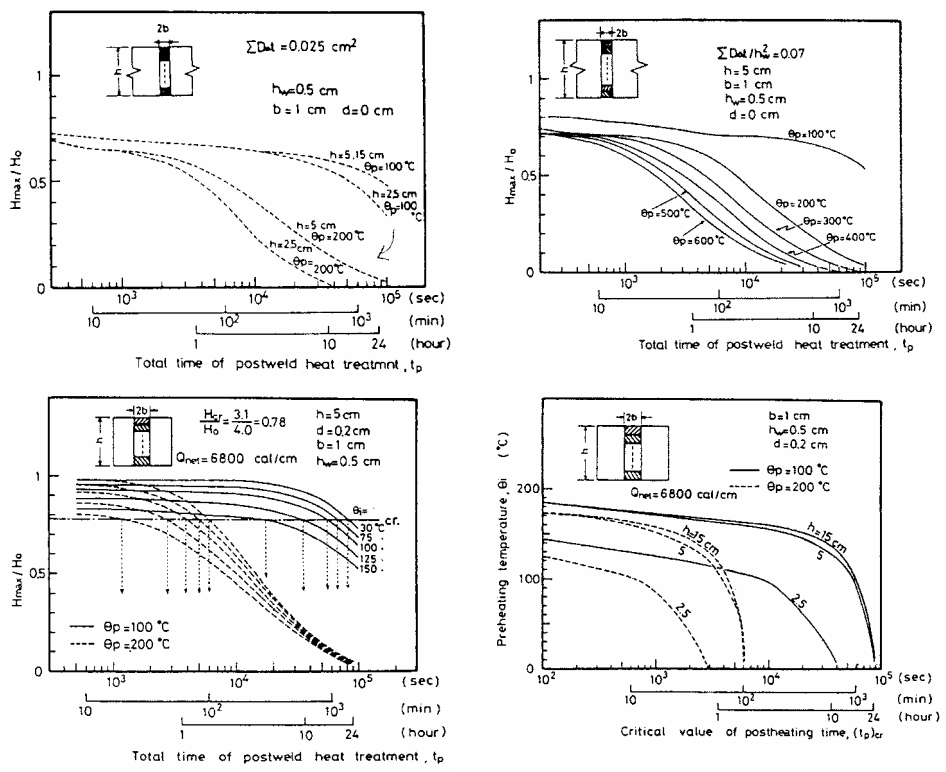

Fig 38. Final maximum hydrogen concentration – initial hydrogen content -ratio H_{max}/H_0 in multipass weld as a function of post-weld heat treatment in terms of heating time t_p and post-heating temperature θ_p[20].

Apart from preheating, or sustaining the elevated interpass temperature during welding, applying retarded post-weld cooling, or post-weld heat treatment, is known to effectively reduce hydrogen cracking risk by promoting hydrogen effusion. Examples[20] of such post-weld treatments for multiple-pass welds are shown in *Figs 38a–38c*.

According to *Fig. 38*, post-weld heat treatment at temperatures about 200°C appears, in the case of multipass welds, somewhat more effective in lowering the H_{max}/H_0 than the use of elevated preheat/interpass temperatures[20], compare *Fig. 38* and *Table 31*.

Applying post-weld heat treatments in accordance with *Fig 38*, the H_{max}/H_0 is seen to become depressed to around 0.30–0.50[20]. *Table 31*, in turn, shows that in order to gain H_{max}/H_0 values equal to or less than 0.50 requires the T_0/T_i levels higher than 200°C. It should be highlighted, however, that comparatively long holding times are required in these cases for the treatment to affect more effectively than preheating. In order to achieve H_{max}/H_0 values less than 0.50, for example, around 3–5 hours at the temperature of 200°C are necessary[20], as shown in *Fig 38*.

5.12 Derivation of the prediction formulae for the estimation of safe preheat/interpass temperatures for multipass weld metals

A 'second line of defence' against WM hydrogen cracking consists of engineering formulae for predicting the required preheat/interpass temperatures T_0/T_i for the avoidance of cracking, once the other controlling factors: strength and hydrogen are such that the Cracking region c.f. *Figs 34–36* is inevitably entered.

This analysis comprises two steps: (i) re-analysis of the former SMAW and GMAW Y-Groove data sets of Nippon Steel Corp. (NSC), and (ii) analysis of the SAW U-Groove cracking test results of the present thesis for optimised prediction of 'safe' T_0/T_i estimates.

5.12.1 Re-analysis of the NSC Y-Groove data sets

A data set consisting of former Y-Groove cracking tests[12] made at NSC is given in *Appendix 5*. These data comprise SMAW and GMAW multipass welds of ultimate tensile strengths around 820 and 750 MPa, weld build-up thicknesses of 20, 30 and 40 mm and weld diffusible hydrogen in the range of about 2 to 11 ml/100 g DM (IIW). It was concluded[12] that the critical preheat/interpass temperature T_{cr} for the avoidance of WM hydrogen cracking can be expressed in terms of WM tensile strength R_M, weld build-up thickness a_w and weld diffusible hydrogen content H_D.

Both Okuda et al.[2] and Yurioka et al.[3] have demonstrated the decisive role of WM strength and weld hydrogen more or less accordingly. For the present re-analysis, weld R_M is approximated using weld chemical composition in terms of CET as defined in Eq. (43b). Unlike Yurioka, Okuda found[2] the influence of weld build-up thickness on WM cracking susceptibility quite minimal and hence insignificant in the 20–80 mm thickness range. The U- and V-Groove test results of the present thesis, however, demonstrate that plate thickness does affect the WM cracking occurrence – at least when transferring from 40 mm to 6 mm weld build-up thickness, compare *Tables 4* and *10*. Inclusion of weld build-up thickness a_w as a parameter into the prediction formulae of T_{cr} is therefore regarded imperative.

For the purposes of ‘safe’ predictions of ‘engineering accuracy’, a general expression of the form of Eq. (40a) was taken as a primitive approximation to describe the crack controlling factors in multipass welding, as explained in Section 3.3.3. As first attempt to estimate T_{cr}, the former NSC Y-Groove data set[12] was fitted by the following empirical equation obeying a general form of Eq. (40a), as:

$$T_{cr} = 700 * CET + 9 * a_w^{0.86} + 134 * H_D^{0.40} - 498 \ (°C) \quad (60)$$

where CET is the carbon equivalent (%) according to SFS-EN 1011-2 : 2001 Method B[1b] calculated from the all-weld metal chemical composition, a_w is weld build-up thickness (mm) and H_D is weld diffusible hydrogen content (ml/100 g DM) according to ISO/IIW 3690-1977[57].

Table 32 summarises the required T_0/T_i values for some of the extra-high strength *Y-80C, L-80* and *L-74* weld metals from the NSC Y-Groove cracking experiments[12]. These experimentally determined T_0/T_i values are then compared with calculated T_{cr} estimates according to the Okuda-formula[2] and Eq. (60) derived in the present thesis. *Table 32* reveals that compared to the experimental Y-Groove data[12], the Okuda-formula[2] puts more weight on weld hydrogen, which is mainly due to the logarithmic dependence of T_{cr} on H_D, see *Appendix 1*. This is seen to weaken the accuracy of T_{cr} predictions towards the ends of the applied H_D range, consequently, T_{cr} tends to become somewhat underestimated at very low H_D levels, whereas the highest H_D levels result in overestimation of the required T_{cr}. Furthermore, the Okuda formula[2] disregards the effect of weld build-up thickness a_w, thereby implicitly assuming that the same T_{cr} estimate originally[2] derived for the 40 mm weld thickness would apply over the 20–40 mm range. This is undoubtedly a safe presumption; however, *Table 32* shows it yields even unnecessarily conservative estimates of T_{cr} in the case of 20 and 30 mm weld thickness.

Table 32. Predicted T_0/T_i estimates for extra-high strength Y-80C, L-80 and L-74 weld metals from the NSC experiments[12] – comparison of T_0/T_i estimates according to Okuda-formula[2] and VTT formulae Eqs (60) and (61) with the required T_0/T_i based on the experimental NSC Y-Groove cracking test data[12].

Filler material	Weld metal strength R_M [1] (MPa)	Weld metal alloying CET [2] (%)	Weld build-up thickness a_w (mm)	Weld hydrogen H_D (ml/100 g DM IIW)	Preheat / Interpass temperature T_0/T_i (°C)			
					NSC Y-Groove experi-ments[12]	Okuda-formula[2]	VTT Eq. (60)	VTT Eq. (61)
Y-80C	852	0.321	40	2.0	75	65	118	74
L-80-1	825	0.312	20	4.3	75	155	79	82
			30		125		128	131
			40		175		175	179
L-80-2	814	0.300	20	6.7	100-125	209	117	121
			30		175		166	170
			40		> 200		214	217
L-80-3	807	0.293	20	10.4	150	266	167	152
			30		200		217	202
			40		> 200		264	249
L-74-1	744	0.278 (0.248)	30	4.0	75	95	76–98	78–99
L-74-2	745	0.248	20	6.7	> 50	167	81	85
			30		≤125		130	134
			40		175		177	181
L-74-3	733	0.280 (0.248)	20	9.9	> 75	213	129–151	117–140
			30		≤150		178–200	167–189
			40		200		226–248	214–236

[1] measured NSC tensile test data acc. to Ref.[12]

[2] calculated acc. to Eq. (43b) applying analyses of WM chemical compositions given in Ref.[12]

According to *Table 32*, Eq. (60) derived in the present study yields surprisingly accurate estimates of T_{cr}, in view of the fact that a single expression is applied to describe the whole dataset, instead of three sub-equations as the Yurioka-formula[3] does, see *Appendix 1*. An obvious shortcoming of Eq. (60) is, however, that it does not allow for adequate relaxation of T_{cr} at very low weld H_D levels, thereby resulting in an unnecessarily high T_{cr} estimate in the case of the *Y-80C* weld with only 2.0 ml/100 g DM (IIW) hydrogen, for example.

In order for adjusting Eq. (60) to reward lowering hydrogen, an alternative expression is derived so that the logarithmic effect of weld hydrogen H_D on T_{cr} would become more accentuated, particularly at the lower tail of the H_D range. Eq. (40b) in Section 3.3.3 gives a general form of this revised formula. Applying a general formulation in accordance with Eq. (40b), the NSC Y-Groove datasets[12] in *Table 32* were fitted by a revised formula of the form:

$$T_{cr} = 700 * CET + 9 * a_w^{0.86} + \{[2800 * \ln(H_D)] / (12 * H_D^{0.21})\} - 505 \ (°C) \qquad (61)$$

Table 32 shows that within the examined NSC datasets[12], Eq. (61) yields a desired improvement of accuracy of the T_{cr} predictions associated with both low and high weld hydrogen contents of $H_D \approx 2.0$ and 9.9–10.4 ml/100 g DM (IIW), respectively.

It is noteworthy that on account of the available NSC data[12], the following validity limits for Eqs (60) and (61) should be considered:

$20 \leq T_{cr} \leq 200$ (°C)
$0.24 \leq CET \leq 0.33$ (%)
$20 \leq a_w \leq 40$ (mm)
$2.0 \leq H_D \leq 10.4$ (ml/100 g DM (IIW))

Consequently, in view of the analysed NSC Y-Groove datasets[12], Eqs (60) and (61) provide a realistic description of the required T_{cr} for extra-high strength multipass welds. In the case of either very low, or comparatively high, weld H_D, Eq. (61) is concluded to provide 'realistic' and 'safe' estimates of T_0/T_i, consequently Eq. (61) should be preferred to Eq. (60) for these cases.

5.12.2 Comparison of the NSC Y-Groove and VTT U-Groove data sets in view of required preheat/interpass temperatures

In the light of the results of the present thesis, Eqs (60) and (61) that both rest entirely on the NSC Y-Groove data[12], seem to overestimate the 'true' T_0/T_i that was actually required to prevent cracking in the SAW U-Groove cracking tests, compare *Table 7* and *Table 32*. This finding is endorsed by the NSC Y-Groove data[12] on lower strength *L-60* weld metals, see *Appendix 5*.

Contemplating the outcome of all the cracking tests in *Tables 3–8* and *Table 32*, it looks evident that WM cracking susceptibility according to the present VTT cracking experiments is lower than anticipated from the NSC Y-Groove data[12], or according to the formulae of Okuda et al.[2] and Yurioka et al.[3]. This applies particularly to welds of moderate strength in the $R_M \approx 600$–700 MPa range.

Table 33. Examples of differences in T_0/T_i estimates according to the VTT and NSC cracking test results for SMAW multipass weld metals.

Electrode	Weld metal strength R_M (MPa)	Weld thickness a_w (mm)	Weld hydrogen H_D (ml/100 g DM IIW)	Preheat / Interpass temperature T_0/T_i (°C)	
				NSC Y-Groove experiments[12]	VTT Y- and U-Groove experiments
OK 75.78	965	40	3.3	290	≈ 100–110
	965	40	4.3	310	> 110
Nittetsu L-80	845	40	4.0	175	< 90–100
	845	40	10.9	> 200	≈ 100
OK 74.78	650	50	10.0	150	< 90–100
	650	50	18.9	180	> 110

Examples of differences in the cracking test results between the present VTT experiments and the former ones at NSC[12] are given in *Table 33*. It shows, whenever preheating was necessary to prevent cracking, the Y- and U-Groove experiments of the present thesis indicate lower required T_{cr} levels than the former NSC Y-Groove tests[3b,12]. The present Y- and U-Groove cracking tests also demonstrate preheating not to become necessary until at WM strength and weld hydrogen levels notably higher than in the case of the NSC Y-Groove tests[12], compare *Table 4* with *Table 32* and *Appendix 5*. It is worth highlighting that with respect to *Nittetsu L-80* welds, the Y-Groove specimen geometry and the weld metal strength, thickness and diffusible hydrogen content all were equivalent between the NSC[12] and the VTT cracking experiments, compare *Table 3* and *Table 32*.

The reason for this discrepancy between the VTT and NSC cracking test results has yet remained unexplained. Since the time from the completion of welding to NDT inspection was not reported for the former NSC experiments[12], differences in the outcome of the cracking tests at NSC and VTT could, in principle, arise from different time periods applied in the experiments made at these two institutes. This would also explain why the attempts made in the present thesis to reproduce the former NSC Y-Groove test results[12] were unsuccessful, as shown in *Tables 3* and *33*. The lack of recorded time data for the former NSC experiments, however, prevents one to draw any sound conclusions on possible effects of time from welding to NDT in these cases. The results from a recent study[117] on hydrogen cracking in multipass SAW weld metals allow one to draw a conclusion that the time factor becomes increasingly important towards lower strength weld metals, whilst the extra-high strength welds resembling the *L-80* exhibited cracks already within a much shorter period of time. Lowering the contents of alloying elements in the weld metal was reported[117] to result in longer fracture times. This is in line with the recognised responses of the different weld metals investigated in the present thesis to the time period before NDT, as the influence of time from welding to NDT was recognised particularly in the case of the moderate strength *OK74.78* weld metal of $R_{p0.2} \approx 550$ MPa, see *Table 4* and *Figs 34–36*.

Another possible explanation may lie on the fact that all the SMAW weld metals investigated in the present work, except perhaps *Atom Arc 12018*, had very low impurity levels, i.e., S < 0.006% and P < 0.013%. Of these, *Nittetsu L-80* with 0.001% S and 0.005% P produced the cleanest weld metal, as shown in *Appendix 7*. Thus, weld metals may simply have become cleaner over the decades; the trend similar to what had been recognised[7, 34] in the case of modern steel that nowadays meet extremely low impurity levels, in comparison to conventional steel.

Once in a while, certain doubts have been expressed[27–30] on that lowering steel's impurity level inevitably reduces the number of non-metallic inclusions acting as sites for ferrite nucleation. This, in turn, would manifest itself as increased hardenability that actually results in elevated hydrogen cracking risk[27–30]. Earlier work[7, 34, 52, 53] at VTT, however, demonstrated outstandingly high HAZ hydrogen cracking resistance of some low-carbon modern TMCP steels, in spite of their low impurity contents. It was concluded[34, 52, 53] that lowering carbon contents of modern steel counterbalance the adverse effects of increased hardenability due to cleanliness. As a result, the overall

hydrogen cracking risk in modern low-carbon steel is actually reduced, compared to conventional medium carbon steel.

It is known[40, 75] that not only inclusions, but dislocations, vacancies and prior-austenite grain boundaries can act as traps to hydrogen in ferritic steel. That HAZ cracking in clean steels tends, even at high hydrogen contents, to occur predominantly as transgranular rather than intergranular cracking[39] implies that cleanliness of steel can impede grain boundary decohesion that is usually promoted[75] by increasing hydrogen contents. Consequently, at comparable strengths, modern steel with low carbon and impurities tolerates higher hydrogen contents than conventional steel without the occurrence of hydrogen cracking[7, 34, 39, 52, 53].

Analyses of the SMAW weld metals of the present thesis, for example, showed[5b, 36] the presence of substantial amounts of inclusions acting as traps to diffusible hydrogen, which further manifested itself as remarkably lower hydrogen diffusion coefficients measured for the weld metals than in the case of the HAZ or parent steel[5b], see *Table 20*. Low weld impurity content can therefore be expected to reduce WM hydrogen cracking sensitivity, analogously to that in clean steels, without concomitant, undesirable increase in hardenability or disappearance of hydrogen traps.

5.12.3 Analysis of the first SAW U-Groove dataset for optimised prediction of preheat/interpass temperature estimates for multipass welds

The U-Groove cracking test results of the first set of SAW experiments of the present thesis demonstrated that the cracking sensitivity of weld metal is, above all, governed by its strength, as shown in *Tables 7–8*. Whilst all the 7 specimens welded with *OK Tubrod 15.27S* and *OK Tubrod 15.29S* displayed characteristic WM transverse hydrogen cracks, none of the 4 specimens welded with *OK Tubrod 15.26S* revealed any cracks. Whether WM cracking did, or did not, occur, both these phenomena took place totally irrespective of the other parameters: weld hydrogen, heat input and preheat/interpass temperature. This is considered rather obscure and it would certainly be doubtful to interpret or generalise these results in such a way that the other parameters would be totally inconsequential in relation to strength.

The apparent insensitivity of parameters, other than strength, to the occurrence of WM cracking is likely to be a consequence of a deficient hydrogen range in the first SAW test series. *Table 8* shows that the measured weld H_D contents not only had fallen from the target values, but also that the range of the measured values had narrowed substantially from the intended target levels. As a result, the inherent influence of factors such as hydrogen, heat input or preheat/interpass temperature on weld metal cracking was probably impeded, whilst the effect of the most decisive factor from the standpoint of hydrogen cracking, i.e., strength, remained and became accentuated, as shown in *Table 7*.

5.12.3.1 Optimisation of the T_0/T_i prediction with respect to weld metal strength

As *Table 34* shows, applying Eqs (60) and (61) to predict the required T_{cr} for the present SAW U-Groove dataset tends to result in overestimation of the T_0/T_i actually needed for the avoidance of cracking in the case of *OK Tubrod 15.26S* weld metals. Both these equations, however, were demonstrated to describe satisfactorily the former NSC Y-Groove dataset[12], as shown in *Table 32*. This implies, again, that WM strength asserts an even greater influence on the cracking occurrence than anticipated previously. Consequently, Eqs (60) and (61) derived from the NSC data[12] on extra-high strength welds in the $R_M \approx 750–850$ MPa range result in overestimation of the required T_0/T_i in the case of lower strength weld metals in the $R_M \approx 600–700$ MPa range.

Thus, in order to obtain 'realistic', but still safe, estimates of T_{cr} for the SAW U-Groove dataset created in the present thesis, Eq. (61) was re-adjusted with the aim of pursuing optimisation of T_{cr} predictions. Applying this re-adjusted formula of the form in accordance with Eq. (61), the experimental data from the SAW U-Groove multipass cracking tests in *Table 7* were fitted by a formula that puts more weight on the effect of WM strength via its CET, as:

$$T_{cr} = 2310 * CET + 9 * a_w^{0.86} + \{[2800 * \ln(H_D)] / (12 * H_D^{0.21})\} - 1145 \ (°C) \qquad (62)$$

A comparison of T_0/T_i values applied in the SAW U-Groove experiments is presented in *Table 34*, with the numerical predictions of T_0/T_i using the Okuda formula[2] c.f. *Appendix 1*, in conjunction with the VTT formulae Eqs (60)–(62). According to *Table 34*, the re-adjusted Eq. (62) yields more realistic T_0/T_i estimates than the former Eqs (60)–(61), as far as the SAW U-Groove cracking test results of the present thesis are concerned. This is particularly the case for weld metals of moderate strength in the $R_M \approx$ 600–700 MPa range, such as *OK Tubrod 15.26S*.

Table 34. Comparison of the applied T_0/T_i temperatures in SAW U-Groove cracking tests with the predictions for T_0/T_i using Eqs (60), (61) and (62) for the estimation.

Specimen No	SAW tubular cored wire OK Tubrod	Arc energy (kJ/mm)	CET (%)	Weld hydrogen H_D (ml/100 g DM (IIW))	Crack / No crack	Applied interpass temperature T_0/T_i (°C)	Prediction for the required T_0/T_i (°C)			
							Okuda formula[2] (1)	VTT Eq. (60)	VTT Eq. (61)	**VTT Eq. (62)**
U395	15.26S	2.0	0.333	4.9	NC	100	130–167	203	209	105
U396	15.26S	3.0	0.334	6.1	NC	125	135–172	227	232	130
U397	15.26S	4.0	0.332	8.4	NC	150	177–213	263	260	154
U398	15.27S	2.0	0.396	6.1	**C**	150	248–290	270	276	273
U399	15.27S	3.0	0.388	8.4	**C**	100	288–330	303	299	284
U400	15.27S	4.0	0.402	4.9	**C**	125	217–260	251	257	264
U401	15.29S	2.0	0.399	8.4	**C**	125	344–390	310	307	309
U402	15.29S	3.0	0.402	4.9	**C**	150	260–304	251	257	264
U403	15.29S	4.0	0.419	6.1	**C**	100	316–362	287	292	326

(1) T_0/T_i range calculated acc. to Appendix 1 from the weld metal HV data converted into weld R_M estimates using Eq. (48b) and Ref.[119]

Since the No Crack region for the extra-high strength *OK Tubrod 15.27S* and *OK Tubrod 15.29S* weld metals was not reached in the first SAW U-Groove test series c.f. *Table 7*, the absolute safety of Eq. (62) for weld metals in the $R_M \approx 820$–1000 MPa range cannot be guaranteed. Anyway, *Table 34* shows that for these extra-high strength welds, the T_0/T_i estimates according to Eq. (62) are very similar to those given by Eqs (60) and (61) that were based directly on the former NSC Y-Groove data[12] and can hence be expected to lie on the safe side for modern high-strength weld metals.

5.12.3.2 Role of heat input and interpass time in optimisation of the T_0/T_i prediction

According to *Tables 7* and *34*, *heat input* does not assert any notable effect on WM cracking susceptibility. What still requires further experiments is the assessment of the effect of plate/weld build-up thickness, a_w; the present data is yet too sparse to allow for accurate quantification of the thickness factor. Nevertheless, the T_{cr}–a_w dependence employed in Eq. (62) conforms with the dependence reported[3,12] for the former NSC Y-Groove experiments[12], thus being compatible with the Yurioka formula[3] c.f. *Appendix 1*.

As far as *interpass time* t_i is concerned, the present experimental results imply that it does not affect the WM cracking boundary conditions to any significant extent either, as shown in *Table 4*. According to the SMAW U-Groove test results in *Table 4*, provided that WM strength and hydrogen are sufficiently high to cause cracking, it takes place

irrespective of t_i in the range of 3 to 15 min. Similarly, in the cases where strength and hydrogen are too low to cause cracking, crack-free welds are obtained over a wide t_i range from 3 to 15 min. These findings suggest, it is not imperative to include t_i as a separate factor into the predictive formulae assessing the required T_0/T_i for the avoidance of WM cracking in multipass welds.

From *Figs 34–36*, it is recognised that only few of the recorded cracking test incidents actually lie very close to the Crack – No Crack boundary line, whilst the vast majority of the data locates entirely either deep within the Cracking, or the No Crack, region. Presumably, *heat input* affects cracking sensitivity of weld metal within only a narrow region in the immediate vicinity of the Crack – No Crack boundary of a certain WM strength – hydrogen -combination. Therefore, the effect of Q seldom becomes notable and is hence difficult to reveal intentionally in the cracking tests. The same explanation probably applies to *interpass time* t_i. Otherwise, it would be difficult to consider theoretical reasons why no effect of t_i on hydrogen cracking was apparent in the SMAW cracking experiments c.f. *Table 4*. A nearly fivefold reduction in t_i from 15 to 4 sec should lead to a corresponding reduction in thermal factor of diffusion $\Sigma D\Delta t$ during the time between two successive passes and throughout the welding operation. That the effect of t_i would be so effete it only becomes notable for those data points locating immediately adjacent to the Crack – No Crack boundary line, would thereby explain why the changes in t_i did not affect the final outcome of the cracking tests c.f. *Table 4*.

5.12.3.3 Optimisation of the T_0/T_i prediction with respect to plate/weld build-up thickness

The reviewed studies[2, 3, 12, 76] consistently report that plate/weld build-up thickness a_w affects WM cracking most prominently in the 20–50 mm range. Above 50 mm, the effect of a_w gradually starts to level off as thickness increases further, whilst lowering a_w will progressively reduce the cracking risk. This has been attributed[2, 3, 12, 76] mainly to a nearly constant level of weld residual stress above 50 mm thickness, whereas local hydrogen can accumulate still further with the increase in thickness[2]. The results of the present thesis demonstrate that the cracking risk becomes insignificant at weld build-up thickness less than 10 mm, regardless of high weld metal strength and hydrogen content, see *Table 10*.

Considering this, it can be realised that the power-law function applied to describe the effect of a_w on T_{cr} in Eqs (60)–(62) is not an optimum expression for the thickness effect. According to *Table 35*, a term of the form: $T_{cr}(a_w) = \{9 * a_w^{0.86}\}$ in Eqs (60)–(62) yields comparatively realistic estimates in the 20–40 mm a_w range when compared with the actual weld thickness effect pertaining to the NSC Y-Groove experiments[12]. With greater thicknessses, however, this is not true and the power-law expression c.f. Eq. (60) is seen to exaggerate the effect of a_w remarkably, without any abate of the effect, even when coming up to a_w values as great as 100 mm.

Table 35. Assessment of the plate/weld build-up thickness effect – comparison of the effect of a_w on ΔT_{cr} prediction between the outcome of the experimental NSC data[12] and the VTT based expressions according to Eqs (60) and (63).

Plate/weld build-up thickness a_w (mm)	ΔT_{cr} *) acc. to NSC Y-Groove experiments[12] (°C)	Thickness Factor acc. to Eq. (60) – NSC data fit based (in°C)	Thickness factor acc. to VTT SAW U-Groove data fit c.f. Eq. (63) (in°C)
6		42	36
10		65	60
15		93	90
20		118	118
	$\Delta \approx 50$	(Δ 50)	(Δ 51)
30		168	169
	$\Delta \approx 50$	Δ 47	(Δ 45)
40		215	214
50		260	250
60		304	280
70		348	302
80		390	319
90		431	332
100		472	342

*) Δ : shift in the T_{cr} when moving from smaller weld a_w to a greater one (i.e., 20 $\rightarrow$ 30 and 30 $\rightarrow$ 40 mm)

Therefore, an alternative expression was derived in the present thesis by replacing the power-law form c.f. Eqs (60)–(62) with a hyperbolic *tanh* function of the form:

$$T_{cr}(a_w) = \{367 * \tanh(a_w / 60)\} \quad (63)$$

As the thickness effect was not systematically assessed in the present thesis, the former NSC Y-Groove data[12] was applied to derive Eq. (63). This simultaneously ensured compatible treatment of the thickness effect in Eq. (63) with the outcome of the NSC data[12] in the a_w range of 20–40 mm, i.e., the range where experimental NSC results were available at the first place, see *Table 35*.

It can be seen that, in comparison to the expression c.f. Eq. (60), the optimised expression of the effect of a_w obeying Eq. (63) results in (i) the desired gradual abate of the a_w effect at thicknesses greater than about 70–80 mm, (ii) greater reward of lowering a_w at thicknesses less than 15 mm, and (iii) excellent compatibility with the outcome of the actual NSC Y-Groove experiments[12] in the 20–40 mm a_w range.

Furthermore, Eq. (63) is also consistent with the treatment of the plate thickness effect in the case of predicting T_{cr} for the avoidance of hydrogen cracking according to EN 1011-2 : 2001[1b].

5.12.3.4 Optimisation of the T_0/T_i prediction with respect to weld hydrogen content

It is widely accepted[1–3, 12, 13, 20–25, 28–30, 63, 69, 77, 101] that the effect of weld hydrogen H_D on T_{cr} is not linear, but rather of logarithmic nature. Still, different formulations are applied to describe this logarithmic dependence. For instance, Okuda et al.[2] use direct [$a * \log (H_D)$] expression, whereas Yurioka et al.[3] apply [$a * \log (H_D/b)$] type formulation resulting in somewhat more abating increase of T_{cr} with H_D. Standard EN 1011-2 : 2001[1b], in turn, uses a power-law expression of the form: [$a * (H_D)^b$, where $b < 1$] to describe the ceasing increase of T_{cr} with H_D.

Therefore, the outcome of different types of formulations for the logarithmic hydrogen effect on ΔT_{cr} were compared against the measured values of the ΔT_{cr} recorded from the former NSC Y-Groove cracking tests[12], see *Table 36*. Weld H_D levels taken to this comparison are compatible with the NSC Y-Groove experiments[12], as far as the 2.0–10.4 ml/100 g DM (IIW) range is concerned. The intention for seeking various expressions for the effect of H_D on ΔT_{cr} was to find a description that (i) would match with the recorded effect in the NSC Y-Groove experiments[12] in the 2.0–6.7 ml/100 g DM (IIW) range where data was available, without (ii) simultaneously exaggerating the effect at either end of the examined H_D range. The alternative expressions for the H_D effect applied in the comparison are in accordance with Eqs (60b), (61b), (64), (65) and (66), as:

$$T_{cr} (H_D) = \{134 * (H_D)^{0.40}\} \quad (60b)$$

$$T_{cr} (H_D) = \{[2800 * \ln(H_D)] / (12 * H_D^{0.21})\} \quad (61b)$$

$$T_{cr} (H_D) = \{351 * \log(H_D)\} \quad (64)$$

$$T_{cr} (H_D) = \{[2310 * \ln(H_D)] / (12 * H_D^{0.15})\} \quad (65)$$

$$T_{cr} (H_D) = \{323 * \tanh (H_D / 5.0)\} \quad (66)$$

It can be seen that Eqs (60b) and (61b) that were the first attempted fittings based on the NSC Y-Groove test data[12], both describe quite satisfactorily the effect of H_D on ΔT_{cr} in the 4.3–10.4 ml/ 100 g DM (IIW) range. However, owing to its *power-law* form, Eq. (60) does not allow for an adequate relaxation of T_{cr} at very low weld H_D levels of about 2 ml/100 g DM (IIW), whereas Eq. (61) applying a combined *ln-power-law* form is seen to accentuate the effect of lowering H_D on ΔT_{cr} somewhat too much to be safe, or realistic, any longer. A simple *log*-function c.f. Eq. (64), in turn, seems to overstate the effect of H_D on ΔT_{cr} at low and moderate weld hydrogen levels around 2–8 ml/100 g DM (IIW), although leading to compatible description with the *power-law* form c.f. Eq. (60) at high weld H_D contents of around 10–16 ml/100 g DM (IIW).

Table 36. Assessment of the weld hydrogen effect – comparison of the effect of H_D on ΔT_{cr} prediction between the outcome of the experimental NSC data and the VTT based expressions according to Eqs (61), (64), (65) and (66).

Weld hydrogen H_D (ml/100 g)	Recorded ΔT_{cr} *) acc. to NSC Y-Groove experiments[12] (°C)	Hydrogen Factor acc. to various Equations – influence on ΔT_{cr} (in°C)				
		NSC data-based 'power-law' fit c.f. Eq. (60)	NSC data-based 'ln-power-law' fit c.f. Eq. (61)	VTT based 'log'-fit c.f. Eq. (64)	VTT SAW U-Groove data-based, 'ln-power-law'-fit c.f. Eq. (65)	VTT SAW U-Groove data-based, 'tanh'-fit c.f. Eq. (66)
2.0		177	140	106	121	123
	$\Delta \approx 100$	$\Delta \approx 63$	$\Delta \approx 111$	$\Delta \approx 116$	$\Delta \approx 104$	$\Delta \approx 102$
4.3		240	251	222	225	225
	$\Delta \approx 50$	$\Delta \approx 47$	$\Delta \approx 47$	$\Delta \approx 68$	$\Delta \approx 50$	$\Delta \approx 56$
6.7		287	298	290	275	281
	$\Delta \approx 25$–50	$\Delta \approx 55$	$\Delta \approx 36$	$\Delta \approx 67$	$\Delta \approx 42$	$\Delta \approx 32$
10.4		342	334	357	317	313
	–	$\Delta \approx 43$	$\Delta \approx 20$	$\Delta \approx 45$	$\Delta \approx 25$	$\Delta \approx 8$
14.0		385	354	402	342	321
	–	$\Delta \approx 21$	$\Delta \approx 7$	$\Delta \approx 21$	$\Delta \approx 10$	$\Delta \approx 1$
16.0		406	361	423	352	322

*) Δ : shift in the T_{cr} when moving from lower weld H_D to a higher one (i.e., 2.0 → 4.3; 4.3 → 6.7; 6.7 → 10.4; 10.4 → 14.0 and 14.0 → 16.0 ml/100 g)

According to *Table 36*, both of the two new expressions derived in the present thesis: the revised, combined *ln-power-law* form acc. to Eq. (65) and the hyperbolic *tanh* form acc. to Eq. (66) result in (i) the desired gradual abate of the H_D effect at weld hydrogen contents greater than about 11–14 ml/100 g DM (IIW), (ii) realistic reward of lowering H_D in the 2–4 ml/100 g DM (IIW) hydrogen range, and (iii) excellent compatibility with the outcome of the actual NSC Y-Groove experiments[12] in the 4–10 ml/100 g DM (IIW) H_D range.

Of the two expressions, Eq. (66) applying the *tanh* form is seen to yield an abatement of the H_D effect which, at weld hydrogen levels of around 14 ml/100 g DM (IIW), already becomes so accentuated that it may no longer be realistic. This may lead to underrating of the effect of H_D on ΔT_{cr} at high weld hydrogen contents when using Eq. (66). Thus, the use of Eq. (65) applying a combined, revised *ln-power-law* form is presumably more safe in this sense, and is hence advised to be preferred to the other functions examined in the present thesis.

5.12.4 Final analysis of the SAW U-Groove data for optimised prediction of preheat/interpass temperature estimates for multipass welds

Table 37 summarises the database comprising the SAW U-Groove cracking tests on thick plate welds and made under different levels of preheat/interpass temperature T_0/T_i. The objective here was to elevate the applied T_i until crack-free welds were obtained for the investigated SAW weld metals: *OK Tubrod 15.26S*, *OK Tubrod 15.27S* and *OK Tubrod 15.29S*.

Table 37. Comparison of the T_0/T_i estimates derived according to different prediction formulae against the required T_0/T_i temperatures in the SAW U-Groove cracking tests – thick plate data from experiments made at ESAB U.K. and Mäntyluoto Works.

Specimen No	SAW tubular cored wire OK Tubrod	Arc energy (kJ/mm)	CET (%)	Weld hydrogen H_D (ml/100 g DM (IIW))	Crack / No crack	Applied T_0/T_i (°C)	Prediction for the required T_0/T_i (°C)				
							VTT Eq. (67a)	VTT Eq. (67b)	Yurioka formula[3] 3)	Okuda formula[2] 3)	VTT Eq. (62)
U395	15.26S	2.0	0.333	4.9	NC	100	105	105	143–193	130–167	105
U396	15.26S	3.0	0.334	6.1	NC	125	130	131	128–177	135–172	130
U397	15.26S	4.0	0.332	8.4	NC	150	155	159	149–197	177–213	154
U400	15.27S	4.0	0.402	4.9	**C**	125	257	257	259–316	217–260	264
U398	15.27S	2.0	0.396	6.1	**C**	150	267	268	277–333	248–290	273
U399	15.27S	3.0	0.388	8.4	**C**	100	278	282	297–354	288–330	284
W1[1)]	15.27S	2.0	0.39	6.5	**C**	175	260	261	280–336	255–297	265
W2[1)]	15.27S	2.0	0.39	6.5	**C**	200	260	261	280–336	255–297	265
W3[1)]	15.27S	2.0	0.39	6.5	**C**	225	260	261	280–336	255–297	265
U402	15.29S	3.0	0.402	4.9	**C**	150	257	257	315–374	260–304	264
U403	15.29S	4.0	0.419	6.1	**C**	100	317	318	368–429	316–362	326
U401	15.29S	2.0	0.399	8.4	**C**	125	302	307	371–432	344–390	309
M1[2)]	15.29S	4.0	0.41	6.0	**C**	250	296	297	347–407	299–345	304
M3[2)]	15.29S	4.0	0.41	6.0	**C**	275	296	297	347–407	299–345	304
M4[2)]	15.29S	4.0	0.41	6.0	NC	285	296	297	347–407	299–345	304
M2[2)]	15.29S	4.0	0.41	6.0	NC	300	296	297	347–407	299–345	304

[1)] weld metal CET estimate calculated as a mean value of the measured values for the OK Tubrod 15.27S welds

[2)] weld metal CET estimate calculated as a mean value of the measured values for the OK Tubrod 15.29S welds

[3)] T_0/T_i range calculated acc. to Appendix 1 from the weld metal HV data converted into weld R_M estimates using Eq. (48b) and Ref.[119]

Table 37 introduces three VTT equations based on weld metal CET to describe the effect of WM strength on the required T_0/T_i. This stems from the outcome of the present SMAW and SAW cracking tests, which demonstrated that cracking sensitivity of weld metal is, besides hydrogen, above all governed by its strength, see *Tables 3–8*. According to *Table 34*, WM strength is seen to have an even greater influence on the cracking occurrence than anticipated previously. This is consistent with the recent findings[117] that showed, the risk of WM hydrogen cracking increases abruptly when transferring from intermediate strength weld metals associated with CETs of 0.33–0.36% to extra-high strength weld metals exhibiting CETs of 0.40–0.42%. This manifested itself as considerably higher required T_0/T_i in the case of the extra-high strength weld metals, compared with the intermediate strength ones, as shown in *Fig. 39*.

For the purposes of comparison, two new equations, Eq. (67a) and (67b) were thereby introduced in addition to former Eq. (62), all of them with slightly different formulations to account for the effects of weld metal chemical composition CET, weld build-up thickness a_w and weld diffusible hydrogen H_D. The two new expressions are of the form:

$$T_{cr} = 2195 * CET + 9 * a_w^{0.86} + \{[2800 * \ln(H_D)] / (12 * H_D^{0.21})\} - 1106 \ (°C) \qquad (67a)$$

$$T_{cr} = 2195 * CET + 367 * \tanh(a_w/60) + \{[2310 * \ln(H_D)] / [12 * H_D^{0.150}]\} - 1081 \ (°C) \qquad (67b)$$

Table 37 shows, despite their slightly different formulations all the three equations yield more or less similar estimates of T_0/T_i. In the cases where the Crack-No Crack boundary is known from the results of the U-Groove experiments, as for the *OK Tubrod 15.26S* and *OK Tubrod 15.29S* welds, all the three equations are seen to yield safe predictions of T_0/T_i. For the rest of the cases where the Crack-No Crack boundary remained unknown, the equations predict T_0/T_i estimates that accord satisfactorily well with those given by the Okuda method[2] and, as it comes to the estimates based on weld metal strength acc. to Eq. (48b), also the Yurioka method[3]. Thus, there is good reason to believe that all the three VTT equations derived here result in safe predictions of T_0/T_i also for the rest of the cases in *Table 37*.

Although Eq. (67b) is intentionally adjusted to fit into the former NSC database[12] as it comes to the effects of a_w and H_D on the estimated T_0/T_i and obeying Eqs (63) and (65), respectively, it can be seen that for the majority of the cases in *Table 37* the use of Eq. (62) yields slightly higher estimates of T_0/T_i than Eq. (67a) or (67b). As a consequence, among the three equations used to assess the required T_0/T_i for the experiments in *Table 37*, Eq. (62) is likely to yield the safest T_0/T_i prediction for the entire dataset.

In order to extend the T_0/T_i assessment towards thin plate welds and greater hydrogen contents, additional experimental cracking test data from *Tables 10* and *6* were incorporated into *Table 38*. These include (i) V-Groove cracking test data for two-pass SAW and SMAW welds of 6 mm build-up thickness a_w, and (ii) preliminary SAW U-Groove cracking test data up to 13.6 ml/100 g DM (IIW) weld hydrogen, H_D. Here, the effects of a_w and H_D on T_0/T_i were taken as defined in Eqs (63) and (65), respectively, thus ensuring that their descriptions conform to the former NSC Y-Groove cracking test database[12], see *Tables 35* and *36* and *Appendix 5*.

Table 38. Comparison of the T_0/T_i estimates derived according to VTT prediction formulae based on weld CET, $HV_{5(ave)}$ and $HV_{5(max)}$ against the required T_0/T_i temperatures in the SAW U-Groove cracking tests – complete database comprising all the thick and thin plate welds.

Specimen No	SAW Tubular Cored Wire OK Tubrod		Weld CET (%)	Weld HV	Weld hydrogen H_D (ml/100 g DM (IIW))	Crack / No crack		Applied T_0/T_i (°C)	Prediction for the required T_0/T_i (°C)			
			ave	max				Yurioka formula[3] 4)	Okuda formula[2] 4)	Eq. (67b) CET	Eq. (68a) HV_{ave}	**Eq. (68b) HV_{max}**
SU1	15.24S	0.263	225	235	6.2	NC	88	70–115	92–126	RT	83	86
U395	15.26S	0.333	265	277	4.9	NC	100	143–193	130–167	105	129	128
U593	15.26S	0.345	264	277	4.9	NC	100	140–191	128–166	131	127	128
U396	15.26S	0.334	251	262	6.1	NC	125	128–177	135–172	131	128	128
U397	15.26S	0.332	249	262	8.4	NC	150	149–197	177–213	159	157	160
SU4	15.26S	0.302	234	241	13.6	**C**	93	144–191	217–252	136	172	168
–												
U400	15.27S	0.402	315	345	4.9	**C**	125	259–316	217–260	257	219	238
U594	15.27S	0.387	344	362	4.9	**C**	125	326–386	268–313	224	271	265
U398	15.27S	0.396	315	336	6.1	**C**	150	277–333	248–290	268	219	248
W1[1, 3)]	15.27S	*0.39*	*322*	*346*	6.5	**C**	175	280–336	255–297	261	263	271
W2[1, 3)]	15.27S	*0.39*	*322*	*346*	6.5	**C**	200	280–336	255–297	261	263	271
W3[1, 3)]	15.27S	*0.39*	*322*	*346*	6.5	**C**	225	280–336	255–297	261	263	271
SU2	15.27S	0.382	313	334	7.2	**C**	71	285–342	267–309	254	257	262
U399	15.27S	0.388	330	367	8.4	**C**	100	297–354	288–330	282	303	330
SU3	15.27S	0.383	314	335	9.1	**C**	71	305–361	301–343	279	281	286
T1 6mm	75.75	0.254	273	280	14.4	NC	68			RT	69	58
S1 6mm	15.27S	0.341	257	266	16.0	NC	60	–	–	56	48	44
–												
U402	15.29S	0.402	339	362	4.9	**C**	150	315–374	260–304	257	262	265
M1[2, 3)]	15.29S	*0.41*	*346*	*368*	6.0	**C**	250	347–407	299–345	297	297	298
M3[2, 3)]	15.29S	*0.41*	*346*	*368*	6.0	**C**	275	347–407	299–345	297	297	298
M4[2, 3)]	15.29S	*0.41*	*346*	*368*	6.0	NC	285	347–407	299–345	297	297	298
M2[2, 3)]	15.29S	*0.41*	*346*	*368*	6.0	NC	300	347–407	299–345	297	297	298
U403	15.29S	0.419	354	376	6.1	**C**	100	368–429	316–362	318	314	313
U401	15.29S	0.399	345	367	8.4	**C**	125	371–432	344–390	307	330	330

1) weld metal CET estimate calculated as a mean value of measurements for the OK Tubrod 15.27S welds

2) weld metal CET estimate calculated as a mean value of measurements for the OK Tubrod 15.29S welds

3) weld HV_{ave} and HV_{max} estimates calculated as mean values of measurements for the corresponding weld metals

4) T_0/T_i range calculated acc. to Appendix 1 from the weld metal HV data converted into weld R_M estimates using Eq. (48b) and Ref.[119]

It is known that the effect of weld metal strength R_M on required T_0/T_i can be expressed either via (i) weld metal chemical composition CET hence conforming to SFS-EN 1011-2[1b], or using (ii) weld metal Vickers hardness HV_5 as the results of the present thesis strongly indicate, see *Fig. 36*. The advantage of applying the HV based approach rests on the fact that it incorporates the effects of both chemical composition and weld thermal cycle. Thus, it was deemed necessary to investigate, whether the use of HV based estimation of weld metal R_M, in place of the CET based estimation, would bring any extra advantages e.g., in terms of improved accuracy of the T_0/T_i prediction. Two additional VTT equations, Eqs (68a) and (68b), were therefore derived from the experimental data. These formulae use the measured values of average and maximum weld metal Vickers hardness HV_{ave} and HV_{max}, respectively, being of the form:

$$T_{cr} = 1.80 * HV_{ave} + 367 * \tanh(a_w/60) + \{[2310 * \ln(H_D)]/[12 * (H_D)^{0.150}]\} - 803 \quad (68a)$$

$$T_{cr} = 1.62 * HV_{max} + 367 * \tanh(a_w/60) + \{[2310 * \ln(H_D)]/[12 * (H_D)^{0.150}]\} - 776 \quad (68b)$$

Table 38 shows the comparison of the T_0/T_i estimates calculated for the complete cracking test dataset and applying: (i) the CET based approach obeying Eq. (67b), (ii) the two new HV based approaches as defined in Eqs (68a) and (68b), and (iii) the estimates given by the Okuda[2] and Yurioka[3] formulae. Overall, it can be seen that in the cases where the Crack-No Crack boundary is known as an outcome of the U-Groove experiments, i.e., *OK Tubrod 15.26S* and *OK Tubrod 15.29S* welds, all the three VTT equations yield safe predictions of T_0/T_i. For the rest of the cases where the Crack-No Crack boundary remained unknown, the equations predict T_0/T_i estimates that, again, accord satisfactorily well with those given by the Okuda-formula[2] and, as it comes to the estimates based on the weld metal strength acc. to Eq. (48b), also the Yurioka-formula[3].

It is noteworthy that, irrespective of the predictions in *Table 38*, the use of T_0/T_i temperatures above 300°C may be detrimental due to the possibility of austenite being retained throughout welding, even if the predictive formulae suggest higher values.

Looking the T_0/T_i estimates calculated using the CET, HV_{5ave} and HV_{5max} based formulae and given in *Table 38* in more detail, the following observations, conclusion and recommendations can be drawn:

(1) In general, the interpass temperature estimation can be realistically based on either weld metal chemical composition or weld Vickers hardness. The VTT formulae based on weld metal CET, HV_{ave} and HV_{max} were all proven applicable for the T_i estimation, hence resulting in realistic description of the required interpass temperature T_i.

(2) For the majority of the examined cases, the HV_{max} based formula is found to yield the highest T_0/T_i estimates among the three evaluated VTT formulae, consequently, the HV_{max} based Eq. (68b) is likely to result in the most safe T_0/T_i predictions for these cases.

(3) The VTT formulae based on weld metal hardness HV seem plausible in predicting realistic T_i estimates also in the case of thin plate two-pass welds and to thicknesses less than 10 mm.

(4a) Should the difference between weld metal average hardness and the individual maximum HV value be exceptionally great, i.e., equal to or more than 20 HV units, it is advisable to apply the HV_{max} based formula instead of the HV_{ave} based one.

(4b) Should the difference between weld metal average hardness and the individual maximum HV value be abnormally small, i.e., less than 10 HV units, it is advisable to apply the HV_{ave} based formula instead of the HV_{max} based one.

(5) With low CET values less than 0.30%, the two HV based formulae are likely more safe than the CET based formula. In these cases the use of the CET based formula may yield unconservative estimates of T_i.

(6) For thin plate (< 10 mm) and essentially 2-dimensional heat flow conditions resulting in prolonged weld cooling rates, it is advisable to use the CET based formula instead of the HV based ones, unless CET is very low (< 0.27%) in which case the use of the HV_{ave} based formula should be preferred instead of the HV_{max} or CET based formulae.

(7) The Okuda-formula[2] is seen to overestimate the need of T_i towards increasing weld hydrogen contents, particularly at H_D levels exceeding 10 ml/100 g DM (IIW).

(8) The Yurioka-formula[3] is found to overestimate the need of T_i at very high levels of weld metal strength, i.e., R_M > 900 MPa.

(9) In conjunction with Yurioka's strength-hardness formula[119], the methods according to both Okuda and Yurioka will overrate the need of T_i. This implies that Yurioka's formula may exaggerate weld tensile strength at a given level of weld metal hardness HV. Coupled with the VTT strength-hardness description as defined in Eq. (48b), the Okuda and Yurioka formulae are seen to predict comparatively realistic T_i estimates that are compatible with those given by the VTT formulae, i.e., Eqs (67b), (68a) and (68b).

Based on the VTT formulae derived from the data in *Tables 35–38* and in *Fig. 39*, the proposed procedure for predicting safe T_0/T_i temperatures for the prevention of hydrogen cracking in multipass weld metals is outlined in Section 5.12.6.

5.12.5 Postulated mechanism for transverse hydrogen cracking in extra-high strength multipass weld metals

The large- and small-scale Y-Groove and the U-Groove cracking tests all demonstrated that for SMAW and SAW weld metals, at equivalent levels of interpass temperature and weld hydrogen, the cracking risk of $R_{p0.2} \geq 690$ MPa welds was significantly higher than that of $R_{p0.2} \approx 550–590$ MPa welds. This, in turn, accords with a recent study[117] that showed how the occurrence of WM hydrogen cracking increased abruptly when transferring from intermediate strength welds associated with CETs of about 0.33–0.36% to extra-high strength weld metals exhibiting CETs of 0.40–0.42%. As regards to the findings of the present study, this is thought to explain the need of using considerably higher interpass temperatures for the extra-high strength weld metals of $R_{p0.2} \geq 750$ MPa, compared with the intermediate strength ones, see *Fig. 39*.

Nonetheless, the steepness of increase in the required T_i level with the weld metal's CET value c.f. *Fig. 39* still is somewhat peculiar, considering how T_i affects weld residual stress σ_{res}. A recent study[124] concerned with measurements of σ_{res} distributions

in multipass weldments reports that the σ_{res} values for the specimens welded at the T_i of 100–120°C already remained lower than the specimens welded with the T_i below 30°C. Thus, the beneficial effects of elevating the interpass temperature should not be restricted to intensifying hydrogen removal only, but also to reducing weld residual stresses, both of which lower the risk of hydrogen cracking. This leads back to the conclusion drawn from the data in *Table 31* (p. 167) suggesting that, at an equivalent level of weld H_0, elevating the T_0/T_i is less beneficial in lowering the H_{Rmax} in the case of multiple-pass welds than single-pass welds, see Section 5.11.

The Vickers hardness measurements in *Table 30* (p. 161) reveal that a rise in WM strength from $R_{p0.2} \approx 550–590$ to 750–900 MPa was accompanied by a steep increase in local macrohardness mismatch within the multipass SAW weld metals. This mismatch manifested itself as 50–80 HV difference in hardness between an individual maximum and a minimum HV_5 value. Since macrohardness translates to ultimate tensile strength R_M as defined e.g. in Eq. (48), the recorded hardness difference should manifest itself as a corresponding difference in local strength of the different WM microstructures. As these were not microhardness measurements and hence cannot reveal microscale properties, such as nature of the phase interfaces, the results are considered merely an indication of substantial differences in strength of local microstructural regions, which was found a characteristic feature of the extra-high strength multipass SAW weld metals in the present thesis. That the local variation of microstructures actually controls the location of hydrogen cracks in multipass weld metal, is supported by a recent study[121] on extra-high strength SAW welds. This study reported[121], most of the cracks were densely populated in the weld region in which the microhardness increased gradually, but were not necessarily related to that particular individual microstructural phase exhibiting the highest microhardness.

Metallographic examination of the present thesis revealed that the presence of larger amounts of GBF did not directly accentuate WM cracking, although cracks were found to sometimes grow intergranularly along the GBF-matrix interface. The crack propagation path revealed mainly transgranular, but occasionally, intergranular cracking modes. This is consistent with a recent study[124] that reported, the formation of transverse hydrogen cracks did not follow the GBF phase, rather, they propagated across the grains. Furthermore, fracture morphology implied[124] that these cracks had occurred in the highly stressed areas of the weldment. In the extra-high strength WMs of $R_{p0.2} \geq 690$ MPa studied here, transverse cracks growing normal to the weld surface and perpendicular to the axis of the weld interface was a predominant mode, whereas in $R_{p0.2} \approx 550$ MPa welds Chevron cracking showing a characteristic 'staircase' pattern and propagating at 45° angle to the surface in weld thickness direction was recognised, compare *Figs 20–22* against *Fig. 23* and *Figs 24–26* against *Fig. 27*. This is in line with a recent study[117] on fracture surface appearance in multipass SAW welds, showing that the amount of crystalline area resembling cleavage/quasi-cleavage fracture increased with the WM carbon equivalent and, hence, its strength. In the present thesis, WM hydrogen cracks were found to initiate in the filling runs beneath the final weld bead layer, and propagated perpendicularly to the axis of the weld interface into approx. 1/3-thickness of the weldment. This accords with a recent study[124] on 50 mm thick multipass weldments

where transverse hydrogen cracks were detected at depths of 9–14 mm from the weld interface.

Analytic calculations showed that in multiple-pass welding, elevation of the preheat/interpass temperature is less effective in removing weld hydrogen than in the case of single-pass welds, see *Table 31*. On the other hand, reported indications[117] on extra-high strength welds have shown that cracking in multipass welded specimens made applying comparatively low T_i of around 80°C had frequently occurred soon after welding and at welding temperatures higher than those traditionally associated with hydrogen cracking, i.e., close to 300°C, on cooling to the applied T_i. Furthermore, the amount of ductile area in the fracture surfaces of cracked specimens was reported[117] to increase with the applied T_i.

Contemplating all these observations leads to conclusion that extra-high strength weld metals require considerably high T_i temperatures, not only to remove hydrogen, but also to promote conditions that will favour ductile fracture micromechanism in these weld metals that due to their strength tend to be inherently more prone to brittle cleavage/quasi-cleavage fracture.

Considering this against the recent findings made elsewhere[117, 121, 124] suggest, local variations in microstructure resulting in gradients of hardness and strength may contribute to the formation of hydrogen cracks at the GBF-matrix interface in extra-high strength weld metal. High strength of the matrix microstructure allows the build-up of great level of residual stress, while the presence of hydrogen at the interface is awaited to weaken the interfacial cohesion. During weld cooling to the applied T_i, the build-up of weld residual stresses coupled with continuous accumulation of hydrogen towards the filling layers presumably favour crack initiation at the interface of two regions, of which one exhibits plastic deformation behaviour while the other still behaves practically linear elastically. Provided this causes formation of microcrack(s) at the interface, the situation should be more or less analogous to that in a pre-cracked specimen, in which case it has been shown[38], a combination of adjacent weld regions with mismatching mechanical properties, rather than the presence of a single weak region, frequently resulted in unstable crack growth under external load. Here, a heavily restrained multipass welded specimen enables elevation of weld residual stress to amount the WM yield strength, which thereby corresponds, in that sense, well enough to the conditions prevailing in an externally loaded small specimen.

Overall, the findings suggest that the abrupt increase in multipass WM cracking sensitivity when transferring from intermediate strength to extra-high strength weld metals can be explained by the combination of: (i) steeply elevating *weld residual stress*, (ii) increased *matrix macrohardness* of the weld microstructure in conjunction with pronounced *local hardness and, hence, strength mismatch*, and (iii) inherent propensity of the microstructure to *brittle cleavage/quasi-cleavage fracture micromechanism*.

5.12.6 Proposed procedure as to provide the necessary precautions for the avoidance of hydrogen cracking in multipass weld metal

The Procedure outlining the necessary precautions against hydrogen cracking in multipass weld metals comprises two steps. These are: *Step 1*: Calculation of the 'worst case' lower-bound estimate of weld critical hydrogen content H_{cr} to assess the Crack – No Crack conditions, and *Step 2*: Calculation of a 'safe' estimate of the preheat/interpass temperature T_0/T_i needed for the avoidance of weld metal hydrogen cracking when operating within the Crack region (according to *Step 1* estimation).

The idea behind the Procedure is that the built-in conservatism decreases through the sequence: *Step 1*, *Step 2 Level 1*, *Step 2 Level 2*. This way, the procedure penalises the user with the minimum amount of required data for the assessment, and rewards the user who is willing to create more than the minimum amount of required data and/or analyses.

Step 1: Calculation of the worst case lower-bound estimate of weld H_{cr} *using the Crack-No Crack Diagrams*

Use one of the three methods to compare between the actual weld diffusible hydrogen content H_D ($\equiv H_0$) and the weld critical hydrogen content H_{cr}.

Method A : Stress based approach that assumes that weld $R_{p0.2} = \sigma_{resL}$ and uses the true yield strength (MPa) of the multipass weld metal in question.

$$H_{cr} = 250 * 10^{(-0.00235 * R_{p0.2})} \quad \text{[ml/100 g DM (IIW)]}$$

Method B : Weld P_{cm} based approach that uses the actual chemical composition of the weld metal in question in terms of the P_{cm} (%) weldability index as defined in Eq. (43a).

$$H_{cr} = 175 * 10^{(-6.460 * P_{cm})} \quad \text{[ml/100 g DM (IIW)]} , \quad \text{or}$$

$$H_{cr} = 116 * (0.295 - P_{cm}) \quad \text{[ml/100 g DM (IIW)]}$$

The lower value of the two H_{cr} estimates calculated using the given formulae, is then applied.

Method C : Weld HV_{max} based approach that uses the measured individual maximum hardness value of the weld metal in question in terms of Vickers hardness HV_5.

$$H_{cr} = 280 * 10^{(-0.00585 * HV_{max})} \quad \text{[ml/100 g DM (IIW)]}$$

Choose the method to be applied either: (i) according to the most relevant actual data that is available, or can be generated, for the case in question or, (ii) provided there is enough data to apply all the three methods, take the one giving the lowest value of H_{cr}.

Compare the thereby calculated H_{cr} value to the actual weld diffusible H_D value measured for the weld metal in question using the single-pass hydrogen test conforming to ISO/IIW 3690.

If $H_{cr} > H_D$, there is no risk of transverse WM hydrogen cracking in multipass welds for the case in question and in conditions referring to normal welding fabrication, provided $T_i \approx 100°C$.

If $H_{cr} \leq H_D$, the possibility of having a risk of weld metal hydrogen cracking in multiple-pass welding must be considered. In this case, one should either: (i) take protective measures such as adjusting the welding procedure and/or changing to another filler material to lower the actual weld diffusible hydrogen content H_D, or (ii) consider additional precautions against cracking such as the use of elevated preheat/interpass temperature in which case one should proceed to *Step 2*.

Validity limits of the equations in *Step 1*:

$480 \leq R_{p0.2} \leq 890$ (MPa)
$210 \leq HV_{max} \leq 370$ (HV_5)
$0.130 \leq P_{cm} \leq 0.300$ (%)
$0.180 \leq CET \leq 0.420$ (%)
$1.3 \leq Q \leq 5.0$ (kJ/mm)
$2.0 < H_{cr} < 19.0$ (ml/100 g DM (IIW))
$80 < T_i \leq 300$ (°C)

Note that until more cracking test results are available for weld metals with $P_{cm} < 0.130\%$, $HV_{max} < 210$ HV or $CET < 0.180\%$, it is advisable for safety reasons to use a cut-off of the H_{cr} level for this regime. That is, the same H_{cr} value corresponding to either weld metal's $P_{cm} = 0.130\%$, $HV_{max} = 210$ HV or $CET = 0.180\%$ is applied also to any other weld metal having lower P_{cm}, HV_{max} or CET value.

Step 2: Calculation of a safe estimate of T_0/T_i *to prevent weld metal hydrogen cracking in multipass welds*

Step 2 comprises two Levels, of which the latter one provides three Options. The selection among these depends on the accuracy of the required T_0/T_i estimate, as well as on certain case-related factors such as the actual weld build-up thickness and weld diffusible hydrogen content.

Level 1: Screening Test: Rough scaling of the required T_0/T_i range as a function of weld metal CET and weld hydrogen H_D applying a "Three-Zone Diagram" illustrated in *Fig. 39*.

The Diagram in *Fig. 39* consists of three zones defined according to the range of weld metal's CET value in question. The level of safe T_0/T_i thereby depends on the range of weld metal CET and weld H_D. The Diagram can be applied provided the CET and H_D values are within the ranges indicated separately for each Zone.

Zone 1: $0.26\% \leq CET \leq 0.33\%$

$H_D \leq 5.0$ ml/100 g DM (IIW) => $T_0/T_i = 100$°C
$H_D \leq 6.0$ ml/100 g DM (IIW) => $T_0/T_i = 125$°C
$H_D < 8.5$ ml/100 g DM (IIW) => $T_0/T_i = 150$°C

Zone 2: $0.33\% < CET \leq 0.39\%$

$H_D \leq 6.0$ ml/100 g DM (IIW) => $T_0/T_i \geq 100 + 3340 * (CET - 0.33)$ (°C)

Zone 3: $0.39\% < CET \leq 0.42\%$

$H_D \leq 6.0$ ml/100 g DM (IIW) => $T_0/T_i = 300$°C

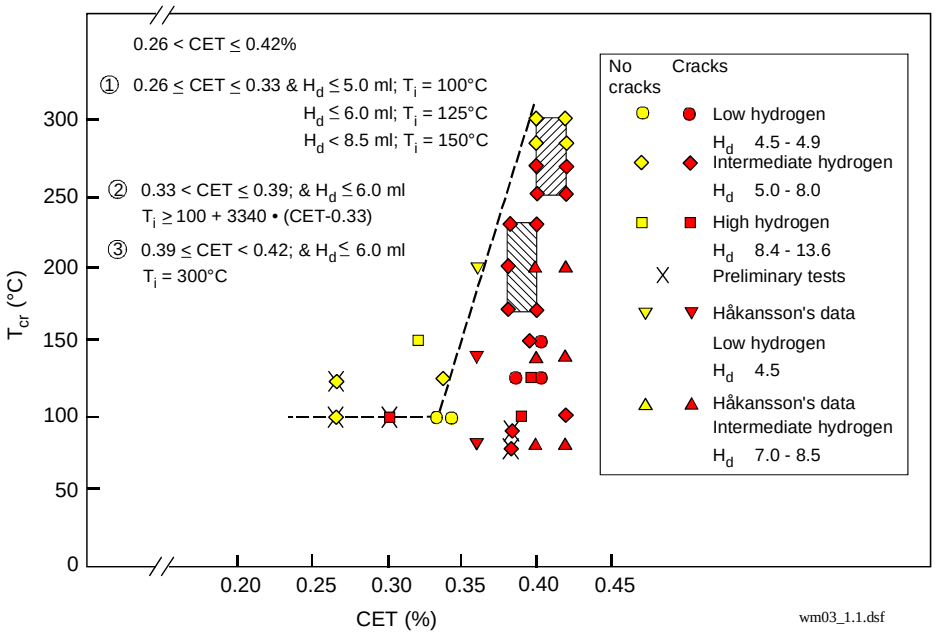

Fig. 39. Critical preheat/interpass temperature T_0/T_i as a function of weld metal CET for multipass SAW weld metals according to the U-Groove test – Screening of Scale. Data from Håkansson[117] added. Note: for deriving recommendations as the applied T_0/T_i values referring to Zone 1, also the data in Tables 37–38 have been used. Filled (red) symbols: cracking; open (yellow) symbols: no cracking.

Should any of the Level 1 estimations yield T_0/T_i values greater than 300°C, then set T_0/T_i = 300°C.

Should the validity limits set for the weld CET or H_D become violated, one should go to Level 2.

Level 2: Calculation of a safe T_0/T_i estimate of the required T_{cr} using weld metal strength in terms of either weld CET or weld metal HV_{max}, weld build-up thickness a_w and weld diffusible hydrogen H_D as controlling factors:

Option 1: If $20 \leq a_w \leq 40$ mm and provided conservative estimates are regarded as satisfactory:

$$T_{cr} = 2310 * CET + 9 * a_w^{0.86} + \{[2800 * \ln(H_D)] / (12 * H_D^{0.21})\} - 1145 \quad (°C)$$

Option 2: When best estimates are required and the estimation is based on weld metal chemical composition:

$$T_{cr} = 2195 * CET + 367 * \tanh(a_w/60) + \{[2310 * \ln(H_D)] / [12 * H_D^{0.15}]\} - 1081 \quad (°C)$$

Option 3: When best estimates are required and the estimation is based on weld metal hardness:

$$T_{cr} = 1.80 * HV_{ave} + 367 * \tanh(a_w/60) + \{[2310 * \ln(H_D)] / [12 * (H_D)^{0.15}]\} - 803 \quad (°C)$$

$$T_{cr} = 1.62 * HV_{max} + 367 * \tanh(a_w/60) + \{[2310 * \ln(H_D)] / [12 * (H_D)^{0.15}]\} - 776 \quad (°C)$$

The validated applicability range of the equations in Level 2 Options 2 and 3 are as follows:

$20 \leq T_{cr} \leq 300$	(°C)
$2.0 \leq Q \leq 5.0$	(kJ/mm)
$0.25 \leq CET \leq 0.42$	(%)
$6 \leq a_w \leq 40$	(mm)
$6 \leq h \leq 70$	(mm)
$2.0 \leq H_D \leq 16.0$	(ml/100 g DM (IIW))

The complete Flow-Charts of the Procedure Step 1 and Step 2 are presented in *Appendix 11*.

Applying the equations given for *Step 1* of the proposed Procedure thereby provides a worst-case estimate of weld critical hydrogen H_{cr} as 'first line of defence' against transverse hydrogen cracking in multipass weld metal. For the assessment, weld diffusible hydrogen content H_D according to single-pass hydrogen test conforming to ISO/IIW 3690, and either the true yield strength $R_{p0.2}$, chemical composition in terms of P_{cm}, or actual maximum hardness HV_{5max} of the multipass weld metal, is required.

Should *Step 1* analysis reveal a potential WM cracking risk, *Step 2* provides equations for predicting a safe estimate of the required preheat/interpass temperature T_0/T_i as 'second line of defence' precautions for the avoidance of WM hydrogen cracking. To conduct this assessment requires (i) weld diffusible hydrogen content H_D, (ii) weld build-up thickness a_w and (iii) either weld metal true chemical composition in terms of CET, or actual weld metal hardness in terms of HV_{5ave} or HV_{5max}, as input parameters.

5.12.7 Areas of non-applicability of the Procedure

The Procedure has its fundamental basis on multipass cracking experiments shown descriptive of transverse hydrogen cracking occurring in the filling runs. Therefore, it should not be applied to assess hydrogen cracking susceptibility of single-pass welds.

The experiments of the present thesis demonstrated that weld H_{cr} levels for weld metals having their $HV_{max} \leq 210$ HV, $P_{cm} \leq 0.130\%$ and $R_{p0.2} \leq 480$ MPa become so high that cracking is very unlikely in practice welding fabrication. Every now and then, fabricators and, occasionally, even laboratories[8] are still experiencing cases of hydrogen cracking in the welding of structural steel and in weld metal, which are associated with weld strengths lower than those anticipated to provoke cracking. The reasons for the occurrence of cracking in these cases have often remained unexplained. Until more

cracking test data are generated for these low strength weld metals, it is therefore advisable, for safety reasons, to use a cut-off of the H_{cr} level for weld metals with P_{cm} < 0.130%, HV_{max} < 210 HV or CET < 0.180%. That is, the same H_{cr} value corresponding to either weld metal P_{cm} = 0.130%, HV_{max} = 210 HV or CET = 0.180% is applied also to any other weld metal having lower P_{cm}, HV_{max} or CET.

It should be highlighted that the Crack-No Crack diagrams describing the 'worst-case' conditions with respect to WM cracking risk in *Step 1* are, after all, based on cracking tests involving T_i = 70–100°C. Any practice welding conditions where the actual T_i might, at some stage during welding, go under the 70–100°C temperature level, can therefore represent an acute risk of cracking.

It is noteworthy that the use of T_0/T_i temperatures above 300°C may be detrimental due to the possibility of austenite being retained throughout welding, even if the predictive formulae applied in *Step 2* suggest higher values.

The Procedure rests essentially on the outcome of the SMAW and SAW multipass cracking tests. The analysis of other cracking test data from literature[76] implies that the Procedure can presumably be applied to FCAW process, as well. However, such assessments should be treated with caution. The applicability of the Procedure to welding processes other than SMAW, SAW and FCAW cannot be guaranteed without performing additional experiments.

Apart from the experiments of the present thesis, any exceptional welding conditions and/or configurations may possess additional sources that can provoke cracking. Such are, for example, welding with cellulose electrodes, welding of highly stressed thick multipass fillet welds, multiple-pass single/double-bevel T butt joints in thick plate welded from both sides and, finally, welding at an open air where welds could become directly exposed to moisture or rain.

6 Conclusive remarks

This doctoral thesis summarises experimental findings and analytical calculations on controlling factors that govern hydrogen cold cracking in high-strength multipass weld metal. The work is concerned with heavily restrained Y- and U-Groove multipass cracking tests of shielded metal arc (SMAW) and submerged arc (SAW) weld metals of yield strengths in the range of 455–900 MPa.

Overall, the results demonstrated that *transverse hydrogen cracking* in multipass welds occurred predominantly at extra-high strength levels of $R_{p0.2} \approx$ 580–900 MPa. Within this range, *weld metal strength* and *diffusible hydrogen* have a substantial influence on cracking sensitivity. Whereas at $R_{p0.2} \approx$ 680–690 MPa strength level, weld hydrogen contents of $H_D \approx$ 7–10 ml/100 g $_{DM(IIW)}$ were necessary to induce cracks, already $\approx$ 3 ml/100 g $_{DM(IIW)}$ weld H_D was sufficient for cracking to occur in the $R_{p0.2} \approx$ 880–900 MPa weld metals.

In the case of low strength SMAW weld metals of $R_{p0.2} \leq$ 480 MPa, it appeared impossible to create conditions severe enough to result in WM cracking under any hydrogen levels examined in the range of 5 to 11 ml/100 g $_{DM(IIW)}$.

At intermediate strengths of $R_{p0.2} \approx$ 500–550 MPa, WM cracking occurrence was found to depend decisively on the *time from welding to NDT inspection*. Cracking in SMAW welds appeared in the cases when this holding time was prolonged from the 'standard' 16 hours[1] to 168 hours (7 days), in conjunction with high weld H_D of $\approx$ 15 ml/100 g $_{DM(IIW)}$. Was the period of 16 h applied, none of the welds showed any cracks with hydrogen levels in the range of $H_D \approx$ 3–18 ml/100 g $_{DM(IIW)}$. In the case of SAW welds of $R_{p0.2} \approx$ 585 MPa, cracking took place when moving from the weld H_D of $\approx$9 to $\approx$13 ml/100 g $_{DM(IIW)}$. The crucial role of holding time that ought to be long enough to allow for hydrogen crack occurrence is consistent with the recent findings made elsewhere[117]. These demonstrated, the period of 16 h specified in EN 1011-2[1b] can, in some cases, be much too short to allow for complete hydrogen diffusion and/or cracks of critical size to be developed in the case of thick multipass welds.

Weld residual stress measurements made for thick multipass weldments indicated that the *weld longitudinal tensile residual stress* σ_{resL} approaches the weld metal yield strength $R_{p0.2}$, provided that the weld is long enough, i.e., at least 300 mm but, preferably, 500–800 mm. Transverse residual stresses were found accordingly high.

These stresses are presumably accompanied by high stress triaxiality. For thin plates, weld residual stresses in the weld transverse and thickness directions are practically non-existent. Unlike for heavy plates, the build-up of the σ_{resL} depended on how the plate was fixed: (i) using bolted clamps the stress became partly relieved once the bolts were removed after welding, consequently, the stress remained remarkably lower than the WM yield strength; (ii) with welded strong-backs ensuring absolute rigidity of the weldment throughout the welding and NDT, the σ_{resL} approached the WM yield strength.

The results of the double-welded large-scale Y-Groove, small-scale Y-Groove and the U-Groove *cracking tests* for thick multipass weldments were all proven compatible. These experiments employing rigidly bolted specimens subjected to intensified cooling were shown to maximise the development of σ_{resL} and enable low *interpass temperature* T_i and short *interpass time* t_i to be obtained simultaneously. According to diffusion theory, the combination of low T_i and short t_i should minimise the effusion of hydrogen during multiple-pass welding, thereby accentuating the accumulation of hydrogen and hence the elevation of the *local final hydrogen concentration* H_{max} in the filling runs.

The *cracking tests* demonstrated that for both SMAW and SAW weld metals, at equivalent levels of interpass temperature and weld hydrogen, risk of hydrogen cracking in the $R_{p0.2} \geq 690$ MPa weld metals was significantly higher than in the $R_{p0.2} \approx 550–590$ MPa welds. This accords with a recent study[117] that demonstrated how the occurrence of cracking in multipass weld metal increased abruptly when transferring from intermediate strength welds associated with CETs of 0.33–0.36% to extra-high strength welds exhibiting CETs of 0.40–0.42%. Cracking seemed[117] to have frequently occurred at temperatures higher than those traditionally associated with hydrogen cracking, i.e., close to 300°C on cooling to lower interpass temperatures, T_i. The amount of ductile area in the fracture surfaces of cracked specimens was also found[117] to increase with the T_i. As regards to the present study, these phenomena are thought to explain the need of considerably higher T_i for the extra-high strength welds of $R_{p0.2} \geq 750$ MPa, compared with the intermediate strength ones.

Weld metal Vickers hardness showed good correlation with cracking susceptibility, provided the actual WM maximum hardness $HV_{5(max)}$ is applied. The measurements indicated, a rise in WM strength from $R_{p0.2} \approx 550–590$ to 750–900 MPa was accompanied not only by a rise in the individual $HV_{5(max)}$, but also by a steep increase in local hardness mismatch within the weld metal. This manifested itself as a 50–80 HV difference between an individual maximum and minimum value and is considered merely an indication of great differences in strength properties of local microstructural regions, which was found a characteristic feature of the investigated extra-high strength multipass SAW welds. A recent study[121] on similar SAW welds supports the view that the local variations of microstructure can control the appearance and location of hydrogen cracks in multipass weld metal.

Metallography revealed that the presence of larger amounts of grain-boundary ferrite (GBF) did not accentuate WM cracking, although cracks were found to sometimes grow intergranularly along the GBF-matrix interface. The crack propagation path consisted of both transgranular and intergranular cracking modes. This accords with a recent study[124] reporting that the formation of transverse hydrogen cracks did not follow the GBF phase, rather, they propagated across the grains and concentrated on the highly stressed areas of

the weldment. In the extra-high strength weld metals of $R_{p0.2} \geq 690$ MPa studied here, transverse cracks growing in the weld thickness direction normal to the weld surface and perpendicular to the axis of the weld interface was a predominant mode, whereas in the $R_{p0.2} \approx 550$ MPa welds Chevron cracking showing a 'staircase' pattern and propagating in the weld thickness direction at 45° angle to the weld surface was recognised. This is in line with a recent study[117] on fracture surface appearance in multipass SAW welds, showing that the amount of crystalline area resembling cleavage/quasi-cleavage fracture increased with the WM carbon equivalent and, hence, its strength. In the present thesis, WM hydrogen cracks were found to initiate in the filling runs beneath the final weld bead layer, from where they had propagated perpendicularly to the axis of the weld interface into ≈1/3-thickness of the weldment. This is in agreement with the experience gained elsewhere[2, 3, 12, 76, 124].

Sorted out according to their actual weld chemical composition and WM hardness, the present SAW U-Groove data in the $R_{p0.2}$ range of 500–900 MPa was found to comply well with the *Crack-No Crack boundaries* derived from the SMAW data. The present SAW cracking test results do not therefore assign any need to modify the Crack-No Crack boundaries derived from the SMAW data.

Overall, the present thesis found the *cracking risk of multipass weld metal* somewhat lower than expected on the basis of previous experience[2, 3, 12], even under the most stringent conditions applying the combination of short interpass times and low interpass temperatures of 3–4 min and 80–90°C, respectively. For instance, any attempts to reproduce the former NSC Y-Groove test results[12] were unsuccessful. It is thought that lowered impurity contents of modern welding consumables and hence weld metals can impede grain boundary decohesion that otherwise tends to occur under the presence of increasing accumulation of hydrogen. Thus, grain boundaries in clean welds can have higher tolerance to the presence of hydrogen, which then elevates their resistance to intergranular hydrogen cracking in a similar manner to that reported[39] for clean steels.

In all the cases where WM hydrogen cracking took place, it did so irrespective of *interpass time* t_i, even though t_i was varied over a range from 4 to 15 min. Thus, t_i seems to have no measurable (significant) influence on WM cracking risk. This was attributed to the dominant role of weld strength and hydrogen, which presumably overrides any effect t_i might have, unless the cracking test manages to produce a result that lies in the immediate vicinity of the Crack-No Crack boundary line. Owing to the crude nature of the applied cracking experiments, this would be considered as a rare event.

According to the SAW U-Groove experiments, *heat input* Q in the range of 2–5 kJ/mm seems to have no measurable effect on WM cracking susceptibility. Besides the dominant role of weld strength and hydrogen, this is explained by the finding that heat input affected the hardness in multipass weld metal to a much lesser extent than expected on the basis of parent steel HAZ hardenability.

Equations were derived to describe *average hardness* HV_{5ave} of SMAW and SAW weld metals as a function of their chemical composition in terms of P_{cm} and CET. The effect of arc energy on hardness was incorporated into the equations, although it was found very modest in the range of 1.6–3.2 kJ/mm. Weld metal *ultimate tensile strength* R_M was shown to be reliably estimated as a function of HV_{5ave}; a linear expression was derived and shown to have good agreement with the present SMAW data, as well as with

the earlier FCAW data. In the case of knowing only the weld chemical composition, estimates of weld HV_5 and R_M can be calculated using the formulae given here. Weld metal's $R_{p0.2}$ can then be estimated within reasonable accuracy using its yield-to-tensile ratio based on nominal strength. Analysis of separate data from former works[12,118,119] showed good agreement with the present results, thereby validating the approach outlined in the present thesis.

Analytical calculations showed that the *local final hydrogen concentration* H_{Rmax} in multipass weld becomes considerably higher than the *remaining diffusible hydrogen content* $H_{R100max}$ in single-pass weld, even though the initial diffusible hydrogen contents, H_0, were identical. This was attributed to diffusion and accumulation of hydrogen towards the filling runs during multiple thermal cycles, which counterbalances the effusion of hydrogen during the cooling stage of each weld pass. Such accumulation does not occur in single-pass welds, consequently, the $H_{R100max}$ always becomes lower than H_0. Moreover, calculations implied, under equivalent weld thermal cycle and initial hydrogen in terms of $\Sigma D\Delta t$ and H_0, respectively, the H_{Rmax} could become higher in SAW than SMAW multipass welds. This was attributed to higher weld bead overlap in the case of SAW. As greater bead size results in longer diffusion distances, values of the H_{Rmax}/H_0 close to, and even beyond unity were obtained especially for SAW and over a wide range of investigated welding conditions. According to calculations, the H_{Rmax} did not, even under extreme conditions, exceed the H_0 by more than ≈ 10%. Thus, $H_{Rmax} = H_0$ can be taken as a general approximation for the predictive formulae assessing cracking risk of multipass weld metal, while $H_{Rmax} \approx 1.1 * H_0$ is considered appropriate for SAW welds in thick plate. Values of H_0 (= H_D) can be determined from single-pass weld hydrogen test conforming to ISO/IIW 3690.

Incorporating all the results showed that WM cracking occurrence was primarily governed by (i) the *weld metal ultimate tensile strength* R_M, (ii) *weld longitudinal residual stress* σ_{resL} amounting the WM yield strength $R_{p0.2}$ and (iii) *weld diffusible hydrogen* H_D (= H_0). *Weld build-up thickness* a_w was found to affect cracking in that, at comparable levels of strength and hydrogen, the occurrence of cracking vanished when transferring from 40 to 6 mm thick multipass welds. The implications of the *time from welding to NDT* were much more significant than anticipated previously, whereas the *interpass time* t_i and *heat input* Q are regarded as being of secondary importance.

As '*first line of defence*', experimentally verified numerical formulae defining Crack-No Crack diagrams are provided for calculating worst-case estimates for the *weld critical hydrogen content* H_{cr} when knowing either: (i) *weld metal yield strength* $R_{p0.2}$, (ii) *weld chemical composition* P_{cm}, or (iii) *weld metal maximum hardness* HV_{max}. All the three approaches yielded essentially the same results and similar ranking of the examined SMAW and SAW weld metals as individual datasets and in terms of their cracking susceptibility, thereby indicating good descriptive potential in assessing hydrogen cracking sensitivity of multipass weld metals. Differences in the relative ranking between the SMAW and SAW welds were recognised, suggesting tubular SAW filler wires may produce weld metals that, in relation to their strength, are inherently more crack sensitive than the SMAW weld metals. In view of the descriptive potential of these approaches for the entire spectrum of the SMAW and SAW welds, the $HV_{5(max)}$ based approach was found to accommodate the actual cracking susceptibility of the different WM strength

grades most realistically. That weld H_{cr} depends on its hardness as defined here is consistent with a former work[122] on hydrogen cracking in weld metals. Furthermore, analysis of separate cracking test data[76, 117] showed that, with the exception of one individual result and the $R_{p0.2}$ based approach, applying the cracking diagrams outlined in the present thesis would have yielded correct predictions of cracking occurrence for the rest of the data. These are considered as plausible evidences on the validity of the approaches defined in the present thesis.

An estimate of *maximum final hydrogen concentration* H_{max} in multipass welds can be calculated as a function of (i) weld initial diffusible hydrogen content H_0, (ii) thermal factor of hydrogen diffusion $\Sigma D\Delta t$ approximated using weld t_{100} data and (iii) individual weld bead layer thickness h_w accounting for the weld overlap effect d/h_w, using the given formulae. Comparing the weld H_{cr} and the H_{max} values then enables the assessment of the boundary conditions for hydrogen cracking in multipass weld metal.

As '*second line of defence*' and for the cases where $H_{cr} < H_{max}$, equations were derived for the calculation of safe preheat/interpass temperature estimates, T_0/T_i, for the avoidance of cracking. Analysing the whole dataset, a formula incorporating: (i) weld metal tensile strength as linear functions of either weld metal CET or weld $HV_{5(max)}$, (ii) weld build-up thickness a_w in the form of *tanh* based expression and (iii) weld diffusible hydrogen H_D in terms of a combined [*ln / power law*] based expression was found descriptive.

The results imply that (i) precautions against WM hydrogen cracking in *low-strength multipass welds* in thick plate, as well as (ii) the possible dependency of the *critical holding time before NDT* on weld metal strength grade, should deserve increasing attention in the future.

The identification of the primary causal factors governing hydrogen cracking in multipass weld metals in the present thesis further enables the *local approach treatise* of hydrogen effects. The assessment of the hydrogen-crack tip interactions applying local approach treatise of damage-based parameters according to continuum based mechanics, coupled with local stresses, actual hydrogen concentration, microstructure and actual failure mechanism, provide the latitude for performance of analyses utilising the micromechanical descriptions of hydrogen cracking.

7 Summary of final conclusions

- Hydrogen cracking occurred predominantly in extra-high strength weld metals of $R_{p0.2} \approx 580–900$ MPa. Within this range, cracking depended essentially on weld strength and hydrogen.
- At intermediate strengths of $R_{p0.2} \approx 500–550$ MPa, cracking in SMAW welds took place in the cases where the time from welding to NDT was prolonged to 7 days and at high weld hydrogen of $H_D \approx 15$ ml/100 g DM (IIW).
- Low strength weld metals of $R_{p0.2} \leq 480$ MPa did not exhibit hydrogen cracking under any conditions examined.
- Results of the large-scale Y-Groove and the small-scale Y- and U-Groove cracking tests were all compatible in the sense of ranking multipass weld metals according to their cracking susceptibility. The experiments employing rigidly bolted specimens subjected to intensified cooling were shown to maximise the development of longitudinal σ_{resL} and enable low interpass temperature and short interpass time to be obtained simultaneously.
- Despite a range of heat inputs and interpass temperatures, all the SAW cracking test results, when sorted according to their actual weld composition and hardness, fell within the Crack-No Crack regions derived from the SMAW experiments.
- According to analytical calculations, H_{max} can – with equivalent weld thermal cycle and initial hydrogen – become higher in SAW than SMAW multipass welds. Setting $H_{max} \approx 1.1 * H_0$ is considered appropriate for SAW welds in thick plate, while $H_{max} = H_0$ can be taken as a general approximation. Here, $H_0 = H_D$ and denotes to weld diffusible hydrogen determined from a single-pass hydrogen test.
- Equations were derived to describe weld HV_5 as a function of its chemical composition in terms of P_{cm} and CET, as well as to calculate weld R_M as a function of HV_{5ave}. Separate data from previously published works[12, 118, 119] accord well with the present results, thereby validating the outlined approach.
- As '*first line of defence*', equations were derived to assess the weld critical hydrogen content H_{cr} corresponding to the Crack-No Crack conditions as a function of either weld metal P_{cm}, yield strength $R_{p0.2}$ or weld hardness $HV_{5(max)}$. All these parameters were shown to rank the separate datasets of the examined SMAW and SAW weld metals accordingly with respect to the occurrence of hydrogen cracking. Separately

published cracking test data[76, 117, 122, 123] show good agreement with the present results.

- As '*second line of defence*', equations were derived for the calculation of safe T_0/T_i estimates for the avoidance of cracking. Analysing the whole dataset, a formula incorporating: (i) weld metal strength as a linear function of either weld CET or HV_{5max}, (ii) weld build-up thickness a_w in the form of *tanh* based expression and (iii) weld diffusible hydrogen H_D in terms of a combined [*ln / power law*] based expression was found descriptive.
- In thick multipass welds hydrogen cracking occurrence was, above all, governed by the weld metal tensile strength, weld diffusible hydrogen and the weld σ_{resL} amounting to the true weld yield strength.
- Plate/weld build-up thickness was found to affect WM cracking risk in that, at comparable levels of strength and hydrogen, the occurrence of cracking vanished when transferring from 40 to 6 mm thick multipass welds.
- The implications of time from the completion of welding before NDT were much more significant than anticipated previously. A period of 16 h from welding to NDT in accordance with SFS-EN 1011-2 appeared far too short in the case of thick multipass welds.
- Interpass time and heat input showed no measurable effect on the WM hydrogen cracking sensitivity, hence turning out to be less important than previously believed.
- Precautions against WM hydrogen cracking in low-strength multipass welds in thick plate, as well as the possible dependency of the critical holding time before NDT on strength grade, deserve increasing attention.
- The identification of the primary causal factors governing hydrogen cracking in multipass weld metals in the present thesis further enables the local approach treatise of hydrogen effects at the crack tip.

8 Future work

Whilst the principal *causal factors* contributing to hydrogen cracking in multipass weld metals are nonetheless comparatively well understood, investigation of *intrinsic factors* as it comes to local conditions prevailing in a microstructure under the presence of hydrogen and stress, have so far received much less attention. For instance, the effect of welding residual stress on the weld cracking risk has traditionally been encountered using robust, causal parameters, i.e., level of longitudinal stress and applying regression analyses[1–5, 11, 19, 26, 67b], instead of sophisticated local approach based numerical modelling capable of determining local stresses and distributions at and near the crack tip, or phase interface. Thus, assessments of hydrogen-interface interactions based on local approach treatise of damage mechanics parameters using continuum based mechanics, coupled with local stresses, actual hydrogen concentration, microstructure and actual failure mechanism, are yet relatively rare and poorly understood. The results of the analyses of mass diffusion of hydrogen, for example, are difficult to quantify in terms of cracking risk since no reliable coupling between the local hydrogen concentration and material damage has been presented.

As an introduction, local approach based numerical analyses of the interactions between hydrogen diffusion and accumulation and the associated effects on the material's cracking resistance in the case of multipass weld metals has recently been initiated[120] at VTT Industrial Systems. Former numerical modelling[21,22] performed at Nippon Steel, Japan, has been analysed and applied as background data. Numerical analyses enables solution of hydrogen diffusion in welds having complex geometries. A finite difference method (FDM) based temperature solution can be used as an input to a finite element transient mass diffusion analysis. In the mass diffusion problem, a three-dimensional residual stress field is to be used as input to describe the pressure stress dependency of the transient diffusion process. The resulting concentration profiles are considered by use of a novel damage mechanics material model in a finite element analysis (FEA) cell modelling framework, which links the local concentration to a continuum mechanics damage description. The use of the damage mechanics constitutive material model will thereby provide means to evaluate the conditions for hydrogen cracking risk in multipass welds.

The first results[120] of the mass diffusion analysis seem to be in harmony with the experimental findings and measured hydrogen concentrations of the present thesis. These imply, the damage mechanics analysis will provide means for evaluating the rupture process by the use of continuum mechanics. These modelling work[120] are currently underway at VTT Industrial Systems. Still, open questions to solved are, for instance, consideration of time for crack development at different strength levels, as well as how to treat crack nucleation event. Existing constitutive models, as such, do not set limitations to model the crack initiation event, however, from the fracture mechanics viewpoint crack tip considerations are only appropriate to the growth of an existing crack whose initial size hence needs to be postulated. An obvious difficulty is that there is practically no experimental evidence whatsoever, from which it could be reliably concluded whether the incubation period from welding to crack appearance, if being as long as hundreds of hours, is essentially for (i) the nucleation of a crack, or (ii) growth of an already initiated crack into critical size.

The results of the present thesis clearly demonstrated that *the effect of time from welding to NDT* is very important. In practice, the welding engineer is concerned with ensuring freedom from hydrogen cracking in his structure for the whole of its lifetime. It is of little consolation to know that there will be no cracking up to 16 hours after welding, as specified in SFS-EN 1011[1] if cracks may appear after 7 days or whatever. In real structures welding residual stresses are not relaxed after, say, 16–48 h, for example. Thus, welding engineers need to estimate the time under restraint before NDT to be sure that all possible hydrogen cracks have formed for any given weld.

Therefore, the possible dependency of the *critical holding time before the NDT* on weld metal strength grade should deserve increasing attention in the future. An indication of its magnitude is available from the present results on the lower strength welds, whereas the question whether the time effect appears similarly also in the high-strength welds remains yet to be answered. Anyway, separate results from a recent study[117] on hydrogen cracking in multipass SAW weld metals allow one to conclude that the time factor becomes increasingly important towards lower strength weld metals, whilst the high strength welds exhibited cracks already within a much shorter period of time. This is consistent with the recognised responses of the different weld metals investigated in the present thesis to the time period before NDT. This would mean that as far as the higher strength regime is concerned, the present results should ensure freedom from hydrogen cracking when applying weld H_{cr} levels given by the formulae and diagrams of the present thesis.

Still, the scope of the work carried out in the thesis does not allow accurate answers to be given in these questions. Therefore, the holding time under restraint to ensure that all cracking is captured during NDT is obviously an area requiring further work. Therefore, additional quantitative data should be produced to further convince and validate the conclusions made in the present thesis, as regards to the dependence of holding time on strength.

References

[1a] *EN 1011-1:1998*: 'Welding – Recommendations for welding of metallic materials – Part 1: General guidance for arc welding'. CEN/TC 121, CEN 1998. 18 p.

[1b] *EN 1011-2:2001*: 'Welding – Recommendations for welding of metallic materials – Part 2: Arc welding of ferritic steels'. CEN/TC 121, CEN 2001. 113 p.

[2a] Okuda N, Nishikawa Y, Aoki T, Goto A & Abe T: 'Hydrogen-induced cracking susceptibility of weld metal'. *IIW-Doc. II-1072-86 / II-A- -86*. Kobe Steel Ltd./The International Institute of Welding, Japan, 1986. 16 p.

[2b] Okuda N, Ogata Y, Nishikawa Y, Aoki T, Goto A & Abe T: 'Hydrogen-induced cracking susceptibility in high-strength weld metal'. *Welding Journal* 66 (1987): May, pp. 141-s – 146-s.

[3a] Yatake T & Yurioka N: 'Studies of delayed cracking in steel weldments (Report 3)'. *Journal of the Japan Welding Society (JWS)* 50 (1981) 3, pp. 291–296.

[3b] Suzuki H & Yurioka N: 'Prevention against cold cracking in welding steels'. *Australian Welding Journal* 27 (1982) 1: Autumn 1982. Pp. 9–27.

[4] Nevasmaa P & Karppi R: 'Implications on controlling factors affecting weld metal hydrogen cold-cracking in high-strength shielded-metal arc (SMAW) multipass welds'. *Report AVAL64-011043: WM-HICC VTT/3. IIW-Doc. IX-1997-01*. VTT Manufacturing Technology, Espoo 2001. 94 p. + Apps 26 p.

[5a] Nevasmaa P: 'Controlling factors influencing hydrogen cold cracking in high-strength multipass weld metals – Status Review report'. *Report VAL A:WM-HICC VTT/1*. VTT Manufacturing Technology, Espoo 2000. 51 p. + Apps 4 p.

[5b] Nevasmaa P, Kantanen M-S & Pan L: 'Hydrogen cold-cracking in high-strength shielded-metal arc (SMAW) multipass weld metals: experimental findings'. *Report AVAL64-001029:WM-HICC VTT/2*. VTT Manufacturing Technology, Espoo 2000. 66 p. + Apps 23 p.

[5c] Nevasmaa P: ‘Controlling factors affecting hydrogen cold-cracking in high-strength multipass weld metals: comparison of the cracking test results between SMAW and SAW welds’. *IIW-Doc. No IX-2027-02*. VTT Industrial Systems, Espoo 2002. 46 p. + Apps 14 p.

[6] Nevasmaa P & Karppi R: ‘Avoidance of hydrogen cracking in modern high-strength steel multipass welds’. Proceedings of the "*17th Nordic Welding Meeting (NSM’97)*", Copenhagen, 14–16 May 1997. Copenhagen: Danish Welding Society, 1997. 17 p.

[7] Nevasmaa P & Karppi R: ‘Welding for the economic and safe use of modern high-strength steels in order to avoid hydrogen cracking in multipass welds’. *Research Report VAL B 202*. VTT Manufacturing Technology, Espoo 1997. *Jernkontorets Forskning TO 40-39*. Jernkontoret, Stockholm 1998. 81 p.

[8] Pargeter RJ: ‘Effects of arc energy, plate thickness and preheat on C-Mn steel weld metal hydrogen cracking’. *TWI Research Report (CRP) No. 461/1992*. The Welding Institute, UK, November 1992.

[9] Kinsey A.J: ‘Weld metal hydrogen cracking during welding 450 N/mm^2 yield strength steel using tubular cored electrodes’. *TWI Research Report (CRP) No. 655/1998*. The Welding Institute, UK, October 1998. 24 p.

[10a] *Standard: SFS-EN 288-3:1992*: ‘Hitsausohjeet ja niiden hyväksyntä metallisille materiaaleille’. Osa 3: Terästen kaarihitsauksen menetelmäkokeet’, Suomen Standardisoimisliitto, 1992. *(in Finnish)*

[10b] *Final Draft Standard: prEN ISO 15614-1*: ‘Specification and qualification of welding procedures for metallic materials – Welding procedure test – Part 1: Arc and gas welding of steels and arc welding of nickel and nickel alloys’. CEN/TC 121 N 998. CEN/ISO, 2002. 28 p.

[11] Thier H, Eisenbeis C & Winkler R: ‘Untersuchungen zur Absicherung der Berechnung der Mindestvorwärmtemperatur beim Mehrlagenschweissen’. *Schweissen und Schneiden* 49 (1997) 7, pp. 426–430. *(in German)*

[12] Yurioka N: ‘Test results of cold cracking in multi-pass weld metal’. *IIW-Doc. IX-1903-98*. Nippon Steel Corporation, The International Institute of Welding, Japan, 1998. 11 p.

[13] Karppi R, Ruusila J, Toyoda M, Satoh K & Vartiainen K: ‘Predicting safe welding conditions with hydrogen cracking parameters’. *Scandinavian Journal of Metallurgy* 13 (1984), pp. 66–74.

[14] ‘Guide to the light microscope examination of ferritic steel weld metals’. *IIW-Doc. IX-1533-88*. The International Institute of Welding, 1988. 5 p.

[15] Tihekari H & Karppi R: ‘Mikrorakenteen vaikutus hienoraeteräksen hitausliitoksen sitkeyteen arktisissa olosuhteissa’. *Technical Research Centre of Finland*. Valtion teknillinen tutkimuskeskus (VTT), Espoo, 1984. 40 p. *(in Finnish)*

[16] Wildash C, Cochrane RC, Gee R & Widgery DJ: ‘Microstructural factors affecting hydrogen induced cold cracking in high strength steel weld metal’. Proceedings of the "*5th International Conference on Trends in Welding Research*", June 1998, Pine Mountain, Georgia, 1–5 June 1998. U.S.A 1998.

[17] Wildash C, Gee R, Cochrane RC & Widgery DJ: ‘The influence of hydrogen and microstructure on the tensile properties of high strength steel weld metal’. Proceedings of the "*9th International Conference on Joining of Materials*", Helsingör, May 1999. Denmark. Institute for Joining of Materials, 1999. Pp. 335–340.

[18] Wildash C, Gee R & Cochrane RC: ‘Designing a microstructure to resist HIC in HS steels’. *Welding & Metal Fabrication* 68 (2000): April, pp. 15–20.

[19] *Japanese Welding Association Standard WES 1105-1985*. ‘Cracking test for single-bevel groove multi-layer welds’. Japanese Welding Association, Japan 1985. 38 p.

[20] Osaka University & Nippon Steel Interim Report on weld metal hydrogen cracking applying numerical modelling of hydrogen distribution – *Interim Report*. *(in Japanese)*

[21] Yurioka N, Ohshita S, Nakamura H & Asano K: ‘An analysis of microstructure, strain and stress on the hydrogen accumulation in the weld heat-affected zone’. *IIW-Doc. IX-1161-80*. Nippon Steel Corporation, The International Institute of Welding, Japan, 1980. 18 p.

[22] Yurioka N: ‘A review of numerical analyses on the hydrogen diffusion in welding of steel’. *IIW-Doc. IX-1553-89*. Nippon Steel Corporation, The International Institute of Welding, Japan, July 1989. 15 p.

[23] Yurioka N: ‘Predictive methods for prevention and control of hydrogen assisted cold cracking’. *IIW-Doc. IX-1938-99*. Nippon Steel Corporation, The International Institute of Welding, Japan, 1999. 16 p.

[24] Karppi R: ‘Effect of weld hydrogen content and preheat temperature on the Implant fracture strength of a few heat resisting pressure vessel steels’. *Publication No 1/1976*. Helsinki University of Technology, Laboratory of Materials Technology, Espoo 1976. 422 p.

[25] Karppi R: ‘A stress field parameter for weld hydrogen cracking‘. *VTT Publications 9*. Technical Research Centre of Finland, Espoo 1982. 119 p.

[26] Wong RJ: ‘Hydrogen cracking resistance of high strength steels in single-pass and multiple-pass weldability tests’. Proceedings of the "*Materials Week '95" Symposium "Welding and Weld Automation in Shipbuilding*", Cleveland, Ohio, 29 October – 2 November 1995. Ed. R. SeNale. The Minerals, Metals and Materials Society, Pennsylvania, USA 1996. Pp. 33–46.

[27] Boothby PJ: ‘Weldability of offshore structural steels. Part 1 & 2’. *Metal Construction* 17 (1985): August & September, pp. 2–14.

[28] Hart PHM & Harrison PL: ‘Compositional parameters for HAZ cracking and hardening in C-Mn steels’. *Welding Journal* 66 (1987): October, pp. 310–322.

[29] Hart PHM, Matharu IS & Jones AR: ‘The influence of reduced carbon equivalent on HAZ cracking in structural steels’. Proceedings of the "*7th International Conference on Offshore Mechanics and Arctic Engineering*", Houston, Texas, 7–12 February 1998. Ed. M. Salama et al. U.S.A: The American Society of Mechanical Engineers (ASME), 1998. Vol. III. Pp. 111–120.

[30] Hart PHM & Harrison PL: ‘Compositional parameters for HAZ cracking and hardening in C-Mn steels’. *Rivista Italiana della Saldatura* No 2, 1990. Pp. 27–43.

[31] Private information. Discussion, R Pargeter & P Hart, TWI, in 21st February 2000.

[32] Yang LJ, Chandel RS & Bibby MJ: ‘The effects of process variables on the weld deposit area of submerged arc welds’. *Welding Journal* 72 (1993): January, pp. 11-s – 18-s.

[33] Gunaraj V & Murugan N: ‘Prediction and optimization of weld bead volume for the submerged arc process – Part 1 and 2’. *Welding Journal* 79 (2000): October & November, pp. 286-s – 294-s and 331-s – 338-s.

[34] Nevasmaa P, Cederberg M & Vilpas M: ‘Weldability of accelerated-cooled (AcC) high strength TMCP steel HT50’. *VTT Research Notes 1410*. Technical Research Centre of Finland, Espoo 1992. 30 p. + Apps. 8 p.

[35] Private information. Discussion, N Yurioka, Nippon Steel Corp. (NSC), June 2001.

[36a] Kantanen M-S: ‘Controlling Factors Influencing Hydrogen Cold Cracking in High-Strength Multi-Pass Weld Metal – Microstructure and tensile properties’. *Interim Report*, Oulu University, Oulu 2001.

[36b] Pan L: ‘Literature search on hydrogen diffusion data and permeation measurements’. *Interim Report*, Oulu University, Oulu 1999.

[37] Wang WW, Wong RJ, Liu S & Olson DL: ‘Use of martensite start temperature for hydrogen control’. Proceedings of the "*Materials Week '95*" Symposium "*Welding and Weld Automation in Shipbuilding*", Cleveland, Ohio, 29 October – 2 November 1995. Ed. R. SeNale. The Minerals, Metals and Materials Society, Pennsylvania, USA 1996. Pp. 17–31.

[38] Nevasmaa P, Laukkanen A & Ehrnstén U: ‘Fracture resistance and failure characteristics of AISI 304/ SA508 bimetallic weld in ductile regime’. Proceedings of the “*13th European Conference on Fracture – Fracture Mechanics: Applications and Challenges (ECF 13)*”, San Sebastian, 6–9 September 2000. Eds. M Fuentes & D Eastbury. Spain: Engineering Materials Advisory Services Ltd., 2000. Paper No 1N.49. 8 p.

[39] Liimatainen J & Martikainen H: ‘New high-purity cast steels for offshore applications’. Proceedings of the “International Conference Welding-90: Technology, Materials, Fracture”, Geesthacht, 22–24 October 1990. Ed. M. Kocak. Germany: Institute for Industrial Technology Transfer, France 1990.

[40] Coe FR: ‘Welding steels without hydrogen cracking’. The Welding Institute, Cambridge, United Kingdom, 1973. 68 p.

[41] Baillie JG: ‘Underbead and toe cracks’. British Welding Journal 14 (1967) 2, pp. 51–61.

[42] Gooch TG & Cane MWF: ‘Fractographic observations of hydrogen induced cracking in steel. Practical implications of fracture mechanics’. *Institution of Metallurgists: Spring meeting*, Newcastle upon Tyne, 27–29 March 1973. Institution of Metallurgists, London 1973. Paper No 10. Pp. 95–102.

[43] IIW: ‘Note on the underbead hardness and cold cracking susceptibility’. *IIW-Doc. IX-600-68*. The International Institute of Welding, Warsaw 1968. 3 p.

[44] Inagaki M, Nakamura H, Inoue T, Takeshi Y, Minami K & Kanazawa S: ‘Delayed cracking in high-strength steel weld with angular distortion’. *Transactions of the Japan Welding Society* 4 (1973) 1, pp. 19–29.

[45] Ito Y & Iwanaga H: ‘The effects of alloying elements on weldability’. *Journal of the Japan Welding Society (JWS)* 36 (1967) 9, pp. 56–64. *(in Japanese)*

[46] Matsuda F, Nakagawa H, Tsuji T & Tsukamoto M: ‘Fractography of cold crack of various carbon steels and alloy steels by means of the Implant test’. *Transactions of the Japan Welding Research Institute (JWRI)* 7 (1978) 1, pp. 71–85.

[47] Randall MD, Monroe RE & Rieppel PJ: ‘Causes of microcracking and microporosity in ultra-high strength steel weld metals’. *Welding Journal* 41 (1962) 5, pp. 193-s – 206-s.

[48] Satoh K, Terai K, Yamada S, Nagano T & Matsumura H: ‘Study on weld cracking in multiple pass welds of high-strength steel’. *Transactions of the Japan Welding Society* 1 (1970) 1, pp. 112–118. *IIW-Doc. IX-678-70*. The International Institute of Welding, 1970. 7 p.

[49] Satoh K, Matsui S, Nishimura I, Hyama H & Chiba N: ‘Effect of intensity of bending restraint on weld cracking in multipass weld’. *Transactions of the Japan Welding Society* 8 (1977) 1, pp. 42–49. *IIW-Doc. IX-960-76*. The International Institute of Welding, 1976. 13 p.

[50] Gedeon SA & Eagar TW: ‘Assessing hydrogen-assisted cracking fracture modes in high-strength steel weldments’. *Welding Journal* 69 (1990): June, pp. 213-s – 219-s.

[51] Beachem CD: ‘A new model for hydrogen-assisted cracking (hydrogen embrittlement)’. *Metallurgical Transactions* 3 (1972) 2, pp. 437–451.

[52] Nevasmaa P, Cederberg M & Vilpas M: ‘Weldability of new HT-50 and HT-80 class thermomechanically rolled high strength steels’. Proceedings of the "*5th Conference on Joining of Materials – JOM-5*", Helsingör, 10–12 May 1991. Eds. RL Apps & O Al-Erhayem. The European Institute for the Joining of Materials, Denmark 1991. Pp. 387–394.

[53] Nevasmaa P, Cederberg M & Vilpas M: ‘Weldability of direct-quenched and tempered (DQ-T) high strength steel HT80’. *VTT Research Notes 1406*. Espoo 1992. 32 p. + Apps. 12 p.

[54] Graville BA: ‘A survey review of weld metal hydrogen cracking’. *Welding in the World* 24 (1986) 9/10, pp. 190–199.

[55] Matsuda F, Nakagaura H & Matsumoto T, *Transactions of the Japan Welding Research Institute (JWRI)* 10 (1981) 1, pp. 81–87.

[56] Interrante CG & Stout RD, *Welding Journal* 43 (1964): April (Research Supplement), pp. 145-s – 160-s.

[57] *ISO/IIW 3690-1977 E*: ‘Determination of hydrogen in deposited weld metal arising from the use of covered electrodes for welding mild and low-alloy steels’. International Organisation for Standardisation, 1977. 4 p.

[58] Moreton J & Coe FR: ‘A survey of the sources, distribution and movement of hydrogen in weld metal’. *IIW-Doc. II-512-69*. The International Institute of Welding, 1969. 21 p.

[59] Coe FR & Chano Z: ‘Hydrogen distribution and removal for a single bead welding during cooling – Part 3’. *Welding Research International* 5 (1975) 1, pp. 66–80.

[60] Schwarz W & Zitter H: ‘Determination of diffusible hydrogen in the weld metal deposited by means of coated electrodes’. *IIW-Doc. II-A-258-70*. University of Mining and Metallurgy, Leoben 1970. The International Institute of Welding, 16 p.

[61] Gerberich WW, Chen YT & St John C: ‘A short-time diffusion correlation for hydrogen-induced crack growth kinetics’. *Metallurgical Transactions A* 6A (1975) 8, pp. 1485–1498.

[62] Savage WF, Nippes EF & Homma H: ‘Hydrogen cracking in HY-80 steel weldments’. *Welding Journal* 55 (1976) 11, pp. 368-s – 380-s.

[63] Terasaki T, Karppi R & Satoh K: ‘Relationship between critical stress of HAZ cracking and residual diffusible hydrogen content’. *Transactions of the Japan Welding Society* 10 (1979) 1, pp. 53–57.

[64] Lazor RB & Graville BA: *Canadian Welder & Fabricator* 74 (1983) 7: July, pp. 21–23.

[65] Satoh K, Ueda Y & Kihara H: ‘Recent trend of researches on restraint stresses and strains for weld cracking’. *IIW-Doc. IX-788-72, X-659-72*, Osaka University, 1972. 39 p. /*Welding in the World* 11 (1973) 5/6, pp. 133–155.

[66a] Matsui S: ‘Reaction stresses and weld cracking in restrained butt joints’. *Doctoral Thesis*. Osaka University, Japan 1967. 109 p. *(in Japanese)*

[66b] Satoh K & Matsui S: ‘Reaction stress and weld cracking under hindered contraction’. *IIW-Doc. IX-574-68*. Osaka University, 1968. 22 p. /*Technological Reprints of the Osaka University* 17 (1967) 2, pp. 353–375.

[67a] Private information. Discussion, R Leggatt, P Hart & R Pargeter, TWI, Cambridge, 21st February, 2000.

[67b] Leggatt RH: ‘Welding residual stresses’. Proceedings of the "*5th international Conference on Residual Stresses*", Linköping, 16–18 June 1997 (Reprint). The Welding Institute (TWI), Cambridge, United Kingdom 1997. 14 p.

[68] St John C & Gerberich WW: ‘The effect of loading mode on hydrogen embrittlement’. *Metallurgical Transactions* 4 (1973) 2, pp. 589–601.

[69] Matsuda F, Nakagawa H, Shinozaki K, Tabaka S & Kihara H: *Transactions of the Japan Welding Research Institute (JWRI)* 10 (1981) 2, pp. 183–191.

[70] Watkinson F: *Welding Journal* 48 (1969) 9, pp. 417-s – 424-s.

[71] Hart PHM & Watkinson F: *Welding Journal* 54 (1975): September, pp. 288-s – 295-s.

[72] McParlan M & Graville BA: *IIW-Doc. IX-922-75*. The International Institute of Welding, 1975 /*Welding Journal* 55 (1976) 4: April, pp. 95-s – 102-s.

[73] Satoh K & Matsui S: ‘Notation system of joint restrain severity’. *IIW-Doc. X-910-78*. Osaka University & Kawasaki heavy Industries, 1978. 6 p.

[74] Lee HW, Kang SW, Um DS: ‘A study on transverse weld cracks in thick steel plate with the FCAW process’. *Welding Journal* 77 (1998): December, pp. 503-s – 510-s.

[75] Lynch S: ‘Mechanisms & kinetics of environmentally assisted cracking’. *Special Visiting Lecture*. Helsinki University of Technology (HUT), Espoo, 30 May 2002. Aeronautic & Maritime Research Laboratory, Defence Science & Technology Organisation, Melbourne, Australia, 2002.

[76] Kuebler R, Pitrun M & Pitrun I: ‘The effect of welding parameters and hydrogen levels on the weldability of high strength Q&T steel welded with FCAW consumables’. *Australian Welding Journal* 45 (2000): 1st Quarter 2000 – Welding Research Supplement, pp. 38–47.

[77] Satoh K, Terasaki T & Ohkuma Y: ‘Relationship between critical stress of HAZ cracking and residual diffusible hydrogen content’. *Journal of the Japan Welding Society (JWS)* 48 (1979) 4. pp. 248–252.

[78] Porter DA & Easterling KE: ‘Phase Transformations in Metals and Alloys’. Chapman & Hall, London, U.K., 1992. 514 p.

[79] Yurioka N: ‘Diffusion and accumulation of hydrogen in multiple-pass welds’. *Special Visitors Lectures*. Nippon Steel Corporation Research Centre (NSC), Kimitsu, Chiba, 2 July 1999. Nippon Steel Corporation, Chiba, Japan, 1999.

[80] Yurioka N & Nakamura H: ‘Investigation of the mass diffusion equation with activity as a variable’. *Journal of the Japan Welding Society (JWS)* 48 (1979) 9, pp. 726–730.

[81] Steigerwald EA, Schaller FW & Troiano AR: *Transactions of the Metallurgical Society of AIME* 218 (1960) 10, p. 382.

[82] Naiki T & Okabayashi H: *Journal of the Japan Welding Society (JWS)* 40 (1971) 7, p. 675.

[83] Kohira K, Yatake T & Yurioka N: ‘A numerical analysis of the diffusion and trapping of hydrogen in steels and steel weldments’. *IIW-Doc. IX-951-76.* The International Institute of Welding. Nippon Steel Corporation, Chiba, Japan 1976.

[84] Sleptsov OI, Mikhailov VE & Smijan OV: *IIW-Doc. IX-B-179-89*. The International Institute of Welding, 1989.

[85] Volkl J & Alfeld G: ‘Hydrogen in Metals’. Ed. G. Alfeld. Vol. 28 (1978), p. 321.

[86] Johnson EW & Hill ML: ‘The diffusivity of hydrogen in alpha iron’. *Transactions of the Metallurgical Society of AIME* 218 (1960): December, pp. 1104–1112.

[87] Sykes C: ‘Hydrogen in steel manufacture’. *Journal of the Iron & Steel Institute* (1947): June.

[88] Andersson BAB: *Transactions of AIME / Journal of Engineering Materials and Technology* 102 (1980) 1, p. 64.

[89] Phragmen G: *Jernkontorets Annaler* 128 (1944), pp. 537–. *(in Swedish)*

[90] Lange G & Hoffman W: ‘Relation between hydrogen up-take and porosity in iron’. *Archiv für das Eisenhüttenwesen (Steel Research)* 37 (1966) 5, pp. 391–397.

[91] Oriani RA: ‘The diffusion and trapping of hydrogen in steel’. *Acta Metallurgica* 18 (1970) 1, pp. 147–157.

[92] Bockris JO'M & Weck W: ‘The effect of stress on the chemical potential of hydrogen in iron and steel’. *Acta Metallurgica* 19 (1971), pp. 1209–1219.

[93] Terasaki T, Akiyama T & Ohshita S: *Quarterly of the Japan Welding Society (JWS)* 4 (1986) 2, p. 378.

[94] Takahashi E, Iwai K & Horitsuji T: *Journal of the Japan Welding Society (JWS)* 49 (1980) 2, p. 129.

[95] Terasaki T, Yamashita Y & Satoh K: *Journal of the Japan Welding Society (JWS)* 48 (1979) 9, p. 678.

[96] Private information. Discussion, R Gee, Leeds University, Leeds, U.K., November 1999.

[97] Private information. Discussion, M Swallow, Leeds University, Leeds, U.K., November 1999.

[98] Mota JMF & Apps RL: *Welding Journal* 61 (1982) 7: July, pp. 222-s – 228-s.

[99] Allen DJ, Chew B & Morris P: *Welding Journal* 61 (1982) 7: July, pp. 212-s – 221-s.

[100] Takahashi E, Iwai K & Horitsuji T: 'Relation between occurrence of transverse cracking'. *Journal of the Japan Welding Society (JWS)* 48 (1979), pp. 855–872.

[101] Karppi R & Nevasmaa P: 'Contribution to comparison of methods for determining welding procedures for the avoidance of hydrogen cracking'. *IIW-Doc. IX-1673-92. VTT Publications 107*. Technical Research Centre of Finland, Espoo 1992. 37 p. + Apps. 12 p.

[102] Ornig H, Schutz H & Klug P: 'Comparison of methods to determine the preheat temperature for high-strength weld metal'. *Welding in the World* 41 (1998), pp. 144–148.

[103] Beres L, Beres Z & Irmer W: 'New equation for calculating the M_S temperature'. *Schweissen und Schneiden / Welding and Cutting* 46 (1994) 8, pp. E128–E130.

[104] *AWS D1.1:1988*: 'Structural welding code – steel'. American Welding Society (AWS), 1988.

[105] *BS 5135:1984*: 'Process of arc welding of carbon and carbon manganese steels'. British Standards Institution (BSI), 1984.

[106] Takahashi E, Iwai K & Horitsuji T: 'Prevention of the transverse cracks in heavy section butt weldments of 2 1/4 Cr-1 Mo steel through low temperature postweld heat treatment. Correlation between hydrogen concentration and practical welding conditions'. *Journal of the Japan Welding Society (JWS)* 48 (1979) 10, pp. 92–99.

[107] Vuik J, van Wortel JC & van Sevenhoven C: 'Application of very low yield strength consumables in the root pass of weldments to avoid preheating'. *Welding in the World* 33 (1994) 5, pp. 362–369.

[108] Boellinhaus Th, Hoffmeister H & Dangeleit A: 'A scatter band for hydrogen diffusion coefficients in micro-alloyed and low carbon steels'. *Welding in the World* 35 (1995) 2, pp. 83–96.

[109] Devanathan MA & Stachurski Z: 'The absorption and diffusion of electrolytic hydrogen in palladium'. *Proceedings of the Royal Society of London No A270*. United Kingdom, 1962. Pp. 90–102.

[110] McBreen J, Nasis L & Beck W: 'A method for determination of the permeation rate of hydrogen through metal membrane'. *Journal of the Electrochemical Society* 113 (1966) 11, pp. 1218–1222.

[111] Scoppio L: ‘Towards a Unified Approach on a European Scale of Electrochemical Hydrogen Permeation Test Methodologies on Low Alloyed Steels’. *Report No EUR 16790 EN*, Europe, 1997.

[112] Widgery D: *Interim Report*. ESAB, U.K., 2002.

[113] Yurioka N, Wakabayashi M & Motomatsu M: ‘Data sheet of properties of high heat input SAW weld metals’. *IIW-Doc. IX-1868-97*. The International Institute of Welding. Nippon Steel Corporation, Japan 1997.

[114] Lowe G & Bala SR: *Welding Journal* 60 (1981) 12: December, pp. 258-s – 268-s.

[115] Thibau R & Bala SR: *Welding Journal* 62 (1983) 4: April, pp. 97-s – 104-s.

[116] Widgery DJ: ‘Welding of high strength steels – weld metal hydrogen cracking’. *Esab Report TR 907*. ESAB -SSAB Meeting, Oxelösund, 23–24 September 1998. Esab Group (UK), United Kingdom 1998. 10 p.

[117] Håkansson K: ‘Submerged arc welding of Weldox 900E in 50 mm plate thickness – Hydrogen cracking tests’. *IIW-Doc. II-A-117-03*. Kockums AB, Laboratory, Sweden. The International Institute of Welding, 2003. 14 p.

[118] Åström H: ‘Tillsatsmaterial för svetsning av höghållfasta ståhl – utveckling och problemområden’. *Svetsen* 60 (2001) 5, pp. 7–14. *(in Swedish)*

[119] Yurioka N: ‘Prediction of Weld Metal Strength (Report III)’. *IIW-Doc. IX-03*. The International Institute of Welding, 2003. 31 p.

[120a] Nevasmaa P, Laukkanen A & Alhainen J: ‘Evaluation of Risk of Hydrogen Cracking using a Combined Finite-Difference to Finite Element Analysis and Coupling to Damage Mechanics’. Proceeding of the "*9th International Conference on the Mechanical Behaviour of Materials (ICM-9)*". Geneva, Switzerland, 25–29 May 2003.

[120b] Laukkanen A, Nevasmaa P & Alhainen J: ‘Numerical Evaluation of Hydrogen Cracking using Transient Finite Element Analysis and Concentration Dependent Damage Mechanics Constitutive Model’. Proceeding of the "*7th International Seminar: Numerical Analysis of Weldability (NAW-7)*". Graz–Seggau, 29 September – 1 October 2003. Austria: Institute for Materials Science, Welding and Forming (IWS) & Graz University of Technology (TUG), 2003. 16 p. *(to be published*)

[121] Kim HJ & Kang BY: ‘Effect of Microstructural Variation on Weld Metal Cold Cracking of HSLA-100 Steel’. *ISIJ International* 43 (2003) 5, pp. 706–713.

[122] Alcãntara NG & Rogerson JH: ‘A Prediction Diagram for Preventing Hydrogen-Assisted Cracking in Weld Metal’. *Welding Journal* 63 (1984) 4, pp. 116-s – 122-s.

[123] Widgery DJ: ‘Welding Consumable Development – Remaining Challenges’. Proceedings of the "*Welding Engineering Research Centre 2nd International Conference on Recent Developments and Future Trends in Welding Technology*". (Reprint). Cranfield University, United Kingdom 2003. 10 p.

[124] Lee HW & Kang SW: ‘The Relationship between Residual Stresses and Transverse Weld Cracks in Thick Steel Plate’. *Welding Journal* 82 (2003): August, pp. 225-s – 230-s.

Appendices

APPENDIX 1/1

Calculation methods predicting the required preheat T_{cr} to avoid weld metal hydrogen cracking

1. Okuda-evaluation [2]

$$T_{cr} = 1.15 * (5.24\, R_M + 277 \log H_D - 482)$$

where:

R_M : tensile strength of weld metal (kgf/mm^2)

H_D : diffusible hydrogen content in the weld metal (measured by gas chromatography method) (ml/100g DM)

validity range: $77 < R_M < 110$ kgf/mm^2
$1.0 < H_D < 5.1$ ml/100g
$h < 40$ mm (for single-bevel groove)
$h < 80$ mm (for double-bevel groove)

conversion formula: 1 kgf/mm^2 = 1 MPa / 9.81

2. Yurioka-Yatake-evaluation [3]

$$T_{cr} = 120 + 120 * \log (H_D/3.5) + 5.0 * (a_w - 20) + 8 * (R_M - 83)$$

where:

H_D : diffusible hydrogen content of weld metal (measured by JIS glycerine test) (ml/100 g deposited metal)

a_w : weld metal build-up thickness (mm)

R_M : tensile strength of weld metal (kgf/mm^2)

validity range: $0.1 < H_D < 40$ ml/100 g DM
$15 < a_w < 30$–40 mm
$60 < R_M < 90$ kgf/mm^2

$$T_{cr} = 120 + 120 * \log (H_D/3.5) + 5.0 * (a_w - 20) - 0.05 * (a_w - 30)^2 + 8 * (R_M - 83)$$

validity range: as above, except:
$30 < a_w < 50$ mm

APPENDIX 1/2

$$T_{cr} = 250 + 120 * \log (H_D/3.5) + 8 * (R_M - 83)$$

validity range: as above, except
$a_w > 50$ mm

conversion formulae: $H(JIS) = (1/1.26) * (H_{GC} - 2.19)$; acc. to Ref.[12]
$H(JIS) = 0.67\ H(IIW) - 0.68$
$H(JIS) = 0.67\ H(IIW) - 0.80$
$H(JIS) = (0.77 \pm 0.03) * H_{GC} - (0.71 \pm 0.19)$
$H(JIS) = 0.77\ H(IIW) - 0.47$

APPENDIX 2/1

Comparison between the preheat estimates T_0 given by EN 1011-2 Method B and the NSC Y-Groove cracking tests for multipass weld metals

Table 2.1. Weld metals[12] with the tensile strength $R_M \approx 800$ MPa.

Weld	CET (%)	a_w (mm)	H_D (ml/100g DM IIW)	T_0 : EN 1011-2[1] (°C)	T_0 : Y-Groove[12] (°C)	ΔT_0 (°C)
Y80C	0.32	40	2.0	78	75	≈ 0
L80-1	0.31	20		47	75	–28
		30	4.3	75	125	–50
		40		95	175	–80
L80-2	0.30	20		56	125	–69
		30	6.7	85	175	–90
		40		105	225	–120
L80-3	0.29	20		69	150	–81
		30	10.4	97	200	–103
		40		116	*> 200*	*> –100*

Table 2.2. Weld metals[12] with the tensile strength $R_M \approx 750$ MPa.

Weld	CET (%)	a_w (mm)	H_D (ml/100g DM IIW)	T_0 : EN 1011-2[1] (°C)	T_0 : Y-Groove[12] (°C)	ΔT_0 (°C)
L74	0.29	30	4.0	57	75	–18
L74-1	0.25	20		17	50–75	> –33
		30	6.7	45	125	–80
		40		65	175	–110
L74-2	0.28	20		58	–	–
		30	9.9	87	150	–63
		40		106	200	–94

CET: carbon equivalent according to EN 1011-2 : 2001[1b]

a_w: weld build-up thickness in the Y-Groove test

H_D: weld diffusible hydrogen content (ml/100g DM) according to ISO/IIW 3690-1977 E[57]

T_0 : EN 1011-2: required preheat temperature according to EN 1011-2 Method B[1b]

T_0 : Y-Groove: required preheat temperature according to the NSC Y-Groove cracking test[12]

APPENDIX 3/1

Results of the residual stress measurements at Helsinki University of Technology, Finland

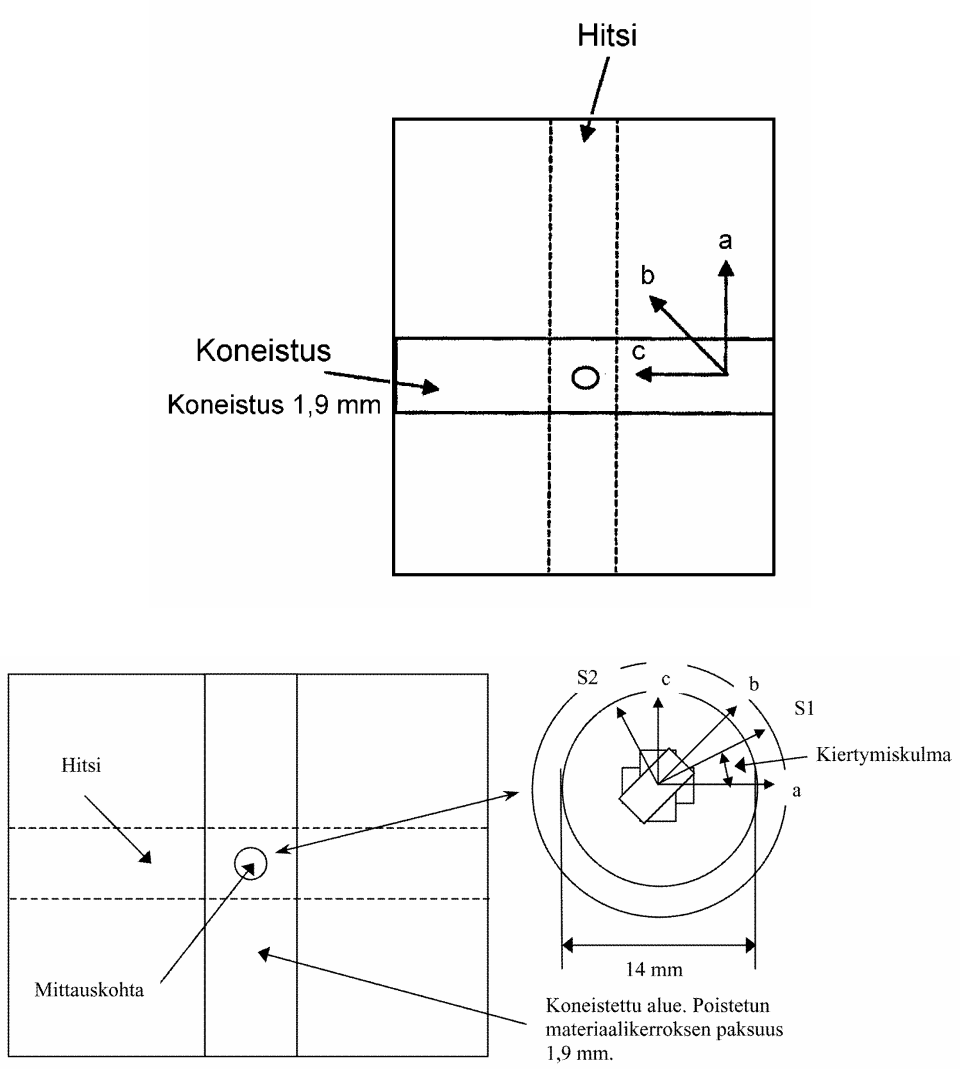

Fig. 3.1. The principles of the Ring-Core test method for determining weld residual stresses in thick plate multipass welds. Plate thickness 40 mm.

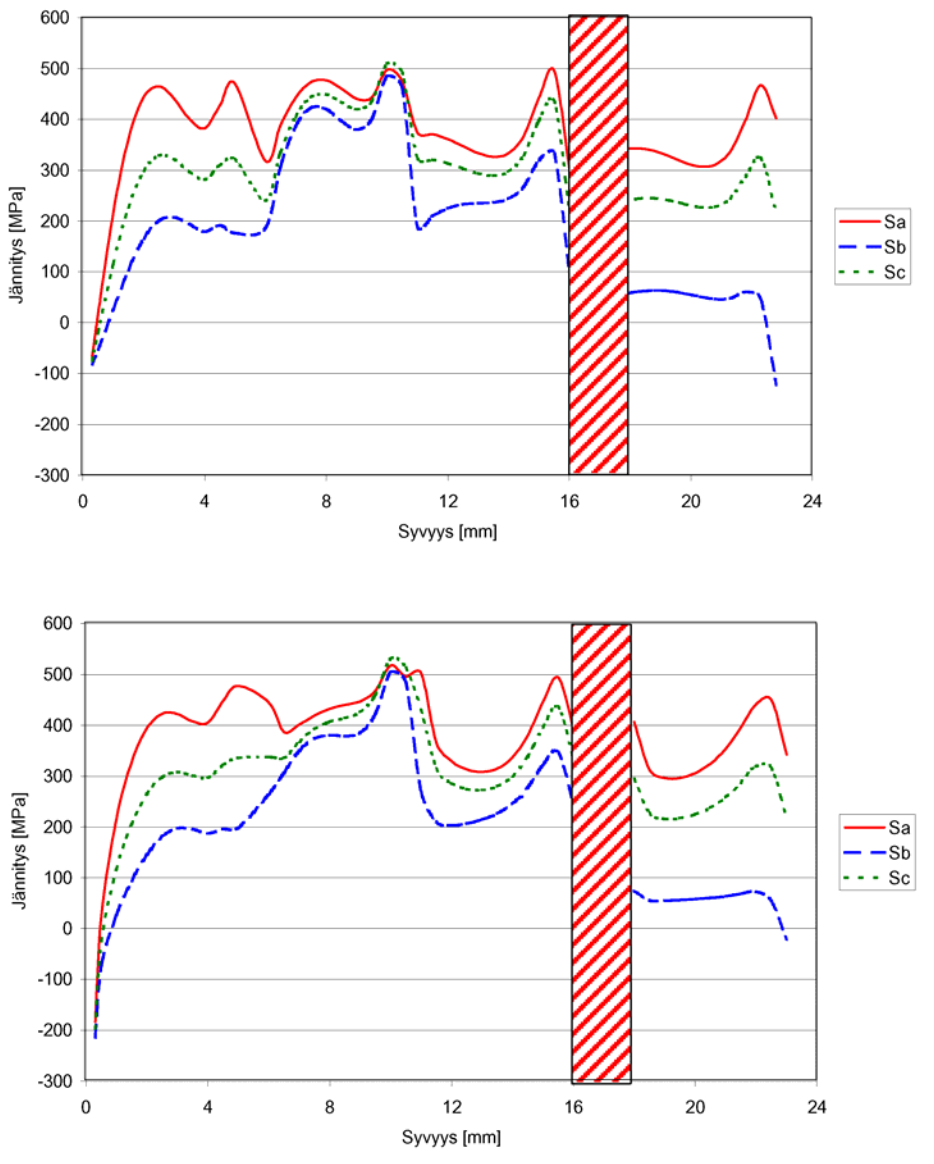

Fig. 3.2. Results of the weld residual stress measurements using the Ring-Core method for the 300 mm long multipass welded specimen (HL40), plotted against the weld depth (mm). Stress components (MPa) into the weld longitudinal direction (Sa), weld transverse direction (Sc) and into the direction of 45° between them (Sb). Analysis made using two different damping calculation functions of HUT Materials Technology Laboratory, Finland (upper figure) and Siemens KWU, Germany (lower figure).

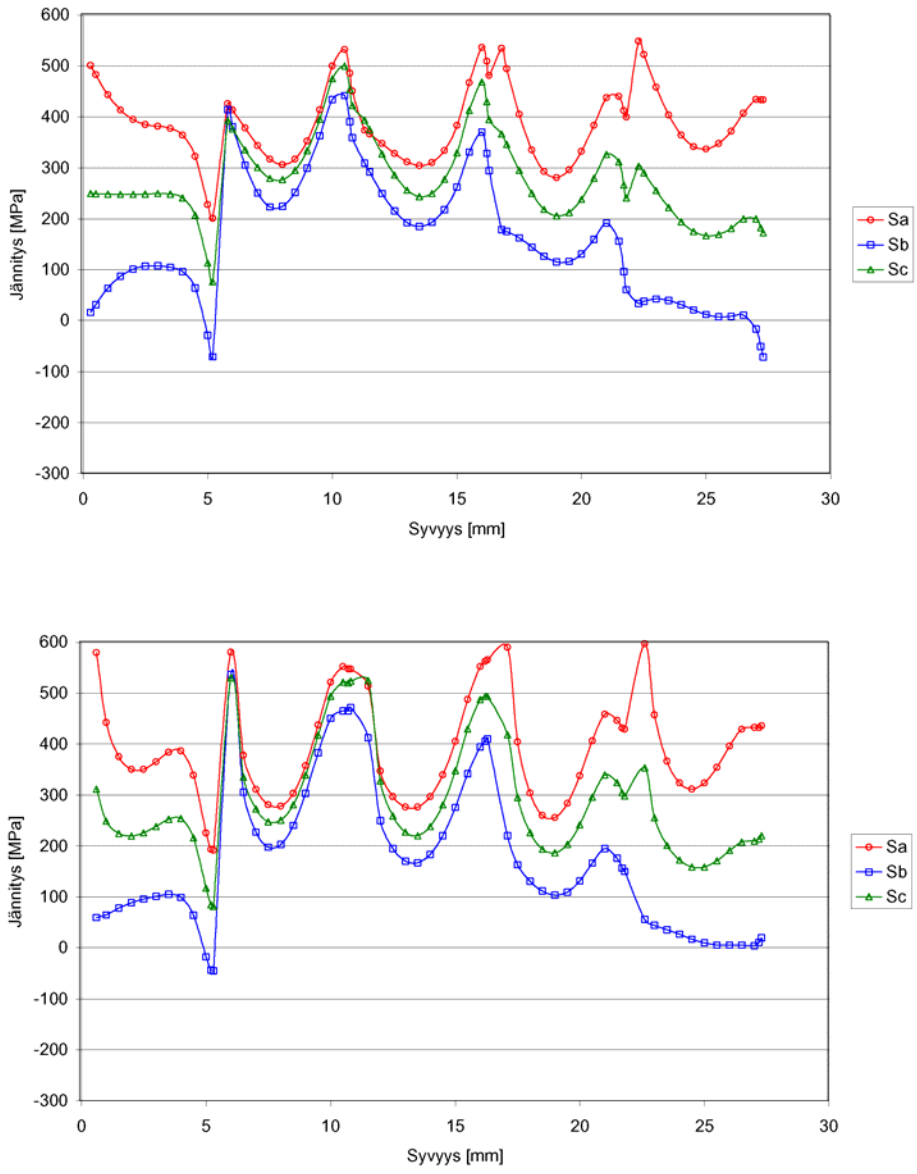

Fig. 3.3. Results of the weld residual stress measurements using the Ring-Core method for the 800 mm long multipass welded specimen (HL402), plotted against the weld depth (mm). Stress components (MPa) into the weld longitudinal direction (Sa), weld transverse direction (Sc) and into the direction of 45° between them (Sb). Analysis made using two different damping calculation functions of HUT Materials Technology Laboratory, Finland (upper figure) and Siemens KWU, Germany (lower figure).

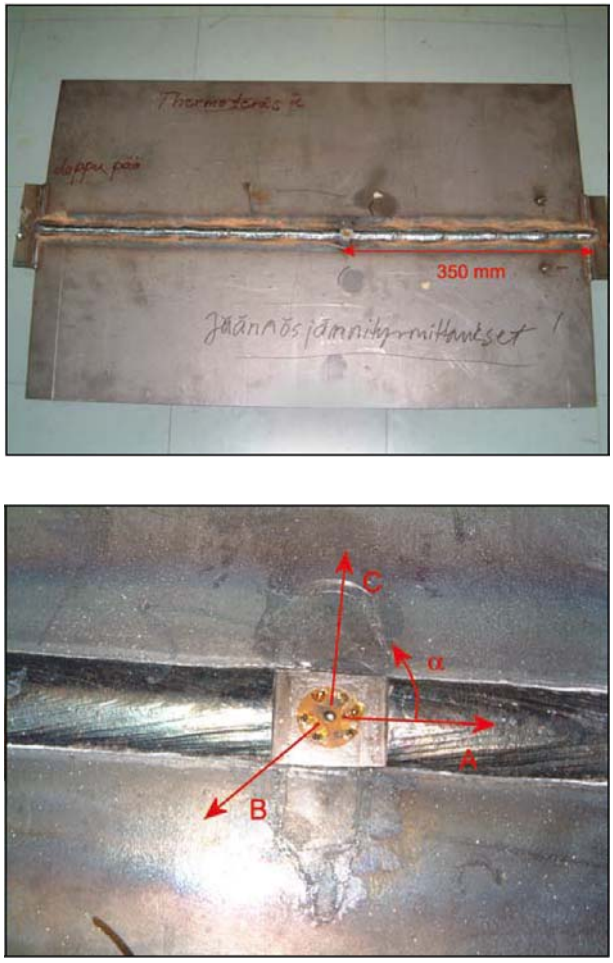

Fig. 3.4. The principles of the hole-drilling test method for determining weld residual stresses in thin plate 2-pass welds. Stress components (MPa) into the weld longitudinal direction (A), weld transverse direction (C) and into the direction of 45° between them (B). Specimen and weld length 800 mm, plate thickness 6 mm. Specimens fixed onto the table using bolted clamps (Appendix 3/5, Fig. 3.5) and welded strong-backs (Appendix 3/6, Fig. 3.6).

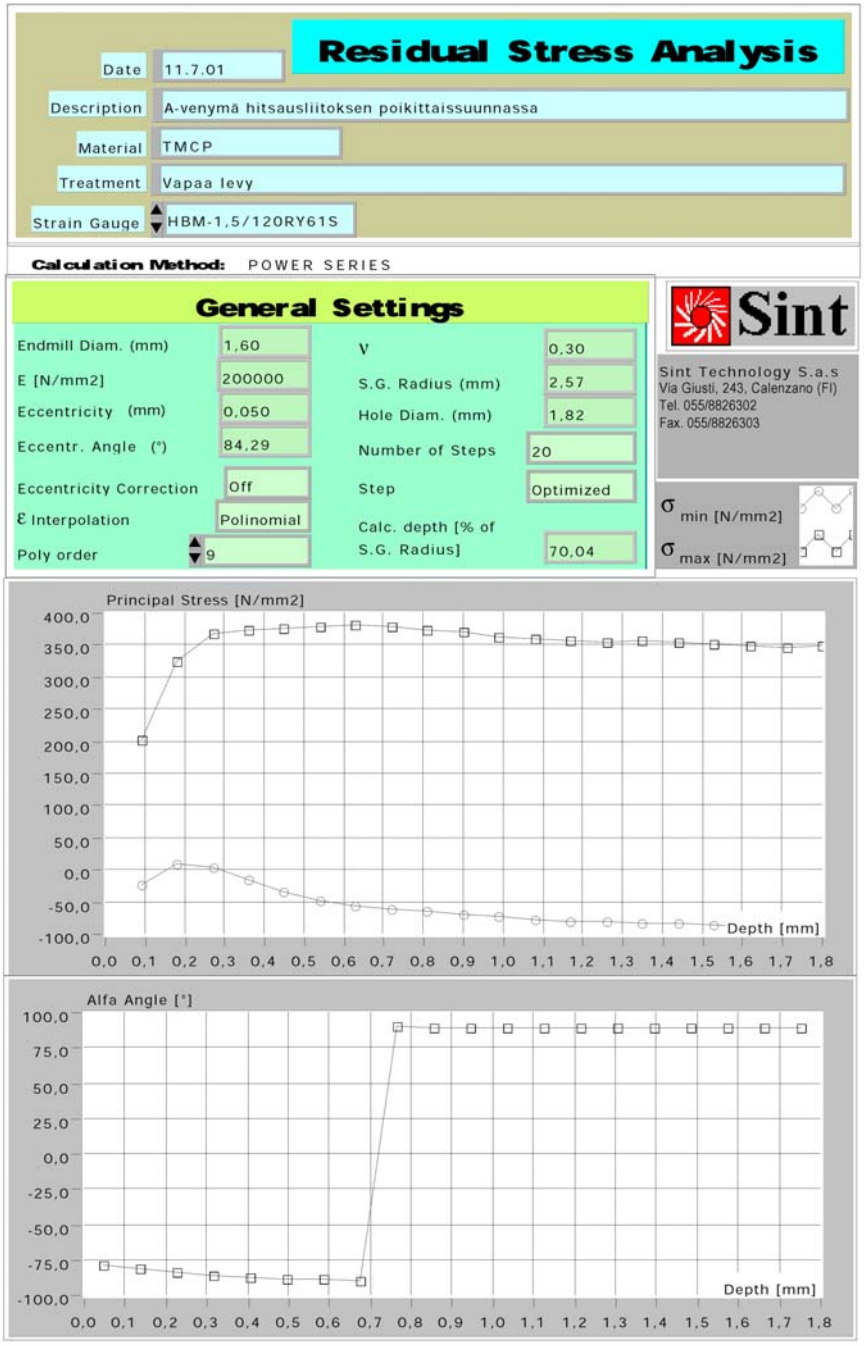
Residual Stress Analysis
Date 11.7.01
Description A-venymä hitsausliitoksen poikittaissuunnassa
Material TMCP
Treatment Vapaa levy
Strain Gauge HBM-1,5/120RY61S
Calculation Method: POWER SERIES
General Settings
Endmill Diam. (mm) 1,60
E [N/mm2] 200000
Eccentricity (mm) 0,050
Eccentr. Angle (°) 84,29
Eccentricity Correction Off
ε Interpolation Polinomial
Poly order 9
ν 0,30
S.G. Radius (mm) 2,57
Hole Diam. (mm) 1,82
Number of Steps 20
Step Optimized
Calc. depth [% of S.G. Radius] 70,04
Sint
Sint Technology S.a.s
Via Giusti, 243, Calenzano (FI)
Tel. 055/8826302
Fax. 055/8826303
σ min [N/mm2]
σ max [N/mm2]
Principal Stress [N/mm2]
400,0
350,0
300,0
250,0
200,0
150,0
100,0
50,0
0,0
-50,0
-100,0
Depth [mm]
0,0 0,1 0,2 0,3 0,4 0,5 0,6 0,7 0,8 0,9 1,0 1,1 1,2 1,3 1,4 1,5 1,6 1,7 1,8
Alfa Angle [°]
100,0
75,0
50,0
25,0
0,0
-25,0
-50,0
-75,0
-100,0
Depth [mm]
0,0 0,1 0,2 0,3 0,4 0,5 0,6 0,7 0,8 0,9 1,0 1,1 1,2 1,3 1,4 1,5 1,6 1,7 1,8

Fig. 3.5.

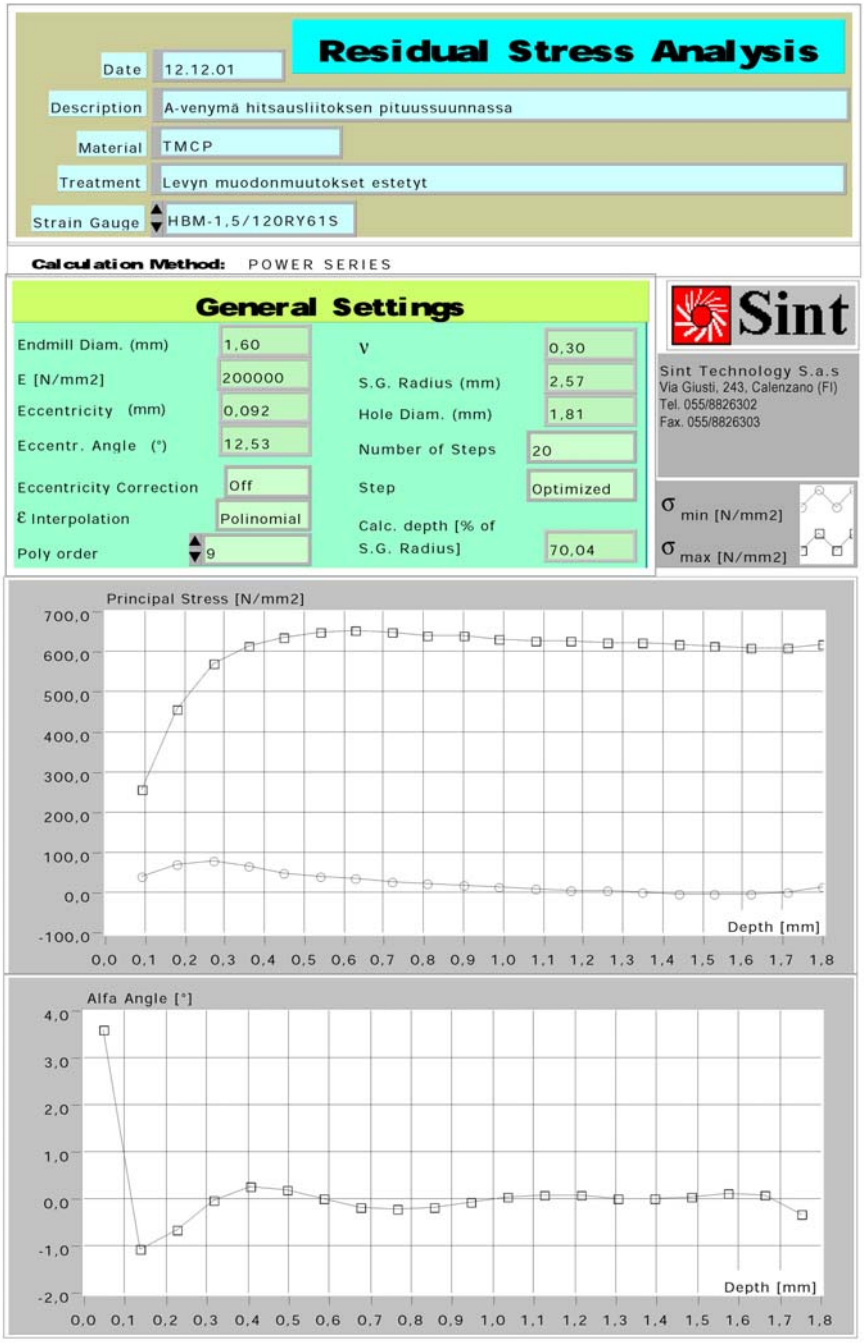
Residual Stress Analysis
Date 12.12.01
Description A-venymä hitsausliitoksen pituussuunnassa
Material TMCP
Treatment Levyn muodonmuutokset estetyt
Strain Gauge HBM-1,5/120RY61S
Calculation Method: POWER SERIES
General Settings
Endmill Diam. (mm) 1,60
E [N/mm2] 200000
Eccentricity (mm) 0,092
Eccentr. Angle (°) 12,53
Eccentricity Correction Off
ε Interpolation Polinomial
Poly order 9
ν 0,30
S.G. Radius (mm) 2,57
Hole Diam. (mm) 1,81
Number of Steps 20
Step Optimized
Calc. depth [% of S.G. Radius] 70,04
Sint
Sint Technology S.a.s
Via Giusti, 243, Calenzano (FI)
Tel. 055/8826302
Fax. 055/8826303
σ min [N/mm2]
σ max [N/mm2]
Principal Stress [N/mm2]
700,0
600,0
500,0
400,0
300,0
200,0
100,0
0,0
-100,0
Depth [mm]
0,0 0,1 0,2 0,3 0,4 0,5 0,6 0,7 0,8 0,9 1,0 1,1 1,2 1,3 1,4 1,5 1,6 1,7 1,8
Alfa Angle [°]
4,0
3,0
2,0
1,0
0,0
-1,0
-2,0
Depth [mm]
0,0 0,1 0,2 0,3 0,4 0,5 0,6 0,7 0,8 0,9 1,0 1,1 1,2 1,3 1,4 1,5 1,6 1,7 1,8

Fig. 3.6.

APPENDIX 4/1

Description of the procedure applied at the University of Oulu for deriving D_H values from the potentiostatic I_a–t curve recorded during the electrochemical permeation test

The background of the electrochemical permeation method [5b, 36b]

During the electrochemical permeation test, hydrogen diffusion can be described by the Fick ´s law:

$$j = D_H \, gradC \quad (1^{st} \; law) \qquad \frac{c}{t} = D_H \, {}^2C \quad (2^{nd} \; law) \tag{1}$$

If D_H is independent on the hydrogen concentration over the distance x, then the Fick´s equation can be written as:

$$J = -D_H \frac{\partial C}{\partial x} \qquad \frac{\partial c}{\partial t} = D_H \frac{\partial^2 C}{\partial x^2} \tag{2}$$

Fick´s law can only resolved under the given boundary conditions.

Because the hydrogen permeation test can meet the Fick´s law boundary conditions, the requirements for the test can be written as:

$t = 0$, $C = 0$ for $0 < x < L$; $t > 0$, $C = C_0$ = constant for $x = 0$, $C = C_L = 0$ for $x = L$.

Following this, the hydrogen diffusion coefficients can be calculated.

The principles of the determination of D_H [5b, 36b]

The potentiostatic curve that displays current on the exit side of the specimen, I_a, as a function of time t in the permeation test. Whilst I_c is the actual charging current applied as constant to the entry side of the specimen, I_a is the recorded current from the reverse (exit) side of the specimen and is hence proportional to the extent and velocity hydrogen permeates through the specimen during the test. Thus, I_a is influenced by the hydrogen diffusion coefficient D_H of the given specimen. Consequently, it is I_a that shows correlation with D_H, not I_c.

The J/J_{max} in the y-axis in Fig. 4.2 is directly proportional to the charging current $I_c/I_{c(max)}$ where I_c corresponds to C_0, i.e., the mean value of hydrogen concentration on the

specimen entry side, see Fig. 1. As long as I_c is kept constant, the recorded I_a–t curve will be an exponential curve. Different D_H values in different materials then manifest themselves as different shapes of the corresponding I_a–t curve.

Before deriving D_H from the I_a–t curve, the s.c. onset point must be determined. In the tests of the present study, the time I_c was applied to the specimen entry side was set as the onset point. After applying I_c, the corresponding I_a–t curve can be recorded. The onset point in the I_a–t curve is then defined as the original zero: $t_0 = 0$, $I_0 = 0$, from which the previous part – being treated as an diffusion independent background, is omitted from the entire transient curve.

There are different ways to calculate hydrogen diffusion coefficients using the I_a–t curve. The value of D_H differs between different calculations, because the I_a–t curve is not an ideally exponential curve.

- $D(t_{1/2})$ is defined to calculate the hydrogen diffusion coefficient by using the half of the whole rising time from onset point ($I_a = 0$) to the maximum of I_a, and $D(t_{1/2}) = 0.138\ L^2 / (t_{1/2})$, where L is the thickness of specimen.
- $D(t_{0.617max})$ is defined to calculate the hydrogen diffusion coefficient by using the 0.617 times of the total rising time from the onset point ($T_0 = 0$, $I_a = 0$) to the maximum of I_a, and $D(t_{0.617max}) = L^2 / 6t_{(0,617max)}$.
- $D(t_1, t_2)$ is defined to calculate the hydrogen diffusion coefficient by using two points (t_1, t_2) in the total rising time from onset point ($T_0 = 0$, $I_a = 0$) to the maximum of I_a, and $D(t_1, t_2) = 0.25\ L\ (t_2 - t_1) / t_2 t_1 \ln[J_2(t_2 / t_1)^{0.5} / J_2]$.
- $D(t_1, t_2, max)$ is defined to calculate the hydrogen diffusion coefficient by using two points (t_1, t_2) and the maximum of I_a in the total rising time from the onset point ($T_0 = 0$, $I_a = 0$) to the maximum of I_a, and $D(t_2, t_1, max) = L^2 \ln[(J\infty - J_1) / (J\infty - J_2)] / \pi^2(t_2 - t_1)$.
- $Dt_b(tg)$ is defined to calculate the hydrogen diffusion coefficient by using the breakthrough time t_b which is the intersection of the time axis with the tangent line to the permeation curve at its inflection point, and $Dt_b(tg) = L^2 / 19.8\ t_b(tg)$.
- $Dt_b(exp)$ is defined to calculate the hydrogen diffusion coefficient by using the breakthrough time t_b which is the intersection of the time axis with the exponent line to the permeation curve, and $Dt_b(exp) = L^2 / 35.2\ t_b(exp)$.

Because the differences among the values calculated with different calculation methods are far too great, a new method to calculate the hydrogen different coefficient was developed.

Derivation of D_H in the present study [5b, 36b]

In the present study, the relaxation time, i.e., the time regarded as being due to finite rate constant for transfer of hydrogen atoms from the surface into the metal phase, approximately equal to 10 sec on the basis of the present experiments, was applied in the analysis. Usually, the point of the first maximum I_a peak detected after the original zero was defined as the end point, see Fig. 4.2.

APPENDIX 4/3

The recorded I_a–t curves were processed before they were applied for calculation of D_H according to the requirement of the Fourier´s solution. Values of $D_{t(0.1)}$, $D_{t(0.2)}$ and $D_{t(0.25)}$ were calculated corresponding to the ratio of J/J_{max} to 0.1, 0.2 or 0.3, respectively[20]. These were found to be more reliable than the commonly determined values for the time lag, breakthrough time, half delay time, etc.[19, 21].

These values were determined as:

$D_{t(0.1)} = 0.1\ L^2 / t$
$D_{t(0.2)} = 0.2\ L^2 / t$
$D_{t(0.25)} = 0.25\ L^2 / t$

where L = thickness of the specimen; t = the relaxation time

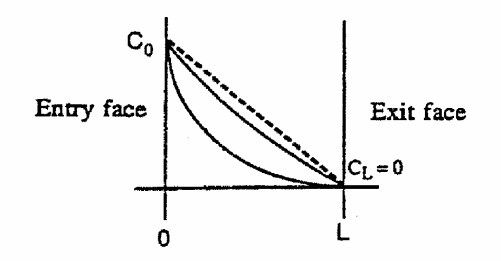

Fig. 4.1. Concentration gradient in a plane sheet during a permeation test (assumption of constant hydrogen concentration on the entry face) (CNRS).

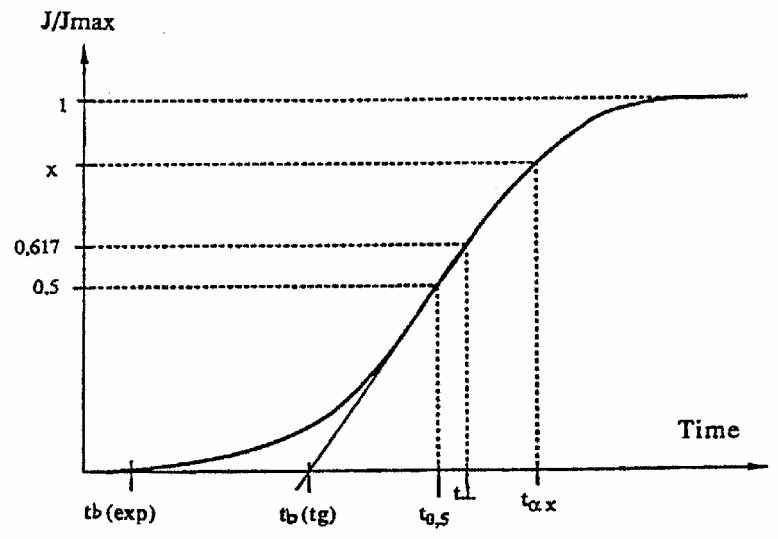

Fig. 4.2. Characteristic time values for D calculation (CNRS).

Explanation:
J/J_{max} in Fig. 4.2 is directly proportional to $I_c/I_{c(max)}$.

$D_{t(0.1)} = 0.1L^2/t$
$D_{t(0.1)} = 0.1L^2/t$
$D_{t(0.1)} = 0.1L^2/t$
L: the thickness of specimen
t: is the time.

For example, how to calculate hydrogen diffusion coefficient with the record data of I_a to calculate hydrogen diffusion coefficient:

I_c = 20–24 mA

Then get a set of I_a data:

Table 4.1.

Times (s)	I_a (uA)
0	15.27
10	15.27
12	15.27
22	15.27
32	15.28
42	15.31
52	15.39
62	15.50
72	15.60
82	15.73
92	15.85
102	15.96
112	16.06
122	16.16
132	16.25
142	16.32

1) determining the maximum value of I_a: 16.85

2) the onset point value I_a: 15.27

3) the difference of the maximum and the onset value is: 16.85 – 15.27 = 1.57

4) the corresponding value $J_1(0.2924J_{max})$: 15.27 + 1.57 x 0.2924 = 15.735

5) determining the time t_1:
15.735 is between 80 second (I_a = 15.73) and 90 second (15.85)
$t_1 = 80 + 2\ (15.735 – 15.73) \times 10/(15.85 – 15.73) = 82.5$

6) determining t_2, t_3 (same as t_1)
t_2 = 157
t_3 = 194

7) determining the relaxation time: 10 seconds

8) calculate the diffusion coefficient:

$D_{(0.1t)} = 0.1\ L^2 / t_1 = 12.45 \cdot 10^{-6}$ (cm^2/s)
$D_{(0.2t)} = 0.2\ L^2 / t_2 = 12.28 \cdot 10^{-6}$ (cm^2/s)
$D_{(0.1t)} = 0.25\ L^2 / t_3 = 12.26 \cdot 10^{-6}$ (cm^2/s)

where L = thickness of the specimen; 0.95 mm.

Also with the data in Table 4.2 can obtain I_a–t curve:

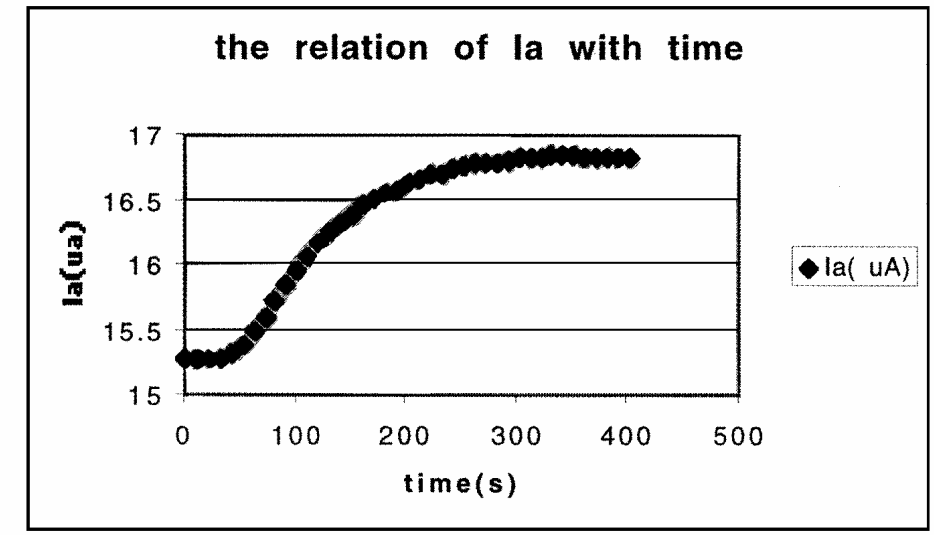

The hydrogen diffusion coefficient can also be calculated with other ways according to Fig. 4.2. Notice that onset I_a in the curve is not zero (I_a is 15.27, time has been 0).

APPENDIX 4/6

Table 4.2.

Times (s)	I_a (uA)
152	16.38
162	16.47
172	16.51
182	16.56
192	16.58
202	16.63
212	16.66
222	16.70
232	16.71
242	16.74
252	16.76
262	16.78
272	16.79
282	16.79
292	16.81
302	16.82
312	16.83
322	16.84
332	16.85
342	16.86
352	16.85
362	16.83
372	16.84
382	16.84
392	16.83
402	16.83

the changing onset point: t = 0

If adopting the formula:

$$D = 0.138L^2/t(1/2)$$

L = 0.95 mm
t(1/2): mean half of the time from the onset point to the maximum (I_a)
the maximum of I_a: 16.86, and the corresponding time: 342 s
the $D = 0.138 \times 0.095^2/(342/)2 = 7.283 \times 10^{-6}$ (cm^2/s).

If adopting other formulas to calculate D, the time (t) must be determined, if the following formula is adopted,

$$D = L^2/19.8\ tb(tg)\ ,$$

the time tb(tg) is only determined from the relation curve of I_a with t, because Tb(tg) is only determined by the intersection of the time axis with the tangent line to the curve I_a–t at the inflection point. Sometimes because of the unidea permeation curve, it is not easy accurately to do so.

APPENDIX 5/1

Y-Groove hydrogen cracking test results of L-80, L-75 and L-60 weld metals made at Nippon Steel [12]

Filler material	Weld R_M MPa	Weld H_D ml/100 g (IIW)	Weld a_w mm	Preheat & Interpass temperature (°C)							
				RT	50	75	100	125	150	175	200
Y-80C	850	2.0	40	●	●	○	○				
L-80	800	4.3	20	●	◎	○					
			30			●	◎	○			
			40					●	●	○	○
L-80 (1)	825	6.7	20			●	◎	○			
			30				●	●	●	○	○
			40					●	●	●	●
L-80 (2)	815	10.4	20			●	●	●	○		
			30				●	●	●	●	○
			40						●	●	●
L-74	735	4.0	30		●	○	○	○			
L-74 (1)	745	6.7	20		●						
			30					○	○		
			40					●	●	○	○
L-74 (2)	745	9.9	20			●					
			30						○	○	
			40						●	●	○
L-60	620	5.1	30	○	○	○	○				
L-60 (1)	645	11.5	30	●	○	○	○				

● : cracked specimens

◎ : both cracked and crack free specimens

○ : crack-free specimens

APPENDIX 6/1

Examples of typical smaw weld metal microstructures – optical microscopy made at the University of Oulu [36a]

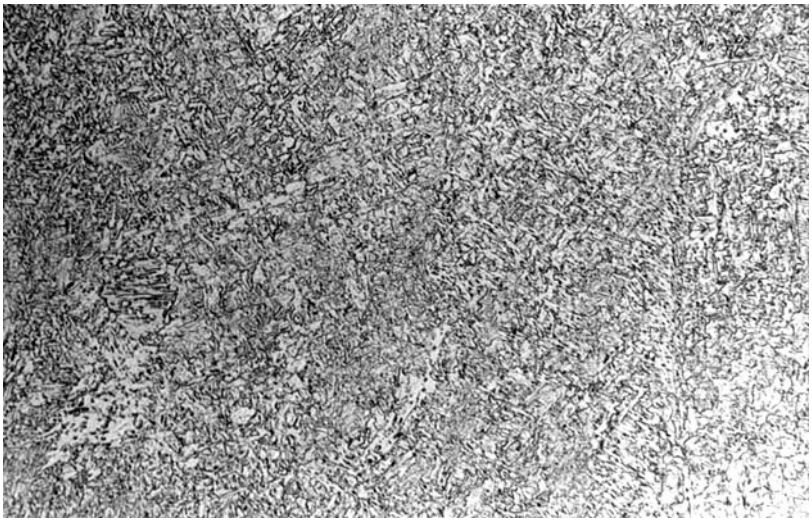

Fig. 6.1. All-weld metal microstructure of NSC15 specimen: arc energy 1.5 kJ/mm (50 x).

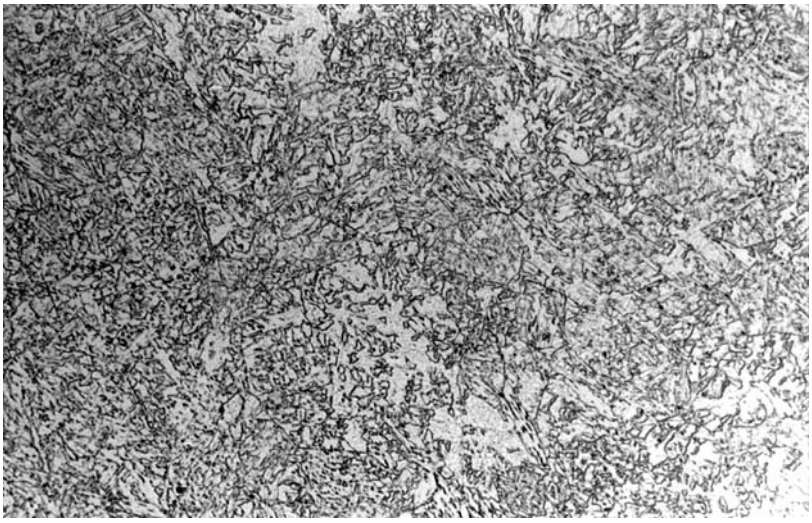

Fig. 6.2 - All-weld metal microstructure of NSC30 specimen: arc energy 3.0 kJ/mm (50 x).

APPENDIX 6/2

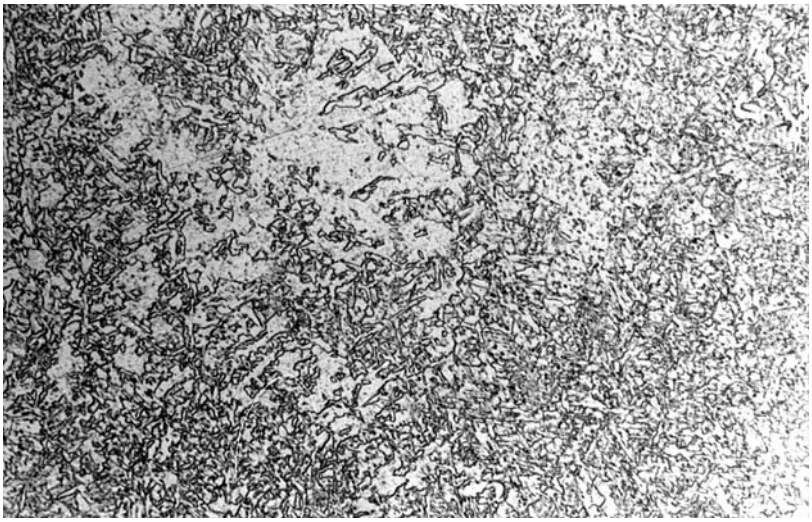

Fig. 6.3. All-weld metal microstructure of NSC50 specimen: arc energy 5.0 kJ/mm (50 x).

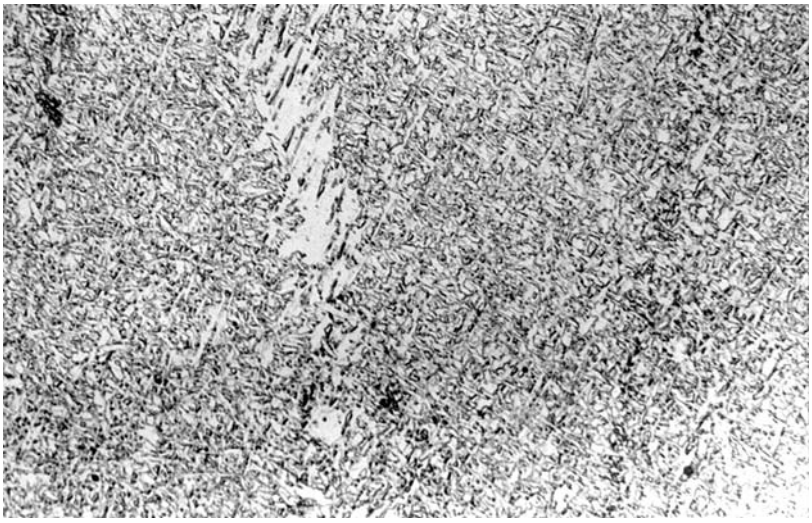

Fig. 6.4. All-weld metal microstructure of VTT1 specimen: arc energy 3.0 kJ/mm (50 x).

APPENDIX 6/3

Fig. 6.5. All-weld metal microstructure of VTT2 specimen: arc energy 3.0 kJ/mm (50 x).

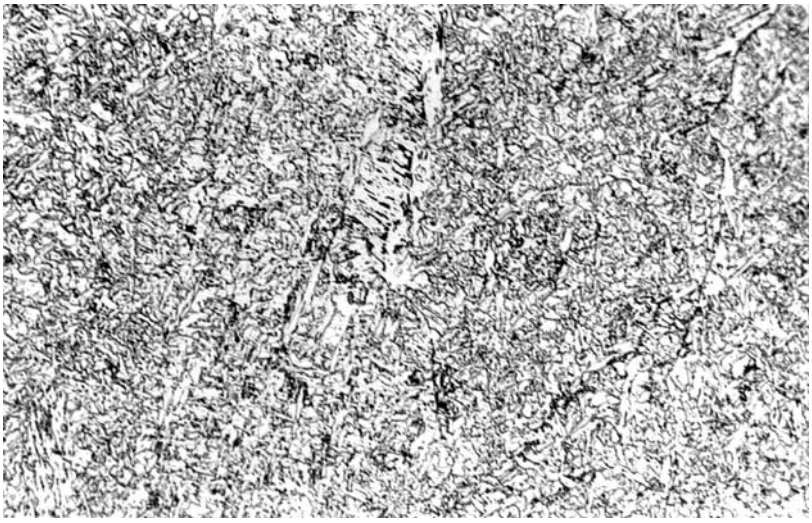

Fig. 6.6. All-weld metal microstructure of OU1 specimen: arc energy 2.4 kJ/mm (50 x).

APPENDIX 6/4

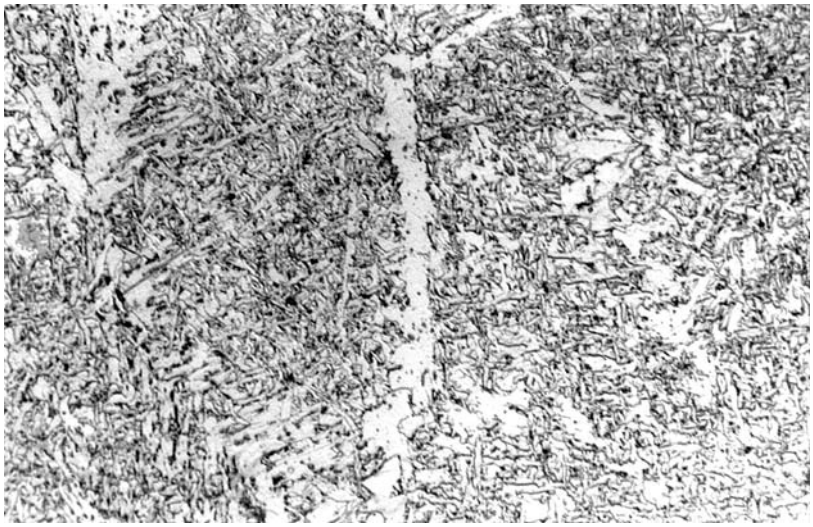

Fig. 6.7. All-weld metal microstructure of OU2 specimen: arc energy 2.4 kJ/mm (50 x).

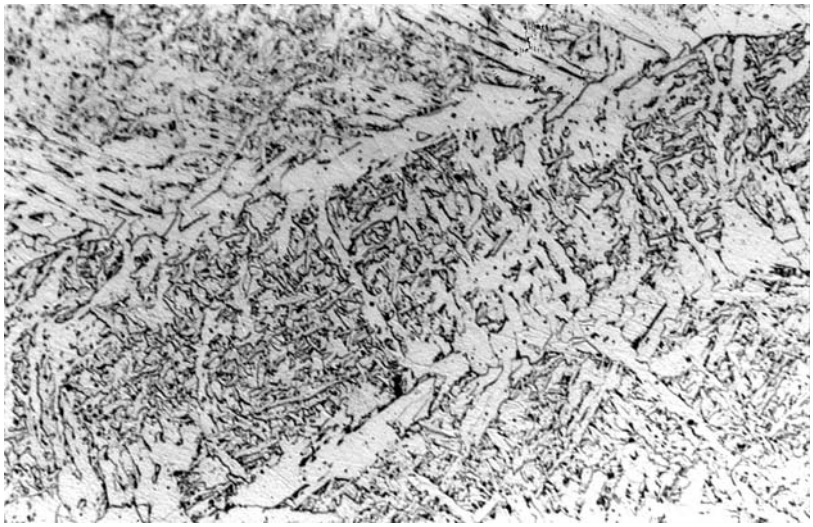

Fig. 6.8. All-weld metal microstructure of OU3 specimen: arc energy 2.4 kJ/mm (50 x).

APPENDIX 7/1

Chemical composition of the smaw and saw weld metals associated with the cracking tests

HICC 2/01

Table 7.1. Chemical compositions of the SMAW electrodes used for experimental multipass weld metals.

Näyte	C	Si	Mn	P	S	Al	Nb	V	Cu	Cr
	Ni	Ce	Mo	Ti	B	Ca	Sn	Pb	Zr	Bi
	Am	Ao	Co	W	As	Sb	Zn	Mg	H (ppm)	O
	N									
OK 48.08 (U7)	0.041	0.330	1.14	0.008	0.0048	0.006	0.005	0.020	0.009	0.030
	0.975	0.002	0.003	0.011	0.0000	0.000	0.002	0.001	0.002	0.000
	0.006	0.000	0.014	0.003	0.001	0.000	0.001	0.001	0.200	0.0309
	0.0080									
OK 74.78 (U20)	0.066	0.214	1.36	0.009	0.0021	0.034	0.031	0.005	0.141	0.018
	0.519	0.001	0.02	0.015	0.0001	0.002	0.001	0.001	0.001	0.000
	0.032	0.002	0.012	0.001	0.001	0.000	0.000	0.001	0.200	0.0327
	0.0169									
Atom Arc (YTT 4)	0.060	0.345	2.02	0.016	0.0113	0.004	0.005	0.009	0.117	0.958
	2.04	0.004	0.492	0.007	0.0002	0.000	0.007	0.009	0.003	0.002
	0.004	0.000	0.009	0.004	0.005	0.003	0.006	0.002	0.700	0.0368
	0.0217									
OK 48.08 (OU1)	0.043	0.356	1.14	0.008	0.0058	0.007	0.004	0.018	0.006	0.030
	0.966	0.000	0.003	0.012	0.0000	0.000	0.001	0.000	0.001	0.000
	0.007	0.000	0.014	0.002	0.001	0.000	0.002	0.001	0.600	0.0402
	0.0046									
OK 74.78 (OU2)	0.049	0.387	1.47	0.011	0.0055	0.004	0.003	0.016	0.015	0.031
	0.038	0.000	0.374	0.012	0.0000	0.000	0.003	0.001	0.001	0.000
	0.004	0.000	0.013	0.001	0.001	0.001	0.000	0.000	0.600	0.0363
	0.0099									
OK 75.75 (OU3)	0.043	0.403	1.65	0.013	0.0051	0.007	0.006	0.021	0.016	0.365
	2.32	0.001	0.360	0.015	0.0001	0.000	0.002	0.004	0.002	0.000
	0.007	0.000	0.015	0.004	0.001	0.000	0.000	0.001	0.400	0.0348
	0.0087									
OK 75.78 (OU4)	0.050	0.245	2.00	0.009	0.0042	0.004	0.005	0.018	0.008	0.427
	2.89	0.003	0.641	0.011	0.0002	0.000	0.002	0.007	0.003	0.000
	0.004	0.000	0.018	0.003	0.001	0.000	0.000	0.002	0.300	0.0328
	0.0103									

VALMISTUSTEKNIIKKA
Metallimiehenkuja 4, Espoo
PL 1703, 02044 VTT
Puh. (09) 4561, Fax (09) 463 118

ANALYYSITODISTUS

SPEKTROKEMIALLINEN ANALYYSI
Optinen emissiospektrometri, Spectrolab S
VAL2-006.2

N:o Liite
Sivuja 1/1

Tilaaja: VTT Pekka Nevasmaa
Saapumispäivä: 11.12.2000

Tilaus: WM-HICC
Analysointipäivä: 15.12.2000

Näyte	Koostumus %																Anal. n:o
	C	Si	Mn	S	P	Cr	Ni	Mo	Cu	Al	W	V	Ti	Co	Sn	As	
OK 48.08	0.04	0.35	1.24	0.004	0.009	0.04	0.97	0.01	<0.01	0.005	<0.01	0.027	0.012	0.015	0.002	<0.003	623/00
OK74.78	0.04	0.32	1.51	0.005	0.007	0.03	0.04	0.38	0.01	<0.003	<0.01	0.021	0.007	0.013	0.003	<0.003	624/00
OK75.75	0.04	0.37	1.66	0.001	0.008	0.34	2.48	0.38	0.01	0.004	<0.01	0.026	0.013	0.021	<0.003	<0.003	625/00
OK75.78	0.05	0.25	2.18	0.001	0.003	0.42	3.10	0.67	<0.01	<0.003	<0.01	0.023	0.011	0.025	<0.003	<0.003	626/00

analyysi on tehty viimeisestä hitsipalkosta
näytteissä merkintä 1.6kj/mm

FINAS AKKREDITOINTI SUOMI FINLAND
T103 (EN 45001)

Espoo 22.12.2000
VTT Valmistustekniikka

Erikoistutkija Jorma Salonen

Erikoistutkija Tomas Törnkvist

Tulos pätee vain analysoiduille näytteille.
Mittausepävarmuustaulukko toimitetaan pyydettäessä.
VAL24-63/2000

VALMISTUSTEKNIIKKA
Metallimiehenkuja 4, Espoo
PL 1703, 02044 VTT
Puh. (09) 4561, Fax (09) 463 118

ANALYYSITODISTUS

SPEKTROKEMIALLINEN ANALYYSI
Optinen emissiospektrometri, Spectrolab S
VAL2-006.2

N:o AVAL24-011044 Liite
Sivuja 1/1

Tilaaja: VTT VAL Pekka Nevasmaa
Saapumispäivä: 9.1.2001

Tilaus: TR-WM-HICC
Analysointipäivä: 10.1.2001

Näyte	Koostumus %																Anal. n:o
	C	Si	Mn	S	P	Cr	Ni	Mo	Cu	Al	W	V	Ti	Co	Sn	As	
OK 48,08	0,04	0,26	1,15	0,005	0,010	0,03	0,97	0,01	0,01	0,006	<0,01	0,024	0,009	0,015	<0,003	<0,003	70/01
OK74,78	0,04	0,27	1,48	0,005	0,008	0,03	0,04	0,40	0,02	0,003	<0,01	0,019	0,007	0,014	<0,003	<0,003	71/01
OK75,75	0,04	0,31	1,62	0,002	0,009	0,35	2,36	0,37	0,01	0,006	<0,01	0,023	0,010	0,020	<0,003	<0,003	72/01
OK75,78	0,04	0,13	1,86	0,001	0,004	0,41	2,99	0,68	0,01	0,004	<0,01	0,021	0,007	0,024	<0,003	<0,003	73/01
Esab atomarc	0,05	0,29	2,00	0,005	0,014	0,91	2,10	0,50	0,01	0,003	<0,01	0,010	0,006	0,016	<0,003	<0,003	74/01
Nittetsu L-80	0,04	0,30	1,36	0,001	0,005	0,25	2,55	0,60	0,02	0,004	<0,01	0,007	0,007	0,007	<0,003	<0,003	75/01

Analyysi on tehty viimeisestä hitsipalosta.
Näytteissä on merkintä 3.2 kj/mm.

FINAS AKKREDITOINTI SUOMI FINLAND
T103 (EN 45001)

Espoo 15.1.2001
VTT Valmistustekniikka

Erikoistutkija Jorma Salonen

Erikoistutkija Tomas Törnkvist

Tulos pätee vain analysoiduille näytteille.
Mittausepävarmuustaulukko toimitetaan pyydettäessä.

TUOTTEET JA TUOTANTO
Metallimiehenkuja 4, Espoo
PL 1703, 02044 VTT
Puh. (09) 4561, Fax (09) 463 118

ANALYYSITODISTUS

Optinen emissiospektrometri, Spectrolab S
Kantokaasumenetelmä, Leco TC-136
(Sisäiset menetelmät VAL2-006.2, VAL2-027.2)

N:o AVAL24-021168 Liite
Sivuja 1/2

Tilaaja: VTT Tuotteet ja tuotanto, PL 1704
Saapumispäivä: 19.4.2002

Tilaus: Pekka Nevasmaa, TR-WM-HICC
Analysointipäivä: 19.4.2002

Näyte	Koostumus %																Anal. n:o
	C	Si	Mn	S	P	Cr	Ni	Mo	Cu	Al	W	V	Ti	Co	Sn	As	
395	0,08	0,17	1,77	0,008	0,010	0,02	0,87	0,52	0,02	0,013	<0,01	0,013	0,004	0,007	0,003	0,003	99/02
396	0,08	0,16	1,79	0,008	0,010	0,02	0,86	0,51	0,02	0,011	<0,01	0,012	0,003	0,007	0,002	0,003	100/02
397	0,07	0,16	1,79	0,007	0,010	0,02	0,85	0,49	0,03	0,011	<0,01	0,016	0,003	0,007	0,002	0,003	101/02
398	0,07	0,22	2,03	0,005	0,007	0,03	2,65	0,54	0,03	0,011	0,01	0,016	0,004	0,012	0,004	0,003	102/02
399	0,07	0,21	2,00	0,004	0,009	0,03	2,52	0,51	0,04	0,011	<0,01	0,017	0,004	0,012	0,004	0,004	103/02
400	0,08	0,23	2,05	0,004	0,008	0,03	2,54	0,50	0,04	0,012	<0,01	0,018	0,004	0,012	0,003	0,003	104/02
401	0,07	0,20	1,90	0,004	0,007	0,25	3,04	0,49	0,03	0,010	<0,01	0,015	0,004	0,014	0,002	0,005	105/02
402	0,07	0,22	1,95	0,004	0,008	0,24	3,00	0,48	0,04	0,011	<0,01	0,017	0,004	0,014	0,004	0,005	106/02
403	0,07	0,23	2,04	0,004	0,008	0,26	3,17	0,51	0,03	0,011	<0,01	0,016	0,004	0,014	0,003	0,005	107/02
593	0,09	0,18	1,80	0,007	0,010	0,02	0,86	0,50	0,05	0,012	<0,01	0,013	0,004	0,006	0,003	0,003	108/02

Näytteen hitsi on analysoitu

Espoo 19.4.2002
VTT Tuotteet ja tuotanto

Tutkimuspäällikkö Simo-Pekka Hannula

Tulos pätee vain analysoiduille näytteille.
Mittausepävarmuustaulukko toimitetaan pyydettäessä.

Erikoistutkija Tomas Törnkvist

TUOTTEET JA TUOTANTO
Metallimiehenkuja 4, Espoo
PL 1703, 02044 VTT
Puh. (09) 4561, Fax (09) 463 118

ANALYYSITODISTUS

Optinen emissiospektrometri, Spectrolab S
Kantokaasumenetelmä, Leco TC-136
(Sisäiset menetelmät VAL2-006.2, VAL2-027.2)

N:oAVAL24-021168 Liite
Sivuja 2/2

Tilaaja: VTT Tuotteet ja tuotanto, PL 1704
Saapumispäivä: 19.4.2002

Tilaus: Pekka Nevasmaa, TR-WM-HICC
Analysointipäivä: 19.4.2002

Näyte	Koostumus %																Anal. n:o
	C	Si	Mn	S	P	Cr	Ni	Mo	Cu	Al	W	V	Ti	Co	Sn	As	
594	0,08	0,28	1,98	0,004	0,010	0,027	2,34	0,46	0,05	0,012	<0,01	0,023	0,006	0,013	0,002	0,003	109/02

Näytteen hitsi on analysoitu

Espoo 19.4.2002
VTT Tuotteet ja tuotanto

Tutkimuspäällikkö Simo-Pekka Hannula

Erikoistutkija Tomas Törnkvist

Tulos pätee vain analysoiduille näytteille.
Mittausepävarmuustaulukko toimitetaan pyydettäessä.

VALMISTUSTEKNIIKKA
Metallimiehenkuja 4, Espoo
PL 1703, 02044 VTT
Puh. (09) 4561, Fax (09) 463 118

ANALYYSITODISTUS

Optinen emissiospektrometri, Spectrolab S
Kantokaasumenetelmä, Leco TC-136
(Sisäiset menetelmät VAL2-006.2, VAL2-027.2)

N:o AVAL24-011103 Liite
Sivuja 1/1

Tilaaja: VAL Nevasma
Tilaus: Termoteräs 3

Saapumispäivä: 4.9.2001
Analysointipäivä: 4 ja 14.9.2001

Näyte	Koostumus %																Anal. n:o
	C	Si	Mn	S	P	Cr	Ni	Mo	Cu	Al	W	V	Ti	Co	O_2	N_2	
T1 hitsi	0,06	0,32	1,33	0,004	0,010	0,16	1,18	0,22	0,02	0,006	<0,01	0,01	0,022	0,014			438/01
SU1	0,05	0,24	1,79	0,004	0,012	0,03	0,83	0,10	0,03	<0,003	<0,01	0,01	0,004	0,010	0,021	0,004	439/01
SU2	0,07	0,25	1,96	0,001	0,011	0,03	2,52	0,50	0,03	<0,003	<0,01	0,01	0,004	0,014	0,018	0,005	440/01
SU4	0,07	0,18	1,61	0,007	0,010	0,02	0,86	0,47	0,02	0,008	<0,01	0,010	0,003	0,008	-	-	203/02

FINAS AKKREDITOINTI SUOMI FINLAND
T103 (EN ISO/IEC 17025)

Espoo 17.9.2001
VTT Valmistustekniikka

Erikoistutkija Jorma Salonen

Erikoistutkija Tomas Törnkvist

Tulos pätee vain analysoiduille näytteille.
Mittausepävarmuustaulukko toimitetaan pyydettäessä.

TUOTTEET JA TUOTANTO
Metallimiehenkuja 4, Espoo
PL 1703, 02044 VTT
Puh. (09) 4561, Fax (09) 463 118

ANALYYSITODISTUS

Optinen emissiospektrometri, Spectrolab S
Kantokaasumenetelmä, Leco TC-136
(Sisäiset menetelmät VAL2-006.2, VAL2-027.2)

N:o AVAL24-021159 Liite
Sivuja 1/1

Tilaaja: TUO Nevasmaa
Tilaus: termoteräs 3

Saapumispäivä: 27.2.2002
Analysointipäivä: 28.2.2002

Näyte	Koostumus %																Anal. n:o
	C	Si	Mn	S	P	Cr	Ni	Mo	Cu	Al	W	V	Ti	Co	Sn	As	
hitsi S1	0.08	0.20	1.87	0.003	0.008	0.02	1.58	0.33	0.01	0.014	<0.01	0.011	0.016	0.012	<0.003	0.004	61/02

FINAS AKKREDITOINTI SUOMI FINLAND
T103 (EN ISO/IEC 17025)

Espoo 1.3.2002
VTT Tuotteet ja tuotanto

Erikoistutkija Jorma Salonen

Erikoistutkija Tomas Törnkvist

Tulos pätee vain analysoiduille näytteille.
Mittausepävarmuustaulukko toimitetaan pyydettäessä.

APPENDIX 8/1

Comparison between the $R_{p0.2}/R_M$ ratios calculated according to the nominal weld metal strength data and actual measured strength values

Weld metal (WM)	$R_{p0.2}/R_M$ ratio acc. to nominal WM strength data	$R_{p0.2}/R_M$ ratio acc. to measured WM strength properties*)
OK 48.08	0.90	0.86–0.87
OK 74.78	0.92	0.85–0.87
Nittetsu L-80	0.90–0.92	0.75–0.92
OK 75.75	0.92	0.84–0.88
Atom Arc 12018	0.90	0.87
OK 75.78	0.95	0.92
OK Autrod 13.27	0.86	0.85–0.88
Filarc PZ 6138	0.91	0.93–0.96

*) measured data: SMAW welds in the arc energy range: 1.6–5.0 kJ/mm
SAW welds with the arc energy of: 5.0 kJ/mm
FCAW welds with the arc energy of: 0.7 kJ/mm

APPENDIX 9/1

Comparison of the calculated R_M estimates according to the estimation methods by VTT and ELGA (Åström) [118]

Arbitrary weld metal P_{cm} range

Applied P_{cm} value (%)	R_M acc. to VTT's estimation (MPa) acc. to Eqs (45a) and (48b)	R_M acc. to Elga's [118] estimation (MPa)	Difference between the two R_M estimates (%)
0.165	695	672	3.3
0.215	836	800	4.3
0.250	935	889	4.9
0.295	1063	1004	5.6

*** VTT's estimation method:**

$R_M = 2.85 * HV_{(ave)}$; $HV_{(ave)} = 993 * P_{cm} + 80$

$R_M = 2\,830 * P_{cm} + 228$ (MPa)

*** ELGA's estimation method (Åström)[118]:**

$R_M = 2\,556 * P_{cm} + 250$ (MPa)

Weld t_{100} cooling time estimation diagram based on the JIS *y*-groove Tekken tests acc. to JSSC [3b]

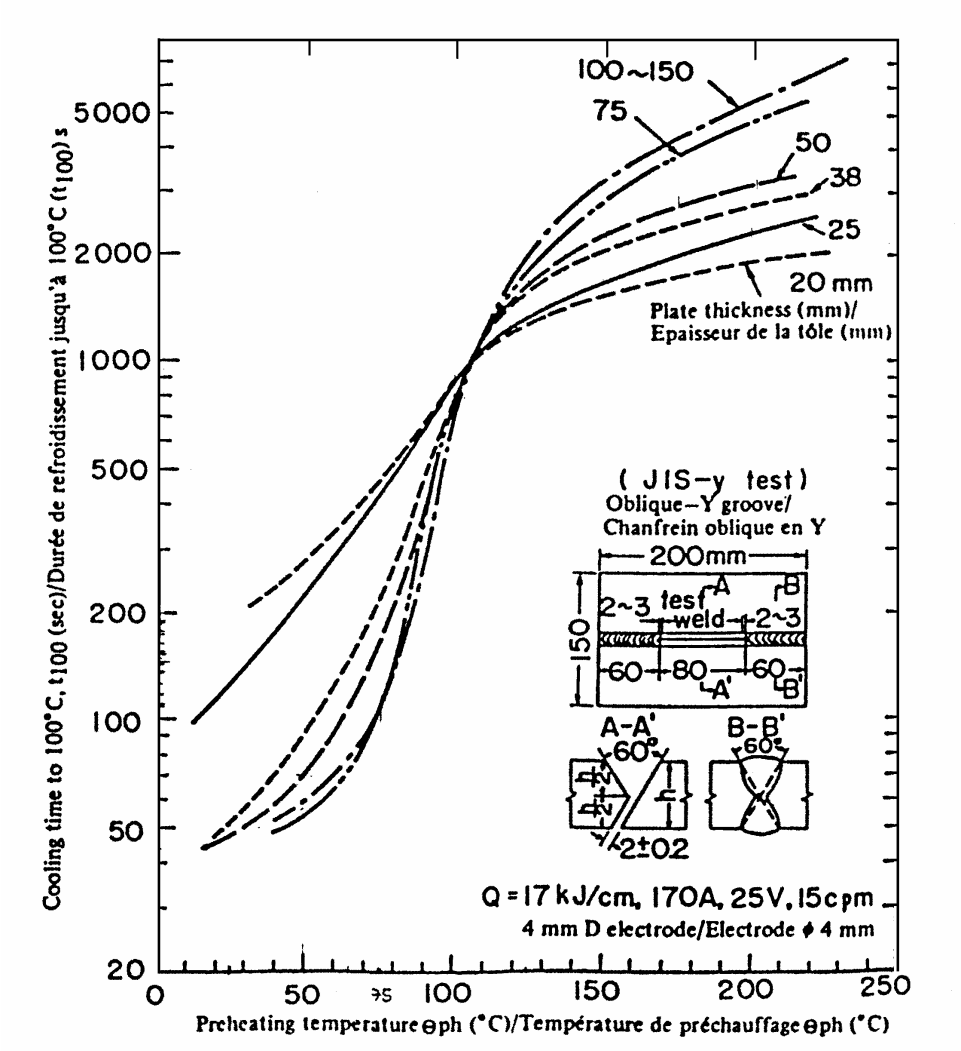

Fig. 10.1. A new cracking parameter for welded steels.

APPENDIX 11/1

Flow-charts of the procedure for the avoidance of weld metal hydrogen cracking in multipass weld metal

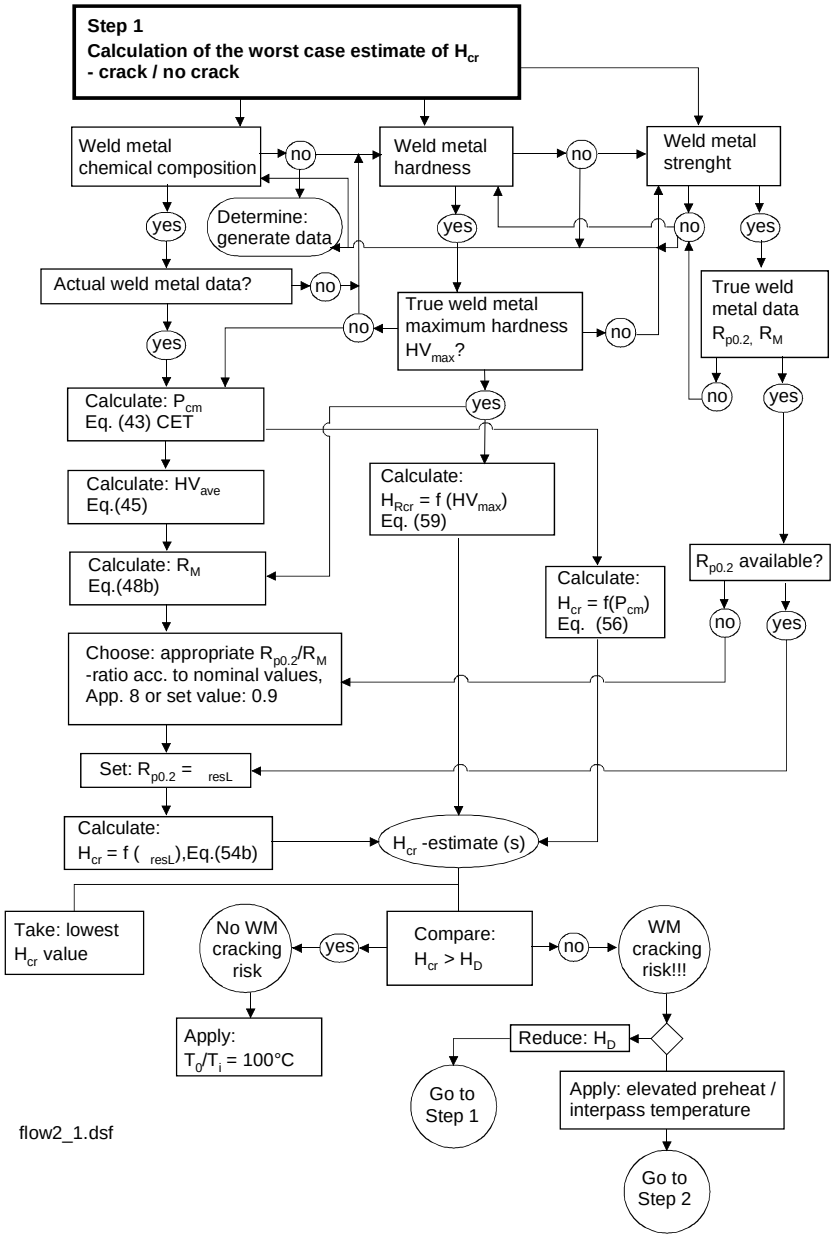

APPENDIX 11/2